Soil-Structure Interaction of a On-shore Wind Turbine from Long Term Cyclic Loading

Rose Mary Claire Hawkswood

A thesis submitted to Newcastle University in partial fulfilment of the requirements for the degree of Doctor of Philosophy within the Faculty of Science, Agriculture, and Engineering

School of Engineering, Drummond Building, NE1 7RU

December 2021

Abstract

Onshore wind turbines are very tall and slender structures that often have shallow foundations. This type of structure is prone to rocking under applied cyclic loading and must withstand millions of cycles over a 20 year design life from the wind and rotation of the blades. Wind loading is complex and highly variable in frequency and magnitude, with storm events causing large increases of horizontal load. In addition to rocking, uplift often occurs under these larger design loads.

A prototype wind turbine was designed for numerical and experimental modelling to investigate the behaviour of an onshore wind turbine with shallow foundations in a slightly overconsolidated kaolin soil, subject to cyclic loading at varying wind speeds. The loading patterns applied were designed to model normal operation of the turbine interspersed with storm events. This allowed investigation of the performance of the structure during and after periods of rocking and uplift. The model was considered to be a two-dimensional (2D) scenario, as the cyclic loading was applied in one plane only.

The experimental modelling was conducted at the University of Dundee, with five cyclic tests conducted at 1g and one cyclic test at 50g in the 3m beam geotechnical centrifuge. The experimental modelling presented three main behavioural characterised determined from the reaction of the structure, describing changes in the force reaction, foundation profile and foundation-soil contact. The three main behaviours are amplification, constant and recovery, these behaviours express the long term behaviour of the soil-structure interaction and the ability for the structure to regain strength after large cyclic events.

The soil-structure interaction was shown to change though recording of the natural frequency of the structure. The natural frequency decreased in all 1g tests, displaying a softening of the soil structure interaction.

Numerical modelling was carried out using 2D finite element analysis in which the soil response was described by the Modified Cam-Clay constitutive model, calibrated using data from experimental testing. The numerical simulations captured many of the mechanisms governing the response of the turbine and allowed for prediction and visual representation of the accumulated deviatoric strain and displacement in the soil body.

The findings presented in this thesis show that on-shore wind turbines foundations can be slightly under designed using less resources. Where current practices see foundation uplift as a failure of the design, it can be used as structural protection against cyclic loads that can cause structural degradation.

For Sue Panteny

Acknowledgement

Dr Helen Mitrani and Dr Mo Rouainia your advice, guidance and encouragement throughout the years have been indispensable and I'll forever be grateful for all the time and energy I've been given. Dr Tom Charlton thank you for your friendship, help and support.

The 1g and Centrifuge modelling was conducted at the University of Dundee and would have been impossible without the guidance from Dr Andrew Breannan. A huge thank you to Dr Scott Robinson - who has such a wealth of knowledge and experience his advice was always spot on, fellow PhD and Post Doc students at Dundee: Dr Katy Oakes, Dr Davide Vitali, Dr Andrew Minto, Dr Efthimios Apostolou, Dr Teng Liang, Gerten, Dr Benjamin Cerfontaine, Dr Craig Davidson, Technical staff Mark Truswell.

My running club, Claremont Road Runners because without them I wouldn't of had the confidence to take on a PhD and without their support over the years I would not have finished the PhD or any of the other adventures that they have supported me in. The feeling you get from a run with friends is such a wonderful place to be in.

My therapist Cat Edmonds, thank you.

This experience has been amazing, but also rough at times. My greatest source of comfort has come from my female friendships I've gained while living in Newcastle. Dr Laura N McGinty, Dr Kath A Rothwell, Dr Helen Mackay, Dr Darci Rush, Dr Kate Osborne, Dr Kirsten Dutton, Sarah Broadbent, Backy Bayliss, Rachel Brown and Dr Katie Gilmore. I know how lucky I am to have these people and many many others in my life supporting and laughing with me.

Finally my family, the clans of Hawkswoods and Howlands who are always brightening my days with daft stories and jokes, you lot really are the most wonderfully weird tribe out there. I love you all, but mostly my nephew and nieces to whom I am their favourite aunty.

Contents

List of Figures

List of Tables

Chapter 1

Introduction

A wind turbine is designed to produce energy by harnessing the wind to rotate the blades which in turn powers a generator. The use of wind energy has been around for thousands of years such as windmills, where wind power was used to grind grain into flour. As climate change is ever increasingly changing the planet, renewable energy resources are being invested and used more than ever before. As wind turbines are developing they are becoming taller structure with more output. The foundations are required to support increasing vertical load, they also need to keep the wind turbine stable throughout the design life.

As wind turbines are relatively new structures there is not a long history of their development and the effects caused from 20 years of cyclic loading. As technology is rapidly developing, Geotechnical Engineers are having to design for more powerful wind turbines with bigger towers and generators. High wind speeds will cause a strong wind load upon the wind turbine, which includes the area of the blades and tower.

Wind turbines are tall slender structures (Figure 1.1) with a heavy mass at the top, these type of structures are prone to rocking under applied loads (Oliveto et al. 2003). A wind turbine is designed to withstand millions of load cycles from the wind, wave and the blade rotation (Lombardi et al. 2013). Wind loading is complex and highly variable in frequency and magnitude, with storm events causing large increases of horizontal load. Structural rocking can occur under the design loads.

Wind loading upon the wind turbine increases the overturning moment of the structure, which will also show that there is more opportunity for the structure to rock if the foundations are designed to rock. A rocking structure can alleviate structural degradation from cyclic loading. The effects of cyclic loading on the superstructure of the wind turbine can be transferred into the foundation, to be dissipated between the foundation and soil.

The destructive forces upon a wind turbine come from environmental and mechanical factors, such as wind, wave and from the rotations of the blades of the wind turbine. This research focused on on-shore wind turbines where the environmental loading will only come from wind loading (Figure 1.2). The mechanical loading comes from the rotation of the wind turbine blades which causes destabilisation at the top of the tower, this has been described by Adhikari and Bhattacharya (2012) as P1 and P3 loading.

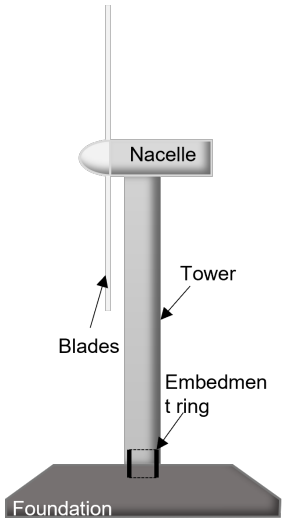

Figure 1.1: A schematic of a Wind Turbine

On-shore wind turbines endure constant cyclic loading throughout their design life, this is due to environmental and mechanical forces. The cyclic forces are:

- a torsional cyclic load from the rotation of the blades (P1) Figure 1.3,
- a cyclic load which occurs when a blade passes the tower (P3) Figure 1.4; this causes a shadowing effect between the blade and the tower and a reduction from the wind loading for that split second,
- a lateral cyclic load from the wind (Adhikari and Bhattacharya 2012).

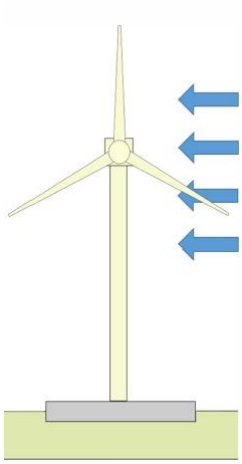

Figure 1.2: The wind load upon a wind turbine

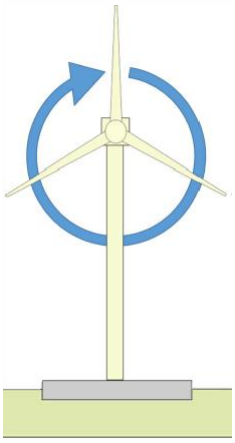

Figure 1.3: The generation of the P1 structural frequency created by a 360 degree rotation of the turbine blades

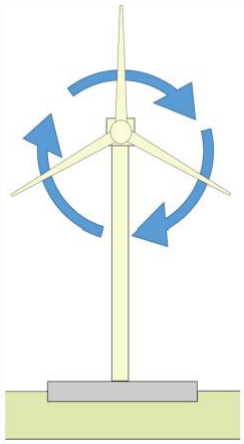

Figure 1.4: The generation of the P3 structural frequency created when the turbine blades pass the tower

The cyclic loads can cause a detrimental effect upon the wind turbine structure. This is because the natural frequency of the structure is finely balanced between the P1 and P3 frequencies. Therefore it is important that the natural frequency of the structure does not

change. If the soil-structure interaction changes due to rocking that will change the soil strength, the stress accumulation or changes to the pore pressure which could change the natural frequency. A change in the natural frequency of the structure is important because must not overlap with the P1 or P3 frequencies.

The mechanical loading comes from the rotation of the wind turbine blades which causes destabilisation at the top of the tower. This has been described by Adhikari and Bhattacharya (2012) as P1 and P3 loading. P1 is the loading caused by the miss alignment of the blades which causes harmonic forces. P3 loading is from the shadowing effect caused when a blade passes the tower.

P1 and P3 are dictated by the mechanical rotations of the tower. It has been demonstrated by Currie et al. (2015) that concrete foundations have required remediation to the embedment ring due to vertical movement between the foundation and tower due to the cyclic loading. It was noted by Salawu (1997) that structural damage is likely to cause changes in the natural frequency and therefore protecting the structure as much as possible, will increase the design life of the wind turbine.

The frequency ranges shown in Figure 1.5 are for a 5MW wind turbine and show the ranges in soft-soft, soft-stiff and stiff-stiff that the natural frequency of the wind turbine can be designed for and more importantly what ranges they must stay within in order to continue being safe.

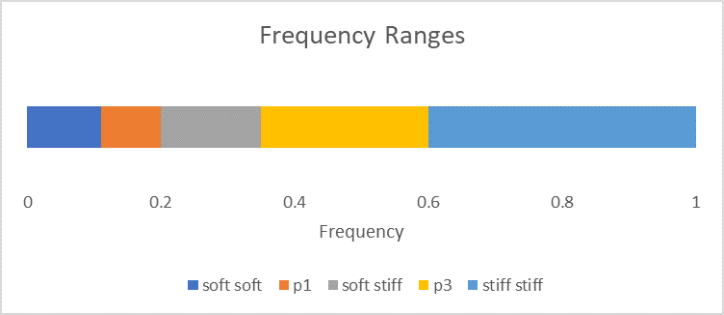

Figure 1.5: The frequency ranges of the P1 and P3 frequencies for a 5MW wind turbine, redrawn from Adhikari and Bhattacharya (2012)

Okawa et al. (2018) measured vertical and horizontal movement of a pile foundation of on-shore wind turbines, these measurements were recorded when the average wind speed was 7.85 m/s (this is to be considered an operational wind speed). The horizontal movement at 0.1405mm was double the vertical movement which implies that these structures were rotating more than uplifting. The foundation being a pile in this research, still requires a connection system to the super structure and similar effects of deformation to the connection has been recorded by Okawa et al. (2018), Oliveira et al. (2018), He et al. (2019) and Currie et al. (2015).

Further research into detection of damage of wind turbines has been conducted by Oliveira et al. (2018) using a vibration based monitoring system which detected changes that brought into question the non-homogeneity of the soil below the foundation, questioning if the soil is a

cause or an effect of the structural changes. He et al. (2019) used strain sensors to monitor the foundation of an on-shore wind turbine, and state that the wind speed and direction dominates the deformation occurring to the foundation with regards to the concrete around the embedment ring, which connects the foundation to the superstructure. The structural components such as the foundation - superstructure connection requires protecting from degradation to ensure for longevity of the wind turbine.

Increasing the design life of a wind turbine will bring a significant number of wind turbines requiring replacing down, as Ziegler et al. (2018) notes that the design life is 20 years. Wind turbines are expected to deal with up to 10^9 cyclic loads over the design life, but there are a significant number of wind turbines that are 15 years or older. It has been estimated by Corbetta et al. (2016) that in 2020 28% of wind turbines will be 15 years or older.

Previous research has shown that rocking changes the stiffness of the soil below the foundations and therefore the natural frequency of the soil-structure system (Lombardi et al. (2013) and Gajan et al. (2005)). It has also been shown to cause the soil profile to round below the foundation resulting in a reduction in contact area (Paolucci et al. 2008), which can affect the performance of the structure even if the system then ceases to rock. However, rocking can also dissipate energy between the soil and the foundations (Gajan et al. 2005). This could be beneficial for structures, especially as there is evidence that currently the embedment ring connection at the base of the tower can suffer substantial movement and require remediation (Currie et al. 2015). Rocking and uplift behaviour has not been investigated for wind turbine structures and needs to be fully understood to ensure their long-term reliability.

1.1 Aims and Objectives

The aim of the project is:
To investigate the effects of long-term cyclic loading upon shallow foundations of an on-shore wind turbine, in order to assess the effects of rocking of the foundation under normal and extreme wind conditions.

The research objectives of the project are:

RO1 To select an appropriate numerical soil model which can predict long-term cyclic loading on an on-shore wind turbine with shallow foundations.

RO2 To design appropriate models which can replicate long-term cyclic loading of an on-shore wind turbine with shallow foundations.

RO3 To investigate the soil behaviour below a shallow foundation under the influence of long-term cyclic loading to assess the long-term stability of the structure.

RO4 To assess soil stiffness degradation and strain accumulation below a shallow foundation of an on-shore wind turbine from the soil-structure interaction due to long-term cyclic loading and associated effects on structural behaviour.

RO5 To use increased understanding of the soil-structure interaction of an on-shore wind to improve the design methods of the foundations to increase the structures design life.

1.2 Scope

The scope of the research is to investigate the changes to the soil-structure interaction when a on-shore shallow foundation wind turbine is allowed to rock, in order to dissipate energy through the soil-structure interaction. The rocking will be due to environmental forces that wind turbines must endure throughout the design life.

The tests were designed from a combination of three wind types, and the environmental loading is the only variable to the test series. The use of different displacements was used to examine the changes which occurred to the soil below the foundation. The tests also increased in complexity of cyclic loading to give insight on the changes to the soil profile due to increased wind speeds and recovery time.

During the test as many cycles as possible were applied the ideal number was 10,000 cycles, in some cases only 350 cycles were applied.

The results are discussed separately with the modelling methods that were used to gain the data. The data has been used to display trends that occur within tests in order to create a profile on how the soil and the structure adapt to the cyclic loading. This includes categorising the different behaviours displayed and the cause and effects of the behaviours.

The tests were all conducted on slightly over consolidated kaolin clay. The surface was a uniform soil strength for each test and this is checked during test preparations, and the same structure was used through out.

This research uses a combination of numerical and experimental modelling to investigate the behaviour of an on-shore wind turbine with shallow foundations, based upon a consolidated clay soil, subject to cyclic loading of varying frequency and magnitude. The loading patterns applied are designed to model normal operation of the turbine interspersed with storm events. This allows investigation of the performance of the structure during and after periods of rocking and uplift.

1.3 Thesis Concept

The thesis design is so that the concept prototype is designed and chapter 4, 5 and 6 are self-contained modelling chapters.

The thesis is laid out as follows:

Chapter 1 is an introduction out lining the issues that on-shore wind turbines face, and the aim, objectives and scope to the research.

Chapter 2 contains insight into relevant literature regarding this research project which includes structural rocking behaviour and mechanisms, structural degradation issues of wind turbines, experimental and numerical modelling of relatable structures and behaviours, cyclic loading common to on-shore wind turbines, and soil-structure interaction behaviour.

Chapter 3 described the method for the design of the soil, structure, foundation, and wind displacement for the experimental and numerical modelling. The methods describe laboratory testing, research and industry design guidances and calculations used for the design.

Chapter 4 is the 1g experimental modelling, which start with how the tests were set up and the instrumentation used. The testing programme is described and the results are displayed from each test. In the discussion of the results a theory of the behaviours is explained and discussed.

Chapter 5 is the centrifuge experimental modelling chapter. There are detailed descriptions of the set-up and alternations made to replicate the 1g experimental modelling. There are details of each test, the instrumentation used and data acquisition methods. The results and discussion regarding behaviours described in chapter 4 and if the two experimental modelling methods are valid and compatible for comparison.

Chapter 6 is the numerical modelling including a literature review on the development of soil models and the choice for this project. The chapter describes the set-up of the model, the simulations runs and the results of the simulation, with a discussion of the results and the comparison with the 1g data.

Chapter 7 is the conclusion, combining the experimental and numerical modelling data and theories to describe how the foundations on on-shore wind turbines.

Chapter 2

Literature Review

This chapter is exploring the existing research of benefit to this project, which ranges from on-shore and off-shore wind turbines of various foundation designs due to having the cyclic effects to manage. The research into rocking structures which allows for the foundation movement to allow for the dissipation of energy from earthquakes for structural protection, is being explored for use in wind turbines. There is also investigation into some expected soil behaviours due to cyclic loading of soils.

Research into the dynamic response of a shallow wind turbine foundation was conducted by Deng et al. (2018). The wind turbine structure has flanges and a ring that connects the foundation to the wind turbine superstructure. The structure was laterally loaded in order to replicate a wind loading by an actuator. The loading patterns were two cyclic patterns which represented 8m/s and 11m/s wind loads and the third was a random loading pattern at 11m/s for a total of 600 seconds for each. The structural reactions were measured with 15 strain gauges, which were placed at the top of the structure, above and below the ring and on the foundation. Settlement and horizontal displacement at the top of the foundation were measured with two LVDTs. Earth pressure cells were also used to record the contact between the foundation and the soil. The cyclic loading produced fewer fluctuating strains around the ring when compared to the random loading, therefore the nature of wind which could be more destructive than an even cyclic load.

Yu et al. (2015) notes that due to wind turbines being structures with irregular masses and stiffness distribution which can cause them to be dynamically sensitive, all the while coping with 10^7 to 10^8 cyclic loads over the 25 to 30 year design life.

Scale model testing is deemed to be essential in furthering the knowledge base of off-shore wind turbine foundations as claimed by Bhattacharya et al. (2018). This must also apply when producing innovative on-shore foundation designs as the representation of forces can be scaled and reactions of the structures can easily be observed and recorded.

2.1 Rocking

Research on the response of rocking structures has been widely based upon experimental testing and furthered with numerical modelling with the aim of providing structural protection from earthquakes/seismic loading. Research in rocking shallow foundations by Gajan et al. (2005) who demonstrated the benefit of a rocking shallow foundation of a single degree of freedom (SDOF) structure to reduce the effects of seismic loading. Protecting the structure but also incurring negative effects of permanent deformation of settlement, rotation and sliding.

Gajan and Kutter (2008, 2009) conducted a series of centrifuge tests on a shear wall to record the structural response to slow lateral cyclic loading and dynamic shaking. Within the testing the soil properties were varied between sand and clay with different densities of sand. The structural components such as height, foundation length, vertical load and foundation embedment depths were also varied. An example from Gajan and Kutter (2008) can be seen in Figure 2.1, where four different critical contact ratios are displayed, 3 on sand and one on clay.

2.1.1 Foundation contact and critical contact area

The critical contact area ratio (A/A_c) is described by Gajan and Kutter (2008) as the ratio between the footing area and the minimum area required to support the vertical load. Gajan and Kutter state that rocking of a footing is a moving contact problem, because the foundation contact area is moving from side to side as seen in Figure 2.1. The energy dissipation, settlement, uplift, and moment are related to the critical contact area ratio.

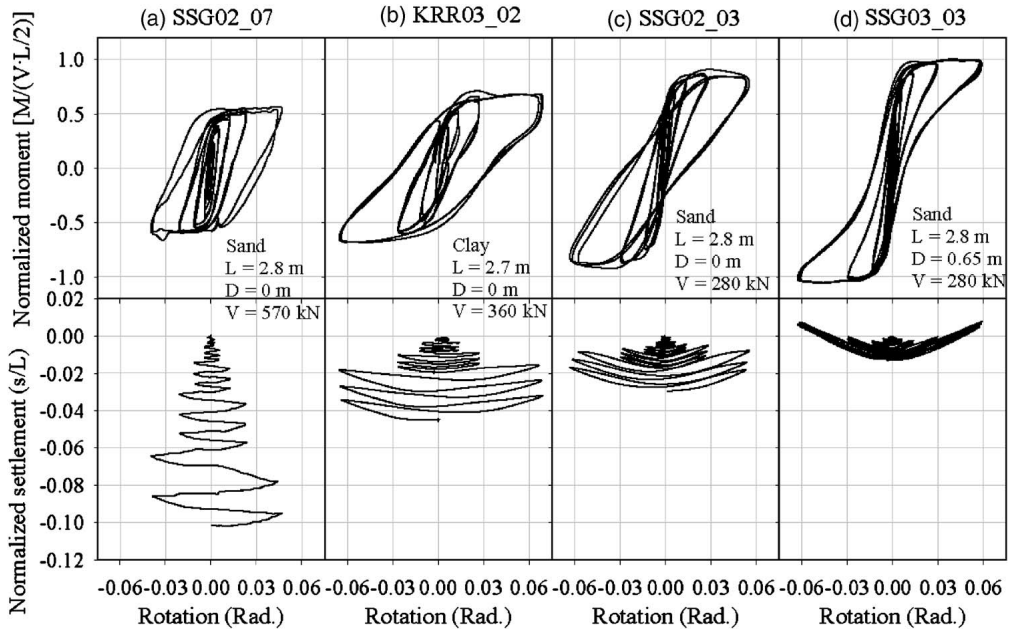

Figure 2.1: The effect of different A/A_c on the moment-rotation and settlement-rotation on a structure during slow lateral cyclic loading, recorded at the centre point of the footing. A/A_c are: (a) 2.2, (b) 3.0, (c) 3.8, and (d) 12.3, taken from Gajan and Kutter (2008)

The rocking behaviour is dependent on the critical contact area ratio of the foundation (Gajan and Kutter 2008), which is similar to Eurocodes (BRITISH-STANDARDS-INSTITUTION

1995) vertical factor of safety. It was noted a foundation had less uplift during dynamic cyclic loading when compared to slow lateral cyclic loads, because the foundation experienced less rotations.

The A/A_c can indicate the expected settlement from a structure, due to smaller values of A/A_c (2.2 for example) incurred more settlement but rotated less. As the larger A/A_c (12.3 for example) structure rotated more but less settlement occurred. Figure 2.1 shows the settlement and the moment normalised due to the test conditions (soil density, foundation size, structure mass) changing. While the structure and the soil are being kept consistent throughout the modelling and the normalised settlement and moment are not required for a comparison.

Deng et al. (2011) focused on the assessment of critical contact area (how much foundation is required to be in contact with the soil) and moment capacity (when a seismic load is applied in centrifuge testing). Ground improvements were investigated in order to reduce structural settlement occurring during the rocking to dissipate energy by placing concrete pads beneath the embedded shallow foundations for support.

The slow cyclic loading caused an uplifting motion to the rocking which was discussed by Anastasopoulos et al. (2012) because the uplifting rocking motion caused less settlement when compared to settling rocking motion. Utilising concrete pads as a form of ground improvement for the structure to be placed upon were shown to be effective in reducing settlement, but this did come at a cost of a reduction of seismic load dissipation into the soil when compared to ground without improvement.

The results were enough for Deng et al. (2011) to declare that ground improvement does warrant further study. They also summarised their opinion that for seismic energy dissipation rocking shallow foundations provide the best protection. The energy dissipation during rocking was rated by creating the Energy Dissipation Rate (EDR) displayed in Equation 2.1:

$$\mathrm{EDR} = \frac{\text{area of hysteresis loop}}{4 \times \mathrm{M_{max}} \times \theta_{\mathrm{max}}} \tag{2.1}$$

Where $\mathrm{M_{max}}$ is the maximum rocking moment and θ_{max} is the maximum footing rotation of the hysteresis cycle.

The higher the rate the more effective the rocking is at dissipating the seismic energy which could damage the structure. A higher EDR would determine the foundation design to be more efficient. Within Deng et al. (2011) research, the foundations required ground improvement to reduce the large settlements.

Investigating other methods which can be utilised to reduce the settlement that can be caused from structural rocking Anastasopoulos et al. (2012) applied a layer of dense sand on the top of a layer of medium density sand as a method of soil improvement. The utilisation of a dense sand cap can also compensate for a potential lack of detailed knowledge of the initial weaker soil properties under a proposed structure. Anastasopoulos et al. (2012) states that the safest solution for this style soil capping for seismic energy dissipation, a depth of $z/B = 1$ (soil thickness/foundation width) for the dense sand. Although depending on design requirements and the formation of the stress bulb below foundations a dense sand thickness of $z/B = 0.5$

could be effective at providing the same structural protection. This also indicates that the zone of interest below the foundation is equal to the width of the foundation.

Kutter et al. (2012) has worked to progress the use of soil yielding for seismic energy dissipation so that the discoveries and knowledge gained though research can be added to design guidance and used by practising engineers. The sharing of knowledge between research and industry was helped with physical and numerical modelling producing similar results which can allow for various designs to be assessed within consultancies. Kutter et al. (2012) states the physical modelling validates and verifies analytical methods, design codes, and numerical modelling. Which are the methods of design most common to designers.

Paolucci et al. (2008) recorded the force the foundation was applying to the soil below with the use of load cells on the base of the foundation. As the structure with a shallow foundation reacted to the cyclic loading the rocking occurred and the foundation uplifted. Figure 2.2 from (Paolucci et al. 2008) shows pressure from the load cells to give an indication of where the foundation and soil are in contact for each phase of the cycle. Allowing for contact area between soil and foundation to be accurately recorded, as well as the distribution of force.

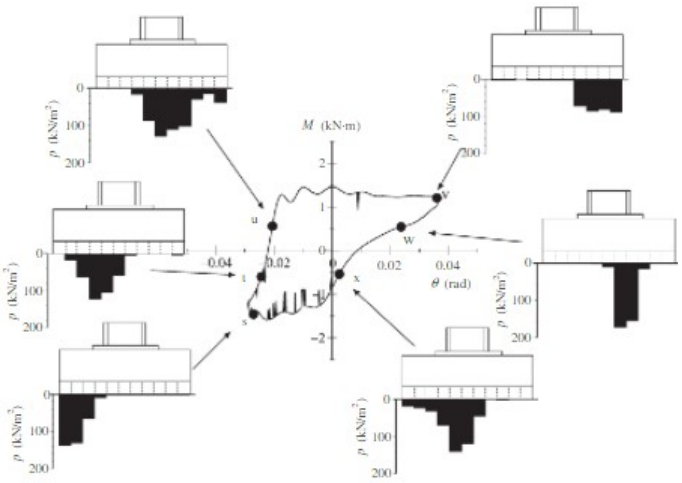

Figure 2.2: The recorded pressures (p) between the soil and foundation during the rotation of the foundation and changes in the moment (M) of the structure Paolucci et al. (2008)

2.1.2 Seismic energy dissipation from rocking: experimental modelling

Anastasopoulos, Gazetas, Loli, Apostolou and Gerolymos (2010) have utilised rocking as a method of seismic dampening. Using real examples of soil failure for structural protection during earthquakes. The example structure was tall and slender (which it could be assumed has a low vertical FoS), from the 1999 Kocaeli earthquake in Turkey (Anastasopoulos, Gazetas, Loli, Apostolou and Gerolymos 2010). Although the structure was unharmed there was excessive rotation, which could lead to collapse or leave the structure unsafe and not fit for purpose. Anastasopoulos, Gazetas, Loli, Apostolou and Gerolymos (2010) declared that the economically efficient earthquake protection requires reappraisal. The conventional design is to use larger and stronger foundations, which do not allow for foundations to rock and therefore prohibits

any soil yielding. Ideally rocking foundations are smaller and therefore require less materials which makes them more economically beneficial. This has been reiterated by Gazetas et al. (2014) which noted that a factor of safety less than one, in seismic geotechnical design is not equal to the same in static design.

Foundation widths or slenderness ratios are critically analysed by testing such as Drosos et al. (2012) investigated through physical modelling of slow cyclic lateral testing and dynamic shake table testing. Using three different foundation sizes of identical SDOF super structures with identical deck loads, the foundations varied in length and width. The vertical factor of safety altered between 7.49 and 2.29 and the earthquake factor of safety to between 1.07 and 0.43. The structure with the smaller factor of safety incurred more settlement but rotated less with smaller moment being created. Showing more energy can be dissipated with the use of soil failure and a reduced factor of safety.

Anastasopoulos et al. (2012) conducted a series of centrifuge testing that investigated allowing slender structures to rock in an uplifting motion rather than settling motion, to reduce the settlement. This was conducted through slow cyclic pushover testing; there were two variables in the testing, the structure weight and soil density. This was conducted using the same Longstone Sand as Drosos et al. (2012), Anastasopoulos, Georgarakos, Georgiannou, Drosos and Kourkoulis (2010) and Anastasopoulos, Gazetas, Loli, Apostolou and Gerolymos (2010), which allows the results to be evaluated against previous works. The light and heavy structure loads were tested on comparable soil densities and more settlement occurred for lower soil densities, where the soil densified under the structure.

Gajan and Saravanathiiban (2011) express dissatisfaction that even with mounting experimental evidence and case histories of foundation rocking that soil yielding remain an unproven / unrealistic energy dissipation mechanism for reducing ductility demands of the structure. The benefit of this research is testing the numerical data against the experimental data, although the focus of the work is on a multi-storey structure which reacts differently to a SDOF structure. The foundation rocking results are still transferable, such as, that energy dissipation is increased with an increase in shaking intensity and similarly with drift. The most important outcome from the work is that foundation rocking has been shown to dissipate 90% of the total seismic input energy when the vertical factor of safety is between 4 and 10. If the vertical factor of safety is increased to 17, the energy dissipation from rocking foundations is reduced to 60% of the seismic energy input. It should be noted that stronger seismic loading had higher percentages of energy dissipation, which will have to be taken into consideration when considering the wind loading is a very different frequency.

Gajan and Saravanathiiban (2011) concluded that it is better economically for foundation rocking as the optimal seismic energy dissipation method, providing settlement and displacement are within tolerable design limits. The implication of the closing conclusion is that settlement is unavoidable, and it is up to the Designer to prepare the structure for such settlement post-earthquake for the structure to continue to be fit for purpose. As wind turbines will have lower forces applied, these will be more continuous throughout the design life. The level of

settlement is expected to be reduced in comparison, while still gaining the desired effects from a rocking foundations.

Hakhamaneshi et al. (2012) investigated the rocking response of a structure when on a medium strength clay, with the use of centrifuge testing, with the view to compare to previous testing on sand by Gajan and Kutter (2008). Identical testing was conducted such as slow cyclic, vertical plate baring and dynamic shaking at 15g, 30g and 60g. The testing confirmed that the sand and clay have similar deformations when dissipating energy through rocking structures, if the vertical factor of safety is in a similar range. The overall verdict is that energy dissipation of rocking structures on clay soils could result in 20% to 40% less settlement than on a sand, although it is noted that with an increasing vertical factor of safety there is a reduction in energy dissipation capacity.

2.1.3 Numerical modelling of rocking structures

Anastasopoulos et al. (2011) replicated the physical modelling conducted by Gajan et al. (2005) in finite element software (ABAQUS), of a shear wall footing under lateral actuation at around the centre of gravity of a structure. Showing a validated constitutive model can effectively capture the response of vertical loading on shallow foundations, the cyclic performance of the foundation capturing moment-rotation and load-displacement. Allowing for the foundation and the soil to have individual computational nodes they are able to move independently of each other and therefore allowing for gapping and sliding between the foundation and the soil. The hysteresis loops which are created from the moment-rotation data displays the energy dissipation between the footing and soil interface. The settlement rotation data showed sharp edges which are indicative of there being gapping, soil yielding and a decrease in the soil-foundation contact. This research shows the correct constitutive model and design allows for accurate representation of wind loading upon a structure. Although this also increased the sliding of the foundation whereas a higher point of actuation would promote more foundation rocking than sliding.

The comparison of seismic energy dissipation by foundation rocking to structures with energy dissipation devices was conducted by Gajan and Saravanathiiban (2011) with the use of physical and numerical modelling. The numerical model output was validated using the results from the physical modelling (shake table tests), although the simulated shear force is less than recorded in the physical model.

2.2 On-shore wind turbines

The investigation into a wind forced vibration response of an on-shore wind turbine by Harte et al. (2012) involves studying the soil-foundation interaction as softer soils can influence a dynamic response from a wind turbine. Where changes to the soil-structure interaction lead to an lengthened vibration period of the wind turbine, and adding to the dampening system. This was also noted by Zania (2014) for off-shore monopile wind turbines.

Yu et al. (2016) researched into the long terms effects of cyclic loading on pile foundations of on-shore wind turbines which addressed the lack of information in the standard of cyclic loading. Noting that current practices do not incorporate the effects of the cyclic loads characteristics and their volume of cycles. With current designs being overly conservative and increased project costs.

Seymour (2018) used numerical modelling to investigate the effects of soil degradation from cyclic loading of a on-shore wind turbine gravity foundation. Using 3 different soil profiles and varying the overturning moment of the structure, which allows for different levels of fatigue, showed that although there were different overturning moments, the effects on the cyclic degradation are not only within periods of storms but in normal operation of the wind turbine. This gives an indication that all cyclic loads no matter how small can affect the wind turbine foundation.

Ntambakwa et al. (2016) discussed the geotechnical design considerations required for on-shore wind turbine gravity foundations. Raising issues such as the bearing capacity and the effects of high overturning moments causing a reduced soil-foundation contact. Also settlement, allowable uplift and minimum foundation stiffness which are dependant on the soil stiffness and the soil-structure interaction.

Taddei et al. (2015) conducted a parametric study into the soil-structure interaction of an on-shore shallow foundation wind turbine upon a layered soil, using a finite element method. The results showed that the natural frequency was not affected by the layering, especially when the layer thickness was the foundation width or greater.

2.3 Monopile off-shore wind turbine

Extensive studies and experiments by Bhattacharya et al. (2011) into wind turbine loading where the research focused on off-shore wind turbine loads and the effects on the foundations. These systems are required to deal with thousands of cycles from P1, P3, wind and wave loading. An investigation into off-shore wind turbine foundations is more complicated than on-shore due to the limited access to the site.

Bhattacharya et al. (2011) investigated the cyclic loading that occurs to pile foundations, by conducting 1g experimental work and numerical simulations on a pile foundation. The foundation is embedded in a normally consolidated clay and subjected to cyclic loading which represents the mechanical and environmental loading that is expected to be applied during its lifetime. The environmental loading being the wind and wave action which is a lateral loading whereas the P1 and P3 are structural loading caused by the rotation of wind turbine blades (Adhikari and Bhattacharya 2012).

The loading styles started as one lateral load to represent all 4 loads, where this has been developed into individual loading methods within the same experiment. This is due to the loads all having different frequencies. The wind turbine was loaded with up to 10,000 cycles which allowed for an expected life cycle to be modelled which is less than other experiments

on wind turbines. LeBlanc et al. (2010) research into pile foundations in sand under a lateral cyclic loading was 8,000 and up to 60,000 cycles.

Bhattacharya et al. (2013) conducted 1g experimental modelling of an off-shore wind turbine with pile foundations. The sand used in the experiment was shown to increase in stiffness with cyclic loading, and therefore caused the natural frequency of the structure to increase. The experimental modelling was used to investigate the free vibration characteristics. Applying uniform and random loading through an actuator and the rotating turbine blades, therefore replicating the wind and wave loading as well as the structural loading of P1 and P3. The structure being non-linear means it is dependant dynamic response amplitude. The drainage in the soil removed potential pore water pressure accumulation, so there cannot be a build-up. Bhattacharya et al. (2013) observed that the sand surrounding the monopile foundation stiffened up due to the increase in densification, and therefore causing changes to the soil-structure interaction.

Lombardi et al. (2013) commented that for off-shore monopile supported wind turbines the foundation vibrations can cause cyclic strains in the soil around the monopile foundation. If these are moderate to high amplitude cyclic loading the soil will change stiffness and strength. To ensure there is no unplanned cross-over in the mechanical frequencies and the structural frequency.

Lombardi et al. (2013) experimental set-up used kaolin clay and a 1:100 model of a 3MV Vesta V90 wind turbine in which 172,000 cycles of P3 loading were applied. The important physical mechanisms and parameters that were identified for the experimental modelling are the repeated cyclic changing the shear strain and the degradation of soil stiffness. The cyclic stress ratio (CSR) which is based upon the ratio between the shear stress and the vertical effective stress at a particular depth, which can be represented as: P/GD^2

The loading rate effects on pore water pressure is to be considered, if there is no available time for the pore water pressure to dissipate there will be build-up. The frequency of loading and the system response with regards to the forcing frequency being close to the natural frequency and therefore risking resonance within the structures system. The dampening of the structures system increased when a higher cyclic stress ratio.

Li et al. (2010) conducted centrifuge modelling of laterally cyclic loading of a mono-pile in sand. To avoid excess pore pressure build up in a drained cyclic response, dry sand was used to replicate the saturated sand properties. When the vertical stress of dry sand is equal to the effective vertical stress of saturated sand, an adjustment to the sample depth can recreate the stresses required.

When the foundation type was changed Bhattacharya et al. (2017) noted that it affected the whole soil-structure interaction, so any information on other foundation types will have to be carefully thought through before using or influencing research directly.

2.4 Suction Caisson off-shore wind turbines

Byrne et al. (2018) used field testing and numerical simulations to improve the design method of monopile foundations by better recording the laterally loaded behaviours. The improved design methods used for monopiles and as Byrne et al. (2018) noted it can also be applied to suction caissons and jacket piles.

Field tests of suction caissons were conducted by (Houlsby et al. 2005, 2006) on sand and clay, the tests included laterally loading the foundations with high and low frequency and amplitude cyclic loading, the results showed there were a variation to the ranges of changes to the stiffness, inertia and dampening effects which depended on the range of the amplitude and frequency that was used to apply the cyclic loading. This is a continuation of other research on suction caissons and how they are affected by the lateral loading conducted by Byrne and Houlsby such as Byrne (2000), Houlsby and Byrne (2000), Houlsby (1999).

Zhu et al. (2012) conducted 1g experimental modelling with a novel cyclic loading rig on wind turbine with a suction caisson foundation which was embedded into a fine silty sand which is representative of the off-shore soils which are found around the UK. The dominant movement was from lateral rotation of the structure, during the testing there is also accumulated settlement which depending on the type of cyclic loading. A one-way loading pattern had less settlement in comparison to a two-way loading pattern. The stiffness is also affected by the pattern of cyclic loading and increased during one-way cyclic loading. Although the experimental modelling did not reach the 10,000 cycles which is the design life of a wind turbine, the lateral loading was along one plane which is not realistic of the multi-directional loading that will occur in nature. Zhu et al. (2012) concluded that in order to reduce the accumulated rotation of the structure is to increase the foundation size or increase the vertical load with the use of ballast. The structure and the foundation are designed to accommodate the accumulated rotation in a one-way loading pattern, whereas two-way loading does not accumulate a similar rotational deformation.

2.5 Strain accumulation

Bhattacharya et al. (2019) notes that element testing can represent the strain accumulation build up, in this it was noted that 100 cycles at a strain rate of 0.5% can have the same results as 19400 cycles at 0.2%. The assumption the strain accumulation is linear will need to be assessed within the results.

Okur and Ansal (2007) investigation into cyclic loading included using cyclic simple shear, cyclic torsional shear and cyclic triaxial devices which show that the dynamic properties of fine-grained soils can be more complex to understand than course grained soils. Even though theoretically there is no dissipation of energy taking place when the strains are below the elastic threshold of strain amplitude. The loading used is at a seismic frequency which allows for the pore water pressure to build up, which will give altered results to tests carried out at a rate in

which the pore water pressure can be dissipated. The degradation stiffness was shown to be dependent on the confining stress in the pneumatic triaxial tests, and the cycle number.

The reduction to stiffness caused by cyclic excitation; changing stress amplitude indicates the reduction of stiffness becomes effective once the critical shear strain level exceeds elastic.

2.6 Pore pressure

Lazcano et al. (2020) investigated the influence of pore pressures in cohesive soil on bearing capacity of shallow foundations under cyclic loading. Which showed that the generation of pore water pressure under cyclic loading depends on the shear stresses, effective vertical consolidation stress and initial void ratio. This lead to numerical calculations to consider the generation of pore water pressures created by cyclic loads in soils with potential for cyclic softening. The effects on the dynamic bearing capacity can be quantified.

2.7 Frequency

Arany et al. (2015) used two different calculation methods to calculate the natural frequency of the structure as treating it as a beam, the more complex (Timoshenko beam model) did not improve the predicted natural frequency when compared to the simpler (Euler-Bernoulli beam model), therefore a simple calculation method would be ok in this project.

2.8 Summary

The main aspects of the literature review to take forward in the wind turbine design and modelling are:

- Rocking has the ability to protect structure from cyclic loading.
- The foundation size with regards to A/A_c during rocking control the settlement of the structure.
- The replication of rocking structures in experimental modelling is well established by Gajan et al. (2005), Paolucci et al. (2008) and Anastasopoulos, Georgarakos, Georgiannou, Drosos and Kourkoulis (2010).
- Anastasopoulos et al. (2011) has successfully replicated the rocking behaviour from seismic loading in finite element analysis.
- There are 3 types of cyclic loads which cause thousands of cyclic loads upon a wind turbine over the life time.
- Experimental modelling of wind turbines on sand and clay is well established with lateral cyclic loading.

- Strain accumulation in fine grained soils is more complex than course grained soils, but the rate of strain accumulation is still linear.
- Pore water pressure in cyclic loading is dependant on shear stress, vertical stress and void ratio.
- The Euler-Bernoulli beam model is suitable for calculation of the natural frequency of the structure.

Chapter 3

Prototype Design

This chapter describes the design process of an on-shore wind turbine with shallow foundations under long-term cyclic loading. This is the second research objective noted in section 1.1. The design process starts with producing a full scale wind turbine the 'Prototype'. The Prototype is the base for the scaled down 'Model' used in centrifuge and 1g experiments and the prototype inputs for the numerical modelling.

3.1 Introduction

The design of an idealised on-shore wind turbine requires consideration of the soil, superstructure, wind loads and foundation. These sections of the prototype were individually designed. They are interconnected into each others designs and this was accommodated throughout the design process. The design of a prototype wind turbine has many requirements which can be split into industrial, research, and practical requirements.

It is important that the wind turbine is representative of current industry designs in use. This was fulfilled by keeping the same slenderness and weight proportions of the superstructure with a large weight at the top replicating the nacelle and blades. The foundation and the wind loading were designed based on industry guidance and a realistic height, diameter and shape of the wind turbine superstructure was used to calculate the wind loading.

The DNV code (Det Norske Veritas 2010) provided guidance for the total design of on-shore and off-shore wind turbines. The DNV code allows the design of the foundation and the wind loading to be aligned with current practices of engineering design, ensuring it is representative of current design practices within the industry.

The research requirements were based upon the aims and objectives of the project. The design of the wind turbine needed to ensure that the structure, soil and cyclic loading are capable of replicating a rocking foundation.

The practical requirements were working within the limitations that exist due to the experimental and numerical methods. Experimentally there are requirements such as the space available for experimental modelling and placement of instruments. There are four aspects to the Prototype; the soil, the superstructure, the foundation, and the loading. Each has their

own requirements for a successful model and their own limitations and constraints due to practicalities of experimental modelling. Each aspect of the design will now be discussed.

3.2 Soil

The soil must support the structure while allowing some yielding of the soil below the foundation to round without extreme settlement. Settlement as soil failure due to the foundation settling over 0.3m ('British-Standard-Intitution' 1990). Another important aspect of the soil in the project is that it is appropriate for the experimental modelling and numerical modelling.

Soil in the UK is made up of varying deposits, which range from clays to gravels ('British-Geological-Socity' 2019), with glacial till being very common. Therefore, an on-shore wind turbine could be built on any soil condition. This means there is no restriction as to the soil type that could be chosen if it is to replicate conditions in the UK. A uniform soil is good for replication and so all the experimental work can be conducted on identical soil with identical properties.

Previous research and studies on structures under long term cyclic loading have been conducted on both clays and sands. For example, experimental modelling conducted by Lombardi et al. (2013), Bhattacharya et al. (2011, 2013) of cyclic loading of a offshore wind turbine is in clays, whereas Li et al. (2010) has researched monopile offshore wind turbines in sands.

Research into rocking structures has been conducted on both sand and clays. Gajan and Kutter (2008, 2009) tested rocking structures from seismic loading using mainly sands, which showed significant settlements and structural rotations. While the tests on clays had less settlement but still retained the rocking features which were present in the tests done with sands Gajan et al. (2005), Gajan and Kutter (2008, 2009). While the source of the cyclic loading is different the decreased potential settlement of clay to sand is worth noting.

For the numerical modelling the use of Modified Cam Clay (MCC) and the Hardening Soil Model with small strain stiffness (HS Small) have previously been used to model clays under cyclic or dynamic loads (Cabangon et al. 2017).

In the laboratory even though it takes longer to prepare the clay due to the consolidation method in the centrifuge (see section 4.2.2), the soil body has a greater consistency between tests when compared to raining sand where layers could have slight differences due to the preparation method. For these reasons clay was decided upon as the soil of choice. Speswhite kaolin clay (Manufactured by Imerys Filteration and Additives) was chosen as it is well documented in other research and the properties are well established. It has been used in research by Bhattacharya et al. (2011), Robinson (2019), Brennan et al. (2016).

3.2.1 Preliminary testing at Newcastle University

The soil to be used in testing has two requirements; to be strong enough to support the weight of the structure but to yield enough so that while the structure is rotating, the edge of the

foundations can deform the soil profile below them. To determine the strength of clay required for the experimental work to be a success some clay slurry was consolidated in a press and shear vanes and an adapted CBR tests was conducted at Newcastle University Geotechnical Laboratories.

The first stage of this initial investigation at Newcastle University Geotechnical Laboratory into the use of clay was consolidating Speswhite kaolin clay mixed into a slurry at a 5:4 clay:water ratio.

In the laboratory 10kg of clay was added to clean barrel, and 7 litres of water was added and a plaster mixer were used to combine into a slurry, with an higher water content than the liquid limit of Specwhite kaolin (65% Robinson (2019)). The mixture's runny consistency ensured that when placed into the clay press no layers formed. The water was added in stages to the clay powder ensuring a smooth slurry.

The clay slurry was poured into a consolidation cell with an volume of 0.005m^3, which is compressed with EnerPac 23 Ton hydraulic ram applying vertical pressure to the cell. A GDS Standard Pressure controller controlled the pressure applied. This cell was calibrated, with the cell full of water and connected to a Budenburge gauge to display the internal cell pressures.

The clay was compressed to pressures of 18.6kPa, 56.4kPa, 132kPa and 201kPa. After each consolidation phase the sample was weighed and had a shear vane test (using Pilcon hand vane tester 13564/3, V206, 19mm to 'British-Standards-Intitution' (1990)) to determine the shear strength of the soil. The shear strength was taken at 3 places in each sample: at the surface, middle of the sample height and at the base of the sample. Figure 3.1 displays the data from all the confining pressures and the three depths at which the test was conducted.

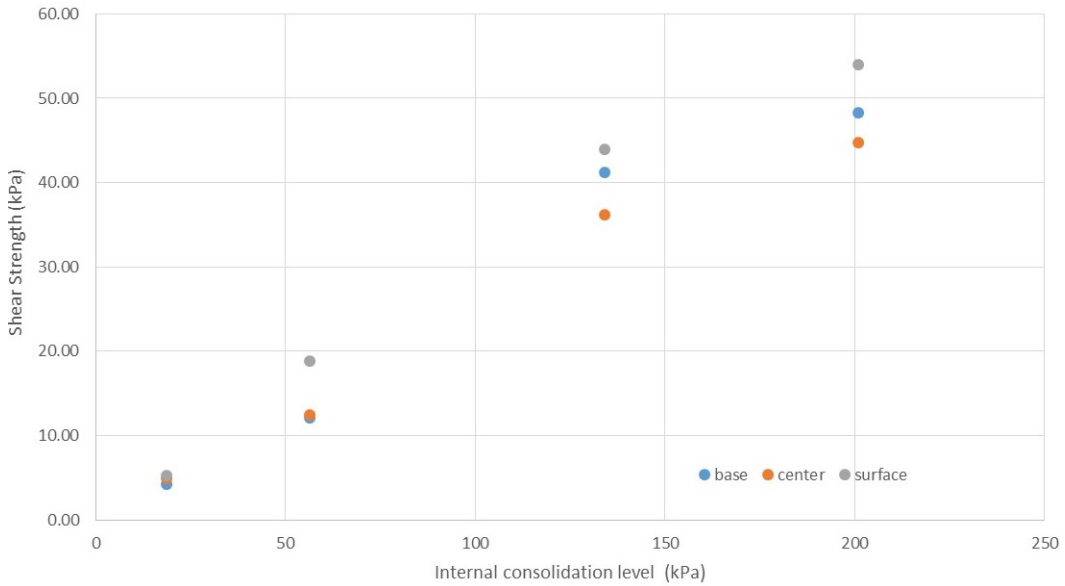

Figure 3.1: Shear strength data from Newcastle clay consolidation

A adapted version of a California Bearing Ratio (CBR) test was conducted to 'British-Standard-Intitution' (1990) after each consolidation phase. The aim of this test is to give an indication on the bearing capacity of the kaolin after each consolidation phase and to see

how the soil reacts to the insertion of a 10mm diameter plate. The CBR test was conducted using an Instron (model 5985L6819, with a 250kN load cell) which moved a plate at a rate of 0.1mm/minute into the clay and would be concluded once it has moved 1mm in to the soil. This was in order to limit deformation of the soil sample so it could continue to be used for further consolidation and testing with minimal disturbance. The results can be seen in Figure 3.2 which shows that when the soil is consolidated to a higher pressure the soil can withstand larger forces. Estimated minimum bearing capacity can be assumed as 0.1 x10^{-3} kN/m^2 at a confining pressure of 18.6kN/m^2, 1.1 x10^{-3} at 56kN/m^2, 2.9 x10^{-3} at 134kN/m^2, and 4.2 x10^{-3} at 201kN/m^2.

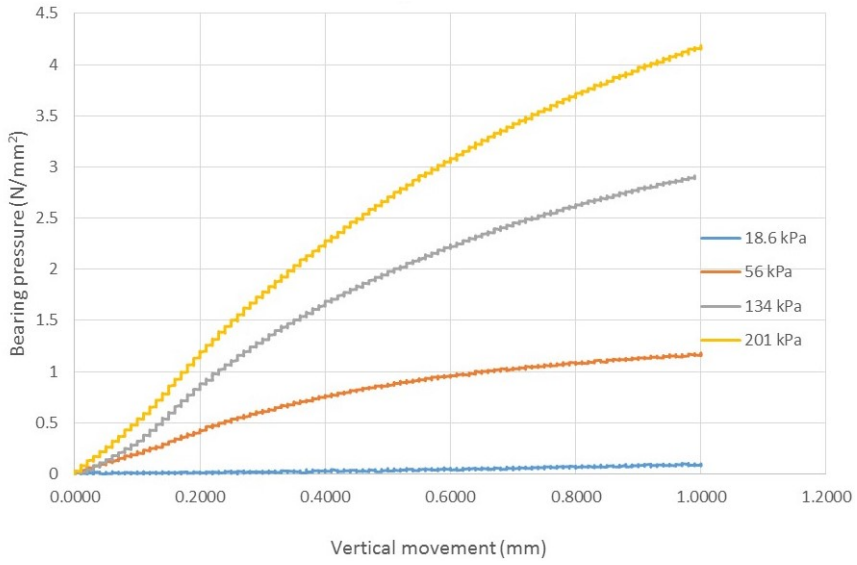

Figure 3.2: The bearing capacity from Newcastle clay consolidation

The height of the sample was measured to calculate volume and the water which was expelled was collected for an estimated moisture content. The moisture contents can be seen in Table 3.1. These can be used to ensure similar levels of consolidation to the soil that is consolidated in the centrifuge, as consolidation methods are different and the soil from the centrifuge will not be uniformly consolidated like the soil that is pressed in a cell.

Table 3.1: Soil water content

Stage of compression	Water Content(%)
Initial	70
18.6 kPa	51
56 kPa	43
134 kPa	37
201 kPa	13

The combination of the shear vane and adapted CBR tests give a profile of the soil and what bearing capacity the soil has for an associated shear strength. The bearing capacity is important because if the soil is too strong it will not yield and the foundation would not embed.

Therefore from these initial experiments the kaolin clay should have a surface c_u of 10kPa which will increase with depth, and the moisture content is expected to be around 35-45%.

The soil body minimum thickness should be no less than the maximum width of the foundation, to avoid boundary effects. Therefore the soil layer is at a minimum of 9m deep, which is detailed in section 3.3.4.

The soil used in the experiments (detailed in section 4.2.2) was processed and tested identically for each test to minimise any variability. T-bar tests were conducted on the soils used in the experimental modelling to ensure the desired shear strength is achieved within the soil body. A T-bar test was developed for normally consolidated clays where the measured penetration resistance is converted into soil strength, using a bearing factor associated with the flow of soil around the bar.

The numerically generated soil does not have issues with replications between simulations, but it does need to accurately represent the soil produced for the physical experiments. This is possible by validating the soil generated numerically in Chapter 6, against that of the results of the t-bar data.

The final details of the prototype soil can be seen in Table 3.2 and the minimum dimensions of the soil body can be seen in Figure 3.3.

Table 3.2: Soil expectations from testing at Newcastle University

Soil properties	
Shear strength (c_u)	10kPa
Moisture content	35-45%
Soil type	speswhite kaolin clay

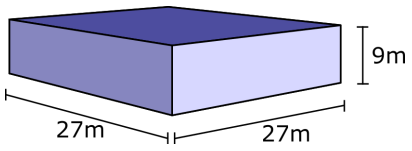

Figure 3.3: The minimum required soil body dimensions

3.3 Superstructure

The important aspects of the on-shore wind turbine to be replicated are the natural frequency of the structure and the weight distribution of a wind turbine. The natural frequency of the superstructure is important as it cannot coincide with the frequency of the applied loads; if they do coincide then resonance can occur and structural damage will result. The aspect of design that can affect frequency are the weight at top of the superstructure, the external and internal dimensions of the tower of the superstructure and the length of the superstructure. The overall weight balance of the structure is important to recreate because this will determine the rocking behaviour and directly influence the natural frequency of the structure.

The start of the design process came from an investigation into current wind turbines such as the Siemens SWT-2.3-93 and the Vesta V90-3.0MW turbines which are of a similar height-weight proportions, the initial Prototype design is idealistic without regards to practical limitation. The Siemens SWT-2.3-93 wind turbine produces 2.3 MW of power from a 3 45m bladed wind turbine hub, the total blade diameter is 93m. The tower is generally 80m although Siemens do specify that each wind turbine is site-specific.

Due to having a more complete set of information for the Siemens SWT-2.3-93 this was used to create the first draft of the prototype wind turbine. This turbine is 80m high and weights for the different parts of the superstructure are shown in Table 3.3.

Table 3.3: Weight distribution of a Siemens SWT-2.3-93, as taken from the Siemens website 2015

Section	Weight
Rotor	60t
Nacelle excluding rotor	82t
Tower	162t
Total	302t

The initial prototype

The initial prototype is an idealistic version of the superstructure, a very tall slender structure with the potential for significant rocking. The superstructure was simplified so there were no rotating blades atop the superstructure but the weight of the blades and the nacelle was included for the normal load at the top of the superstructure.

Based on the weights of the Siemens SWT-2.3-93 shown in Table 3.3, the tower to top weight ratio would be 1.1:1 tower:top mass. The rotation of the blades creates two of the main frequencies that the superstructure must avoid, it is not feasible to recreate blade rotations in the centrifuge. The focus of the test is on creating the displacement of the superstructure from wind loading to cause the foundation to uplift. The details of this initial prototype and associated 1g and centrifuge models are shown in Table 3.4.

Table 3.4: The initial deigns of the prototype wind turbine, with model scale dimensions

Scale	Prototype Structure	1g model	50g Centrifuge model
Height (m)	78.3	1.566	1.566
Top mass (kg)	128,820	51.530	1.031
Tower mass (kg)	146,936	58.777	1.175
Tower diameter (m)	4.5	0.090	0.090

3.3.1 Practical Limitations and Updated Prototype

There are several size and weight limitations on the structure to allow for small-scale testing in the centrifuge and at 1g. The height of the structure is limited due to the rotation of the centrifuge gondola during flight (see section 5.1 for details), the weight is controlled by what is feasible for a person to move.

The actuator position constrains the height of the tower, as the superstructure needed to be clear of the actuator but able to be pushed by the actuator. This means the superstructure height has to be within a reasonable distance of the actuator. The internal base of the centrifuge strong box to the position of the actuator is 767mm. Within this space a 7mm deep layer of gravel, j-cloth, 4mm Vyon HDPE filter plastic, Fisher scientific qualitative filter paper equivalent to Whatman Grade No. 1 (Brennan et al. 2016) and the consolidated clay (full information on the set up and material used in the experimental modelling can be found in section 4.2.1), which left 575mm for the structure. Reducing the structure height to 575mm would not allow for any variations in the soil thickness with regards to getting the correct soil strength. Making the model structure a maximum of 500mm allows for variations in the soil heights, in prototype scale that is a limitation of 25m. The prototype structure dimensions are the same in model scale for both the centrifuge and 1g modelling.

Due to one model structure being produced for both the centrifuge and 1g modelling the weight of the prototype structure will be heavier at centrifuge scale than at 1g scale, because of the increased gravity in the centrifuge. In order to have the prototype structure weigh the same in 1g modelling as it will in centrifuge modelling would have made it very heavy and impractical to use. The model structure was kept at the same weight for both modelling methods, which means the 1g modelling had a lighter prototype structure.

The height limitations in the centrifuge therefore required a modification of the prototype geometry, reducing the height of the superstructure from 80m to 22.5m. The weight limitations at 1g results in there being two prototype structures and one model structure. The details of the updated prototypes are shown in Table 3.5 below.

Table 3.5: Updated deign of the prototype wind turbine for Centrifuge and 1g Experimental modelling, with the resultant model scale dimensions

Scale	Prototype for Centrifuge	Prototype for 1g	Constructed model
Height (m)	22.5	22.5	0.45
Top mass (kg)	156,250	3,125	1.25
Tower mass (kg)	147,500	2,950	1.18
Tower diameter (m)	0.766	0.766	0.015

To decide the tubing dimensions that should be used for the model, the frequency was calculated and taken into account. Another method for adjusting the frequency is to change the mass at the top of the structure, which is listed below in section 3.3.2.

Figure 3.4 shows the dimensions of the prototype superstructure.

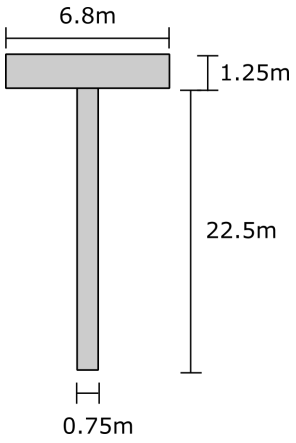

Figure 3.4: The prototype design of the superstructure

3.3.2 Frequency

The frequency of the prototype superstructure should be as realistic as possible and should not be within 10 $\%$ of the P1 and P3 frequencies . The diameter and wall thickness of the superstructure tower and the weight at the top of the superstructure control the natural frequency and therefore are adapted to produce a suitable natural frequency, Det Norske Veritas (2010). Natural frequencies of the superstructure under free vibration and accounting for the foundation soil were calculated as presented below.

Undamped free vibration frequency

A free vibration is created when a structure is disturbed from its static position by a displacement, such as striking the top of the structure with a heavy weight (Chopra 1995). The natural frequency under free vibration ($\mathrm{F_n}$) can be calculated using Equation 3.1.

$$\mathrm{Fn} = \frac{1}{\mathrm{T_n}} \tag{3.1}$$

Where $\mathrm{T_n}$ is the time required for the system to complete one full cycle of free vibration. $\mathrm{T_n}$ can be calculated using Equation 3.2.

$$\mathrm{T_n} = \frac{2\pi}{\omega_\mathrm{n}} \tag{3.2}$$

Where ω_n is the natural angular frequency, can be calculated from Equation 3.3.

$$\omega_\mathrm{n} = \sqrt{\delta_\mathrm{st}} \tag{3.3}$$

Where δ_st is calculated from Equation 3.4:

$$\delta_\mathrm{st} = \frac{\mathrm{m} \times \mathrm{g}}{\mathrm{k}} \tag{3.4}$$

Where g is acceleration due to gravity,
m is mass at the top of the tower,
k is spring stiffness.

For the prototype superstructure a natural frequency of 0.0072 Hz was calculated, which places it in the soft-soft (0 - 0.08) frequency safe zone. The frequency was calculated at model scale (1g), this can be seen in the Table 3.6. The table shows the inputs used to calculate the free vibration frequency for the updated prototype. The frequency has been calculated for the 1g model turbine as a comparison to the recorded experimental modelling frequency tests of the structure.

Table 3.6: Calculated undampened free vibration of the tower (4 significant figures)

	Prototype turbine	1g model turbine
Frequency Fn (Hz)	0.007291	0.2977
Circular Frequency	0.0458	13.2248
Lateral displacement	4674.224	0.05609
Spring stiffness (kN/m)	219	219
Mass (kg)	104167	1.25
Height (m)	22.5	0.45
Inertia (m^4)	0.0104	1.7 x 10^9
Young's modulus for aluminium	8 x 10^{10}	8 x 10^{10}
Second moment of area for a column I_c (m^4)	0.01038	1.660x10^{-9}

Frequency of a Pendulum

If considering the foundation as a fixed point on which the superstructure is attached then a natural frequency of the soil-structure system can be calculated by treating the superstructure like a pendulum, as shown in Equation 3.5.

$$\text{Frequency of a pendulum} = \sqrt{\left(\frac{\text{Acceleration due to gravity}}{\mathrm{R_o}}\right)} \tag{3.5}$$

Where Equation 3.6, shows the calculated frequency for the centrifuge prototype structure.

$$\sqrt{\left(\frac{9.81}{156,250}\right)} = 0.0079 \tag{3.6}$$

The low frequency calculated from Equation 3.6 which would fit in the soft-soft frequency range as shown in Figure 1.5 in section 1.1. This is a realistic frequency for the prototype soil-structure system.

3.3.3 Wind Load

As wind loading is the only variable component of the modelling, the aim of the wind loading is to load the structure to create foundation uplift and rotation. The design of the Siemens SWT-2.3-93 wind turbine is based on functional wind speed ranges in which the wind turbine can safely operate. When wind speeds are higher than the cut off wind speed, the rotation of the blades is stopped until the wind speed has dropped enough to allow the rotation to resume. The wind loading is to be a two-way sinusoidal displacement.

When the wind speed decreases to the cut-in speed the blades restart again. This is what is going to be referred to as 'normal' wind speed, when the wind turbine is in operation. The average functional wind speed is 10m/s and the cut-off is 25m/s and the cut-in is 22m/s (Siemens 2009). A wind turbine is required to be designed for higher wind speeds while the blades are not in rotation, these winds speeds are extreme wind and gust wind.

Table 3.7: Design wind speeds for the SWT-2.3-93 Siemens wind turbine, as taken from Siemens (2009)

Wind type		Wind speed (m/s)
Cut-off wind speed	V_{cut}	25.00
10 minute extreme wind speed at hub height	V_{ref}	48.50
3 second gust wind speed at hub height	$V_{50\mathrm{e}}$	60.30

Three phases of wind loading were therefore adopted, which are shown in Table 3.7. The first phase represents the average wind speed, which will load the superstructure with a wind force that the wind turbine would cope with during normal operation. This type of loading will be the baseline to all the testing and should cause minimal rocking of the foundation. The cut-off speed for the Siemens SWT-2.3-93 is 25m/s so the higher wind speed for normal operations (The-Wind-Power 2019) will be used, to ensure maximum rotation during normal operation. Rather than the average wind speed provided which is 9.85m/s.

The second phase represents high wind speeds such as storms, when the wind turbine blades are no longer rotating. This phase will cause structural rotation and uplift of the foundations, along with rounding of the soil below the foundation. In Table 3.7 the 10 minute extreme wind speed at hub height is 48.5m/s which will be used as a representative of the wind speed that will occur during storms, with the wind speed being nearly double that of the cut off wind speed that is used for the normal operation.

The aim of the third phase is to create a short burst of increased wind speed, similar to a gust, this style of loading will be a very short phase as it will only be a few cycles with the aim that only a few cycles are needed to cause significant changes to the soil profile below the foundation. This will determine if a few larger gust cycles cause more changes to the structure than many storm cycles.

An extra loading phase is an extreme loading, which is not based on a particular wind speed but rather a significant increase on the gust phase. This will be used to see how the soil structure interaction changes when an unrealistic wind speed is applied.

The wind speeds in Table 3.9 have been converted into wind forces (the vertical loading from the wind), using Equation 3.7 (Det Norske Veritas 2010).

Table 3.9 shows the wind force in kN an the displacement of the structure that these wind forces will cause.

$$\mathrm{Fw} = \mathrm{CqASin}\alpha \tag{3.7}$$

Where: C - shape coefficient of the superstructure of the wind turbine
q - Wind pressure
A - projected area of the superstructure
α - angle of wind to the superstructure.

To calculate the wind pressure (q) in , equation 3.8:

$$\mathrm{q} = 0.5\rho\mathrm{vtz}^2 \tag{3.8}$$

Where: ρ - Density of air
tz - Wind velocity average at time interval (t) and height (z).
v - Kinematic viscosity of air.

The projected area (A) is calculated using equation Equation 3.9:

$$\mathrm{A} = 0.5 \times \pi \times \theta \times \mathrm{h} \tag{3.9}$$

Where θ - diameter of the tower,
h - height of the tower.

Further information on the inputs required to calculate the wind force in equation 3.7 can be found in Table 3.8.

Practical Limitations, revised/updated loading

The cyclic loading could either be displacement controlled (where the structure moves the same distance every time, regardless of force) or load controlled (where the force moving the structure is the same regardless of the displacement). The Actidyn centrifuge actuator is displacement controlled, therefore displacement controlled loading was adopted. A load cell was attached and the applied force recorded. The actuator used in the 1g experiments had a maximum rate of displacement which was 6mm/min (GDS-Instruments 2009). Whereas the horizontal speed of the Actidyn centrifuge actuator had a max speed of 420mm/minute, which was not able to be controlled in the x-axis.

While making a mock set-up of the experimental set up the 1g loading actuator was used to apply the displacement calculated and the normal load of 10m/s wind speed did not create any movement of the structure so the normal loading was increased to the cut-in wind speed that the wind turbine had been designed for 22m/s.

To produce the displacement distance the force some initial assumptions were made, such as:

Table 3.8: The inputs and equations used to calculate the wind force

		Units	values	notes
Wind force	Fw	N	18341.1	Vertical loading from the wind.
The wind pressure	q	Kg/ms^2	59.2	calculation from DnV
Density of air	ρ	kg/m^3	1.183	given on data sheet at 1.183, Siemens (2009)
Wind velocity average at time interval (t) and height (z)		m/s	10	from Siemens data sheet normal wind velocity is: 9.85 10 min extreme wind velocity: 48.50 3 seconds gust wind speed: 60.3
Shape coefficient	C		0.2	calculated using Re=(D vtz)/v ; table 5.4 in DnV code 30.5 where if Re>10^6, C=0.20
Projected area	A	m^2	27.06	calculation given in DnV
Angle of wind to exposed surface	α	$\circ$	90	Gives the maximum value when at 90 or 270
Kinematic viscosity of air	v	m^2/s	14.6×10^{-6}	Given in DnV code
circle circumference		m	2.4	
Diameter	θ	m	0.765625	4.5m from Siemens wind turbine design, kept the tower circumference at 4.5m to match the original design rather than the thinner prototype model
Height of tower	h	m	22.5	22.5m from prototype model design sheet

-Wave length and frequency was the same for all the wind speeds,
-The amplitude is in kN (to match the wind force produced in Table 3.8),
-Wave speed and wind speed are assumed to be the same.

The wave speed (m/s) that were used to calculate the wind force, the amplitude (m) of the cyclic load is based upon the displacement that is required.

$$\text{Frequency}(1/\text{s}) = \frac{\text{windspeed}(\text{m/s})}{\text{displacement}(\text{m})} \tag{3.10}$$

The normal and storm loading frequencies are the same, due to the wind speed and the displacement doubling, therefore the frequency of the cyclic loading remains the same.

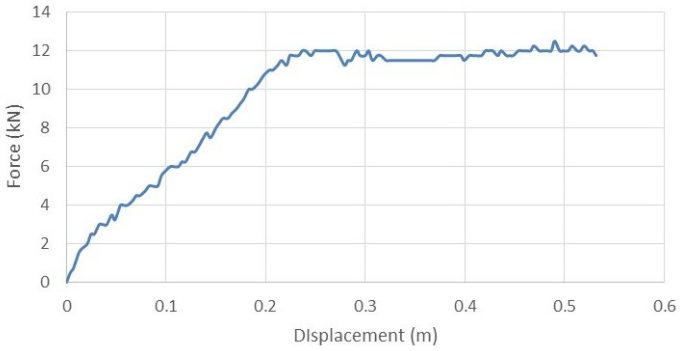

Figure 3.5: Result from a push-over test at 1g

The push-over test (Figure 3.5) conducted at the University of Dundee, using the first batch of soil produced, was the first time the whole set up of the 1g experiment was attempted. It shows the maximum force the structure copes with is 12kN therefore this is the maximum load possible applied to the structure and storm and gust loading will be conducted in this model scale range.

In research by (Bhattacharya et al. 2011, LeBlanc et al. 2010) the loading ranges from being lateral loading of piles, to a complex loading systems such as Yu et al. (2015) in which there was previous loading calculations for a single point loading system, which took into account the force and position the load would be affecting the superstructure. This was then developed into a gearing system in which the frequencies of each loading system (such as P1, P3, wind and wave) is applied in its own individual rhythm, which on occasion could overlap and create a increased load or work against each other to produce a reduced load upon the structure.

3.3.4 Foundation

The basic requirements for a rocking foundation is that the foundation is able to uplift. Gravity base foundations are common for on-shore wind turbines as they are simple in design and construction when compared to pile foundations, and cheaper. The effect of the rocking motion on the foundation requires it to lift up and cause the opposite edge to embed into the soil below. The rocking motion occurring on repeat the soil below the foundation will begin to

Table 3.9: Wind forces and displacements for each loading type in prototype scale with the wind force in 1g model scale

Name	Wind Speed (m/s)	Wind Force Fw (kN)	Displacement (mm)	Representing
Normal	22	8	150	Normal operational wind loading which allows the wind turbine to produce energy
Storm	45	11.75	300	Where the wind turbine has cut out and stop rotation due to high winds
Gust	60	12	400	A gust is a short spell of increased wind speeds, the wind turbine will not be in operation during this phase
Exaggerated	?	12	600	A unreal wind load to compare against the 'normal' wind loading

round and for that a stiff foundation is required. To minimise settlement a foundation with a higher A/Ac will be used in accordance with Gajan et al. (2005).

Practical Limitations

The foundation is required to fit in the centre 1/3 of the centrifuge strong box to avoid any boundary effects. A square foundation over a round foundation was chosen to better suit the all round modelling process (including numerical not just experimental). A square foundation can be modelled as planar and therefore the stress below the foundation is equal along the z-axis as the structure is being loaded in the x direction only. This proves useful while modelling in 2D numerically, data recording (uniform movement in the z-axis) and allows for a smaller foundation which is easier to keep within the centre third.

3.3.4.1 Design Calculations

The design of the foundations was based on the DNV code chapter 8 (Det Norske Veritas 2010). The geotechnical design comprised checks on the bearing capacity, stability against sliding, settlement, foundation stiffness, and rotation/uplift.

Further information on the design calculations can be found in the DNV code in chapter 8. Table 3.10 show the input information that was used for the prototype design. The foundation width and thickness were chosen in part to not exceed the allowable bearing capacity and to allow for practical limitations.

Bearing Capacity for undrained soil conditions

The bearing capacity for a gravity base foundation can be calculated using Equation 3.11(Det Norske Veritas 2010). The foundation soil is assumed to be undrained. Where the soil angle of friction $\theta = 0$.

$$\mathrm{q_d} = \mathrm{C_{ud}} \mathrm{N_c^0} \mathrm{S_c^0} \mathrm{i_c^0} + \mathrm{p_0} \tag{3.11}$$

Equation 3.11 values used for the foundation design can be found in Table 3.13. These values were taken from Det Norske Veritas (2010), and can also be found in Eurocode 7.

Factors of safety

The Eurocode 7 partial load factor, shearing resistance partial factor and cohesion partial factor were all set to 1.These values were chosen so that the foundation is not over designed, as the aim of the design is to allow the structure to rock and uplift.

Eccentricity and eccentric loading

The eccentricity (e) is the distance from the centre of the foundation to the load centre (LC)and can be calculated using Equation 3.12.

$$\mathrm{e} = \frac{\mathrm{M_d}}{\mathrm{V_d}} \tag{3.12}$$

Where: $\mathrm{M_d}$ - Moment force
$\mathrm{V_d}$ - Vertical force

The foundation will be classified as extreme eccentric loading if eccentricity (e) is a higher value than 0.3 of the foundation width (b) (Det Norske Veritas 2010). In this case e = 2.3m and 0.3 $\times$ b = 2.7m (see Table 3.10 and table3.11), so the foundation is not extremely eccentricity loaded.

Effective foundation area

The effective foundation area serves two purposes for this research. Initially it is included as part of the bearing capacity design and ensuring the foundation is correctly designed, but it gives insight into the potential uplift behaviour of the foundations. The effective width of the foundation can be calculated with equations 3.13, 3.14, 3.15 below (Det Norske Veritas 2010).

$$\mathrm{A_{eff}} = \mathrm{b_{eff}} \times \mathrm{l_{eff}} \tag{3.13}$$

$$\mathrm{b_{eff}} = \mathrm{b} - 2 \times \mathrm{e} \tag{3.14}$$

$$\mathrm{l_{eff}} = \mathrm{b} \tag{3.15}$$

Where b - foundation width
e - eccentricity

The calculated effective area can be seen in Table 3.11. This was calculated by assuming the movement of the foundation due to the loading is symmetrical in the z-axis of the foundation when the loading is along the x-axis.

Sliding resistance

The sliding resistance is important for this project as the tower is being laterally loaded and the foundation must not slide rather than rotate in place. The DNV code states that in undrained conditions in clay, to avoid sliding the applied horizontal force (H) has to be less than the effective area of the foundation multiplied by the undrained shear strength of the soil ($\mathrm{c_{ud}}$) (Equation 3.16). Equation 3.17 can be used to ensure adequate sliding resistance. All the values of the variables in equations 3.16, 3.17 can be seen in Table 3.12.

Table 3.10: Input information for foundation design

Structural dimensions and loads	Symbol	Value	Unit
Vertical force	V	4317	kN
Horizontal force	H	440	kN
Shear force		820	kN
Overturning moment		9908	kNm
Torsion Moment		4300	kNm
Load centre		2.205	m
Eccentricity	e	2.295	m
Foundation diameter/width	b	9.000	m
Foundation depth		1.250	m
Foundation weight		54	kN
Hub weight		31	kN
Tower height		22.500	m
Tower weight		2	kN
Partial load factor		1.00	

$$\mathrm{H} < \mathrm{A_{eff}} \mathrm{c_{ud}} \tag{3.16}$$

$$\frac{\mathrm{H}}{\mathrm{V}} < 0.4 \tag{3.17}$$

Where H - Horizontal force

$\mathrm{A_{eff}}$ - Effective foundation area

$\mathrm{c_{ud}}$ - Undrained shear strength of the soil

V - Vertical force

Critical contact area

The concept of the critical contact area was developed by Gajan and Kutter (2009)and is the area of the foundation required to resist the applied load. The ratio of the foundation area (A) to the critical contact area ($\mathrm{A_c}$), as shown in Equation 3.18 gives an indication of the rocking behaviour of the foundation.

$$\frac{\mathrm{A}}{\mathrm{A_c}} \tag{3.18}$$

$$\mathrm{A_c} = \frac{\mathrm{V}}{\mathrm{gd}} \tag{3.19}$$

When a foundation has a $\mathrm{A/A_c}$ of above 3 there is less settlement to a structure under dynamic loading than a foundation with a $\mathrm{A/A_c}$ of less than 2 (Gajan and Kutter 2009). The $\mathrm{A/A_c}$ of the prototype is 4.03, with the foundation area (A) being 81m2 and the critical foundation area ($\mathrm{A_c}$) of 20m^2 . This means that the foundation is not likely to settle excessively but maintain the capability for rocking behaviour to occur.

Table 3.11: Effective area

	symbol	value	unit
Equivalent horizontal force	H'	440.81	kN
Effective foundation area			
	Square	where load eccentricity is symmetric in respects to l_{eff}	
Length of effective area	l_{eff}	9.00	m
Width of effective area	b_{eff}	4.41	m
Foundation Area	A	81.00	m^2
Effective area	A_{eff}	39.69	m^2
V/qd =	A_c =	20.08	m^2
A/A_c		4.03	
critical contact length	L_c	2.23	

Table 3.12: Eccentric loading, Sliding resistance and Critical contact area

Extremely eccentric loading	e		0.3*b	
Eccentric loading?	2.30	>	2.7	Not
The structure is eccentrically loaded if e >0.3b				
Sliding Resistance				
Undrained conditions in clay	H		A_{eff}*c	
	440	<	794	Resistant
	H/A_{eff}			
	0.10	<	0.4	Resistant
Gajan and Kutter critical contact area				
Footing area	A	81.00	m^2	
Minimum area required to support vertical load	A_c	20.08	m^2	

Table 3.13: Bearing capacity design inputs using guidance from the DNV code Det Norske Veritas (2010)

Bearing Capacity			
For undrained conditions			
Effective unit weight of soil	y'	8.00	kN/m^3
Effective overburden pressure at level of the foundation-soil interface	P'0	0.00	kPa
‘	cd	12.00	kPa
Angle of shearing resistance		6.00	deg
EC7 angle of shearing resistance		6.00	deg
Shear strength	c_u	20	kPa
EC7 shear strength	c_{ud}		
EC7 shearing resistance partial factor		1.00	
EC7 cohesion partial factor		1.00	
Undrained conditions	N_c	6.28	
	S_c	1.10	
	i_c	0.83	

This design results in a 9m by 9m square foundation with a thickness of 1.25m as seen in Figure 3.6. There will be no embedment to the foundation, due to the foundation having sufficient resistance to sliding.

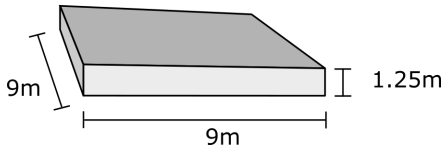

Figure 3.6: The prototype foundation

Due to the model which is being used in the experimental test being the same model for the 1g and 50g scale modelling, one of the tests will not have 'perfect' conversion from the prototype structure. In terms of practicability and viability scaling the model to a 50g centrifuge test will produce the lighter model and therefore be more practical for working in both 1g lab and 50g centrifuge modelling. Creating a structure for 1g lab modelling will produce a heavier structure which would be unfeasible for the 50g centrifuge modelling.

3.4 Resulting Prototype

The resulting prototype wind turbine and soil can be seen in Figure 3.7, with the superstructure geometry shown in more detail in Figure 3.8, this will be numerically modelled (Chapter 6) in prototype scale but will be scaled by a factor of 50 for experimental modelling (Chapters 4 & 5).

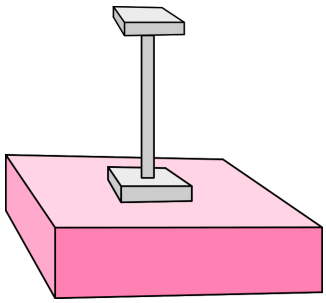

Figure 3.7: The minimum required soil body

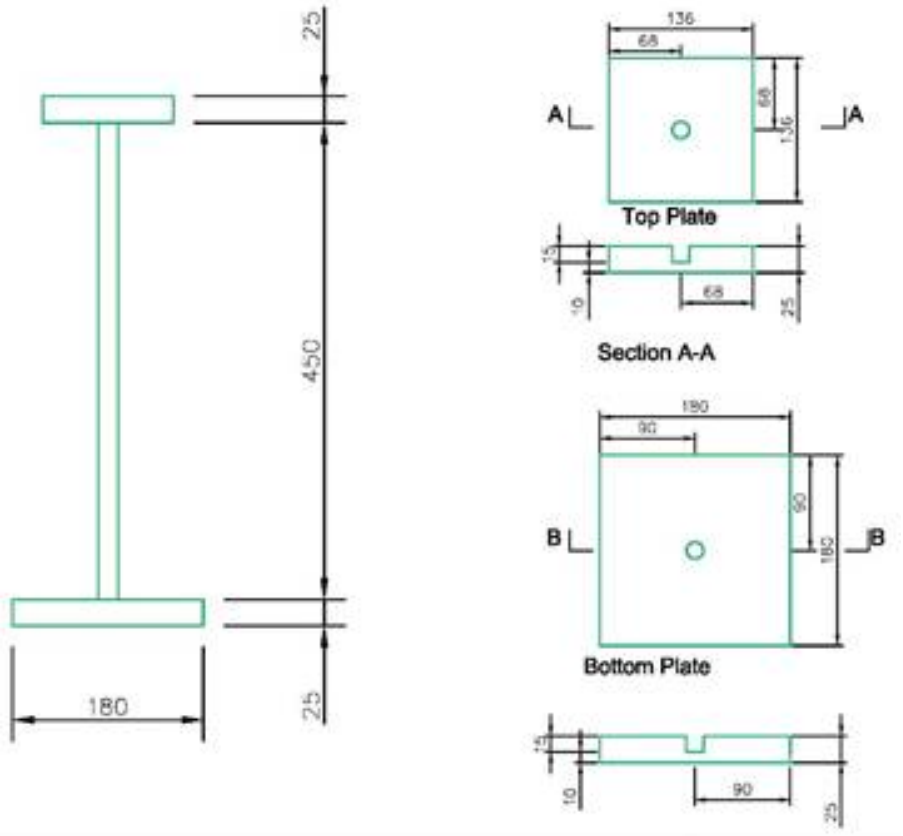

Figure 3.8: The Wind Turbine model for manufacture

Chapter 4

1g Physical Modelling

4.1 Introduction

Small-scale, 1g experimental modelling was conducted at the University of Dundee Geotechnical Centrifuge Centre, with the aim of replicating the rocking behaviour of a wind turbine structure with a shallow foundation, founded on a homogenous soil. The design of the experiments is explained in Chapter 3. In this chapter the methodology of the 1g experimental tests is explained in full, and the results from the testing are presented and discussed.

1g modelling is a form of physical modelling where the gravity is not changed, in contrast to the centrifuge modelling where the gravity level is increased. 1g modelling can be conducted with full scale models but this can be expensive due to their size when replicating a large structure. Alternatively, small-scale 1g modelling can replicate behaviours that occur in at full scale with the use of scaling laws which dictate how a prototype is scaled down to model scale.

4.2 Methodology

All tests were prepared and carried out in the same way, as described in the following sections.

4.2.1 Strong Box Preparation

The strong box (as seen in Figures 4.1 and 4.2) was used in all the experiments, it was designed and made in house by the University of Dundee School of Engineering's Workshop team. The dimensions of the box are 800mm by 500mm with a depth of 467mm and along the length of the strong box the walls are 80mm thick perspex.

The base of the box was filled with a 50mm thick layer of course gravel, seen in Figure 4.1. to allow drainage during the centrifuge consolidation of the clay. The course gravel used is a smooth natural aggregate with a particle diameter of 12.5mm. The gravel was tamped into place to ensure minimal compaction during consolidation and was lined with j-cloth (purchased from Lidl's own range), to prevent any clay seeping into the gravel and reducing the drainage. The j-cloth was kept in place with duct tape to form a continuous seal between the layers above and below the gravel (Figure 4.2).

Figure 4.1: Gravel layer in the centrifuge box

Figure 4.2: j-cloth in the centrifuge box

A 7mm thick grade D Vyon HDPE porous plastic (manufactured by Porvair Sciences) was placed above the j-cloth; this is a porous plastic material made from high density polyethylene which allows water to pass though while retaining small clay particles. The sheet was cut to be smaller than the area of the box for maximum coverage but also allowing for it to be removed when the box is being emptied without damaging the Vyon.

Fisher scientific qualitative filter paper equivalent to Whatman Grade No. 1 is placed on top of the Vyon in order to cover it, the filter paper is A3 in size and 4-5 sheets were used to cover the base per batch. This prolongs the life span of the Vyon only allowing the finest particles through. Before the clay slurry can be poured into centrifuge box, the filter layers were saturated removing the air.

4.2.2 Soil Layer Preparation

4.2.2.1 Mixing Kaolin

A total of No 5 25kg bags of speswhite kaolin was mixed into a 100% water content slurry, in 10 batches of 12.5kg of kaolin and 12.5kg of water in a 90L electric barrel cement mixer until smooth. The slurry was then transferred to the pre-prepared centrifuge box by tremie filling

the box with the slurry. This was achieved by initially saturating the filter layers removing and ensuring there is 100mm of water above the filter layers for the clay slurry to be poured into, minimising air being trapped between the clay layers.

4.2.2.2 Consolidation

The clay was consolidated using the Actidyn C76-23.5m beam centrifuge at the University of Dundee Geotechnical Laboratory. The box was secured in the centrifuge and spun at 70g for 65 hours to consolidate. Two way consolidation was allowed, where water that drains down through the soil comes out of the bottom of the box though taps which are level with the gravel layer, and the water which drains upwards sits in a layer at above the consolidated clay. A benefit of consolidation in a centrifuge is that it speeds up normal consolidation, in this case 70^2 times faster than a 1g consolidation.

4.2.2.3 Validation of Soil Parameters

A 19mm hand shear vane tests were carried out at the soil surface, 100mm and 200mm below the surface to check if the shear strength of the consolidated clay was acceptable. At the surface the soil was extremely soft, the soil failed at 1kPa average. At 100mm below the surface the average result was 3.75kPa, and at 200mm below the surface the average was 8.25kPa. This is lower than the desired 10kPa.

T-bar tests were also conducted to determine the undrained shear strength (c_u) profile over the depth of the clay layer. The T-bar test was designed by Stewart and Randolph (1991), to use on soft clays. The T-bar is inserted into the soil at a rate of 60mm/minute, and the extraction of the T-bar is also recorded to show the strength of the suction (House et al. 2001). The test is repeated at least 3 times on each clay layer in different areas of the box ensuring that the strength profile is consistent.

To carry out the T-bar test, the box of consolidated clay was loaded on to an Instron test frame with a 25kN load cell and the T-bar was attached to the Instron by using tensile grips. The data was recorded via a PC connected to the Instron with Bluehill Universal software.

The undrained shear strength (c_u) of the soil can be calculated by using equations 4.1 and 4.2 (Stewart and Randolph 1991):

$$q_{T-bar} = \frac{\text{recorded load}}{\text{t-bar area}} \tag{4.1}$$

Where: q (kPa) is penetration resistance of the T-bar being inserted into the clay, derived from the recorded load from the Instron (kN) and the T-bar area (m_2). The T-bar area is calculated from the diameter $\times$ length of the T-bar.

$$c_u = \frac{q}{\text{t-bar factor}} \tag{4.2}$$

Where the t-bar factor depends on the roughness of the surface area of the t-bar and is detailed in Stewart and Randolph (1991).

The results from a T-bar test are shown in Figure 4.3 and the strength of the soil increases with depth. In this figure, the shear strength measured when the T-bar is inserted into the soil is shown as positive, while that measured during extraction from the soil is shown as negative. From the results in Figure 4.3 it can be seen that an undrained soil shear strength, c_u of 10kPa occurs at around 100mm below the surface.

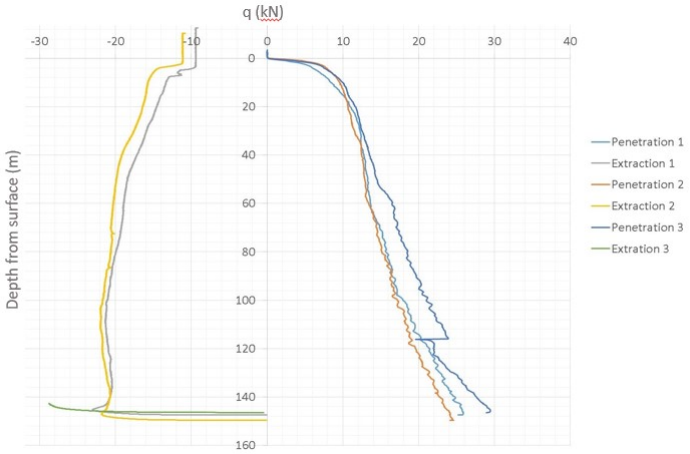

Figure 4.3: Results from the t-bar test

4.2.3 Structure

The structure used for all tests is described in chapter 3 in section 3.3 and 3.3.4. The structure was placed on the surface of the clay layer after soil preparation and strength testing.

4.2.3.1 Data Acquisition

The data acquisition systems used in the experiments are described below, including details on preparing the hardware and software. These are an essential part of any experimental test as they control aspects such as the intervals of data.

National Instruments USB-6009 DAQ

The data acquisition (DAQ) units used were National Instruments USB-6009 DAQ, which provide both analogue and digital data logging functions. Each DAQ has the capabilities for 4 differential analogue inputs in, with a maximum sampling rate of 48k samples per second.

The DAQ is bus-powered (powered through the USB, which also transfers the data) which allows simultaneous recording from each channel, which can also be programmed in LabVIEW (see below) to have different time steps and voltages, as well as having multiple DAQ recording information. More information on the National Instrument products can be found at www.nationalinstruments.com.

Two USB 6009 DAQ were used with 4 analogue channels on each.

LabVIEW

All data was recorded using Laboratory Virtual Instrument Engineering Workbench (LabVIEW), a software designed by National Instruments for data measurement and hardware configuration of DAQ units. It has a graphical interface in which different DAQ units can be set up to record instruments simultaneously. LabVIEW 2016 was used throughout the 1g experimental modelling.

Creating the VI

A virtual instrument (VI) is the interface which connects to the hardware and records to the software. VIs are created in LabVIEW by the user.

For this project the DAQ Assistant and DAQmx (software within the LabVIEW programme) was used to set up the VI and connect to the DAQs. This allows for simple programming to each DAQ used and the individual channels on the DAQ. This allowed recording from sensors using different voltages, through multiple DAQs. The inputs required for each channel for both the long cyclic tests and the free vibration frequency tests are stated below in Tables 4.1 and 4.2.

Table 4.1: Inputs for long cyclic tests

Instrument	Signal output range	Scaled units	Generation Mode	Samples to write	Rate (Hz)
LVDT	10	Volts	Continuous	100	1
Accelerometer	5	Volts	Continuous	100	1
Force sensor	5	Volts	Continuous	100	1
Pore pressure transducer	5	Volts	Continuous	100	1

Table 4.2: Inputs for the free vibration frequency test

Instrument	Signal output range	Scaled units	Generation Mode	Samples to write	Rate (Hz)
LVDT	10	Volts	Continuous	1000	100
Accelerometer	5	Volts	Continuous	1000	100

4.2.4 Instruments

4.2.4.1 LVDTs

To measure displacement of the structure, Linear Variable Displacement Transformers (LVDTs) were used (LDC1000A made by RDP, www.rdpe.com). Unlike the other instruments being used in this experimental work (section 4.2.4.2, 4.2.4.3 and 4.2.4.4) the supplied voltages do not affect the LVDTs therefore the voltage output is much cleaner than other data sources. (with serial numbers 196045 for the edge LVDT, 161617 for the middle and 161616 for the top.) The positions of the LVDTs in each test are shown in Figure 4.4 below, with serial numbers for each instrument included. The LVDTs were held in place using clamps which were attached (with serial numbers 196045 for the edge LVDT, 161617 for the middle and 161616 for the top.)

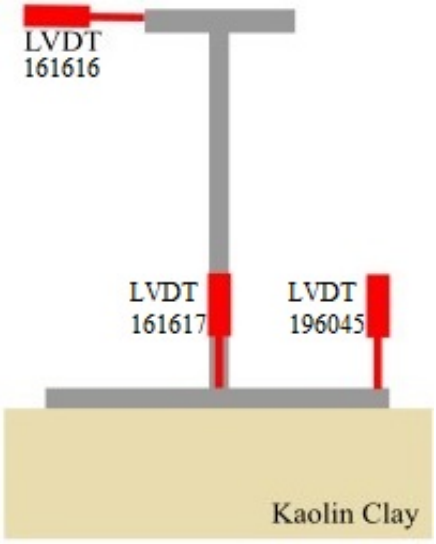

Figure 4.4: Position of the LVDT on the model

A top horizontal position records the maximum movement at the top of the structure, a vertical position at the centre of the foundation records the settlement and any uplift of the foundation, and the third LVDT position is near the edge of the foundation to record the maximum uplift and settlement of the foundation. To ensure this LVDT stayed on the foundation during rotation and didn't slip off, it was placed 5mm from the edge of the foundation.

To calibrate the LVDTs high magnification calibrator scales (manufactured by INSTRON) were used to very accurately displace the LVDTs a known distance and record the voltage. The high magnification calibrator scale has a rotating platform where every clockwise 360° will lift the platform 0.5mm. Each LVDT was placed onto the top of the calibrator and secured with a small weight then the change in voltage was recorded for each 0.5mm movement. Calibration at intervals of 0.1mm was also conducted but this did not significantly improve the accuracy of the calibration and the noise from the instrument interfered with the output voltage.

0.5 mm in model scale is 25mm in prototype scale, which gives defined boundaries for the readings.

$$\frac{\text{Current (volts)}}{\text{calibration factor}} = \text{Displacement (mm)} \tag{4.3}$$

Figure 4.5 shows the data from the calibration. To get the calibration factor to convert output voltages to displacement, lines of best fit can be utilised. The R^2 for the line of best fit are between 0.989-0.998 which indicates a high correlation between the data points and the line of best fit. Figure 4.5 shows that the 3 LVDTs all require different calibration factors, the top LVDT has a calibration factor of 0.087, centre is 0.869 and the edge is 0.126. The LVDTs were calibrated at regular intervals between tests to ensure the calibration was the same thought out the individual tests as well as the experimental modelling programme.

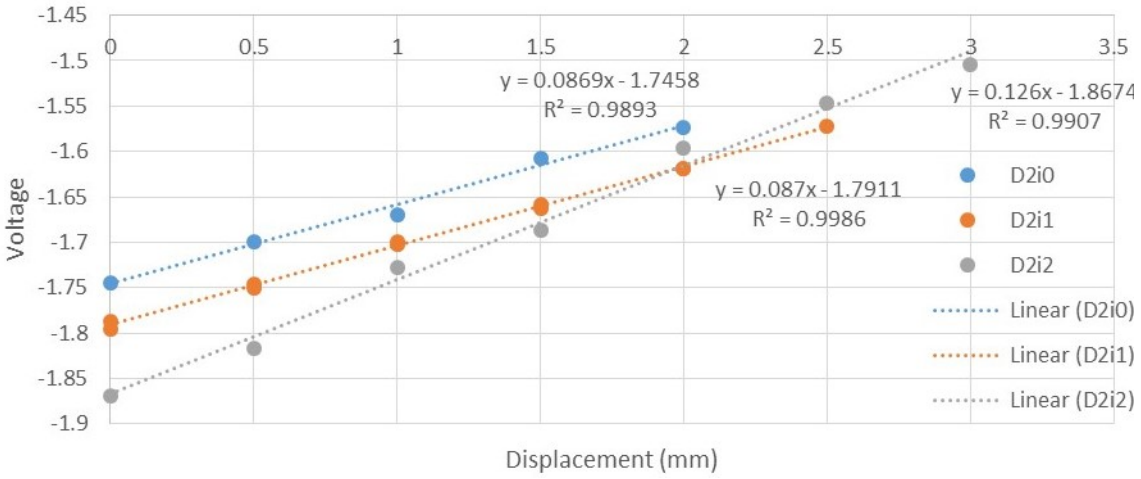

Figure 4.5: Calibration of LVDTs at model scale

4.2.4.2 Force Sensors

Force sensors are used to give an indication of the contact between the foundation and soil during cyclic displacement. The force sensors used are made by Single Tact, they are ultra-thin (0.35mm), which is ideal for placement underneath the structure without altering the contact between the foundation and the soil. The sensors are also only 8mm in diameter (50.3mm^2 area) so the load is evenly applied over the whole sensor area.

1N sensitivity was chosen as most appropriate for these sensors as the maximum force expected is 0.32N. The total structure force on the soil is 34.3N over a 180mm square foundation, which results in a pressure of 0.001N/mm^2 and a total force on each sensor of 0.05N. Under a severe uplift condition, the total force of the structure may only be resisted by 1/6th of the foundation, resulting in 0.32N on each sensor.

The sensors were placed at 3 locations under the foundation, see Figure 4.6. The edge of the foundation is important as here the sensors will record minimal pressure during uplift and higher pressures during embedment of the foundation. The edge force sensor like the edge LVDT is set 5mm from the edge in order to be line with the LVDT and ensuring the whole

sensor is underneath the foundation. From the edge of the sensor to the edge of the foundation there is 1mm.

The force sensors (Figure 4.6) at the centre of the foundation and between the centre and the edge will inform if there is any uplift occurring away from the edge of the foundation. This is important as it can show a reduction in the critical contact area, which can be compared against the critical contact area calculated in the design of the foundation.

Force sensors were only placed on one side of the foundation because the displacement is two-way sinusoidal, the deformation of the foundation will be fairly even and therefore both sides of the foundation should look similar.

Force sensors were only places on one side of the foundation because the displacement is two-way sinusoidal, the deformation of the foundation will be fairly even and therefore both sides of the foundation should look similar.

The sensors are waterproof but the clay still can disrupt them, so to keep the sensors clean and working most efficiently a layer of cling film was placed directly below them.

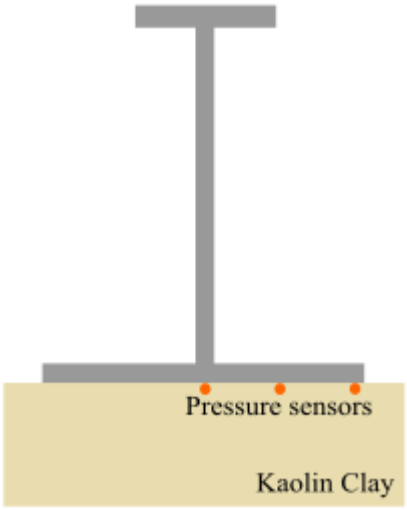

Figure 4.6: Position of the force sensors on the model

The calibration of the force sensors was conducted by adding known masses to the sensors and recording the analogue voltage output in LabVIEW. The calibration can be seen in Figure 4.7. Lines of best fit and R^2 have been calculated which show that there is not a strong correlation in the calibration data. The sensors were calibrated before each test, but it was found that throughout the test the calibration started to drift and calibration at the end of the test was vastly different to that at the start of the test. It is possible that clay particles get into the sensors and cause the drift.

Due to this lack of reliability, it was deemed best to use the force sensor data qualitatively to just indicate contact or loss of contact between the foundation and the soil below.

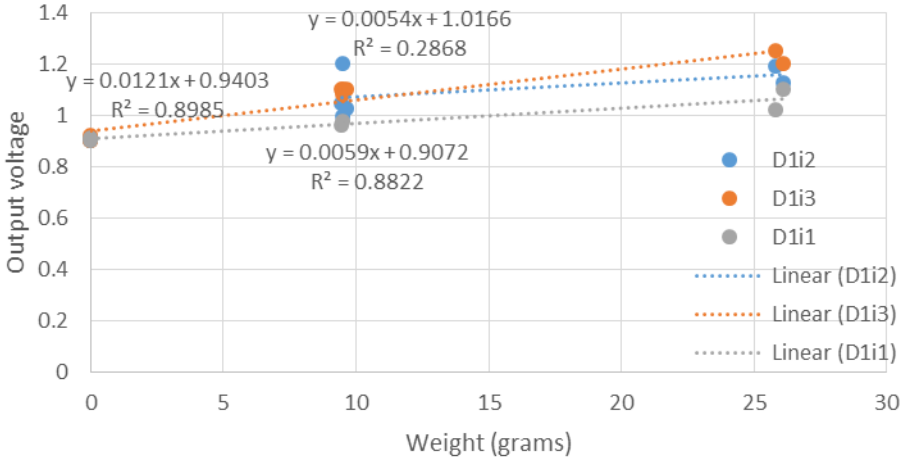

Figure 4.7: Calibration of the force sensors

Data from the force sensors can be recorded either with an analogue system through LabVIEW or an digital system using an Arduino Uno and an I2C bus. An Arduino Uno is an open-source microcontroller board, which can be programmed to control other electronics and an I2C bus is a method of sending and receiving data from multiple sources simultaneously through one data port. Both systems were tried and it proved that the analogue system was more reliable over the long duration of the tests.

In addition, if the NI USB 6009 DAQ is used for all instruments, then they all have the same sampling rate which means that the analogue system is more efficient for data processing as all the instruments are being read at the same time and therefore the data points are comparable.

In the following results section, the data from the pressure sensors is presented alongside the vertical displacement at the edge of the foundation, to show the detail of what uplift and embedment is occurring here and to give context to the qualitative force data. An example of this is shown in Figure 4.8, where the orange line represents the vertical edge displacement and the blue line is the force data. The maximum point of uplift had been noted in figure 3.8 as well as when the foundation edge is embedding.

At the same time as maximum uplift no pressure is being applied to the soil from the foundation and the maximum force is recorded during embedment. It should be noted that the sensors are unable to read negative forces, these are due to the drift of the calibration factor and should be taken to indicate uplift. In addition, there are times when the force upon the sensor is greater than the maximum force it can read, therefore it plateaus off, as shown at the points of maximum embedment. Again, this is a reason why the data should only be considered qualitatively.

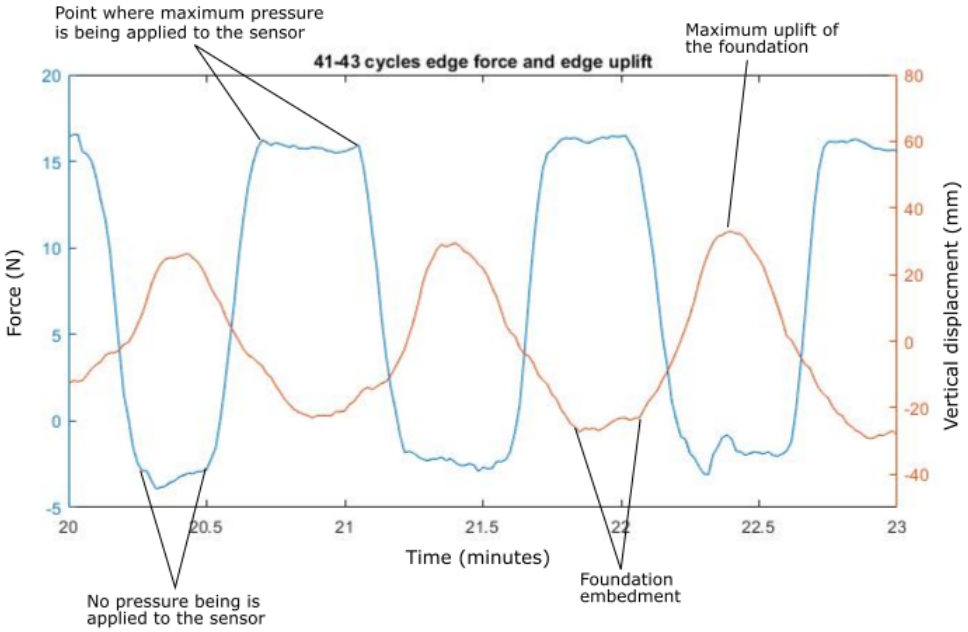

Figure 4.8: Explanation of the force sensor data

4.2.4.3 Pore Pressure Transducers

Pore pressure transducers (PPTs) record changes in the pore pressure below the soil. As the structure is rocking and the foundation is embedding and uplifting it was anticipated that positive and negative pressures could be recorded.

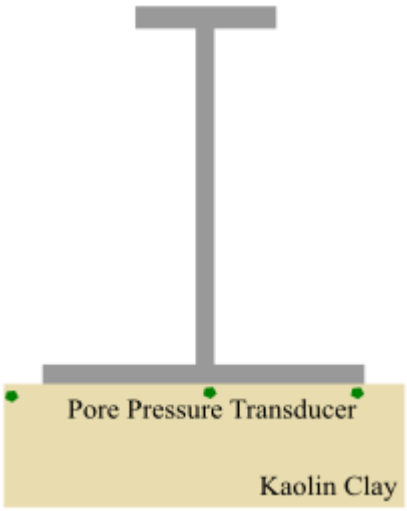

Figure 4.9: Placement of the PPTs on the model

The PPTs were placed at the centre line of the foundation, the edge of the foundation and one away from the foundation in the free field. The PPTs were inserted into the soil by slowly drilling a hole at a 45 degree angle into the clay with a 15mm drill bit to allow the sensor to be inserted into the hole without pushing on the side walls and potentially breaking though the surface. The direction of each hole was perpendicular to the foundation (Figure 4.10), in order to minimise the disturbance to the soil directly below the foundation. The PPTs were calibrated

by applying a known pressure to the sensors. A GDS Advance Pressure/Volume Controller (filled with water) was connected to the sensors via a rubber tube and a few zip ties to tightly secure both ends of the tube. A GDS Advance Pressure/Volume Controller can apply accurate pressures and volume changes, further information can be found at www.gdsinstruments.com. The pressure was applied in intervals of 10kPa, starting at 0kPa and ending at 100kPa. This was recorded using the USB 6009 DAQ and LabVIEW in volts.

Figure 4.10: Placement of the PPTs in the soil, Red line to outline the position of the foundation, Green stars to note the position of the PPTs in the clay

4.2.4.4 Accelerometer

A Miniature iMEMS (ADXL78) accelerometer (manufactured by Analog devices Inc.) was added to the top of the superstructure orientated in line with the displacement direction. The accelerometer was powered with 2mV direct current in order to minimise noise from the power source.

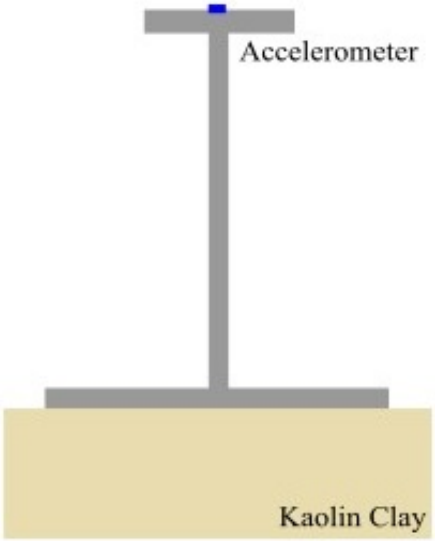

Figure 4.11: Placement of the accelerometer on the model

Because an accelerometer can sense gravity this can be used to calibrate it, so when the accelerometer is horizontal the acceleration is 0. When the accelerometer is rotated 90 degrees from horizontal then the reading should be -1g or -9.81m/s^2. When the sensor is rotated 90 degrees from horizontal in the opposite direction the reading should be 1g or 9.81m/s^2. The results from the calibration can be seen in Figure 4.12, where for inclination the voltage calibration factor is 0.0005, to convert the voltage into a angle, and the calibration factor to convert the voltage to m/s^2 is 0.0045.

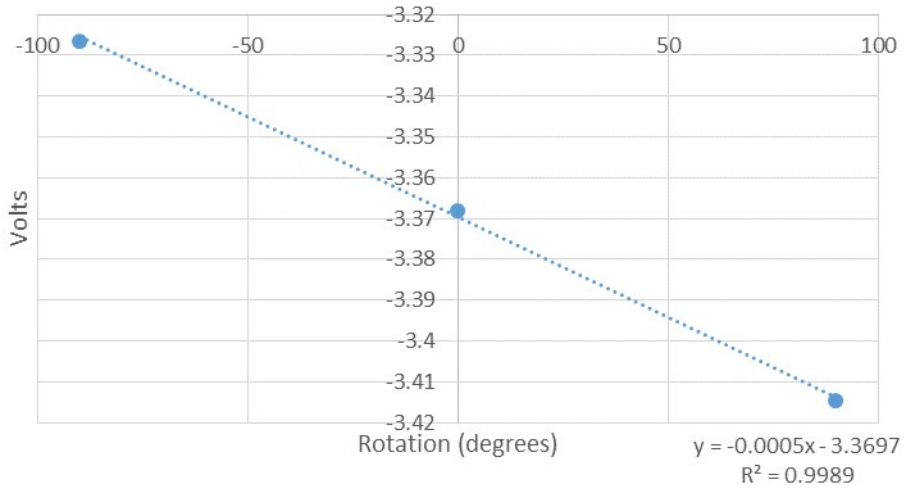

Figure 4.12: Calibration of the accelerometer

4.2.4.5 Actuator

The cyclic displacement was applied to the super structure using a GDS Force Actuator, which can be programmed to apply a linear displacement or force. The GDS Force Actuator is controlled by connecting it to a PC with the GDS software that can be programmed to apply a

range of displacements or forces. The software will also record the displacement and the force used during testing.

The displacement was applied 20m from the base as seen in Figure 4.13. As the displacement is a push and pull motion, an appropriate attachment to the GDS Force Actuator had to be designed. Figure 4.14 shows the attachment that was made at Newcastle University. This can be attached to the load cell and hook around the centre tube of the structure to push and pull the programmed distances, while also allowing the structure to settle.

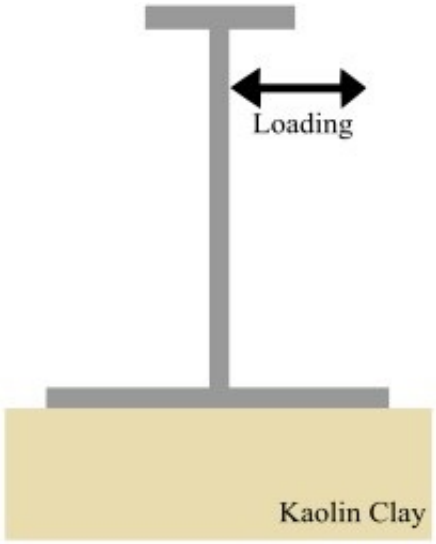

Figure 4.13: Location of applied cyclic displacement on the structure

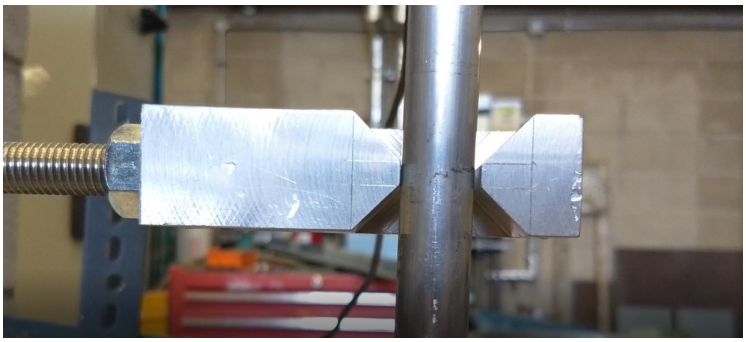

Figure 4.14: The attachment made for the Force actuator to apply the cyclic displacement to the structure

Programming the cyclic displacement

Up to 100 phases of cyclic displacement can be programmed, which allows for a changes in the magnitude of the applied displacement. The larger displacements used also require more time for the GDS force actuator to complete the cycle, so for a 150mm (3mm model scale) cyclic displacement 30 seconds were required. For a displacement of 300mm (6mm model scale) 60 seconds were required and for 400mm (8mm model scale) 120 seconds were required. Extra time was allowed for the 8mm displacement to prevent the actuator from 'repositioning' itself.

Table 4.3: Scaling laws for 1g physical modelling Drosos et al. (2012)

Quantity	Prototype/model
Length/ displacement	n
Area	n^2
Stress	n
Strain	1
Mass	n^3
Force	n^3
Moment	n
Frequency	$n^{-0.5}$
Time (Creep)	1
Time (Dynamic)	$n^{1-\alpha/2}$
Acceleration	1

4.2.4.6 Load cell

The load cell is connected to the GDS force actuator. The load cell is in loop with the GDS force actuator programme which recorded the loads applied. The load cell can be checked to be correctly calibrated by placing weights of known mass and cross referencing that with the kN which is being read by the force actuator.

4.3 Scaling 1g physical work

All small scale physical modelling needs to consider the scaling of the test from prototype scale in the design to model scale for the tests and then back to the prototype scale for the results. Scaling uses the non-dimensional groupings of the physical aspects of the Prototype.

Due to the model which is being used in the physical test being the same model for the 1g and 50g scale modelling, one of the tests will not have 'perfect' conversion from the prototype structure. In terms of practicability and viability scaling the model to a 50g centrifuge test will produce the lighter model and therefore be more practical for working in both 1g lab and 50g centrifuge modelling. Creating a structure for 1g lab modelling will produce a heavier structure which would be unfeasible for the 50g centrifuge modelling. The scaling of the structures physical dimensions:

Scaling laws based on non-dimensional groupings of the relevant physical aspects of the prototype are used to produce a model for small-scale physical testing. These laws are also then used to convert the results back to prototype scale. A summary of the scaling laws used for 1g physical modelling is reproduced from Muir Wood (2004) and shown in Table 4.3.

Further information on scaling laws for geotechnical modelling can be found in Muir Wood (2004).

Table 4.4: Test plan.

Test Name	Total Duration (min)	Total number of cycles	Number of cycles per phase		
			Normal (150mm, 0.283Hz)	Storm (300mm, 0.141Hz)	Gust (400mm, 0.071Hz)
Baseline	180	360	all	none	none
Short Break Storms	3600	5400	50	20	none
Long Break Storms	1800	1920	80	20	none
Gust Storm	280	375	40	20	5
Exaggerated	1150	575	none	none	none

4.4 1g Tests conducted

The purpose of the testing is to explore the impacts of long term cyclic displacement of a shallow foundation onshore wind turbine on the soil and how the soil-structure interaction changes through out the life time of the structure. Each test has been designed to cause different levels of impact upon the foundation from the repetitions of phases of cyclic displacement.

4.4.1 Baseline Test

The aim of this test is to get a baseline response, under operational displacement where minimal uplift and rocking of the foundation is expected. The displacement applied is sinusoidal with an amplitude of 150mm and a period of 30s, as shown in Figure 4.15. The duration of the test was 180 minutes which allowed for 360 cycles.

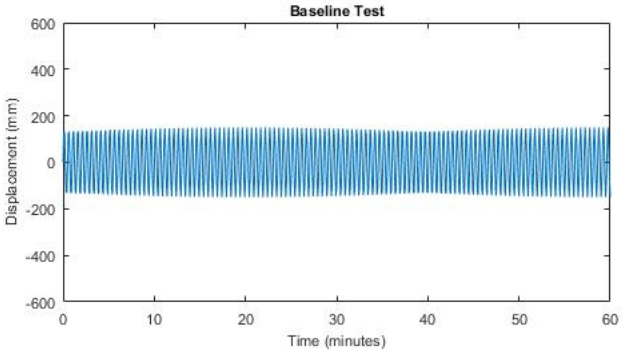

Figure 4.15: Baseline applied cyclic displacement

4.4.2 Short Break Storms Test

The short break storm test is to introduce a larger amplitude cyclic displacement (storm phase) into the test sequence, to create a significant uplift in the foundation and therefore induce rounding of the soil below the foundation. The normal phases in this test are a recovery break from the storm phase displacement and will be compared to the each other in order to show how the structure adapts to changes in the soil below the foundation.

Figure 4.16 shows a phase of normal displacement of an amplitude of 150mm followed by a storm phase of amplitude 300mm and period 60s. The increase in period is due to the extra time the actuator required in order to complete the total movement, as it was displacing the structure at its maximum speed. The short break storm test is replicated in the centrifuge for comparison (section 5.6.2).

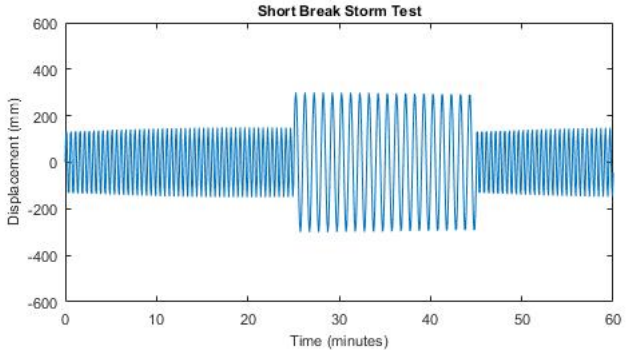

Figure 4.16: Short break storm applied cyclic displacement

4.4.3 Long Break Storms Test

This is the same set up as the short break storms with one difference that the phases of normal displacement are longer, with more cycles. This is for comparison with the short break storm test, to see if the extended duration of the normal phases allow for more recovery or in fact the additional cyclic displacement causes further deformation to the soil below the foundation.

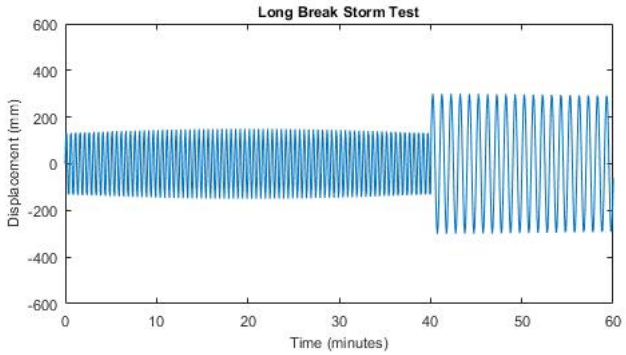

Figure 4.17: Long Break Storm applied cyclic displacement

4.4.4 Gust Storm

The gust storm displacement pattern has the 3 types of displacement in the test sequence, normal (150mm amplitude), storm (300mm) and gust (400mm), as shown in Figure 4.18. The gust phase is to further disrupt the stability of the structure and increase the deformation under the foundation. The displacement is in stages of 40 normal cycles, 20 storm cycles and 10 gust cycles. This test was run for 238 minutes, when the actuator over-displaced the structure and the test was stopped at 280 minutes. This equates to 319 cyclic displacements that were completed without drifting.

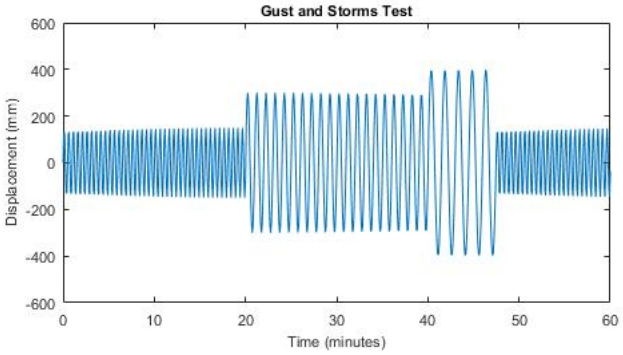

Figure 4.18: Gust Storm applied cyclic displacement

4.4.5 Exaggerated Push Test

The exaggerated push tests are an unrealistic displacement upon the structure, designed to cause an extreme response.

As seen in Figure 4.19 the amplitude is 600mm and the period is 120 seconds. The test lasted for 575 cycles, which is 1150 minutes.

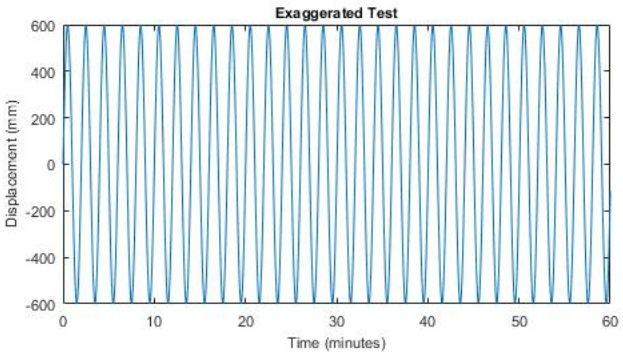

Figure 4.19: Exaggerated Push applied cyclic displacement

4.4.6 Free Vibration Test

A measurement of the free vibration behaviour of the structure was made in every test, before and after the cyclic displacement. This allowed for the recording of the natural frequency of the soil-structure system and how this changes due to the cyclic displacement. The test is conducted by recording the reaction of the structure when hit with a weight, in this instance the same G-clamp was used to strike the top of the structure. The accelerometer and the horizontal LVDT recorded the displacement and the acceleration at the top of the structure. As the response typically lasted less than one second, data was recorded at an increased rate, every 0.01 seconds.

4.5 Results

The results are all displayed in prototype scale therefore can be easily compared to the other forms of modelling that has been conducted in this research project.

Unfortunately no pore pressure data could be obtained from the 1g laboratory as the PPTs did not display any output other than noise which could not be filtered out. If there was any recorded pore pressure data it was not large enough to overcome the noise from the equipment. For this reason no PPT data is presented. The results are presented on the order of horizontal displacement, horizontal force, settlement, settlement-rotation, force-rotation, soil-foundation contact if available and finishes with free vibration frequency.

4.5.1 Baseline test

The results from the baseline tests represent the behaviour of the wind turbine under operational or 'normal' loading and should show the least amount of change to the foundation due to cyclic displacement.

4.5.1.1 Horizontal displacement of the structure - time

Figure 4.20 shows the horizontal displacement of the structure. The displacement should be and does start off a consistent ±150mm as applied by the GDS force actuator. However as the test continues is can be seen that over the course of the test there is a slight drift and there is more displacement applied in the negative direction. This is most likely due to a computational error with the GDS actuator, which is why a LVDT was added to the top of the structure to check the displacement being applied.

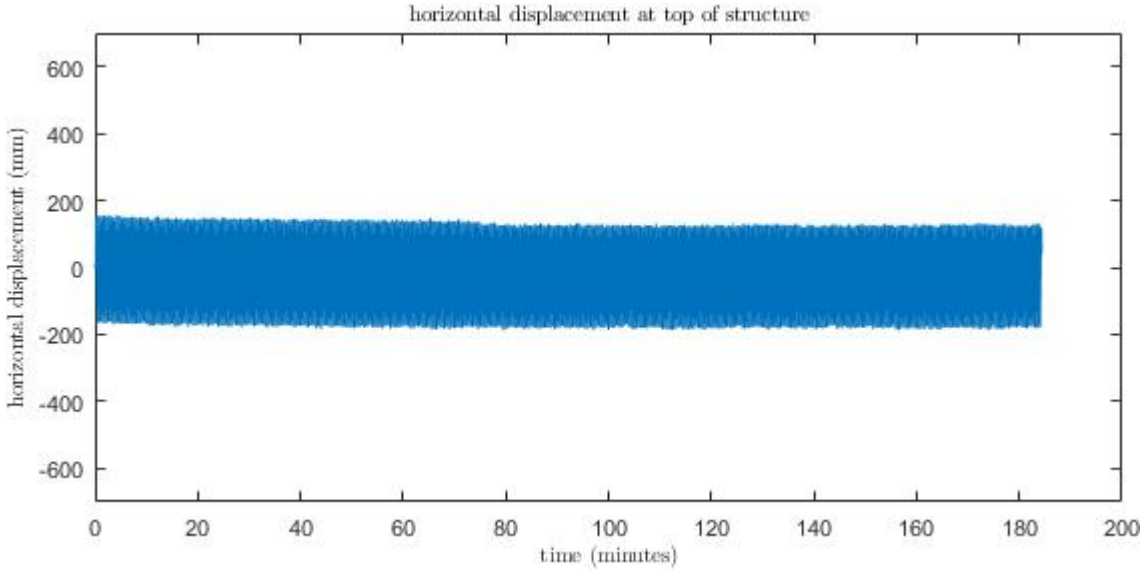

Figure 4.20: Horizontal displacement at the top of the structure

4.5.1.2 Horizontal force - time

The force is displayed with negative and positive forces, the positive force is when the actuator is pushing the structure away from 00mm position. While the negative force is when the structure is being pulled from the 00mm position by the GDS actuator.

Figure 4.21 shows the force required to displace the structure ± 150mm sinusoidally. At the start of the test a higher magnitude of force is required to produce displacements in the first 5 cycles, compared to the force required for the rest of the test. The drift seen in Figure 4.20 does affect the force required and as the test continues the negative force required increases and the positive required force decreases. The total force required to produce a complete cycle of displacement reduces as the test continues, although the reduction in the force required to displace the structure is small from 2400kN to 2200kN, a reduction of 8%. This could be due to the soil yielding to the foundation and the profile below the foundation rounding which would allow for easier rotation of the structure.

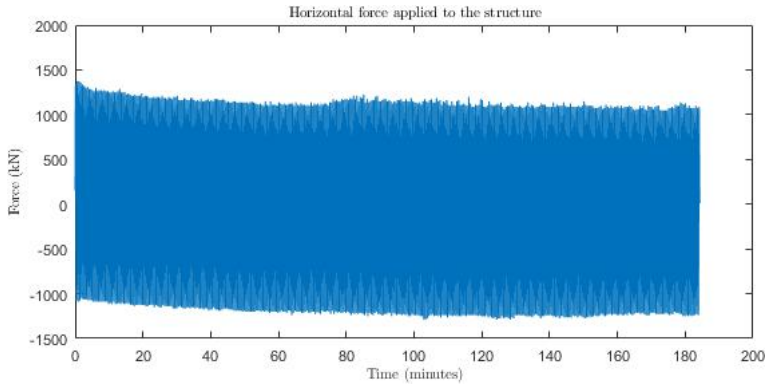

Figure 4.21: Horizontal force required to displace the structure - time

4.5.1.3 Settlement - time

The settlement data is recorded at the edge (blue) and centre (orange) of the foundation and can be seen in Figure 4.22.

Figure 4.22 shows the foundation is settling and also rocking, as some uplift and embedment can be seen at the of the edge of the foundation. Initially in the first 20 minutes of the test (40 cycles), the centre and the edge of the foundation settle at the same rate but by 40 minutes the edge of the foundation continues to embed into the soil while the settlement at the centre of the foundation plateau in comparison. This could be due to the negative drift in displacement from the GDS actuator which would cause further embedment of the foundation where the edge LVDT is recording displacement.

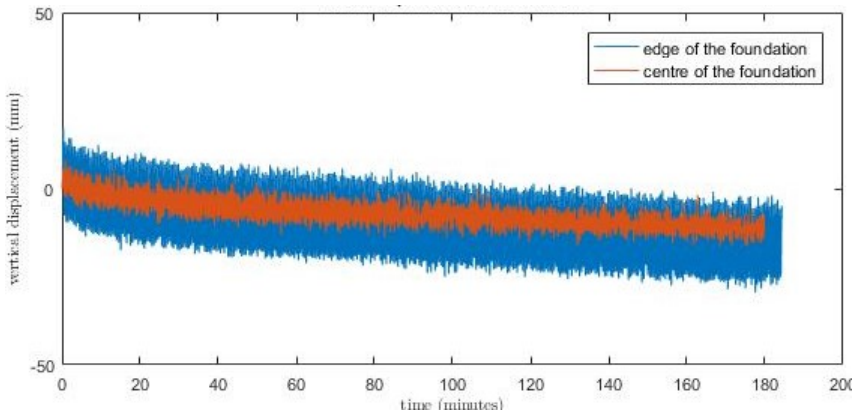

Figure 4.22: Vertical displacement of the foundation

4.5.1.4 Settlement - rotation

The vertical movement of the structure is taken from the centre of the foundation, and the rotation was calculated by Equation 4.4 using the displacement recorded at the top of the superstructure.

In Figure 4.23 the rotation of the shifts to the negative rotational direction which is similar to the horizontal displacement as that too shifted to the negative during the test with increased settlement. This could be due to the the first displacement of the structure is to the left so it might induce more deformation than the right hand side of the foundation.

Figure 4.23 shows the vertical settlement of the structure plotted against rotation, between 1-32 cycles, 168-200 cycles and 328-360 cycles. The vertical movement of the structure is taken from the centre of the foundation and the rotation was calculated with Equation 4.4 using the displacement recorded at the top of the superstructure.

In Figure 4.23 the rotation of the structure shifts slightly towards the negative direction due to the shift in horizontal displacement (see section 4.5.1.2. No uplift at the centre of the foundation is visible.

$$\tan^{-1}\left(\frac{\text{displacement}}{\text{superstructure height (22.5m)}}\right) = \text{rotation (degrees)} \tag{4.4}$$

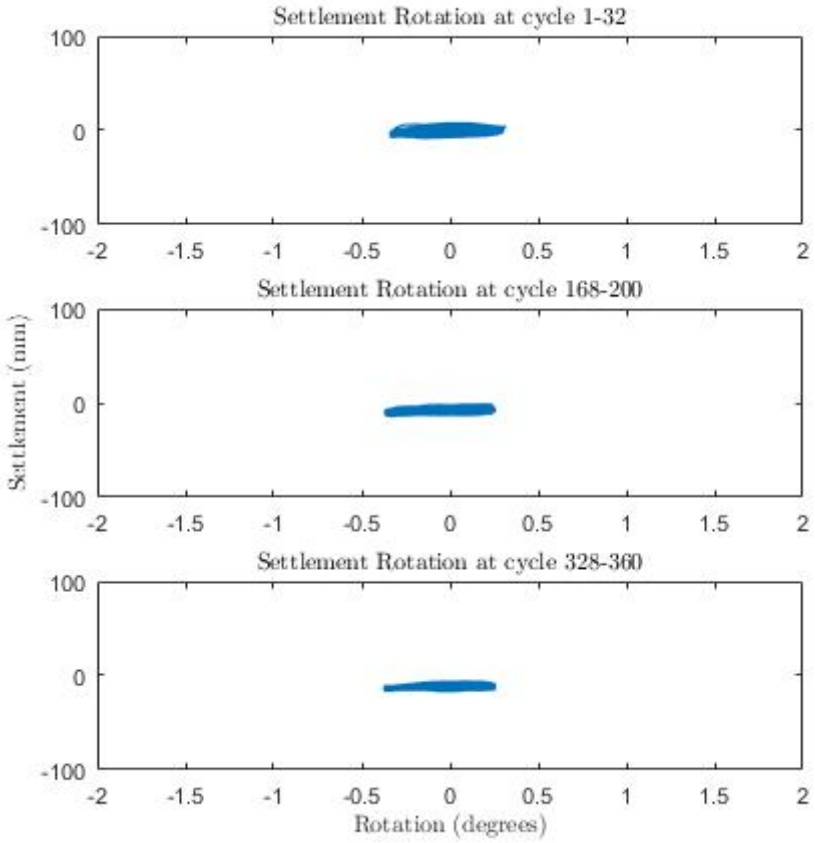

Figure 4.23: Settlement - rotation of the structure during normal loading of the baseline test

4.5.1.5 Force - rotation

Figure 4.24 displays the force plotted against rotation between 1-32 cycles, 168-200 cycles and 328-360 cycles. The overall shape of the loop changes slightly throughout the test from a concave curve initially, to more linear at the end of the test.

The more linear shape is most noticeable in cycles 328-360 between points 0.2°, 400kN and -0.3°, -1200kN. There is also more resistance to rotation at the start of the test, as can be seen by a steeper force-rotation loop. These small changes in behaviour during the test are likely to be due to the edge of the foundation embedding into the soil and rounding the soil below the foundation.

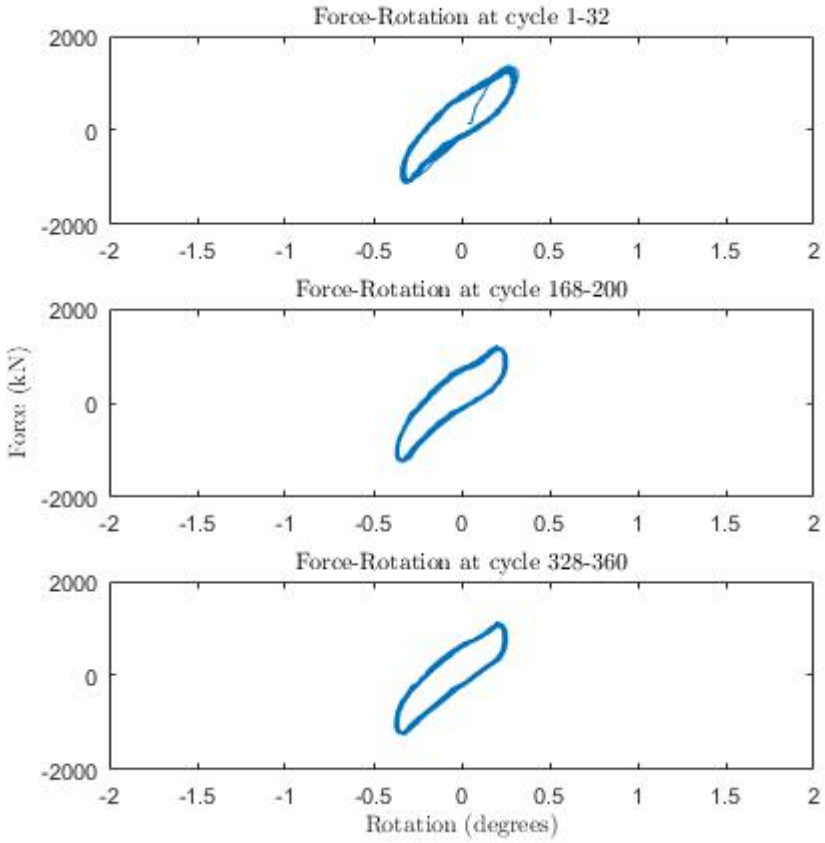

Figure 4.24: Force - rotation of the structure during normal loading of the baseline test

4.5.1.6 Soil-foundation contact

The contact between soil and the foundation was measured using pressure sensors, while thought out the test the sensors gained errors and the calibration at the start and end of the test are different. So the pressure sensors are to be used as a qualitative assessment of the foundation being in contact with the soil or not.

In this test contact data was able to be recorded at the centre, quarter point and edge of the foundation. In Figures 4.25, 4.26 and 4.27 the contact is shown by force applied to the sensors (blue), they all display cycles 1-6, 170-176 and 350-356. Displacement data from the edge of the foundation has also been added to the figures which gives context to the position of the foundation.

The contact force data shown is in N, although this should be taken as a qualitative response as the calibration changed between the start and end of the test.

In Figure 4.25, 1-6 cycles (0-3 minutes) is the start of the test and the pressure at the centre is constant while the the foundation is being displaced. By cycles 170 (85 minutes)the foundation has settled 20mm and the contact is now variable. From the 170th cycle (85th minute) in the contact data it can be seen that the base of the curves are flat, which would indicate that no force is being applied to the foundation. The graph mostly displays a negative force, which these sensors are unable to record. In cycles 350-356 (175-178 minutes) the force

applied is at a larger force amplitude when compared to cycles 170-176. This could mean the force applied at the soil-foundation contact at the centre of the foundation has increased due to a overall reduction of the foundation area being in contact with the soil. It can easily be noted that edge of the foundation embeds to 30mm now, showing further settlement is occurring.

Figure 4.27 shows in cycles 1-6 (0-3 minutes) that at the edge the soil-foundation contact immediately in flux. The troughs are pointed which shows there is little time when there is no contact, when compared to the peaks which are more rounded to show solid contact between the soil and foundation. This is also true in cycles 170-176 (85-88 minutes), when the peaks are much broader indicating the contact is for longer. Cycles 350-356 (175-178 minutes) it is harder to distinguish the cycles in the same way.

In Figure 4.26 which is the quarter point of the foundation and placed between the centre and edge sensors. For cycles 1-6 (0-3 minutes) it is difficult to distinguish any true changes to the soil-foundation contact. By cycle 170 (85 minutes) changes to the soil-foundation contact are notable, showing the force applied at the soil-foundation contact are changing with the movement of the foundation.

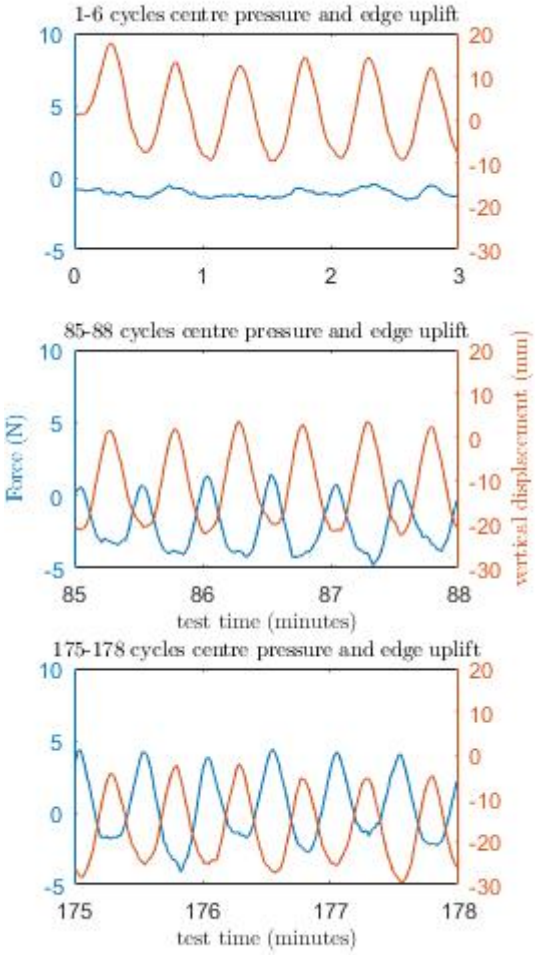

Figure 4.25: The contact force between the foundation and the soil at the centre and the displacement at the edge of the foundation

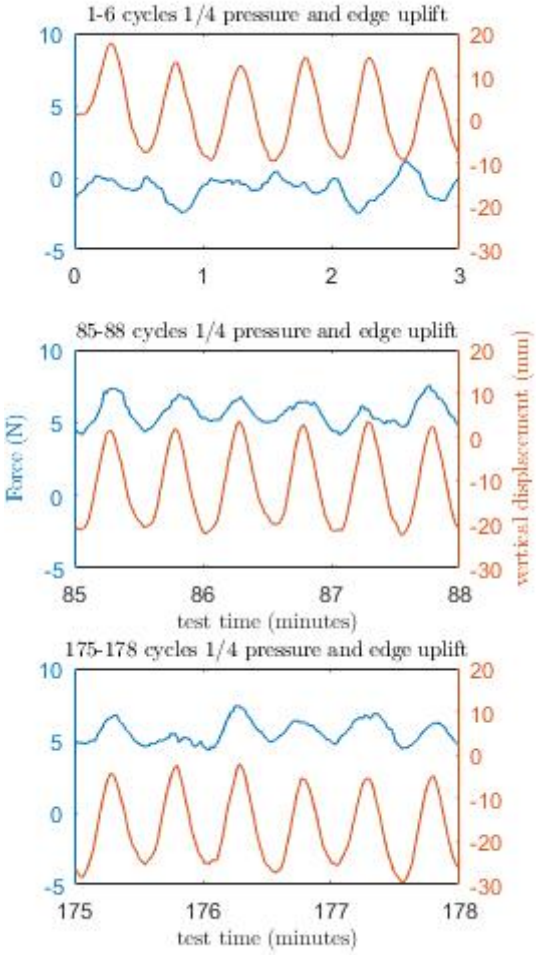

Figure 4.26: The contact force between the foundation and the soil at the quarter point and the displacement at the edge of the foundation

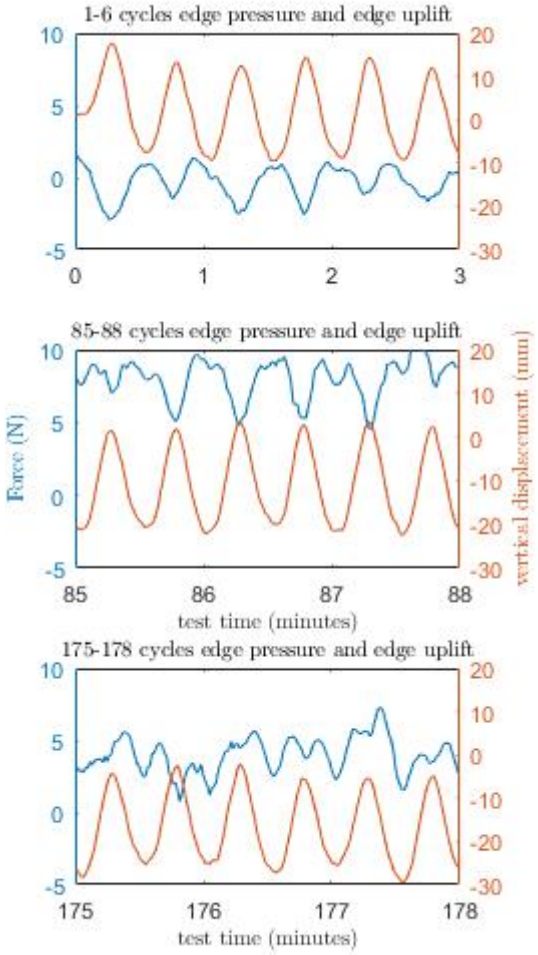

Figure 4.27: The contact force between the foundation and the soil at the edge and the displacement at the edge of the foundation

4.5.1.7 Free vibration frequency

Figure 4.28 shows the free vibration tests, on left is the results from 3 strikes of the structure before cyclic displacement and on the right are the results from a single strike at the end of the test. The data is taken from the LVDT at the top of the structure. The data from accelerometer could not provide clear results including after increasing the sample rate, could not overcome the noise from the power source.

The results from the start of the test are all very similar in wavelength, and have only minor variation to the amplitude, showing adequate repetition. Comparing the results before and after the baseline cyclic displacement is completed it can be seen that the frequency has changed from 6.45 Hz to 6.21Hz, which is minor. Before the cyclic displacement the data disappears into the noise after 3 cycles, but after test there are only 2 cycles to be seen. This shows that the structure does not continue to rock for as long as there is a better dissipation of energy and increased damping.

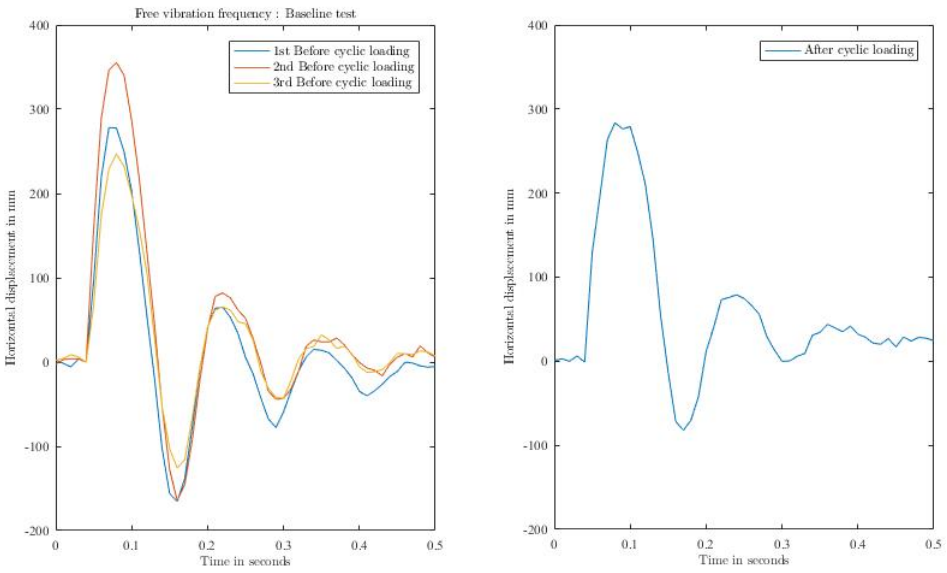

Figure 4.28: Free vibration test of the superstructure at the start and end of cyclic displacement

4.5.2 Short break storms test

There are two data sets from this test, one recording the instruments and one recording the load cell and actuator displacement. After 45 cycles the laptop recording the instruments malfunctioned and no recording took place thereafter, but the load cell was able to keep recording until the test was stopped manually.

4.5.2.1 Horizontal displacement - time

At the top of the structure the displacement was recoded as $\pm$ 180mm for the normal cyclic displacement and $\pm$ 320mm for the storms. The applied displacement is at around 20m whereas the recorded displacement is measured at around 22.25m. The position would change in the test according to the settlement that also occurred. There is no significant drifting of the applied displacement during the test.

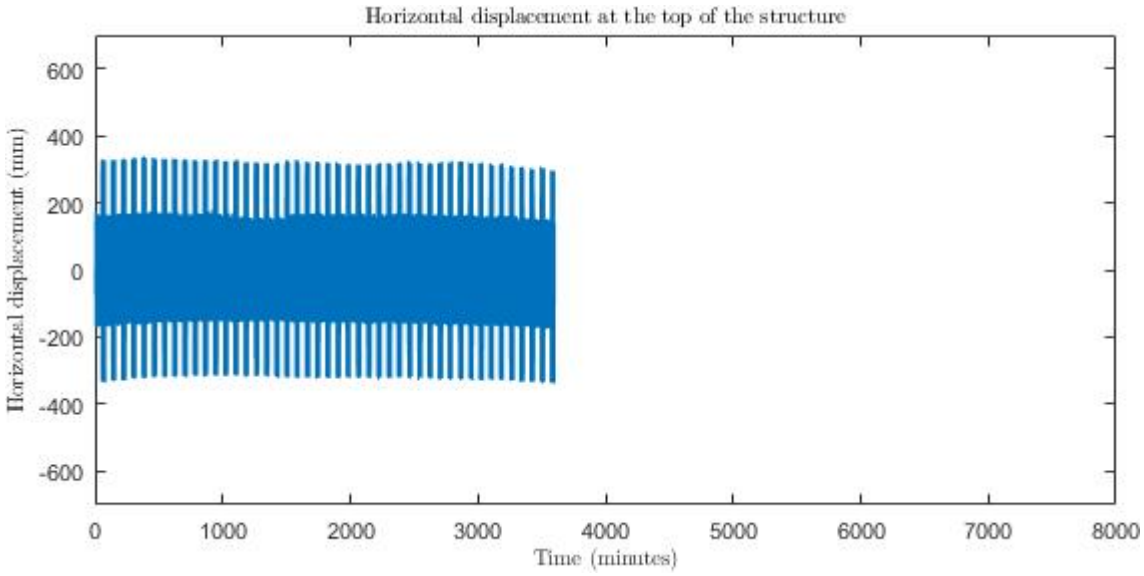

Figure 4.29: Horizontal displacement at the top of the structure

4.5.2.2 Horizontal force - time

Figure 4.29 shows the force required to displace the structure over time. Overall the force required for the displacement in the normal phases is steady compared to the storm phases which require more force than the normal. The storm phases increase in combined force from the first phase till the 10th storm phase (800 minutes), with it being more noticeable in the positive force than the negative force which levels out on the 5th storm phase (400 minutes). Differing required forces indicates that there was initially less resistance in the positive displacement than the negative displacement. A potential result of the initial soil-foundation contact being slightly uneven, that with the cyclic displacement and subsequent settlement has evened the foundational response.

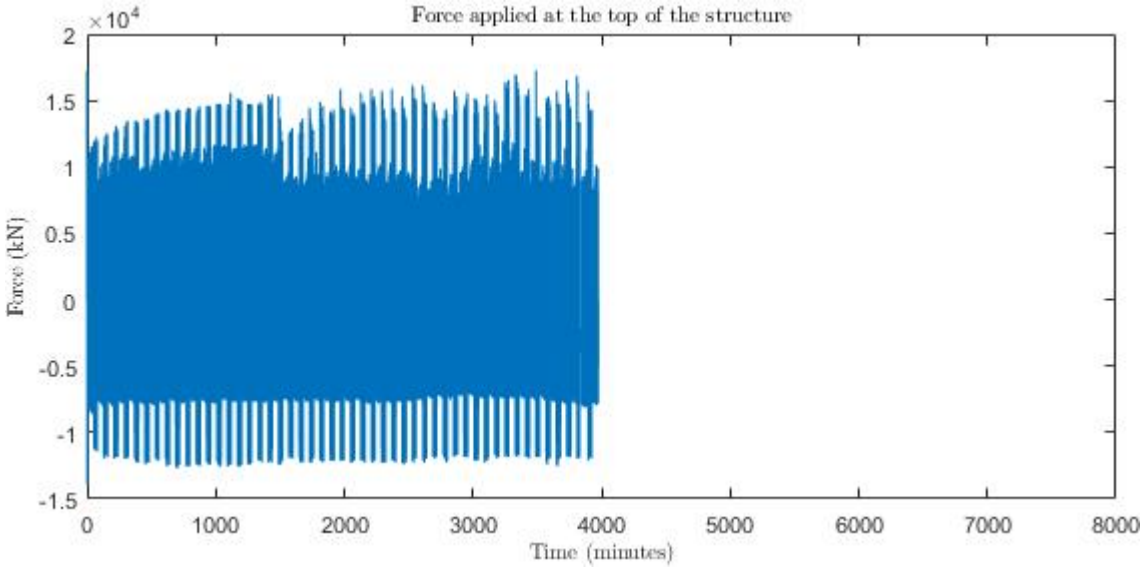

Figure 4.30: Horizontal force required of the structure - time

4.5.2.3 Settlement - time

This Figure 4.31 shows the vertical movement from the foundation at the centre (orange) and the edge (blue). The overall settlement of the structure is 25mm. In contrast to the baseline test, there is considerable uplift at both the edge and the centre of the foundation during the storm phases. This indicates there is likely to be significant reduction in the contact area of the foundation during the storm phases.

The rocking movement of the foundation is not even, with much more uplift than embedment seen at the edge and centre of the foundation due to the soil providing resistance to the rotation of the foundation. During the storm phases the uplift of the edge of the foundation is around 55mm and the embedment is up to 21mm, this is consistent for the majority of the test. In the normal phases, the centre of the foundation has the same vertical movement throughout the test of $\pm$ 5mm which is similar to the behaviour seen in Figure 4.22.

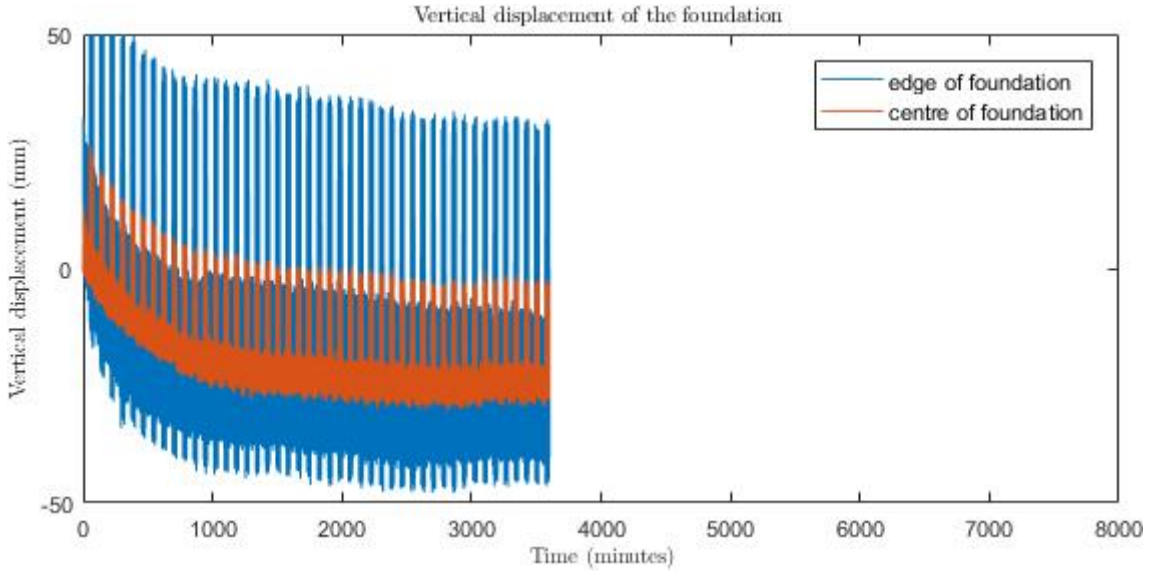

Figure 4.31: Vertical displacement of the foundation

4.5.2.4 Settlement - rotation

The settlement-rotation data has been split up to show specific phases of the testing. This allows the progression of the test to be easily distinguishable. Figure 4.32 display cycles 1-50 (1st phase), 631-680 (10th), 1331-1380(20th), 2031-2080(30th) and 2731-2780(40th) of normal displacement, while Figure 4.33 displays cycles 51-80 (1st phase), 681-700 (10th), 1381-1400(20th), 2081-2100(30th) and 2781-2800(40th) of the storm displacement. As the structure is displacement controlled the rotation does not to change. The calculation of the rotation is described in section 4.5.1.4.

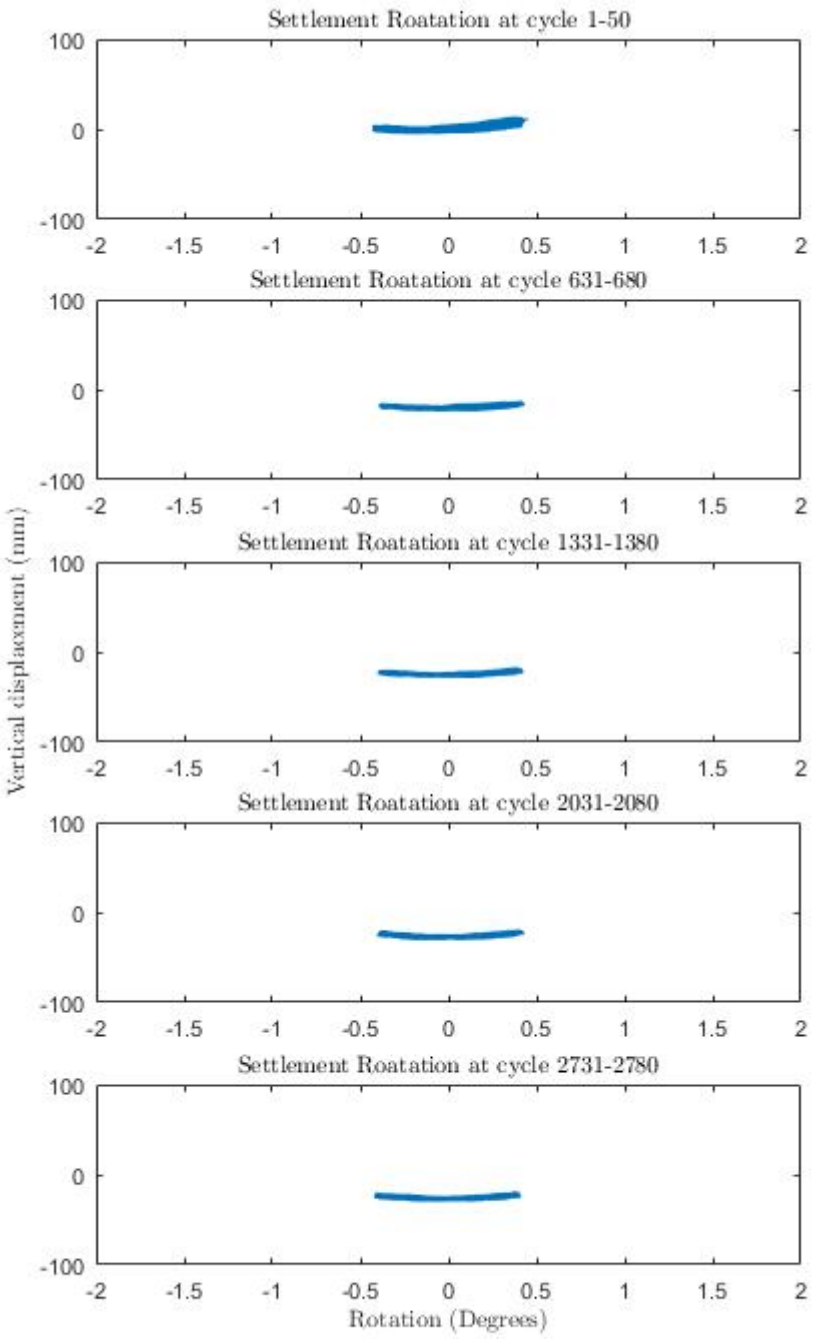

Figure 4.32: Settlement - rotation, normal phases

The settlement in Figure 4.32 shows that there is more vertical movement during cycles 1-50 (1st phase) and the movement is all uplift as the structure is just starting to settle. The uplift is uneven with the positive rotations of the structure uplifting more, which is most significant in cycles 1-50 (1st phase) which can be seen with the data displaying a much thicker line of movement. In general a small amount of uplift is visible in all phases, more than in the baseline test. Cycles 631-680 (10th phase) shows there is settlement occurring throughout the

test, and in cycles 1331-1380(20th), 2031-2080(30th) and 2731-2780(40th) the amount of settlement within the phases are consistent.

The data shown in Figure 4.33 displays the rotation that occurs during the storm phases as well as the settlement. Significant uplift occurs and even the centre of the foundation uplifts when the rotation of the structure is between 0.4 to 0.8°. Cycles 51-80 (1st phase) have more uplift when the structure has a positive rotation than a negative rotation, similarly to the normal phase.

Similar amounts of settlement occur in each phase. In cycles 2781-2800(40th storm phase) there is a slight change to how the structure is moving in comparison to the previous phases, the vertical movement of the structure has reduced when the rotation of the structure is between -0.2 and 0.2°. When the rotation reaches to -0.8 to -0.2 and 0.2 to 0.8° there is an increase in the vertical movement from a changing soil profile.

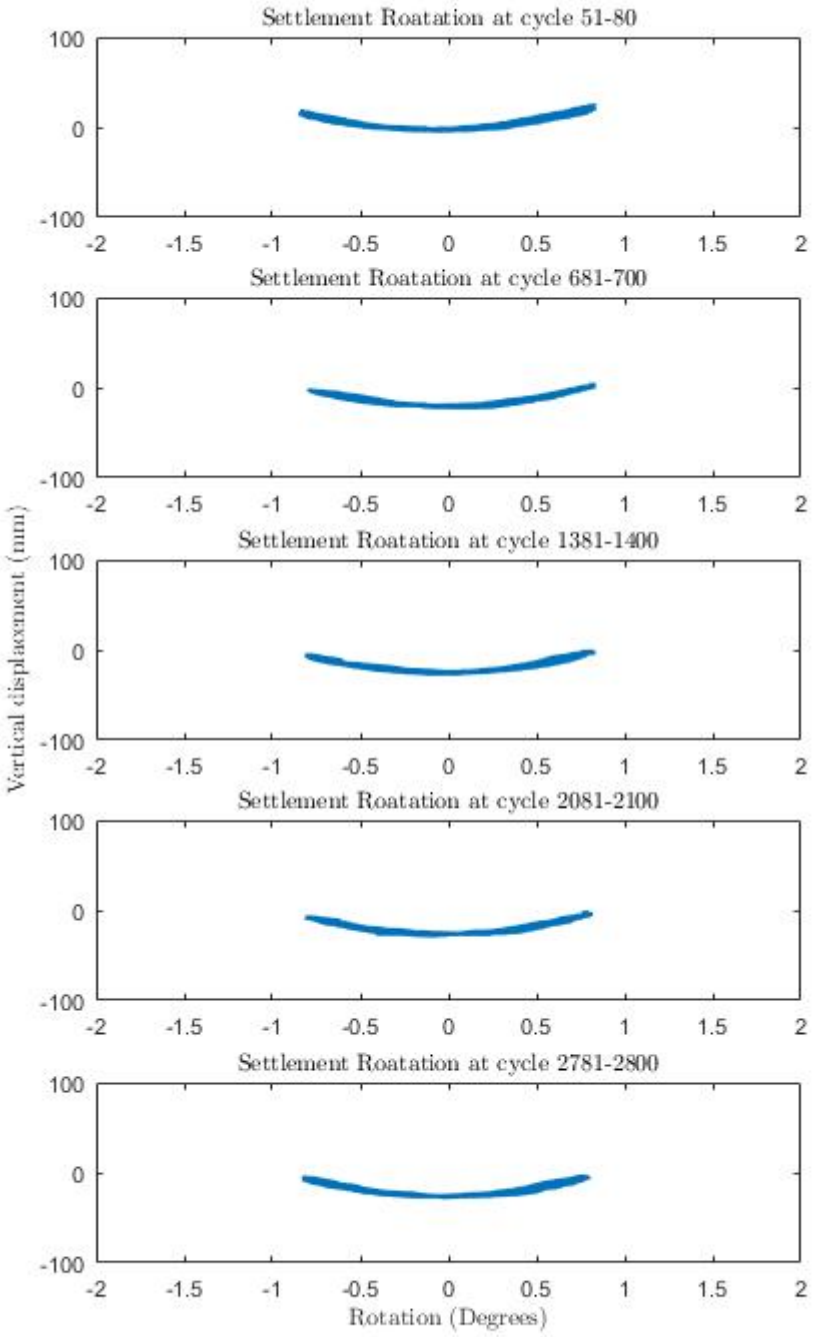

Figure 4.33: Settlement - rotation, storm phases

4.5.2.5 Force - rotation

The amount of force required to rotate the structure is plotted against rotation in Figure 4.34 with cycles 1-50 (1st phase), 631-680 (10th), 1331-1380(20th), 2031-2080(30th) and 2731-2780(40th) of normal displacement. In Figure 4.35 cycles 51-80 (1st phase), 681-700 (10th), 1381-1400(20th), 2081-2100(30th) and 2781-2800(40th) of the storm displacement.

The rotation of the structure increases from 0.4° to 0.8° between the normal and the storm displacement but the force that is required to produce this rotation is not double. In fact, it is only roughly an increase of a third of the force. Cycles 51-80 (1st storm phase) in Figure 4.35, shows the force at its maximum force occurs simultaneously with maximum rotation, while cycles 681-700 (10th storm phase) the maximum force now occurs when the rotation is at 0°. As the test continues into cycles 1381-1400 (20th storm phase) the shape of the force-rotation loop returns to the same as that from cycles 51-80 with the change that the maximum force in the positive now occurs when the rotation is in it's negative maximum.

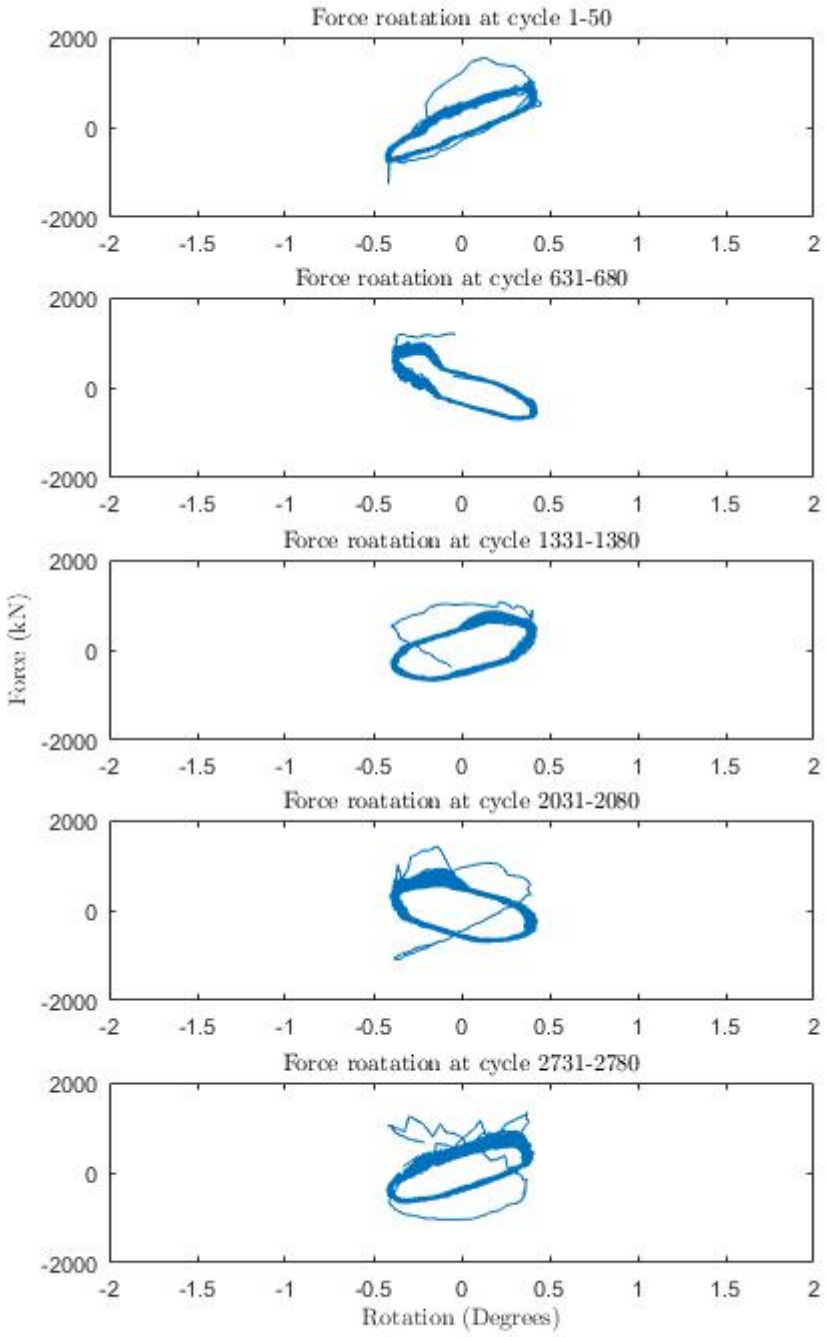

Figure 4.34: Force - rotation, normal phases

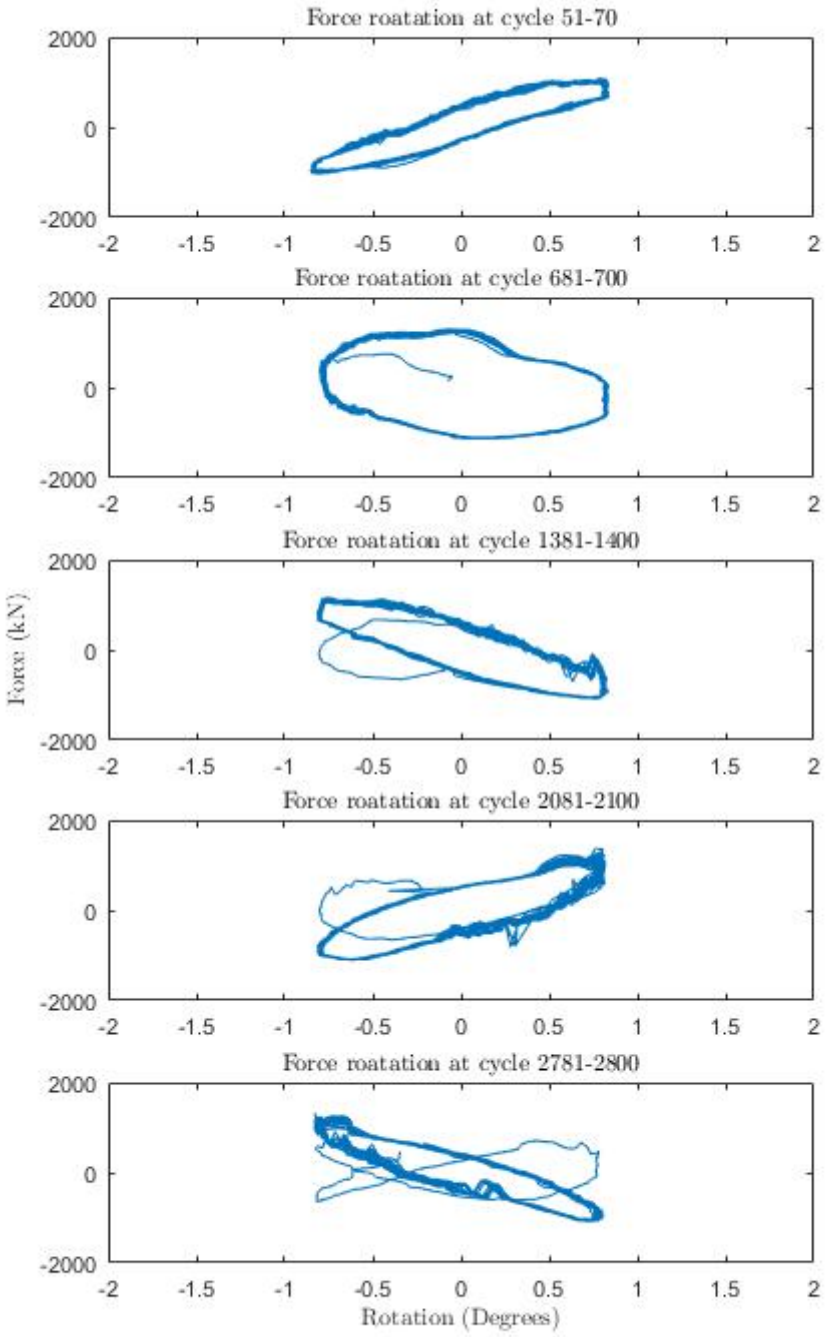

Figure 4.35: Force - rotation, storm phases

4.5.2.6 Free vibration response

Figure 4.36 shows the free vibration response from before and after the cyclic displacement was applied, plotted together to show directly the change in the wavelength and frequency. There is only one cycle distinctly recorded in the frequency test before the cyclic displacement

whereas there are two recorded after the cyclic displacement. The frequency before the cyclic displacement is 5.00 Hz (0.2 second) and the frequency after is 3.33 Hz (0.3 seconds).

The increased number of cycles visible after cyclic displacement shows that there has been a change to the damping and soil structure interaction. When comparing the baseline test frequency (4.28) to the short break storm there is less damping at the end of the short break storm test. The storm phases allowed for increased rotation and therefore a greater change in the soil profile and a reduction in the contact area allowing the structure to rock more than from just normal cyclic displacement.

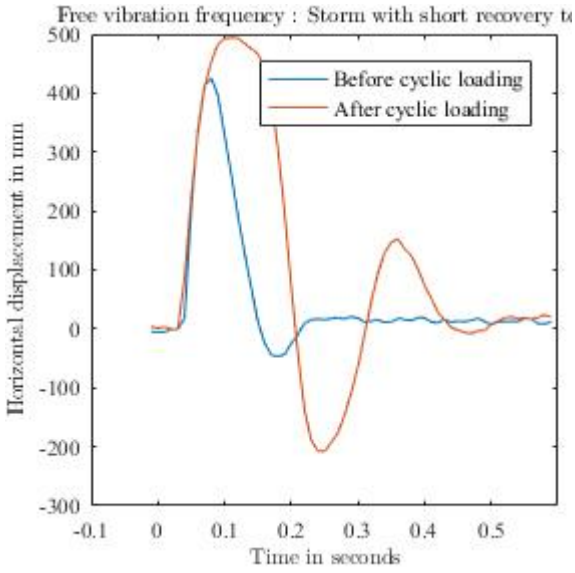

Figure 4.36: Free vibration test of the superstructure at the start and end of cyclic displacement

4.5.3 Long break storms test

The long break storm test didn't go to plan due to the actuator malfunctioning. Near the start of the test there were two interruptions to correct the error and reset the actuator without disturbing the experiment, these breaks occurred after 100 minutes when the GDS actuator stopped due to overextension of the actuator arm and the second was at 700 minutes when again the GDS actuator stared to drift and was manually stopped and reset. The second reset included changing the position of the LVDT at the top of the structure, because it was knocked This was the only time any sensors were moved or tampered within the test. At 1500 minutes into the test the actuator malfunctions and unevenly displaces the structure, which causes uneven deformation to the foundation and makes the data from the test after 1800 minutes unreliable. At 2700 minutes the GDS actuator malfunctions again offsetting the structure by 500mm but continuing the cyclic displacement until it defaults and stops once again. The test was once again restarted at 5000 minutes without The first 1800 minutes of this test has data that can be used as one experiment, as the initial interruptions and errors were minor prior to resetting. The full data set of horizontal displacement with time is shown in Figure 4.37 below to show the dramatic shifts in the displacement caused by the problems with the actuator. The full set of data is also shown for the settlement and force with time. However,

the settlement-rotation figures and force-rotation figures only include data from the first 1800 minutes of the experiment.

4.5.3.1 Horizontal Displacement - time

Figure 4.37 shows the overall pattern of displacement during this test including the breaks and issues that occurred. The break in the test from 100 to 600 minutes no displacement occurred and does not affect the tests results because the foundation was not being disturbed by the cyclic displacement.

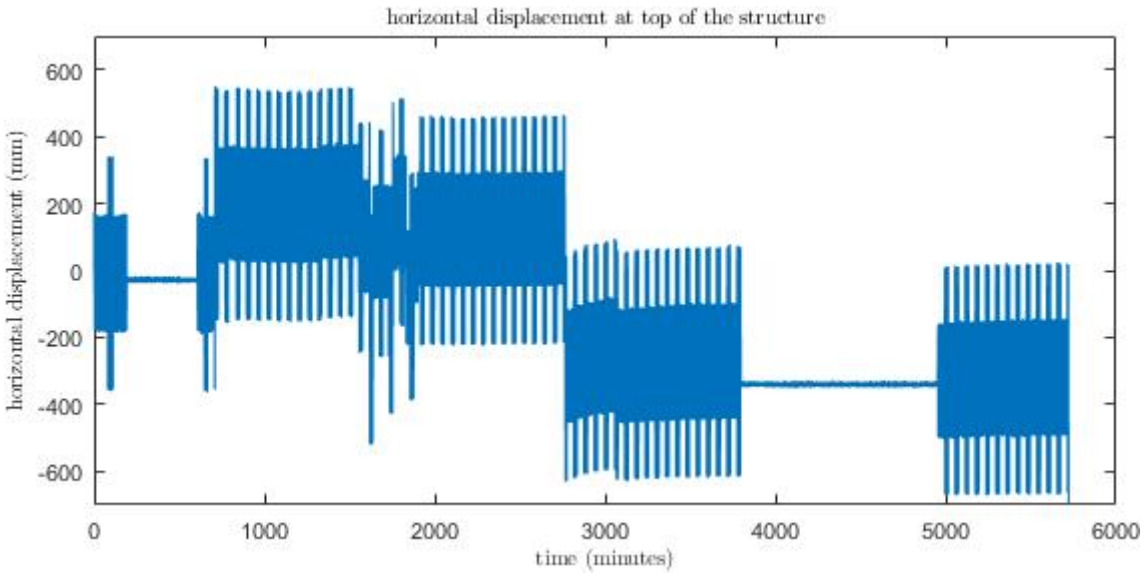

Figure 4.37: Horizontal displacement at the top of the superstructure

4.5.3.2 Force - time

The force has been plotted as individual graphs in Figure 4.38; to allows for the force required to be seen in more detail, while not displaying the stoppages that occurred.

At the top of Figure 4.38 is the first application of displacement (test time 0-100 minutes). Below is the second (test time 600-700 minutes) which both did not run for a long period of time due to being interrupted and reset before significant malfunctioning occurred.

The third graph (test time 700-3700 minutes) where the majority of the cyclic displacement occurs. The third storm phase is where there is distinguishable force between normal and storm phases of displacement. The storm phases now require larger forces to produce additional displacement.

It is also notable round 800 minutes where the displacement is variable so to does the force as a consequence of that, at this stage the data is unreliable.

Whereas the third attempt to continue the test was able to run for around 700 minutes before any issues occurred and in this does sync up to the previous graphs as the first two cycles show little distinction between the normal and storm displacement, and this can be seen

to be changing at the start in the 3rd graph. The storm displacement takes a few more phases before it is distinct.

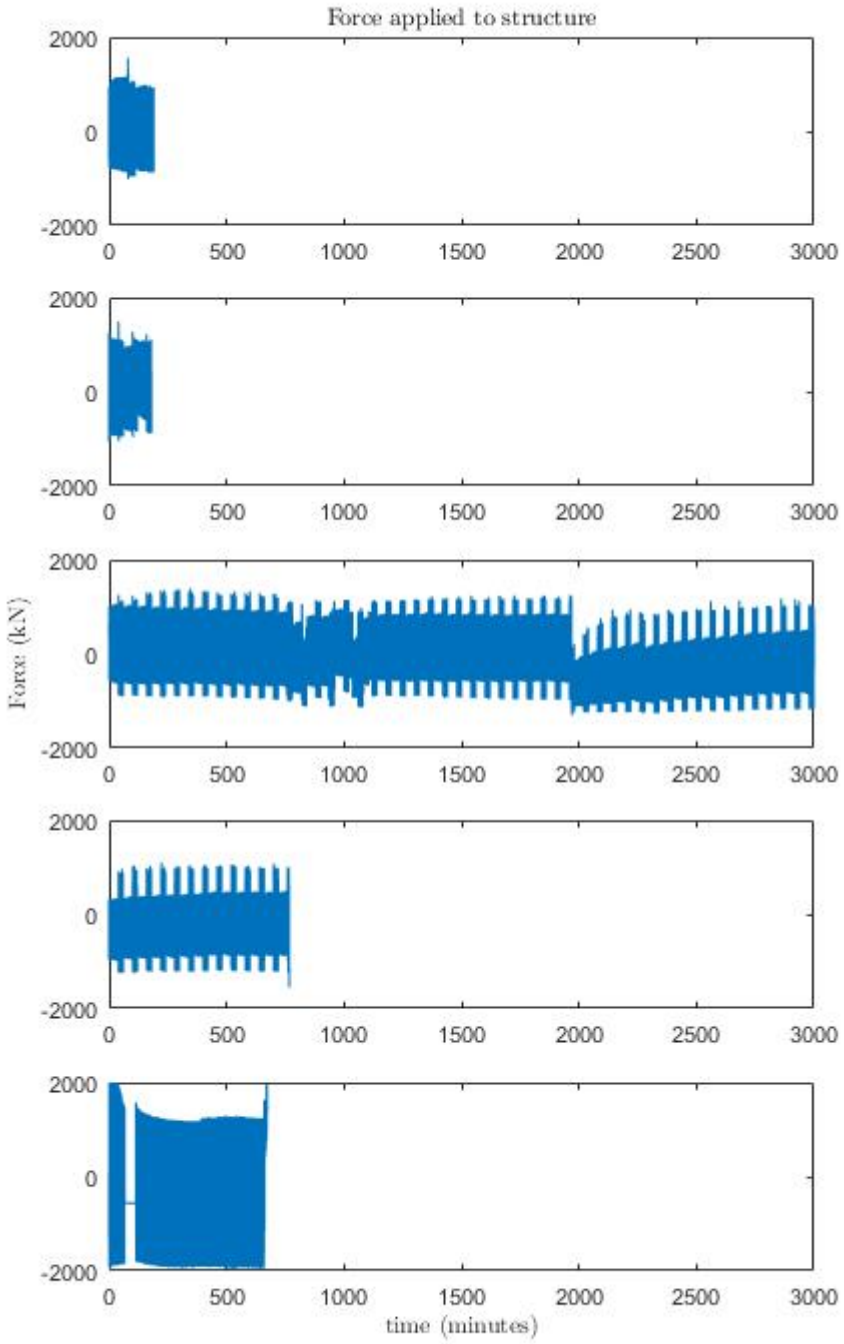

Figure 4.38: Horizontal force required to displace the structure - time

4.5.3.3 Settlement - time

Figure 4.39 shows the vertical movement at the centre (in orange) and the edge (in blue) of the foundation. At the edge of the foundation the amplitude of vertical movement in the normal

phases is 30mm whereas in the storm phases this increases to 80mm, comprising 60mm uplift and 20mm embedment. At the centre of the foundation, the amplitude of vertical movement during the normal phase is 10mm, whereas in the storm phase it is 25mm, and similar to the edge of the foundation there is more uplift than embedment. The centre of the foundation does not have the same embedment characteristic as at the edge of the foundation, as shown in Figure 4.40. This figure shows three phases of normal and storm displacement and the extent of the edge embedment can clearly be seen.

Between 200 and 400 minutes of the test there is no cyclic loading due to the malfunction of the actuator. During this time there is some very minor settlement occurring which is not due to the cyclic displacement but the weight of the structure on the soil. When the displacement resumes the rate of the settlement increases to be similar that in the first 200 minutes of the test. This shows that the weight of the structure does cause some the settlement but the cyclic displacement creates more. By the end of the test the structure as a whole has rotated and the edge LVDT is no longer in contact with the foundation.

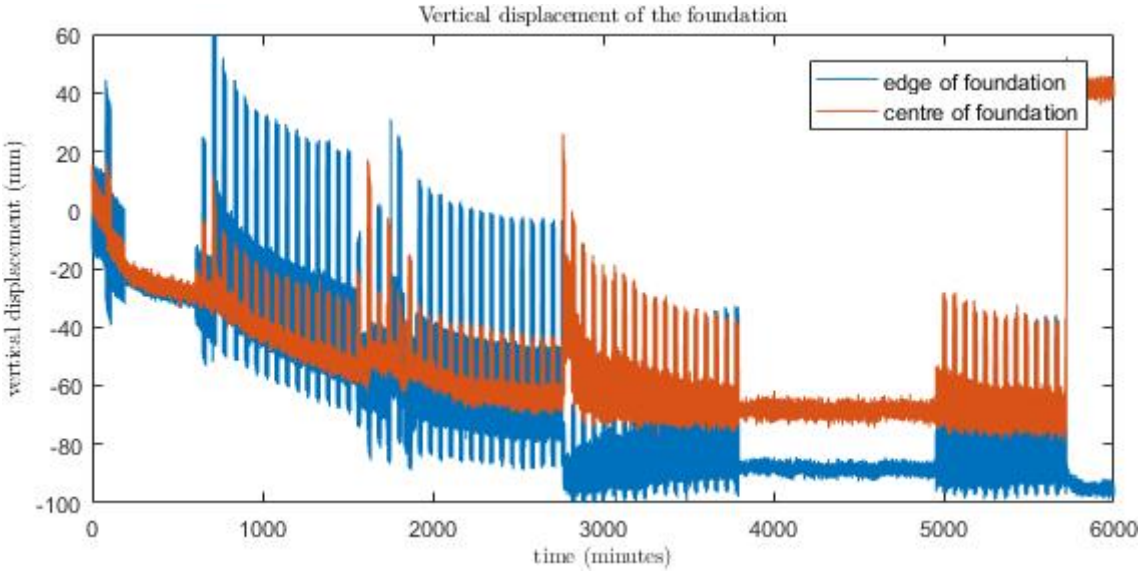

Figure 4.39: Vertical displacement of the foundation

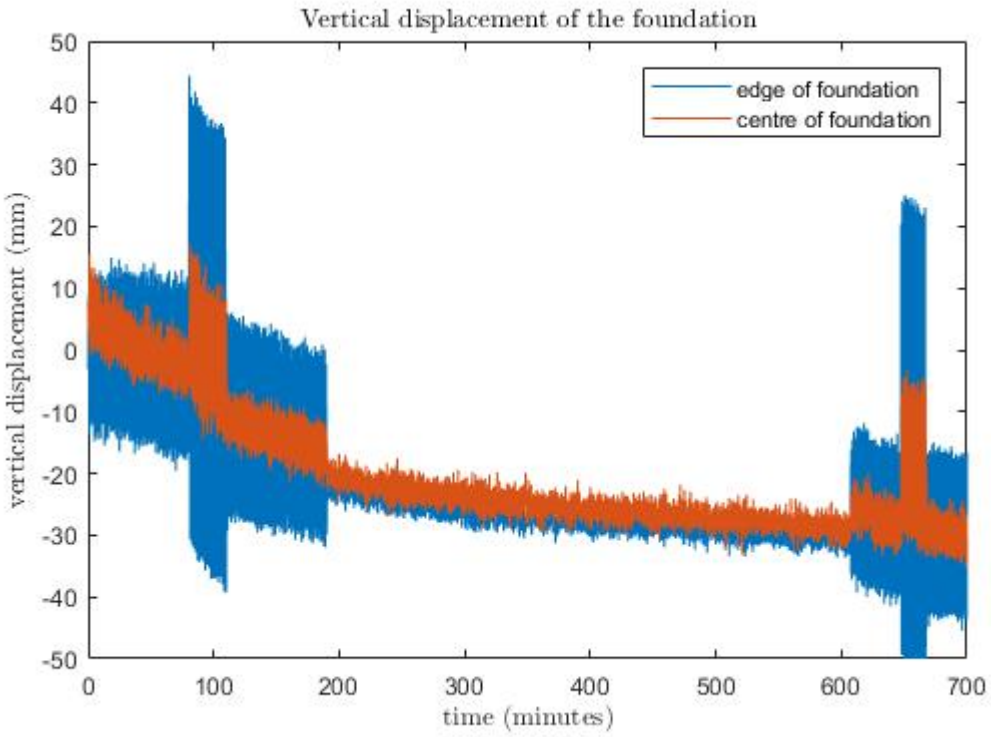

Figure 4.40: Vertical displacement of the foundation between 0-700 minutes

4.5.3.4 Settlement - rotation

Figure 4.41a shows cycles 1-160 (1st phase), 651-730 (5th phase), 1151-1230 (10th phase) and 1651-1730 (15th phase) which are normal cyclic displacements. These intervals where chosen as an incremental progression of the test showing of the changes occurring to the foundation throughout the cyclic displacement. In the 1st phase of normal displacement (cycles 1-160) there is 22mm of settlement and when the structure rotates to the negative there is a small amount of uplift. Little uplift is visible in the subsequent phases of normal displacement. By the 5th phase of normal loading (cycles 651-730) the rotation has shifted to the positive, although the amplitude of rotation is the same as the 1st phase; with them both rotating just less than 1°, the shift of the rotation to the positive side is due to the actuators displacement cycle miss firing.

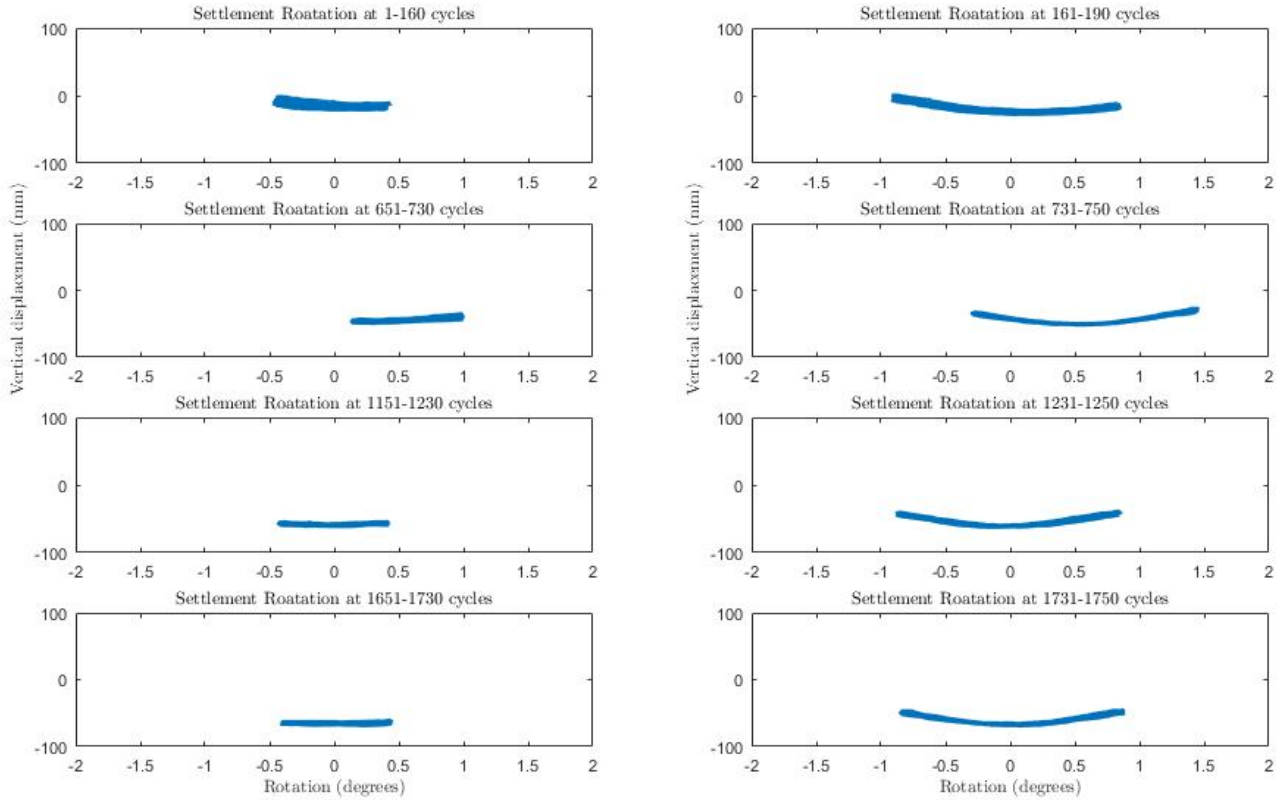

(a) Normal phases **(b)** Storm phases

Figure 4.41: Settlement - rotation, phases 1, 5, 10 and 15 of the long break storm test

Figure 4.41b shows the settlement and rotation during the storm phases on cycles 161-190 (1st phase), 731-750 (5th phase), 1231-1250 (10th phase), and 1731-1750 (15th phase). The overall rotation in each phase is 1.75° and this is even throughout the test. In the first storm phase the structure is evenly rotating with more uplift in the negative rotation. The 10th and 15th phases the uplift is higher in the positive rotation, which is a possible after effect of the drift that occurred around the 5th phase.

The rate of settlement (the most in one phase) is highest in the first phases, at the end of the first storm phase at 0° the structure had settled 28mm, which brings the overall settlement to 40mm. By the end of the 10th storm phase (cycle 1250) the structure settled 12mm the settlement is up to 62mm.

Much more uplift occurs during the storm phases than during the normal phases of cyclic displacement. Figure 4.42 shows a single cycle of the uplift of the centre of the foundation. The storm phase (minute 1140) causes 19mm up lift while during normal phases (minute 1130) the uplift is 3mm, this shows that there is significantly more occurring with greater rotation.

The uplift at the centre of the foundation is up to 19mm during a storm phase, which would indicate the soil-foundation contact area is highly reduced during storm displacement.

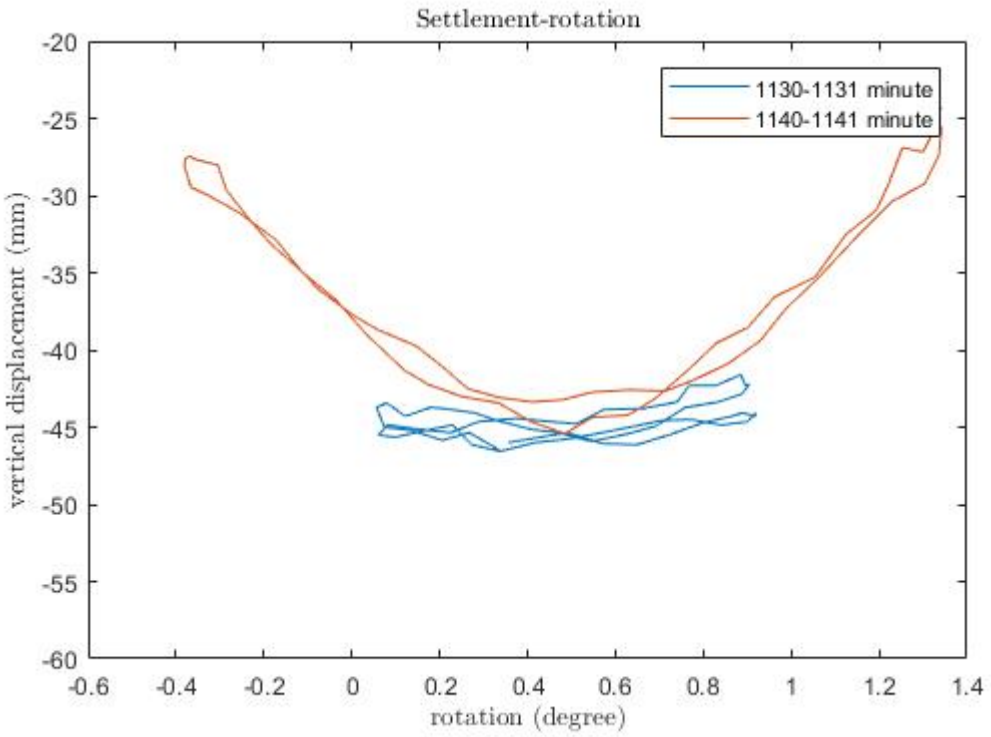

Figure 4.42: Settlement - rotation, comparison between storm and normal displacement

4.5.3.5 Force - rotation

Figure 4.43a displays the force-rotation data from the 1st, 5th, 10th and 15th normal cyclic displacement phases. The rotation data is steady throughout the testing, apart from during the 5th occurrence when the actuator miss fired. Although this isn't reliable for comparison it is important as it has affected the rest of the test due to how the foundation behaviour changed in that time. The force required to displace the structure is positive while the actuator is pushing the structure away from itself and negative while it is pulling it toward itself.

The start of the test is a normal phase and the loop that the force - rotation creates shows that in the positive maximum rotation the force drops steadily without a change to the rotation, whereas the maximum negative rotation the force changes with the rotation. This could suggest that during the peak of the displacement while the structure does not move significantly the force to keep it at positive maximum rotation is no longer required. At the negative maximum rotation as soon as the force is removed from displacement the structure also moves.

By the 10th occurrence of the normal phase (cycles 1151-1230) the maximum positive force occurs before the maximum negative rotation which is a change from how the structure was reacting at the very start of the test in the first normal phase (cycles 1-160). The shape of the loops is now even and both sides of the soil-foundation interface are behaving the same.

Storm phases of the force-rotation can be seen in Figure 4.43b. The 1st phase of storm displacement (cycles 161-190) shows an open loop where the force rate is higher when the structure in being unloaded from the maximum and minimum rotation point to 0° rotation.

This is a similar but larger to the loops from the 1st normal phase in Figure 4.43a. Then when the structure is being displaced away from 0° the force is higher with the rotation increasing from 0, this is from the initial disturbance of the soil.

Whereas in the 5th phase the force applied to the structure is even from the maximum to minimum rotation, the loop appears to look more like a line, the gap is very minimal. It is taking an even effort to displace the structure throughout the loop.

The 10th phase of the storm phase the maximum load is no longer at the maximum rotation, and is now close to the 0° rotation, which means to initially displace the structure takes more force than to take it to maximum rotation. Then during the 15th phase (cycles 1731-1750) the force-rotation seems to have flipped where the maximum force is now negative rotation, whereas previously the maximum force was also the maximum rotation.

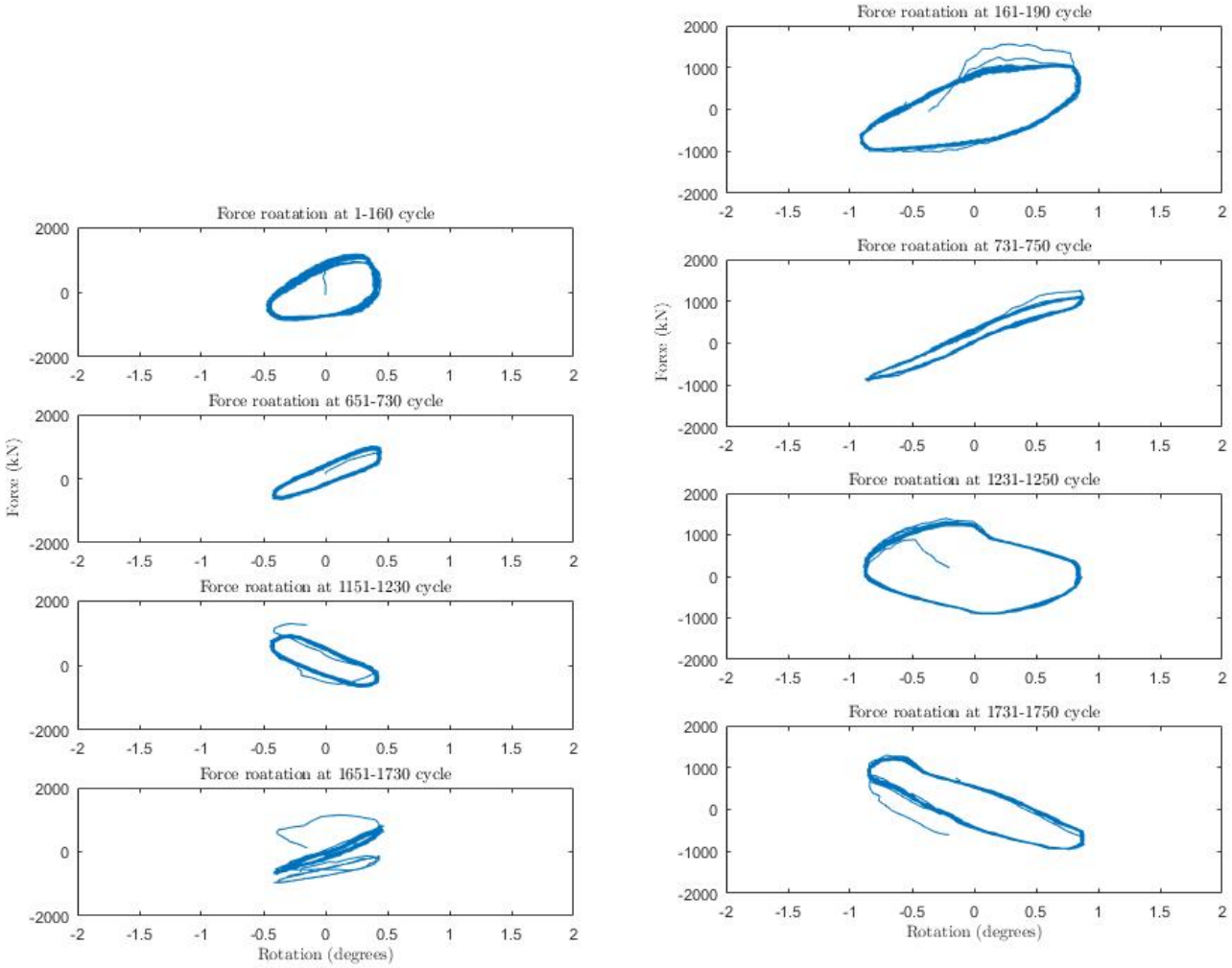

(a) Normal phases **(b)** Storm phases

Figure 4.43: Force - rotation, phases 1, 5, 10 and 15 of the long break storm test

4.5.3.6 Start and end free vibration frequency

The free vibration response of the soil-structure system measured at the start and the end of the long-break storm test is shown in Figure 4.44. The natural frequency measured before the test is 7.3Hz after the cyclic displacement has taken place, this reduces to 2.9Hz.

Comparing this to the short break storm test the changes in frequency are similar in that the before cyclic is a higher frequency than the after, although there is a larger drop in frequency in the long break storms test. This test has more normal cycles, more cycles in general, and GDS actuator issues which can all lead to a alterations in the soil-foundation.

The damping doubles, which the opposite to the short break storm where is decreases. The response before the test has 4 cycles in 0.55 seconds. After the test, the response is only one cycle which lasted 0.35 seconds.

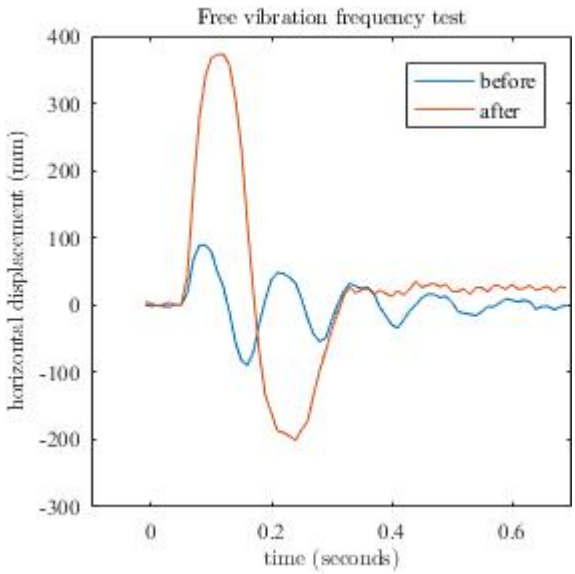

Figure 4.44: Free vibration test of the superstructure at the start and end of cyclic displacement

4.5.4 Gust Storm Test

This test has 3 phases of cyclic displacements of different amplitudes. These are 150mm, 300mm and 400mm, with 40, 20 and 5 cycles each respectively. In this test the actuator malfunctioned at around 240 minutes and shifted the centre of displacement 200mm. After this, the test was re-started which caused the structure to be rotated to an extent that failure occurred and affected the soil profile below the foundation.

The test was then reset by moving the structure and LVDTs back into their original positions and restarted. This resetting had to be carried out 6 times in total, due to continued malfunctioning of the actuator, so the experiment cannot be considered as continuous. Before each reset the frequency of the structure was recorded. Due to the problems with the actuator, the results presented are from the initial 305 cycles of displacement but the full applied displacement can be seen in the following section.

4.5.4.1 Horizontal displacement - time

Figure 4.45 shows this test is very short, which is due to a malfunctioning actuator which at around 240 minutes shifted the centre of displacement 200mm.

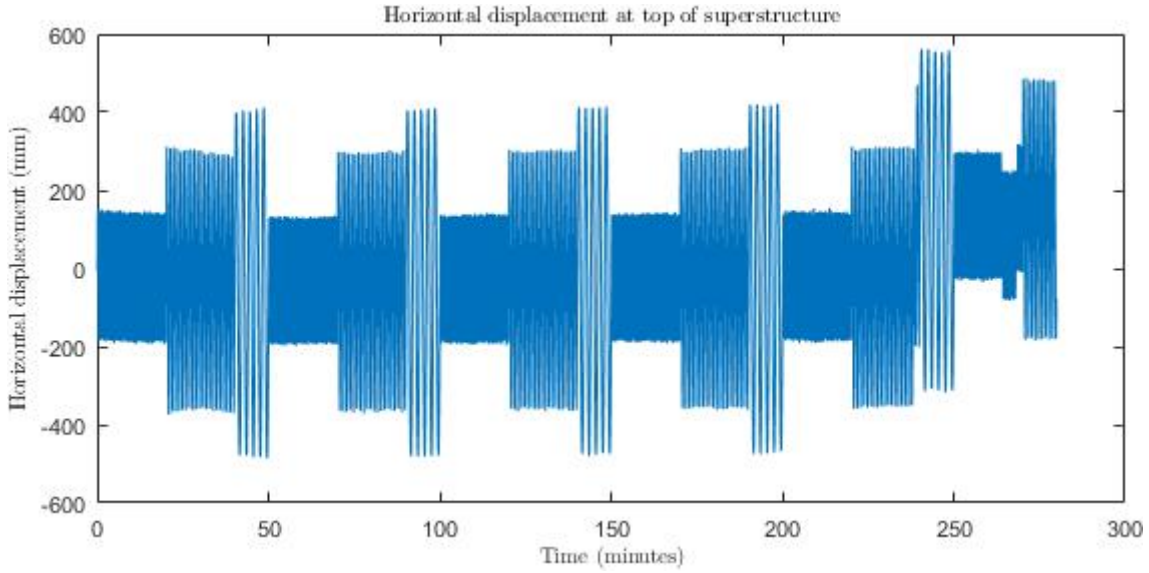

Figure 4.45: horizontal displacement at the top of the superstructure

The test was reset several times after the actuator malfunctioned as can be seen in Figure 4.46.

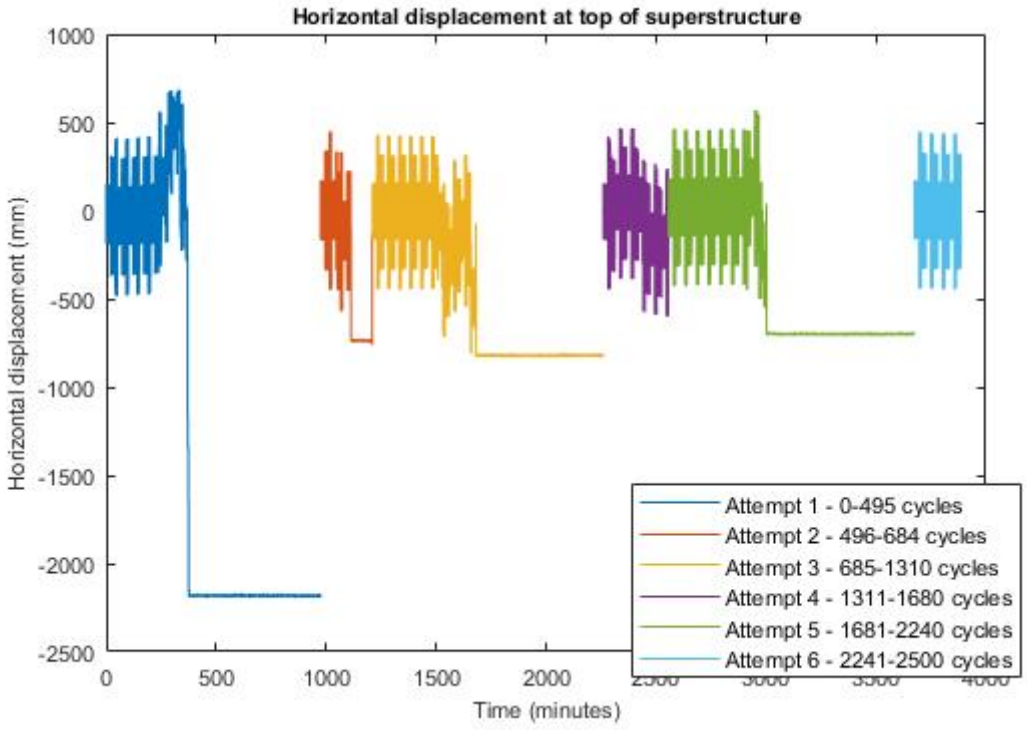

Figure 4.46: All the cyclic displacement applied to the structure for the gust storm test, including displacement when the actuator malfunctions

4.5.4.2 Force - time

Figure 4.47 shows the force required for the applied cyclic displacement.

The force required to displace the structure is significantly larger at the start of the cyclic displacement and at 20 minutes in to the test the largest force is recorded which also coincides with the start of the first storm phase where the displacement changes from 150mm to 300mm.

Within 5 cycles of the storm phase, the force has reduced from 5,500kN to 2,500kN for a full cycle of displacement. The change in required force could be due to the shape of the soil below the foundation changing and allowing for the displacement to occur with less force.

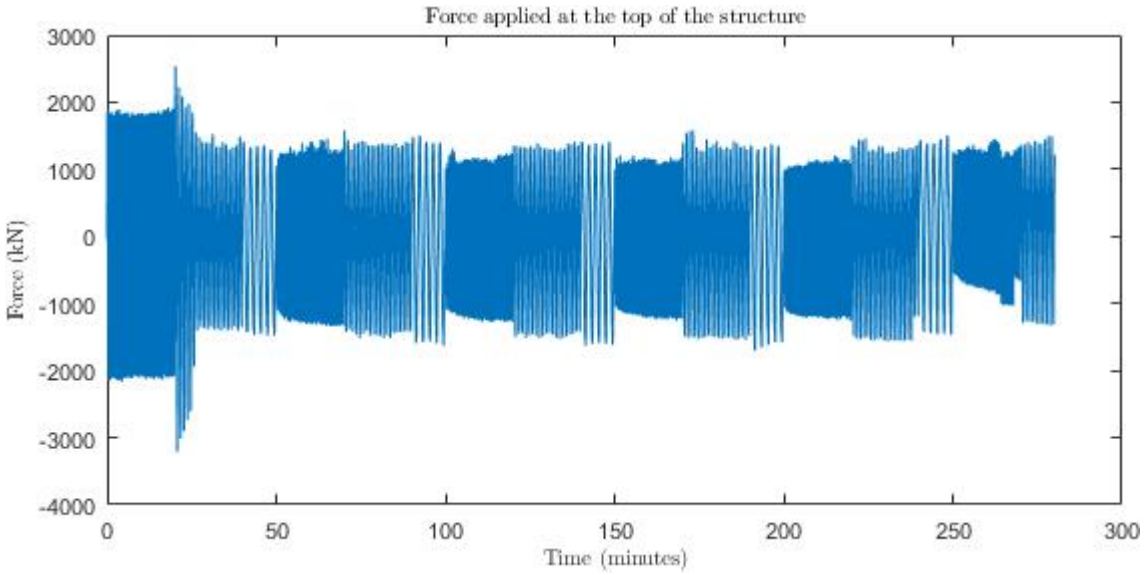

Figure 4.47: Horizontal force required to the structure - time

The normal phases start at 50, 100, 150, 200, and 250 minutes and in each of these the force required is lower in the first 3 cycles of displacement but then increases from 2100kN to 2500kN. The reduced force required at the start of each phase could be a consequence of the larger gust phase displacement before it. The gust displacement will have moved the structure further and have been changing the soil profile, when the normal displacement comes after there is initially a more rounded soil profile while the normal cyclic displacement continues this becomes flatter.

The storm phases start at 70, 120, 170, 220 and 270 minutes and have a reasonably constant force of 2800kN on average throughout the phase. The same can be seen in the gust phases which start at 40, 90, 140, 190, and 240 minutes, where the average force required is 2900kN. The force required for the storm and gust displacements are similar due to the being at the limits of maximum force which has also been noted in figure showing the pushover test.

The reduction of applied displacement after the larger storm and gust phases initially results in a reduced connection between the foundation and the soil and easier movement of the structure. However, as the normal phase continues, the soil appear to increase in density.

4.5.4.3 Settlement - time

In Figure 4.48 the vertical movement of the foundation centre (blue) and the foundation edge (orange) are shown for 0-280 minutes. In the first normal phase (0 to 20 minutes) the centre and the edge of the foundation are moving in unison, with little difference between the two. This unlike the baseline test which in the edge of the foundation moves more than the centre.

At 20 minutes (end of the first normal phase) the overall settlement of the structure is 10mm and the maximum movement occurring in a cycle is 10mm at the centre of the foundation and 15mm at the edge.

In the second phase of the normal displacement (50-70 minutes), there is much more vertical movement in a cycle at the edge of the foundation as it increases to 35mm compared to 12mm at the centre.

The change in behaviour is expected as the previous storm and gust phases have increased the rotations of the structure and changed the soil profile which allows the edge of the foundation to move up and down more than in the first normal phase. The overall settlement at the end of the second normal phase is 17mm.

In the third phase of normal displacement (100-120 minutes) the edge of the foundation vertical movement in a cycle is 38mm in comparison to 17mm at the centre. This is similar to the second phase, which shows that the is a consistent pattern beginning.

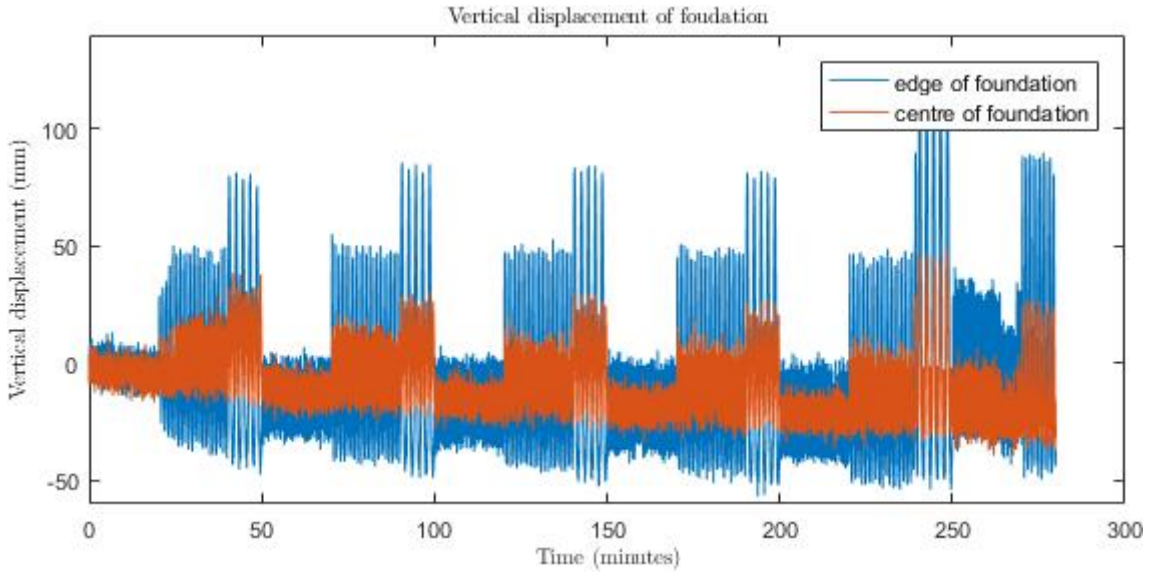

Figure 4.48: Settlement of the structure

The cyclic vertical movement at the centre of the foundation has increased from 10mm to 17mm from the first to the 5th phase of the normal phases of the test.

By 220 minutes the total settlement at the centre of the is 30mm, after this time the actuator starts to malfunction and the data becomes less reliable but is shown because it effects the frequency results.

Where as at the edge of the foundation cyclic vertical movement at 220 minutes has increased to 43mm. This shows towards the end of the test the foundation was still changing

the soil profile in the storm and gust phases of the test and the soil-foundation had not reached an equilibrium yet.

In the storm phases, where increased displacement is applied to the structure, increased uplift can be seen at the edge of the foundation, which is larger than the embedment similar to other tests.

Figure 4.49 shows the vertical movement of the foundation in the first storm phase in more detail. In Figure 4.49 the increase of the movement of the edge is noticeable, but it can also be seen that between 20 and 25 minutes the centre of the foundation uplifts once per cycle and after 25 minutes the centre of the foundation uplifts twice per cycle.

This shows that initially when the storm loading began the increase in the foundation movement is not symmetrical. It is possible that while the structure is being pushed away (positive displacement on Figure 4.45) from the centre by the actuator and the edge and the centre are uplifting simultaneously while the opposite edge of the foundation is embedding into the soil below. Then in the second half of the cycle where the structure is being pulled toward the actuator (negative displacement on Figure 4.45) the foundation edge is embedding into the soil, but the centre of the foundation is resting on the soil. In this time either the foundation is sliding a little in order cope with the structural rotation or the edge has been able to embed into the foundation more than in the first half of the cycle, keeping the soil in contact with the foundation at the centre.

From 20 to 25 minutes the edge of the foundation uplift and embedment increases with each cycle. After 5 cycles of storm displacement (25 minute mark on Figure 4.49) the behaviour changes again. The new behaviour shows the edge of the foundation uplifting and embedding consistent distances, with the edge at 80mm and the centre at 30mm per cycle.

The centre of the foundation uplift occurs with a maximum displacement in both the positive and negative displacement directions. This shows that the soil profile below the foundation is now more symmetrical, with the foundation now embedding on both sides. This behaviour is seen in the long break storm test with uneven uplift cycles at the centre of the foundation, although it is not in the short break storm test.

In the first gust phase (45 minutes) the centre uplifts 40mm but the centre of the foundation does not settle at an increased rate when compared to the previous storm phase. The edge of the foundation is moving 120mm and the edge is embedding 10mm more than it did in the storm phase, this is consistent in the gust phases until 241 minutes when the test was disrupted.

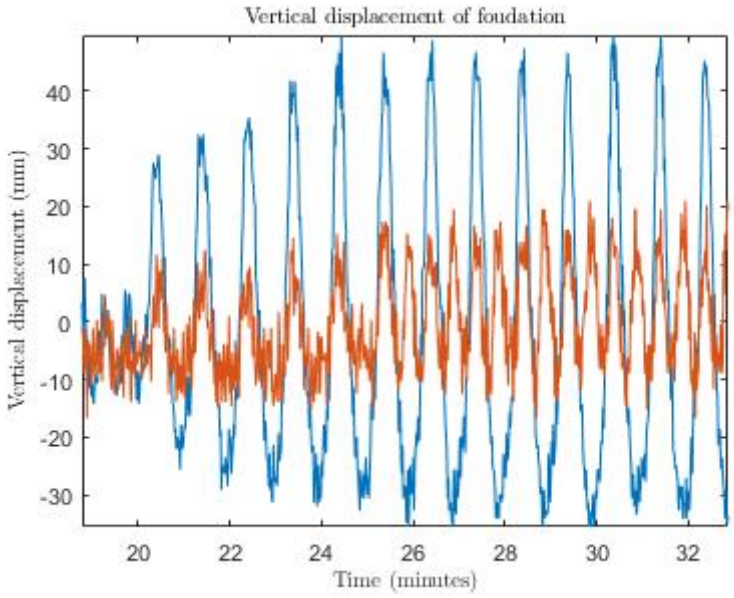

Figure 4.49: Settlement of the structure from 19 to 33 minutes

4.5.4.4 Settlement - rotation

The settlement - rotation are shown in Figures 4.50a,4.50b, and 4.50c. Figures 4.50a and 4.50b display the five phases of the normal and storm cyclic displacement, whereas Figure 4.50c has only 4 phases of the gust cyclic displacement due to the actuator malfunctioning in the 5th gust phase.

Figure 4.50a shows that in cycles 1-40 there no uplift due to the flatness of the results, it does show the structure is undergoing settlement which is similar to that seen in the baseline test. The second phase of normal displacement (cycles 66-105) uplift begins to occur and this continues in the third phase (cycles 131-170) and fourth phase (cycles 196-235). In the 5th phase (cycles 261-300) appear to have a more consistent uplift of 2mm at -0.5° and 0.35°.

Figure4.50b shows the first phase (cycles 41-60) with a changing behaviour in the negative rotation which has two different vertical movements, one where the foundation remains level and the second where the foundation uplifts. This is caused by a changing soil profile, which appears to be a dramatic change in the soil because it is not a slow change cycle by cycle but rather an sudden failure or change in the soil below the foundation. This behaviour is not seen in the short break storms or the long break storm tests.

The foundation uplift in the storm phases of up to 26mm of uplift in the 3rd (cycles 236-255) and 4th (cycle 301-320) storm phases at 0.8°. Showing the soil profile is easily adaptable to allow the structure to embed and deform the soil.

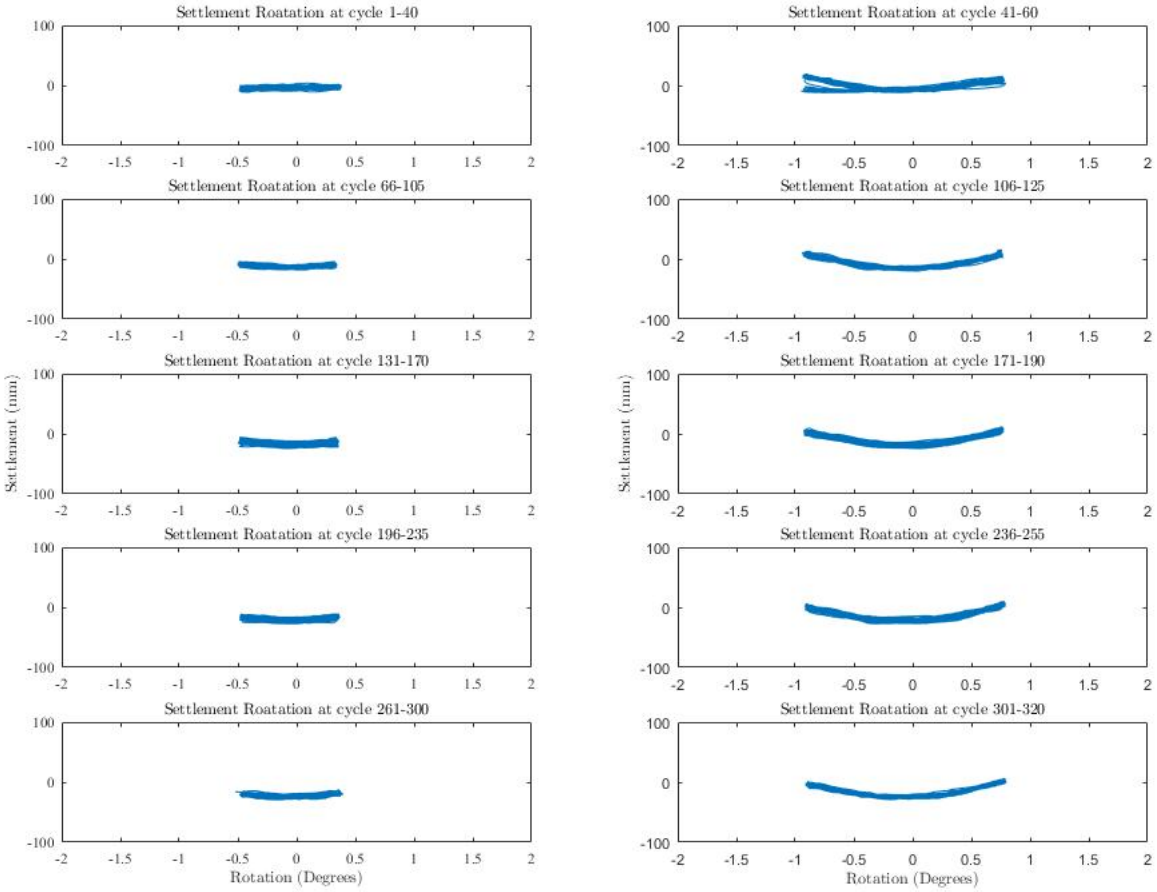

(a) Normal phase

(b) Storm phase

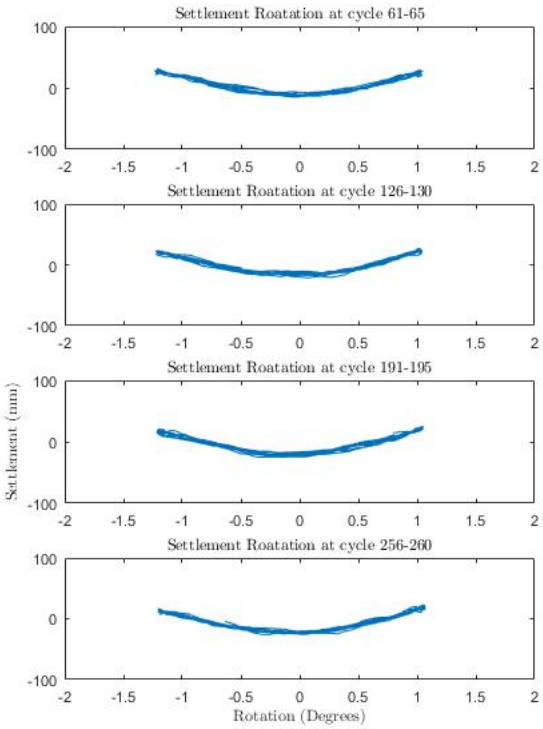

(c) Gust phase

Figure 4.50: Settlement - rotation, phases 1, 2, 3, 4 and 5 of the gust storm test

Figure4.50b shows the first phase (cycles 41-60) with a changing behaviour in the negative rotation which has two different vertical movements, one where the foundation remains level and the second where the foundation uplifts. This is caused by a changing soil profile, which appears to be a dramatic change in the soil because it is not a slow change cycle by cycle but rather an sudden failure or change in the soil below the foundation. This behaviour is not seen in the short break storms or the long break storm tests.

The foundation uplift in the storm phases of up to 26mm of uplift in the 3rd (cycles 236-255) and 4th (cycle 301-320) storm phases at 0.8°. Showing the soil profile is easily adaptable to allow the structure to embed and deform the soil.

Figure 4.50c shows consistent uplift of 40mm in each of the four gust phases of the test, this shows the foundation could manipulate the soil from the start of the first gust phase (cycle 61), and that the storm phase previously had altered the soil profile enough to allow for easier embedment of the foundation in the gust phases.

4.5.4.5 Force - rotation

The force - rotation loops are shown in Figures 4.51a, 4.51b and 4.51c. In Figure 4.50a it shows the 5 normal phases of displacement, in the first phase (cycles 1-40) where the maximum rotation is also the maximum positive force required of 1860N. The loops is slim in shape as the maximum negative force (2110kN) is also the maximum negative rotation.

The second phase (cycles 66-105) required less force to reach maximum rotation, which changed the shape of the loop from long and slim to shorter and slightly wider.

The third normal phase (cycles 131-170) is similar to the second, while the 4th normal phase (cycles 196-235) has changed shape to where the maximum forces required occur before the maximum rotations. Which shows that the changes to the soil below the foundation are now affecting how the structure is horizontally loaded.

In the 5th normal phase (cycle 261-300) the shape of the loop has changed to the maximum positive and negative required forces at 0.05 and 0.1, so when the structure is near the centre. The maximum positive and negative rotations occur when the force required is at 0kN, which shows that the structure requires more force to initially move it from 0°.

In the normal phases of this test there is a very obvious flattening of the angle of the displacement. This appears to most prominent in the normal phases of the cyclic displacement, and a little in the storm displacement phases but it does not seem to have such an effect during the gust displacement. The flattening represents the reduction in force required for the same rotation, and is an indexation of rounding below the foundation.

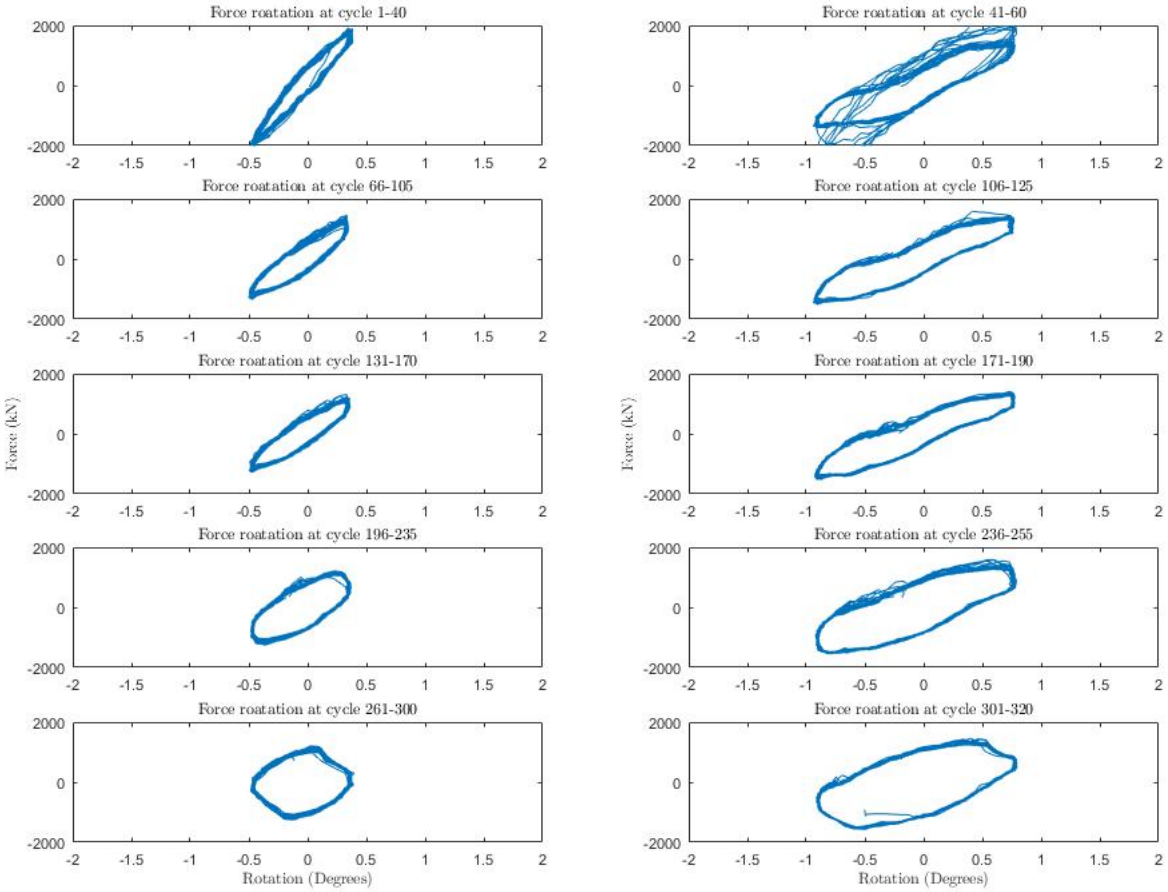

(a) Normal phase

(b) Storm phase

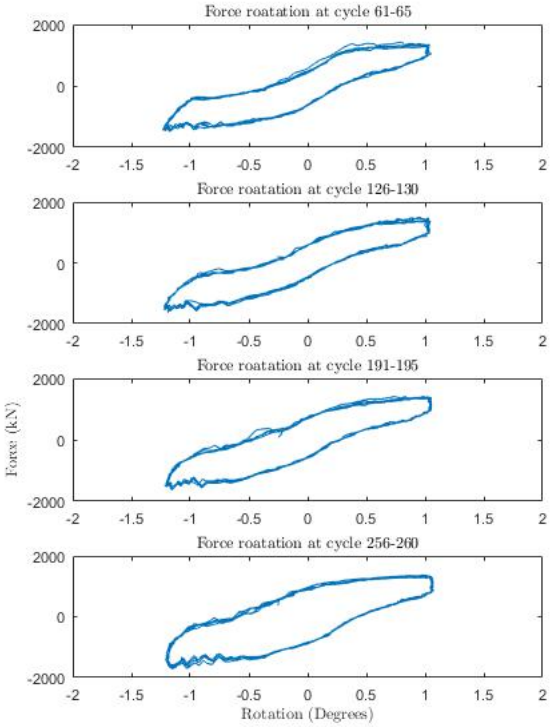

(c) Gust phase

Figure 4.51: Force - rotation, phases 1, 2, 3, 4 and 5 of the gust storm test

In Figure 4.51b the loops in the 1st, 2nd and 3rd storm phases are similar in shape with maximum required forces occur with maximum rotations. The 4th storm phase (cycles 236-255) continues with the maximum rotations and required forces occurring together but the shape of the loop has changed and is wider. In the 5th storm phase (cycles 301-320) the shape has changed again to become more rounded shape where the maximum force required occurs before the structure reaches the maximum rotations. This could indicate that the soil profile has changed so much that once the structure reaches $\pm 0.5^{\circ}$ the structure no longer requires an increasing force, but the soil profile allows the structure to continue rotating.

Figure 4.51c shows four gust phases, the first gust phase (cycle 61-65) loop is similar is shape to a drawn out 's', the top and bottom of the 's' are where the required force has reached a maximum, but the structure is still rotating. The second gust phase (cycle 126-130) is similar to the first gust phase, while the third gust phase (cycles 191-196)

4.5.4.6 Soil-foundation contact

Figures 4.52a, 4.52b, and 4.52c present the pressure sensor data from under the foundation, which has been amplified by 100,000 in order for it to be on a similar scale to the vertical movement data taken from the edge of the foundation.

In figure 3.58 the blue line is the data from the pressure sensor in the normal phases of cyclic displacement, while the orange line is the vertical movement data from the edge of the foundation.

Figure 4.52b shows that initially in cycles 1-6 the pressure between the edge and the centre of the foundation changes, which shows the foundation is uplifting enough to remove pressure off the foundation that when the pressure is near 0 the foundation and soil are not in contact which is corroborated with the edge of the foundation vertical movement as being a period where that section of the foundation was uplifting.

By cycle 66 the foundation uplifting is well established and so to is the pressure only being recorded when the foundation is at -0.3mm or less, this progresses to the pressure being removed from the sensor at -0.5mm or less by cycle 196 and the time between the soil-foundation contact has increased from 0.0117 minutes in cycle 3 to 0.25 minutes in cycle 68, and then to 0.3 minutes in cycles 134, 198, and 263.

The sensor at the edge of the foundation which is also right below the LVDT which measured the vertical movement at the edge of the foundation can be seen in Figure 4.52c. At the start of the test cycles 1-6 even though there is movement at the edge of the foundation it is not enough to remove the pressure from the sensors, so therefore there is continuous soil-foundation contact(maybe there is no contact because the sensor at $1/4$ is in contact and shows a change in pressure). From cycle 66 the recorded pressure changing with the movement of the edge of the foundation.

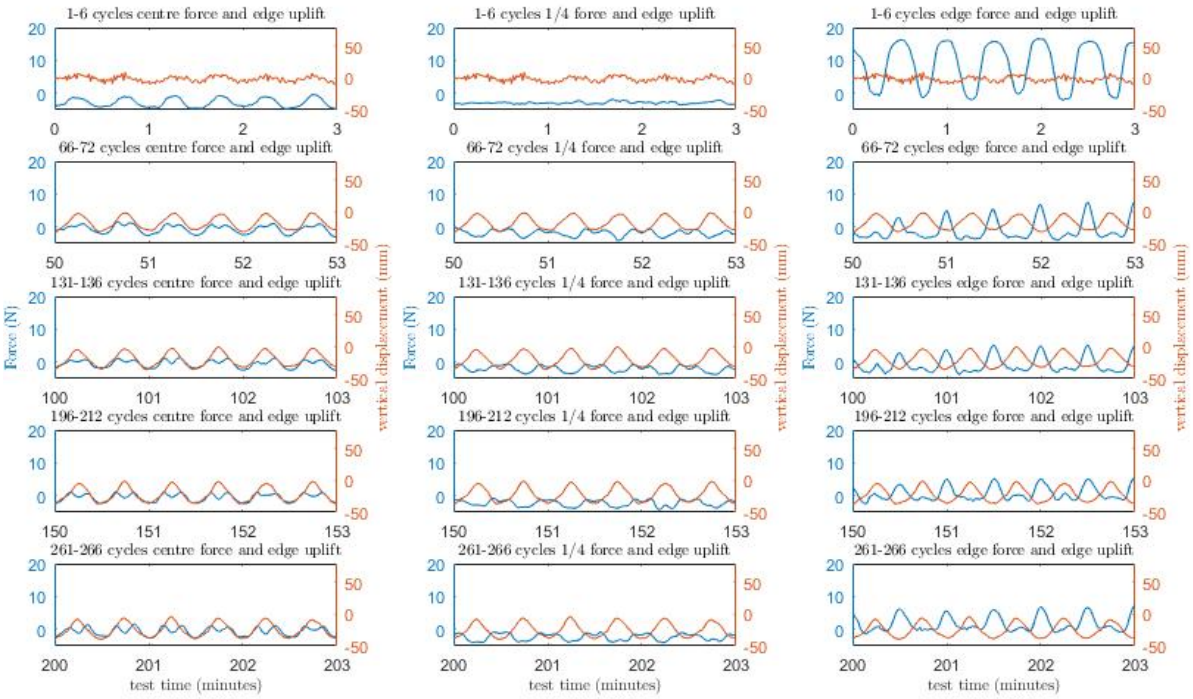

(a) Centre **(b)** Half way **(c)** Edge

Figure 4.52: The contact force between the foundation and the soil, and the vertical movement from the edge of the foundation, during the normal phases

During the storm loading the structure is displaced further and therefore the foundation has a larger vertical movement. The effect this has on the changes in foundation contact can be seen in Figure 4.53c, at cycle 41 (the first storm displacement) the pressure does not change throughout the cycle. At cycle 106; which is the start of the second phase of storm loading, when the foundation is uplifting the pressure reading is a plateau whereas when the foundation is embedding the pressure increases before decreasing below the plateau reading then increase and decrease into the plateau level could be due to the sensor being over loaded as the pressure sensor used does not read negative pressures. This also occurs in the gust loading phases which are shown in Figure 4.54c.

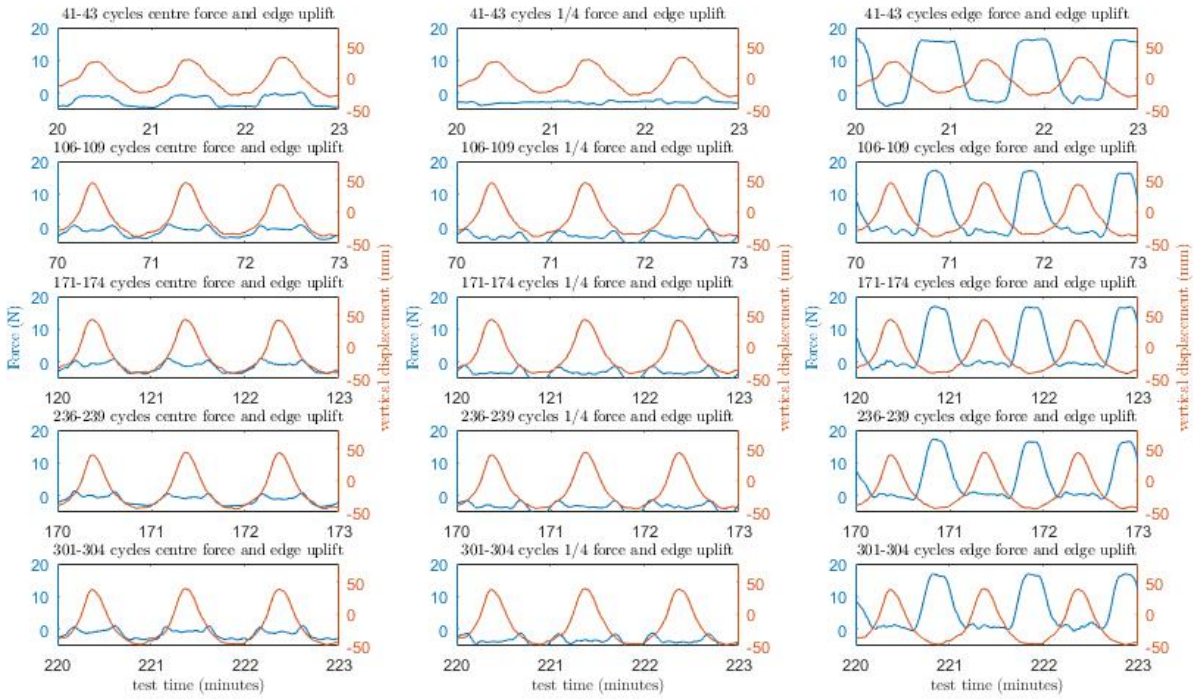

(a) Centre **(b)** Half way **(c)** Edge

Figure 4.53: The contact force between the foundation and the soil, and the vertical movement from the edge of the foundation, during the storm phases

In Figure 4.53c there are 3 cycles displayed in the 3 minute window, which all come from the start of the phase of displacement. The soil-foundation contact time remains steady though out the test at around 48 seconds which in contrast to Figure 4.52c where the soil-foundation contact time is increasing with cyclic displacement. Although neither of these situations are occurring in Figure 4.54c when the gust cyclic displacement is happening, the soil-foundation contact time is initially 75 seconds at cycle 81, whereas by cycle 276 the soil-foundation contact time is 69 seconds.

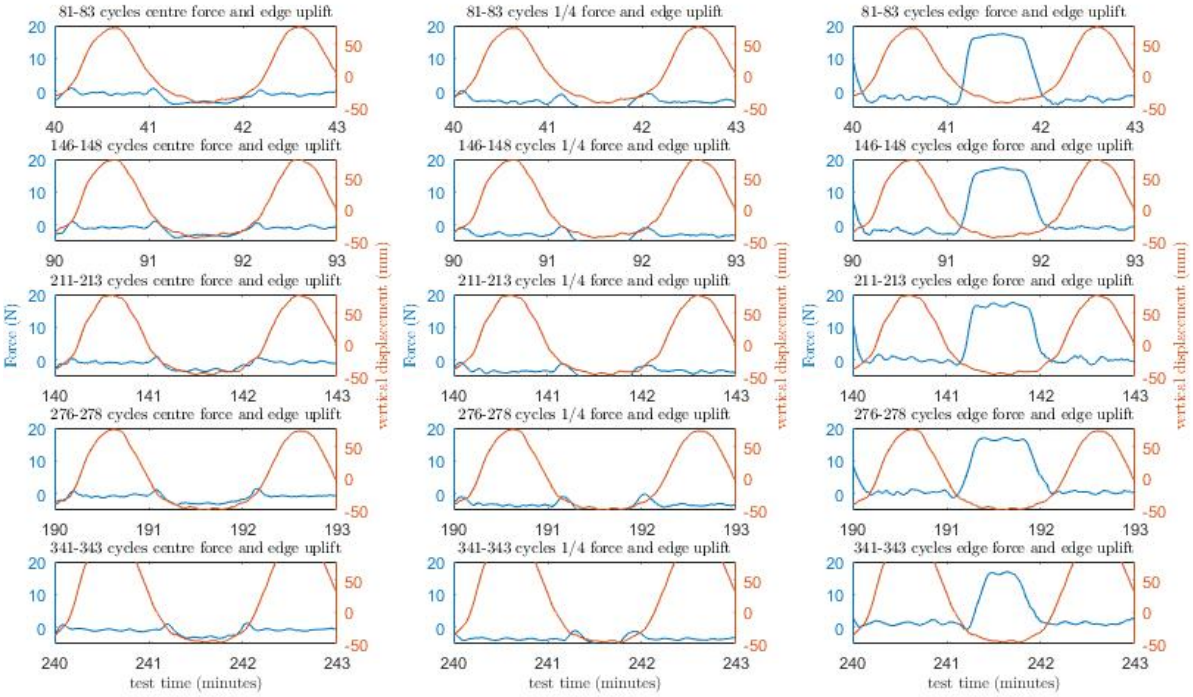

(a) Centre **(b)** Half way **(c)** Edge

Figure 4.54: The contact force between the foundation and the soil, and the vertical movement from the edge of the foundation, during the gust phases

4.5.4.7 Free vibration response

The results from the free vibration test can be seen in Figure 4.55. The results from before the application of cyclic displacement are shown in blue and there is only one well-defined full cycle, with a frequency of 7.49Hz (0.13s period).

The results from after the application of cyclic displacement are shown in orange and the response has a frequency of 7.72Hz. This is only a difference of 0.23Hz (0.004 seconds), showing the frequency has not changed much post cyclic displacement. However, the damping of the structure after the cyclic loading is significantly decreased. The structural response shows 3.5 cycles compared to only one before the start of the test. This is likely because following the severe cyclic displacement, the structure is less stable and able to rock more easily.

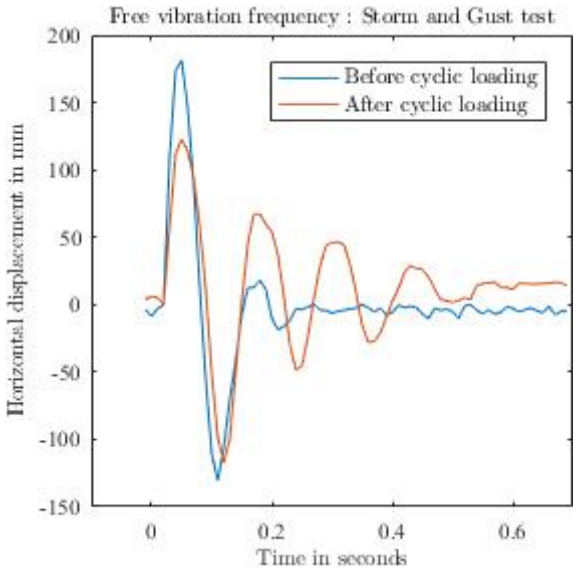

Figure 4.55: Free vibration test of the structure at the start and end of cyclic displacement

The free vibration frequency is affected by the number of cyclic loads which can be seen in Figure 4.46. This figure shows the frequency constantly decreasing with additional cyclic displacements but there is also defined change in frequency between 684 cycles and 1312 cycles from 5.5hz to 3.6hz.

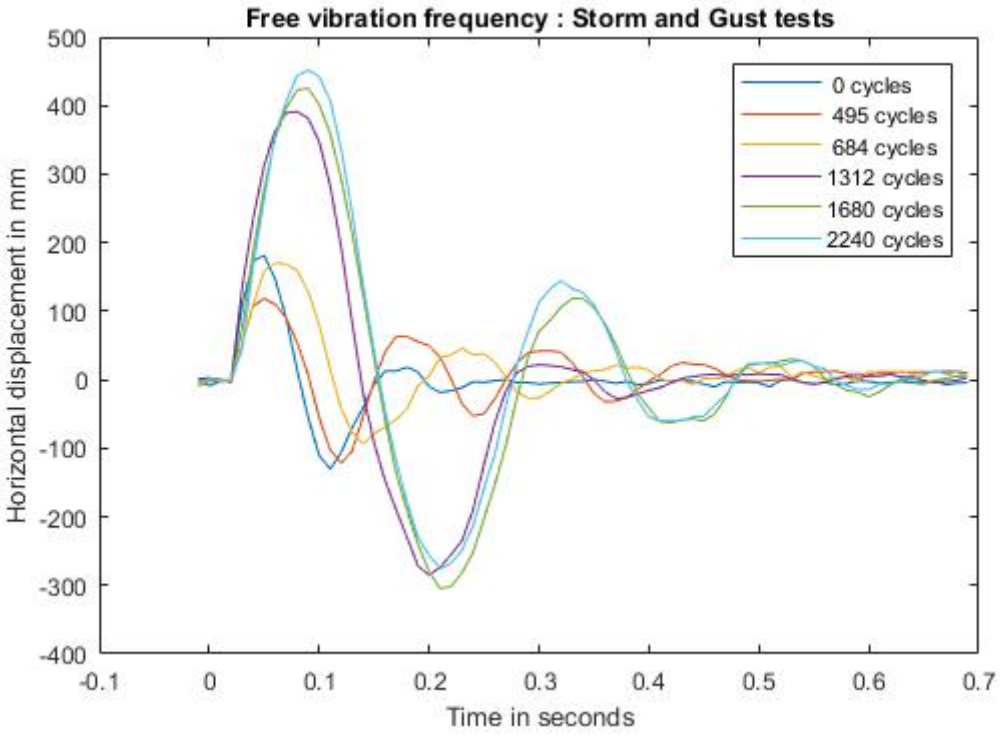

Figure 4.56: Frequency of the structure in between the re-setting of the gust storm test

4.5.5 Exaggerated Displacement

In this test a larger cyclic displacement of 600mm was applied to the structure, in order to obtain an extreme response.

4.5.5.1 Displacement - time

The horizontal displacement applied to the structure is shown in Figure 4.57.

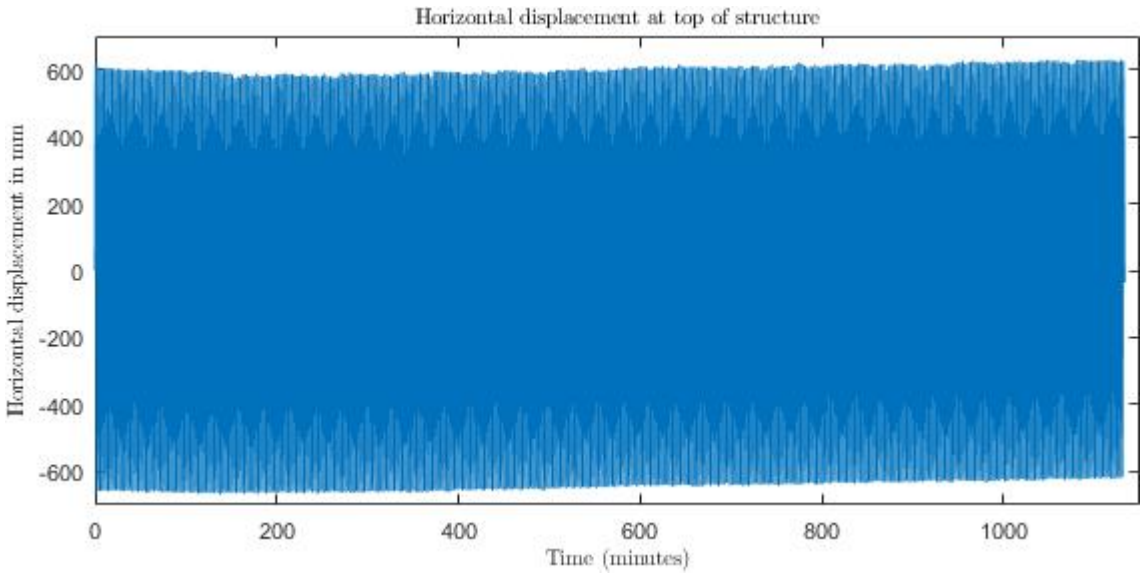

Figure 4.57: Displacement at the top of the super structure

4.5.5.2 Horizontal force - time

The force required to displace the structure can be seen in Figure 4.58. At the start of the test the force required is +1360kN to -960kN but after 75 minutes the negative force begins to increase and by 200 minutes plateaus at -1160kN. The positive force increases from 1360kN to 1475kN around 135 minutes into the test.

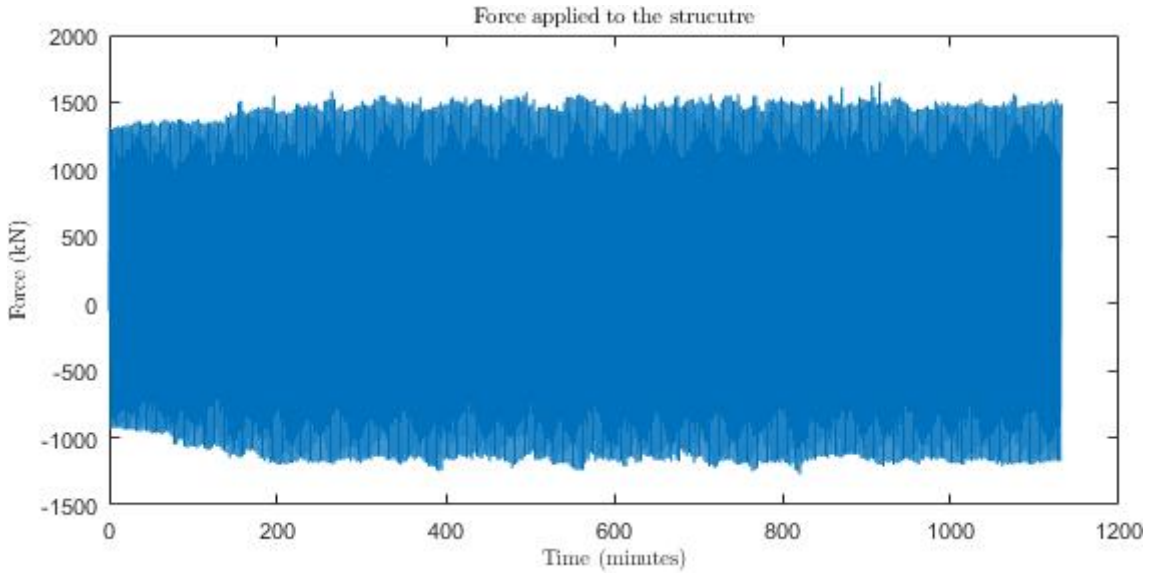

Figure 4.58: Horizontal force required to displace the structure - time

4.5.5.3 Settlement - time

The settlement at the edge (blue) and centre (orange) of the foundation can be seen in Figure 4.59. The settlement is linear throughout the test and a total of 25mm occurs at the centre by the end of the test. The centre of the foundation also uplifts, in the first 10 minutes this uplift is 90mm but by 20 minutes into the test this has reduced to 80mm and remains constant for the rest of the test. No embedment occurs at the centre throughout the test. The reduction in uplift of the centre of the foundation at the start of the test coincides with the edge of the foundation embedding more into the soil. The uplift of the edge of the foundation is significant and is constant throughout the test.

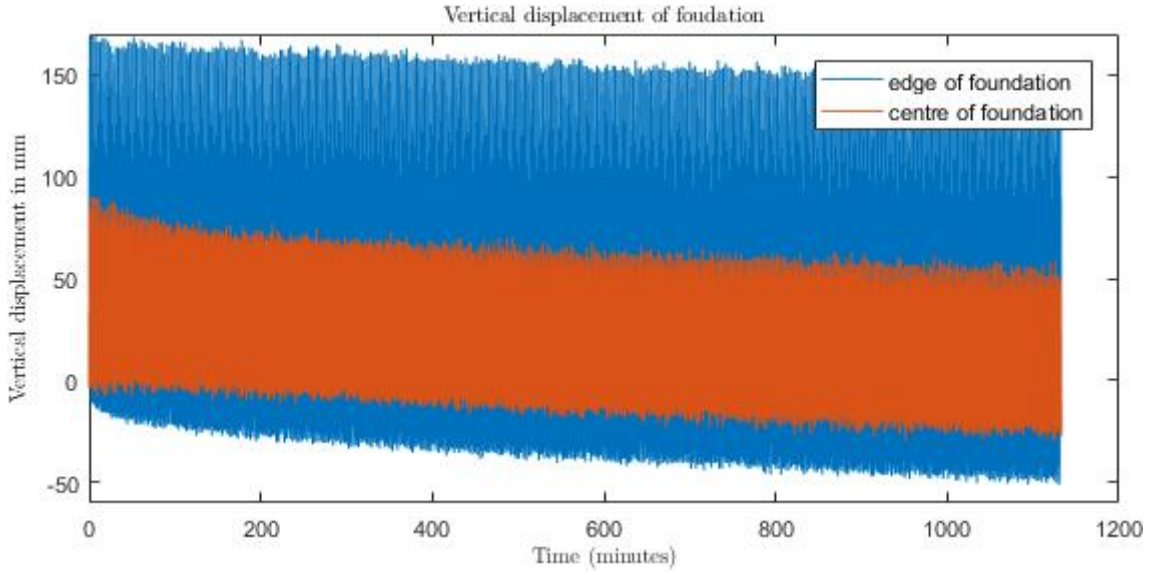

Figure 4.59: Vertical movement of the foundation centre and edge

4.5.5.4 Settlement - rotation

Figure 4.60 shows the settlement - rotation results, segmented into 4 sections of the test (cycles 1-8, 168-175, 335-342 and 501-508). During cycles 1-8 the uplift is 90mm on the negative rotation whereas it is 72mm on the positive rotation. By cycle 168 the uplift is even the positive and negative rotation as the rotation is now 65mm. This stays even until cycle 501 where the positive rotation uplift is 5mm more than the negative.

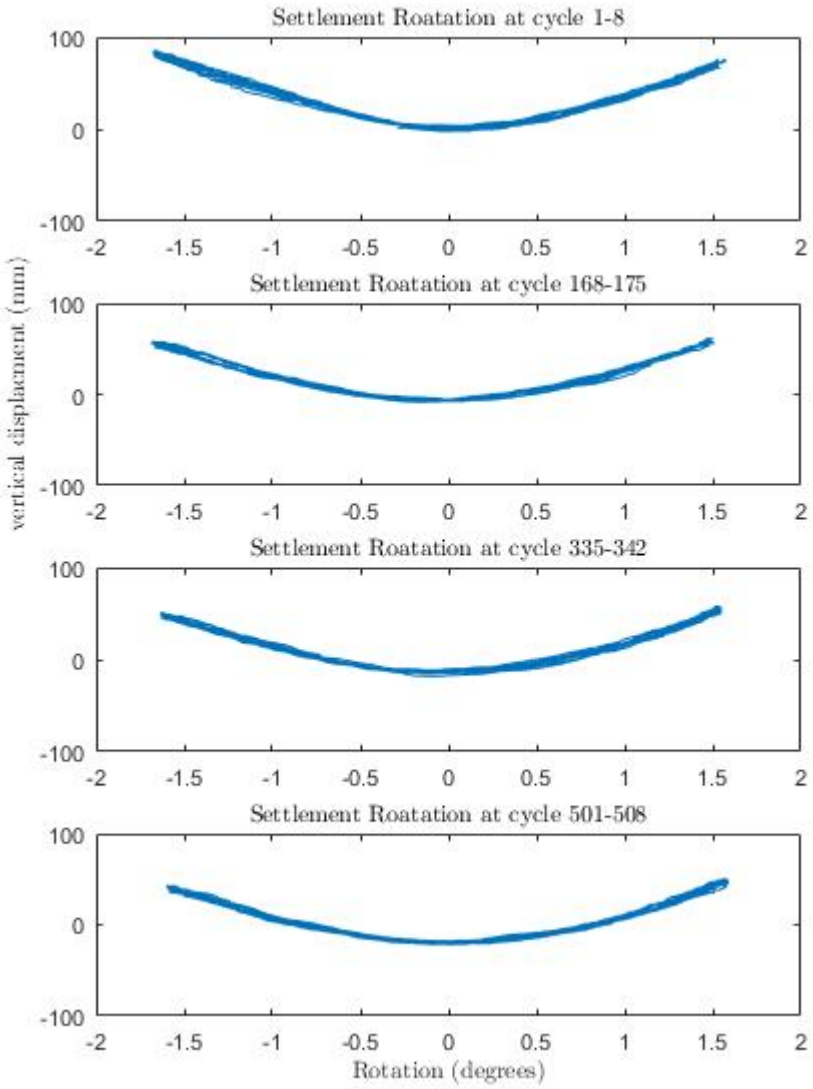

Figure 4.60: Settlement - rotation of the structure during the exaggerated test at cycles 1-8, 168-175, 335-342 and 501-508

4.5.5.5 Force - rotation

Figure 4.61 shows force against rotation for the same four points in the test (cycles 1-8, 168-175, 335-342 and 501-508). At the start of the test the rate of increase of the force is highest around 0°. The force required to rotate the structure away from the centre and

the force required to bring the structure back to the centre is similar. As the test continues, the loop widens, with the force at 0° increasing from 90kN in cycle 1-8 to 500kN in cycle 167-175, 875kN in cycle 335-342 and 1350kN in cycle 501-508. The shape of the loop changed which shows that it takes less force to rotate the structure from 0° as the cyclic displacement continues.

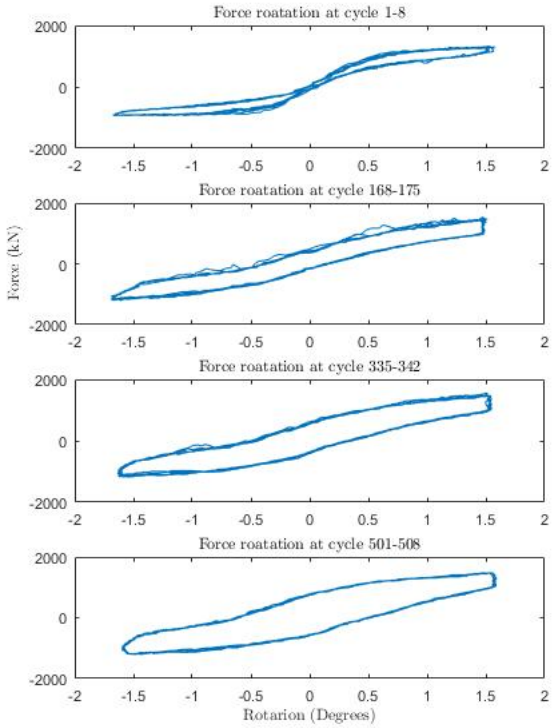

Figure 4.61: Force - rotation of the structure during the exaggerated test at cycles 1-8, 168-175, 335-342 and 501-508

4.5.5.6 Free vibration response

The results from the free vibration tests before and after the cyclic displacement can be seen in Figure 4.62. The frequency before the cyclic displacement is 6.6Hz and after is 4.65Hz. Before the cyclic displacement there appears to be more damping, as the structural responds with one full cycle, whereas after the cyclic displacement the number of cycles increases to 1.5. The exaggerated displacement has caused the soil-structure interaction to change but no more than any of the previous tests.

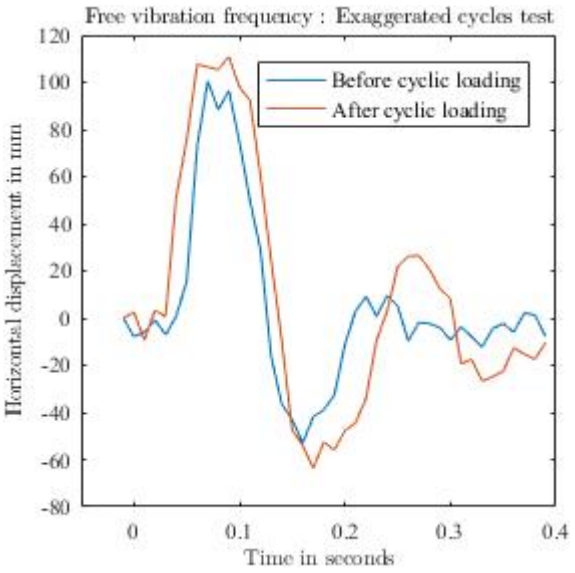

Figure 4.62: Free vibration test of the super structure at the start and end of cyclic displacement

4.6 Discussion

4.6.1 Free vibration frequency

The frequency at the start and the end of each test is shown, and in all tests they free vibration frequency changes, which shows that the cyclic displacement also changes the soil structure interaction. As it is already acknowledged that with time the frequency of a structure will change and that the wind turbines must be designed to be flexible within the soft soft, soft stiff and stiff stiff zones of the frequency to avoid conflicting with P1 and P3 frequencies. this does not add much to what was already known. The rate of change in the frequencies.

The frequency decreases with the change in the soil-structure interaction, as can be seen in short break storm tests, the wavelength of the post cyclic frequency is increased by a third and there is a clear second frequency cycle although diminished. Whereas in the pre-cyclic displacement free vibration frequency test there can only really be one cycle noticed before the noise of the instruments over take the recoding and the response is complete by 0.2 seconds where it is closer to half a second in the post cyclic test response.

The baseline test does not show similar outputs of data, although the wave length is very marginally increased, the number of cycles recorded are far less in the post cyclic test free vibration frequency test when compared to the frequency test that occurs before any cyclic displacement. Which may show that light cyclic displacement such as the 'normal' 150mm cycles are not causing the significant change to the soil structure interaction but it is in fact the larger 300mm and 400mm cycles which represent storms and gusty weather.

The issues with this style of test in this 1g physical series is that before the test starts cyclic displacement is being applied to the structure and this could change in a very small way the soil below the foundation, although this was thought not to cause issue because the displacements occurring from the frequency test are minor in comparison to the displacements in the cyclic displacement test. The test also requires the person conducting the test to use the same force each time the structure is struck.

Using the same person and the same weight (a D-clamp that was also used to keep the force actuator in place), a gentle tap seemed sufficient for a recording. An increase in force would relate to a higher amplitude, but it would not record the damping that is occurring differently. Such as in the baseline test 3 attempts of frequency tests are show which demonstrates different amplitudes but the same general pattern of frequency occurring.

4.6.2 Force required per cycle of displacement

To gain further insight into the changes in force required to produce displacement, the force required to displace the structure in each cycle is plotted for a number of sets of phases throughout each test. This is the total positive and negative force involved in the displacement cycle. The start and end of each phase is logged around any change in displacement amplitude. Which will mean that between test the phases are on differing amount of cycles at the start.

Figure 4.63 shows data from the long break storm test. The force data is plotted from the last 10 cycles of each normal phase, through the storm phase and for the next 25 cycles of the following normal phase. For all the normal phases the force starts fairly constant, then with the increase in displacement amplitude in the storm phases the force required increases which is the start of the amplitude behaviour. As the cycles continue at this higher magnitude displacement, the force required decreases and the structure moves more easily; this is most notable in the 1st and 3rd phase. When the displacement amplitude drops to the next normal phase, the force required significantly drops but as the cyclic displacement continues the force required gradually increases, which is part of the recovery behaviour.

The main difference in behaviour over the duration of the test is that the overall force required for each cycle of displacement reduces with the number of cycles applied. In this test in particular it is very clear that each set of phases shown requires less force than the once previously. The reductions in required force occurs at a higher rate at the start of the test than towards the end of the test.

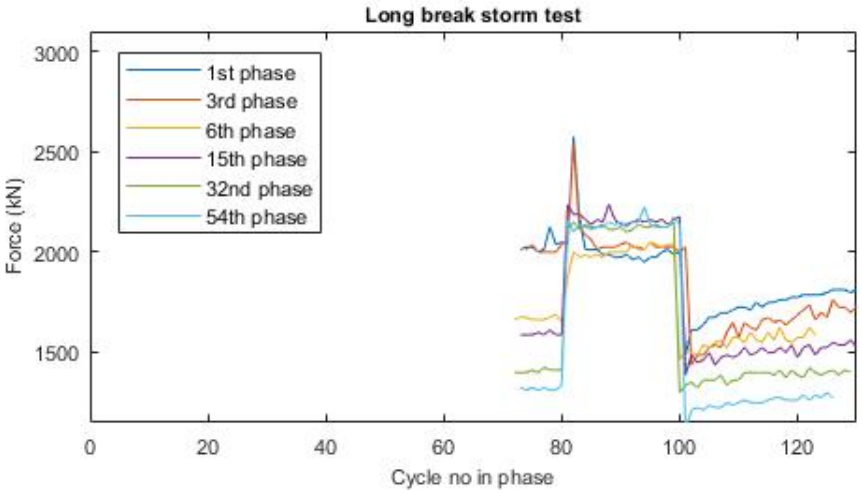

Figure 4.63: The combined force required per cycle to displace the structure during the long break storm test

Figure 4.64 displays 7 sets of phases from the short break storm test, in a similar way to Figure 4.63. The data shows an overall pattern of constant behaviour, then amplitude behaviour when the displacement amplitude increases which levels off into a constant behaviour. Which leads into a recovery behaviour when the displacement amplitude decreases.

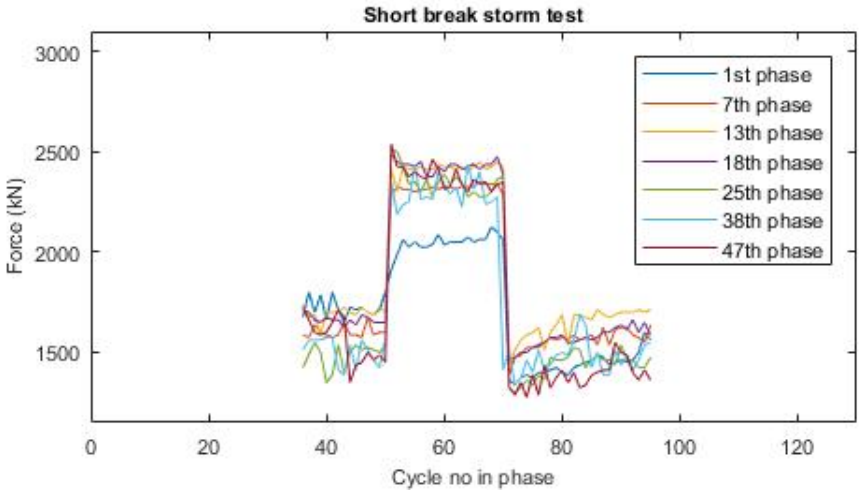

Figure 4.64: The combined force required per cycle to displace the structure during the short break storm test

Figure 4.65 displays the change in force from phase 2-5 in the Gust storm test. The First phase is shown in full in Figure 4.66 and is significantly higher than the rest of the test. Each round of cyclic behaviour displays a small decrease in the required force to displace the structure. The start of the storm phase is at cycle 40 and the start of the gust phase is at cycle 60, for both of these increases in displacement the force required increases substantially before a small decrease with each cycle. At cycle 65 the gust phase finishes and the normal phase beings the force required have a significant drop from 2800kN to 2000kN, which is 400kN less than before the start of the storm phase. There is rebounding of the force required and with additional cycles the force required increases, with each additional phase the rebounding is not as effective.

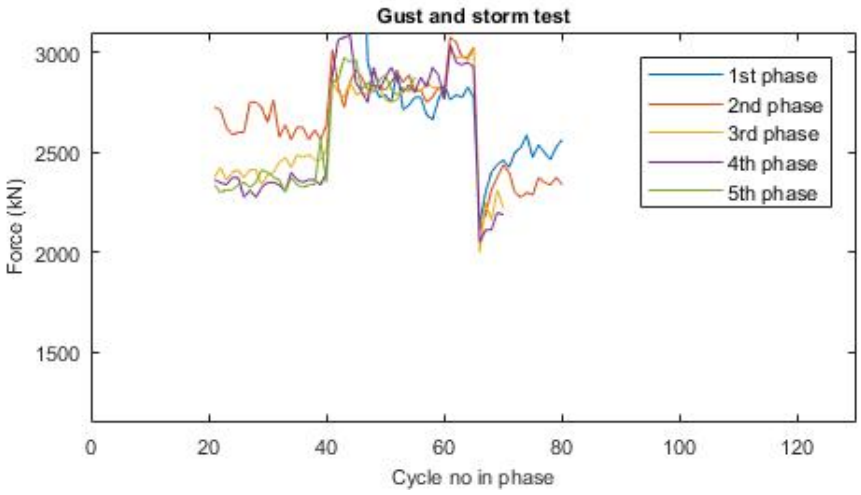

Figure 4.65: The combined force required per cycle to displace the structure during the gust and storms test, not including the first phase

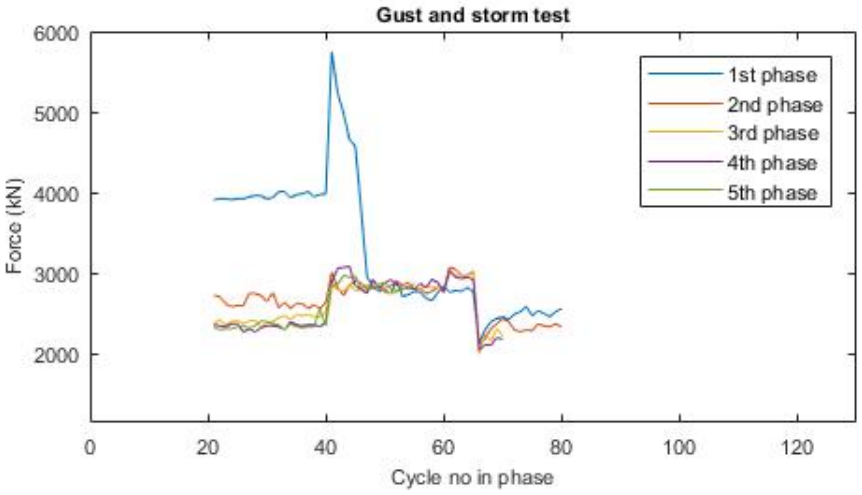

Figure 4.66: The combined force required per cycle to displace the structure during the gust and storms test, including the 1st phase

4.7 Behaviours

There are 5 notable and repeatable behaviours that occur in with the testing. These behaviours depend on the displacement that is occurring and the changes in the amplitude of the displacement. The behaviours can be divided into main behaviours and initial behaviours.

The main behaviours are the *constant behaviour*, *amplification behaviour* and *recovery behaviour*. These three behaviours are always present when two or more different amplitudes of cyclic displacement are applied. If the initial behaviours are present they will be exclusively at the start of the tests. Once the main behaviours have occurred the initial behaviours will not reappear.

4.7.1 Initial behaviour

The initial behaviour occurs at the very start of the testing and is an uneven response to the sinusoidal cyclic loading. The soil below the foundation is starting to be deformed due to the foundation rotation and embedment, but it is not symmetrical to both sides of the foundation. This is represented by the diagrams in Figure 4.67. This behaviour is possibly due to the very first movement causing the structure to embed into the soil and then the second half of the displacement (when the structure moves from +150mm to -150mm) does not cause the same response below the foundation.

The unevenness in structural rotation is best seen in the foundation vertical displacement data. In Figures 4.68a, 4.68b, 4.68c and 4.68d this can be seen as the centre of the foundation is expected to lift up twice per cycle (which is half a minute long). What actually occurs is the centre of the foundation only uplifts once per cycle. In the majority of tests the centre of the foundation uplifts with the positive displacement, apart from in the long break storm test (Figure 4.68d) where the centre of the foundation uplifts during the negative displacement.

The initial behaviour is proceeded by either constant behaviour when the soil below the foundation has a symmetrical soil profile, or the initial amplitude behaviour or amplitude behaviour.

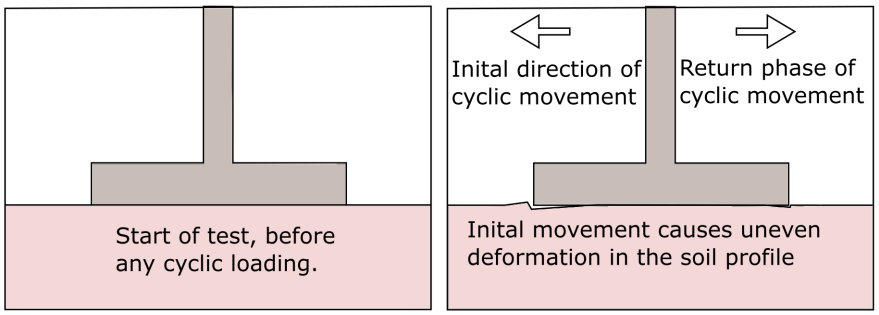

Figure 4.67: The initial movement of the structure and effect on the soil profile

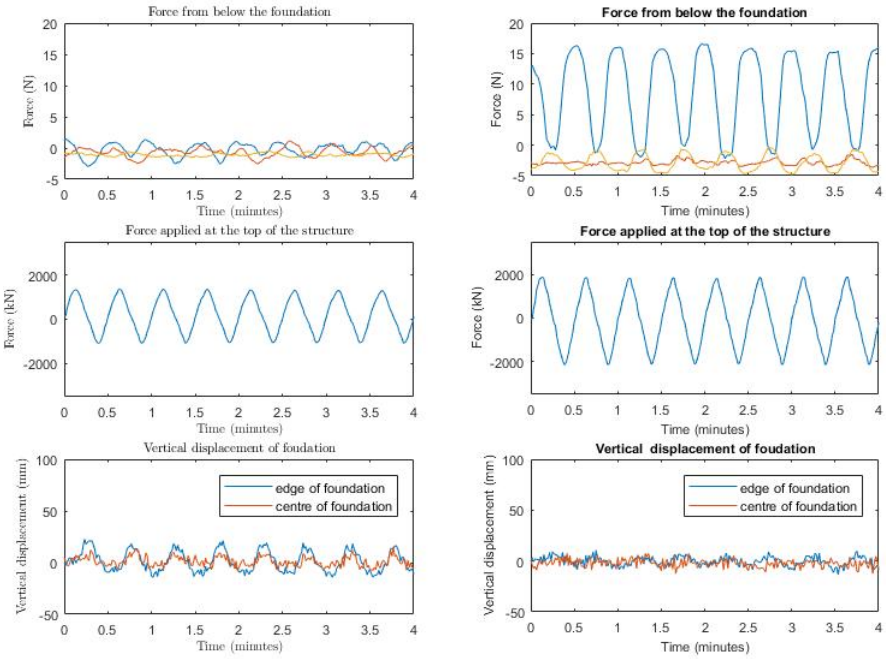

(a) Start of the baseline test, data from the force sensor under the foundation, the force required to displace the structure and the vertical movement of the foundation

(b) Start of the gust test, data from the force sensor under the foundation, the force required to displace the structure and the vertical movement of the foundation

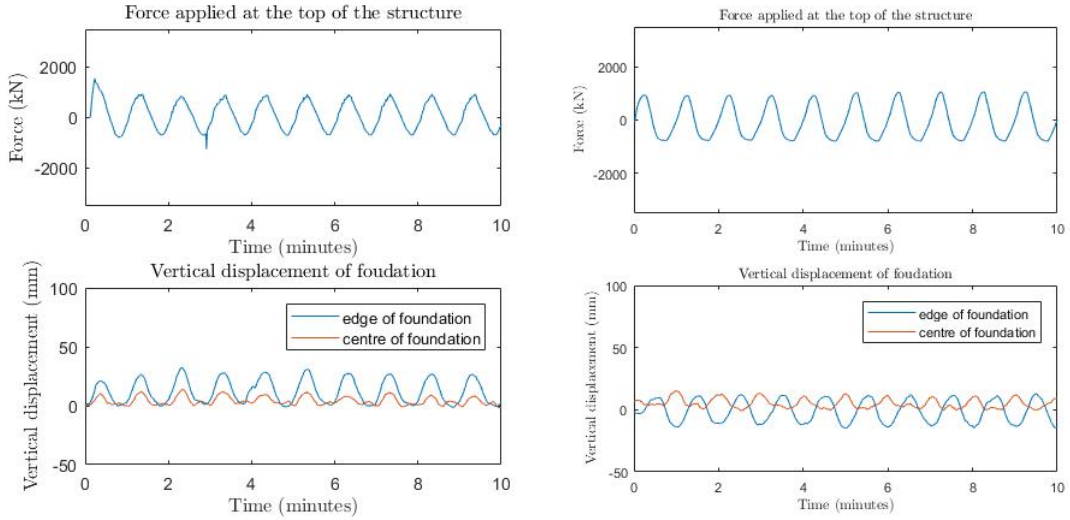

(c) Start of the short break storm test, the force required to displace the structure and vertical movement of the foundation

(d) Start of the long break storm test, the force required to displace the structure and vertical movement of the foundation

Figure 4.68: Initial behaviour

4.7.2 Initial Amplification Behaviour

The initial amplification behaviour (Figure 4.69) occurs only once in a test which has a minimum of two different applied displacements. This behaviour follows on from the initial behaviour, a continuing of the uneven behaviour and the larger displacement evens out the soil profile.

The increase in displacement amplitude results in an increase in the force required for the displacement, but this force is not constant, it is highest at the start of the increased embedment into the soil with the foundation. In Figures 4.70a and 4.70b the force can be seen to increase with the increase in displacement. In Figure 4.70b the foundation vertical displacement at the centre of the foundation can been seen to uplift twice in 60 seconds, but it is still uneven with the centre of the foundation uplifting more when the right hand edge is embedding than lifting up.

The end of the initial amplification behaviour is only when the reactions of the structure and soil are even through out the cycle, which is the constant behaviour. If the behaviour has not become constant it may skip to recovery behaviour when the displacement amplitude decreases.

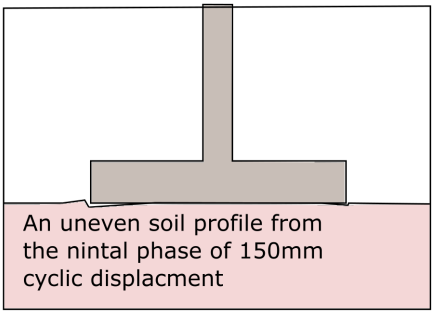

Figure 4.69: The initial amplification behaviour and the effect on the soil profile

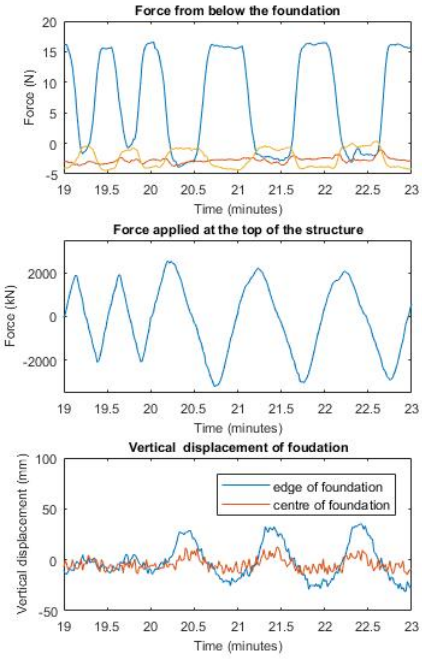

(a) The start of the first storm phase in the gust storm test, data from the force sensor under the foundation, the force required to displace and vertical movement of the foundations

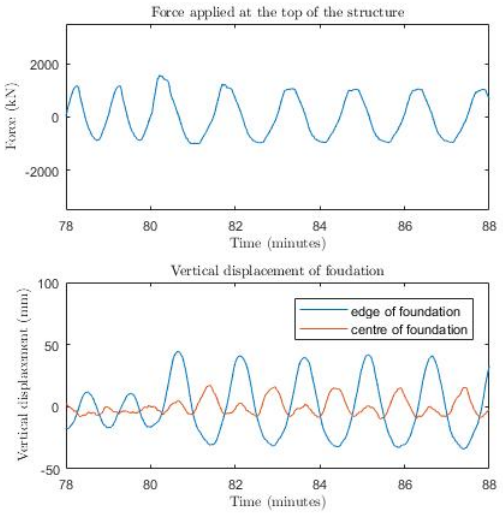

(b) The start of the first storm phase in the long break storm test, the force required to displace and vertical movement of the foundations

Figure 4.70: Initial Amplitude Behaviour

4.7.3 Constant behaviour

The constant behaviour is when repetitive cyclic displacement causes even rotation in each direction, embedment and formation of a symmetrical soil profile . Changes that can occur during this behaviour is settlement of the structure, as shown in Figure 4.71.

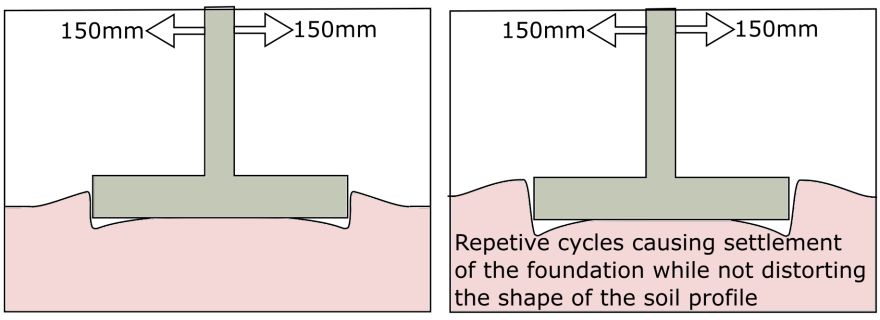

Figure 4.71: The constant phase of movement, causing settlement without affecting the soil profile

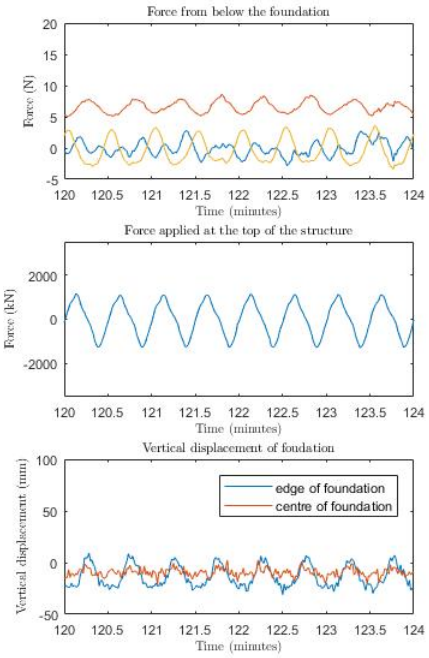

(a) The baseline test, data from the force sensor under the foundation, the force required to displace and vertical movement of the foundations

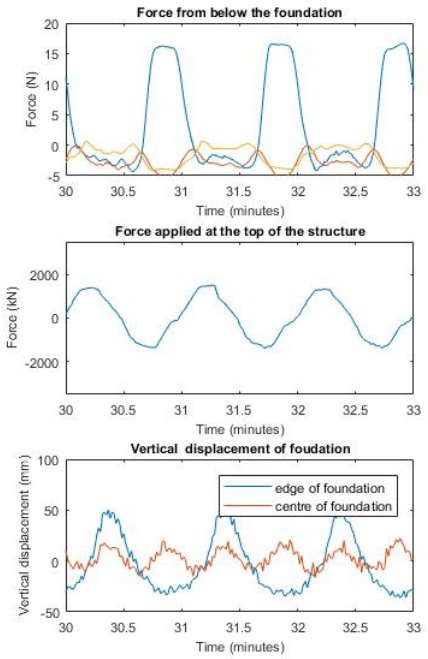

(b) The gust test, data from the force sensor under the foundation, the force required to displace and vertical movement of the foundations

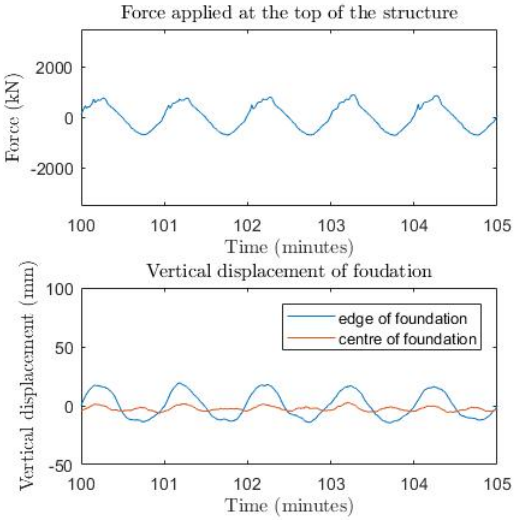

(c) The short break storm test, the force required to displace and vertical movement of the foundations

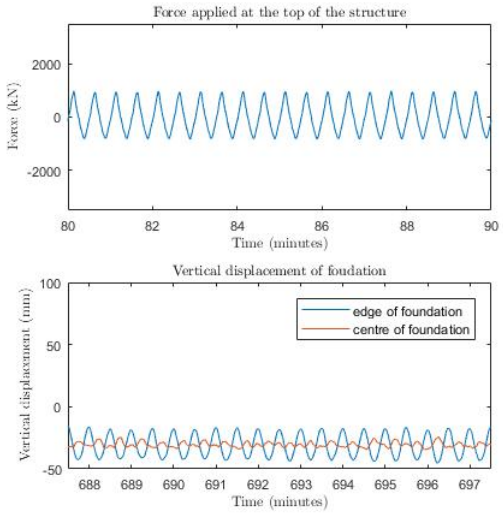

(d) The long break storm test, the force required to displace and vertical movement of the foundations

Figure 4.72: Constant Behaviour

4.7.4 Amplification behaviour

The amplification behaviour occurs during extreme loading (storm and gust phases), when the displacement amplitude increases. Figure 4.73 shows the increase in displacement amplitude leads to a change in the soil profile where the contact between the soil and the foundation

is reduced. The response is symmetrical, with significant uplift, even at the centre of the foundation and there is also an increase in overall settlement.

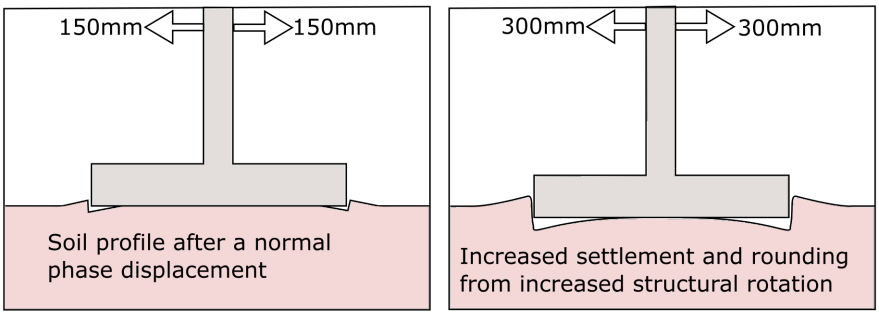

Figure 4.73: Amplification behaviour and effect on the soil profile

The vertical movement of the foundation is symmetrical during the increasing displacement, which is evident in the vertical movement of the centre of the foundation which is uplifting to it maximum with both edges of the foundation also reaching their maximum, this is noticeable in Figures 4.74a and 4.74b.

Another indicator of the amplification behaviour is shown by the force required to displace the structure. When the displacement initially increases so does the force as the additional rotation of the structure causes an increase of foundation edge embedment and for this to happen a greater force is required. However, as each cycle progresses the required force to displace the structure becomes less which is best seen in Figure 4.74c.

The force sensors below the foundation also shows a increased duration of sensors being at their maximum limits in both Figures 4.74a and 4.74b. This shows the time the foundation is in contact with the soil is increasing but also the duration in which the edge of the foundation is not in contact has increased.

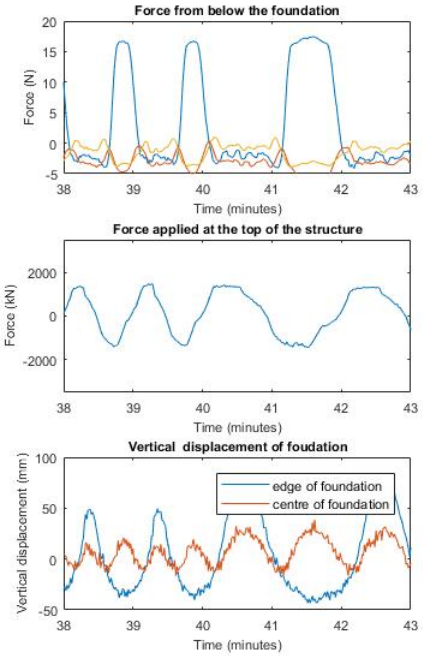

(a) The gust test increasing the displacement from 300mm to 400mm, data from the force sensor under the foundation, the force required to displace and vertical movement of the foundations

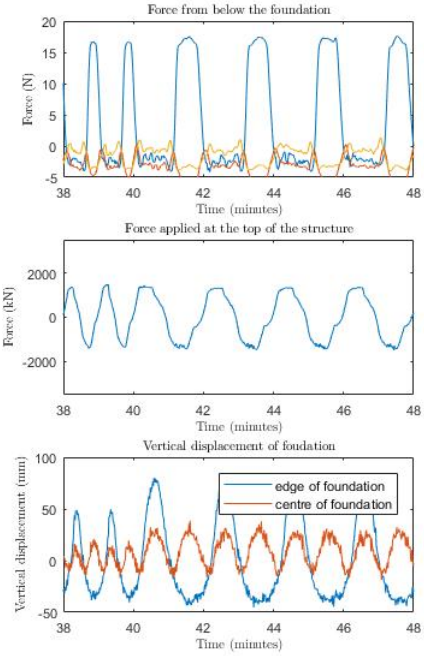

(b) The gust test increasing the displacement from 150mm to 300mm, data from the force sensor under the foundation, the force required to displace and vertical movement of the foundations

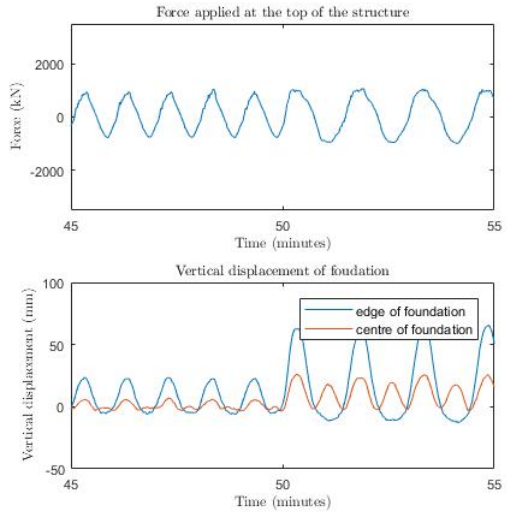

(c) The short break storm test increasing the displacement from 150mm to 300mm, the force required to displace and vertical movement of the foundations

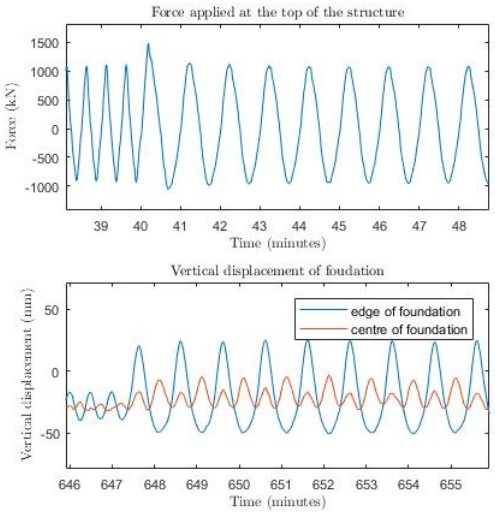

(d) The long break storm test increasing the displacement from 150mm to 300mm, the force required to displace and vertical movement of the foundations

Figure 4.74: Amplitude Behaviour

4.7.5 Recovery behaviour

The recovery behaviour occurs after the displacement amplitude decreases. It is characterised by the force required for displacement gradually increasing. As the structure is rotating and uplifting less, and a flattening of the soil profile occurring and causing an increase in soil foundation contact, as seen in Figure 4.75.

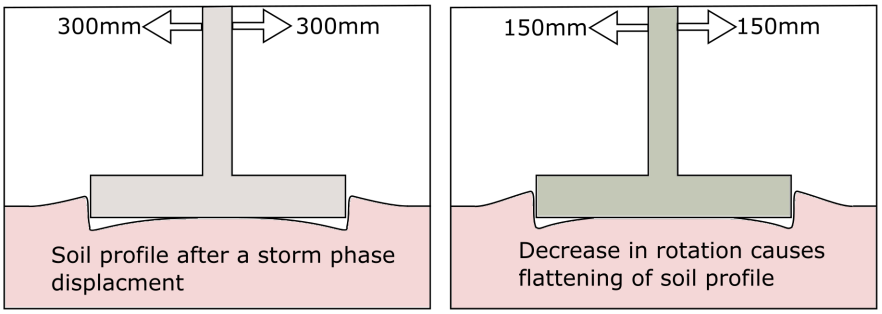

Figure 4.75: The recovery phase flattening the soil profile

In Figures 4.76a, 4.76c and 4.76b the force applied at the top of the structure, the force magnitude decreases with continuing cyclic displacement. The foundation vertical movement differs between 4.76a and 4.76b & 4.76c, in the short break and long break storm tests both the edge and the centre of the foundation reacts to the decrease in displacement, where there is minor movement at the centre of the foundation and a decrease at the edge. The gust test (Figure 4.76a) displacement changes from gust to normal displacement (400mm to 150mm), the change that is noticeable is the pattern in which the centre of the foundation is uplifting significantly more with the edge of the foundations maximum and there is little change to the amplitude of the foundation uplifting.

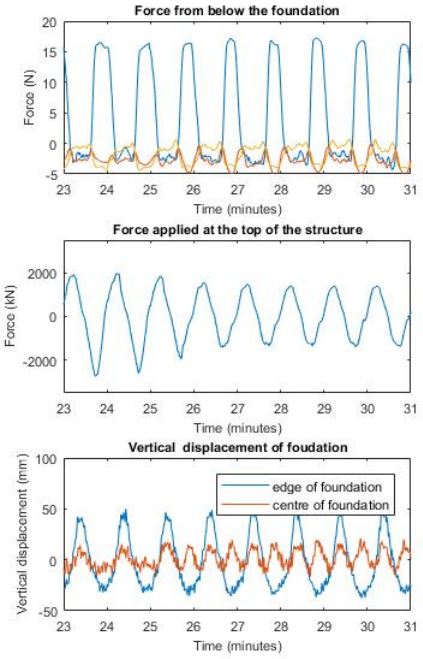

(a) The gust test after a drop in the displacement distance, data from the force sensor under the foundation, the force required to displace and vertical movement of the foundations

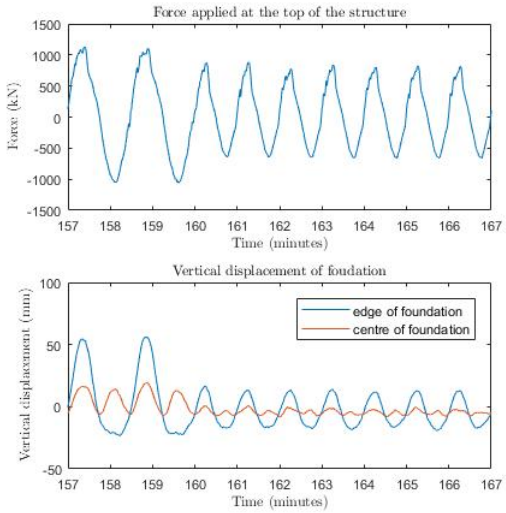

(b) The short break storm test after a drop in the displacement distance, the force required to displace and vertical movement of the foundations

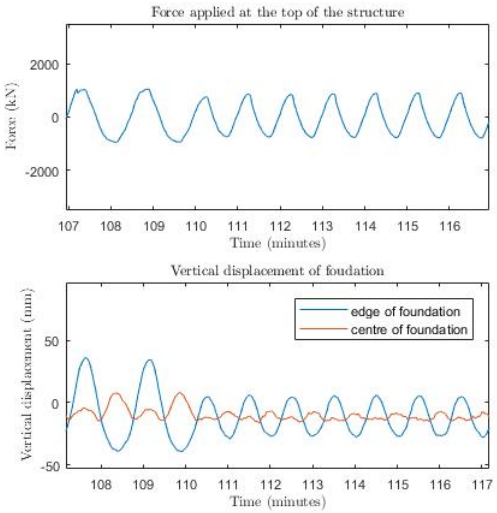

(c) The long break storm test after a drop in the displacement distance, the force required to displace and vertical movement of the foundations

Figure 4.76: Recovery Behaviour

4.8 Conclusion

A shallow foundation wind turbine was modelled with cyclic displacements replicating wind. The model was able to capture the effects of the cyclic displacement, deformation of the soil

profile, and changes in natural frequency. The identification of five behaviours which describe the response between the soil and the foundation from the cyclic loading and changes in the cyclic loading. Two behaviours (the initial and initial amplification behaviours) are if present in a test, are single events and do not repeat. Whereas the Constant behaviour, Amplification behaviour and Recovery behaviour are repeated when there is more than one type of cyclic displacement. The each repeated behaviour has a specific response on the soil profile, this information can allow for rocking structures to be introduced into the design of shallow onshore wind turbine foundations. A foundation can be designed to rock with the knowledge that after a storm event when the soil foundation contact is reduced, the soil profile will alter again and soil foundation contact will increase.

The frequency was shown to decrease after each cyclic test, which if the wind turbine is designed on a soft-soft natural frequency (similar to this prototype) then there is no issue of the changing natural frequency overlapping either the P1 or P3 frequencies.

Chapter 5

Centrifuge modelling

5.1 Introduction

Centrifuge modelling is used to allow reproduction of a prototype's full weight and stress at small scale. Centrifuge modelling was conducted to show how a prototype wind turbine of realistic weight would behave under long-term cyclic loading.

This would indicate if an increase of the structure and soil weight and therefore soil stresses (compared to the prototype used for the 1g modelling) causes a difference of behaviour. The tests conducted in the centrifuge are a push-over test and a short break storm test which is the same as the 1g test described in subsection 4.5.2 and Figure 3.5.

This chapter describes the methodology of setting up and conducting the centrifuge tests, presents the results and discusses how they relate to those from the 1g testing, described in Chapter 4.

5.2 Centrifuge Modelling Theory

Small scale modelling in a centrifuge uses centrifugal acceleration to increase the gravity level and therefore the self weight of the model being tested. This allows the scaled model to reproduce the weight and stresses of the prototype that it is based upon (Deng et al. 2011).

The stress-strain behaviour in soils is non-linear, therefore experimental modelling with an increased gravity level allows for this relationship to remain. The centrifugal acceleration or increased gravity is represented by N, which is the factor which is used to scale the models. The stress profile of the soil is more realistic in centrifuge modelling than in 1g modelling. The increased gravity increases the unit weight of the soil which in turn replicates the soil strength profile seen in reality. The radial acceleration field is the application of the acceleration upon the model. Due to the model spinning to create the acceleration from centripetal forces, the field is circular. Which when applied to a model means there is slight changes in acceleration in the orientation of rotation. To ensure this does not effect the modelling the x and y axis of the model are not in the same orientation of rotation.

5.2.1 Scaling Laws

Scaling must be done in order to relate the behaviours of the model to the prototype. These relationships are essential in accurately scaling down the prototype (chapter 3), but also scaling up the reactions of the model Madabhushi (2014). The scale factor for stress and strain is 1, due to them being identical at prototype and model scales. In Table 5.1 the scaling factors that are important to this project are presented and further information on scaling factors and how they are devised can be found in Muir Wood (2004) and Madabhushi (2014).

Table 5.1: Scaling factors for Centrifuge Modelling, Muir Wood (2004)

Unit	Scaling factor
Time	$1/N^2$
Acceleration	N
Mass	$1/N^3$
Force	$1/N^2$
Length/displacement	$1/N$
Frequency	N

The scaled time in Table 4.3 is for a consolidation event where a diffusion process with in the soil body occurs when excess pore water pressure is generated. Whereas a dynamic time scale the excess pore water pressure in the soil body would build up and in granular soils cause liquefaction under cyclic loading.

5.2.2 Dundee Centrifuge

Centrifuge modelling was carried out using an Actidyn C67-2 3m beam centrifuge (Figure 5.1) at the University of Dundee's Department of Engineering. The 3m refers to the distance between the centre point of rotation to the platform of the gondola. During flight (while spinning) the gondola gently rotates up to a horizontal level and is held there by the g-force, putting the model under a radial gravitational field.

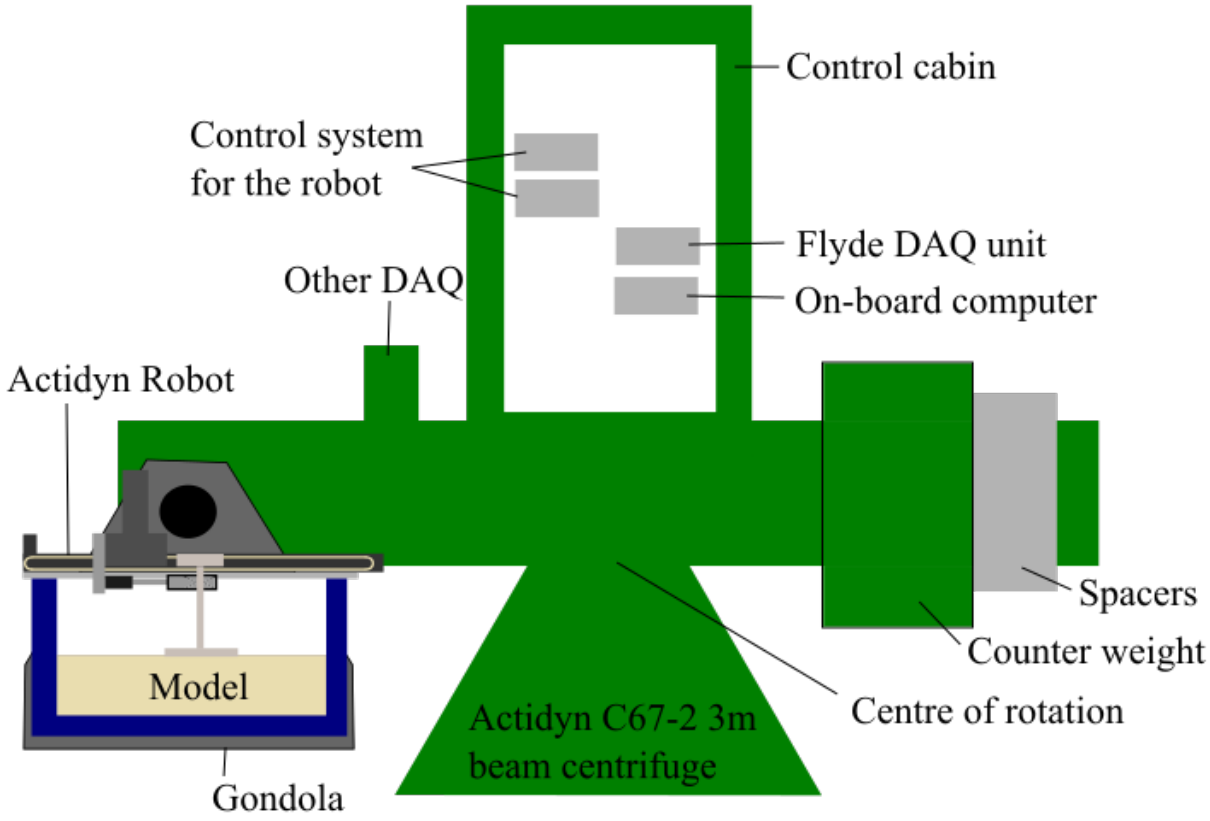

Figure 5.1: A cut through sketch of the centrifuge at the University of Dundee

The centrifuge requires that the package placed on the gondola is evenly balanced with a counter weight at the opposing end of the beam. The spacers shown in Figure 5.1 are used to ensure the correct positioning of the counter weight. While setting up a model on the gondola, each item must be weighed and recorded in order to calculate the position of the counter weight. This ensures there is an even and smooth flight path during testing and protects the centrifuge from damage. Figure 5.2 shows the centrifuge

Figure 5.2: The centrifuge box and robot loaded into the centrifuge ready for the test to begin

5.2.2.1 Boundary effects

To ensure there is accuracy within the centrifuge modelling and the soil is not constrained or affected by the soil being constrained near the wall of the box. The structure is placed in the middle 3rd of the container.

5.3 Instrumentation

5.3.1 Actidyn ACTS C67

The Actidyn Controlled Tool System (ACTS) is a robot which can be remotely controlled or pre-programmed to perform in the centrifuge during flight and is shown in figure5.3. The robot does not fit directly on the box, there is a steel plate which is fixed to the outside of the centrifuge box which is slightly larger than the box and the robot is bolted to the steel plate. The capabilities of the robot are moving in the x and y direction and in the y direction the tool has more control. The ACTS was used to control the displacement of the structure

during flight. It is controlled though Actidyn software which can either be pre-programmed in a txt file with the coding devised by Actidyn or controlled in-flight using the interface on the software. The push-over test was the first use of the ACTS in-flight for testing, which meant that the push-over test was an trial of the robot itself.

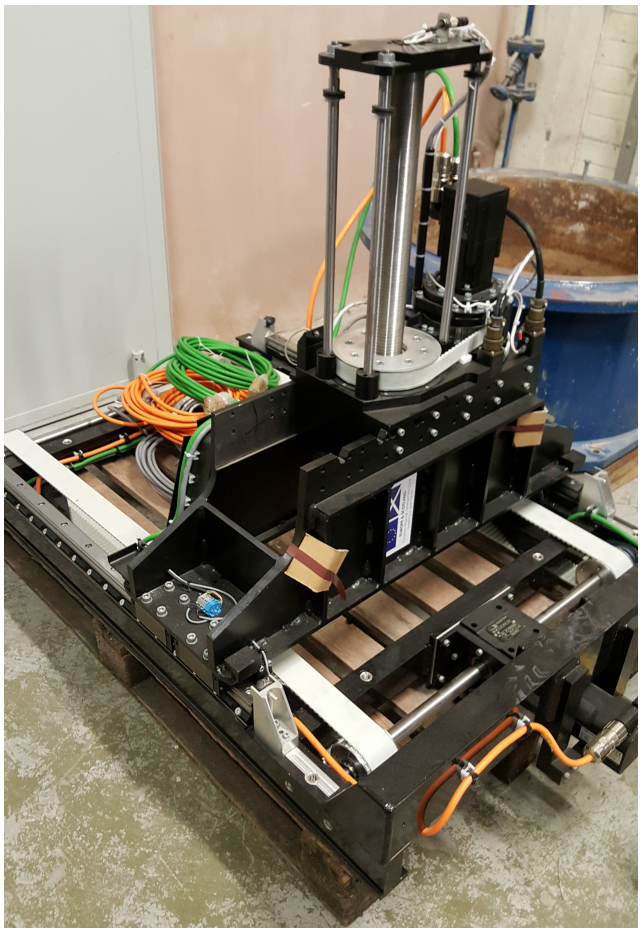

Figure 5.3: The Actidyn C67 Robot

5.3.2 Load cell

The load cell used was a 100kg S - beam load cell SN23903 Mod601RS (PN RS645811). The load cell was attached to the robot using a u-shaped aluminium channel and was used to measure the force required to displace the structure (Figure 5.8). The load cell was calibrated by applying weights and recording the voltage output, following the same method in section 4.2. The calibration was conducted up to 98N (Figure 5.4) in model scale, which is 245kN in prototype scale and sufficiently large enough to cover the loading which is applied during testing. The calibration data was fitted with a line of best fit; which has a R^2 of 0.9998 and gives a calibration factor of -0.0008.

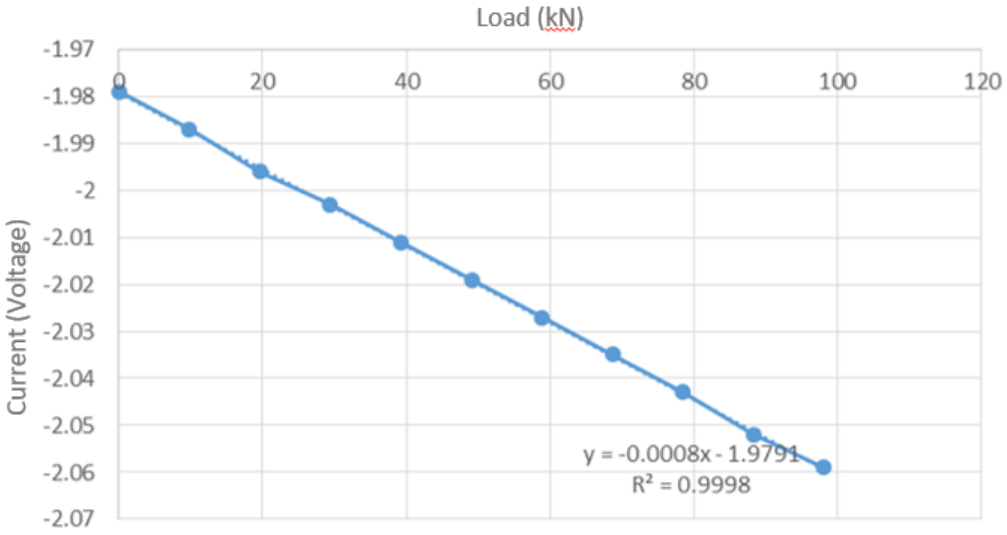

Figure 5.4: The calibration for the load cell

5.3.3 LVDT

The LVDTs used in the centrifuge experiment are the same centre and edge LVDTs which have been described in section 4.2.4.1. The calibration method is the same as for the 1g experiments, with the change that the instruments are connected to the Flyde DAQ (section 5.4.3) in the centrifuge for the cyclic test only. The centre LVDT was calibrated in model scale to 3mm with 0.5mm intervals, which is 150mm and 25mm in prototype scale. For the edge LVDT, the same displacement intervals were used but within one of the 0.5mm intervals 5 readings at 0.1mm intervals (model scale, 5mm in prototype scale) were added. Figure 5.5 shows that the calibration factor for the centre LVDT is 0.086 to convert volts to mm in model scale. The edge LVDT calibration shown in Figure 5.6 has a calibration factor of 0.0868 and a R^2 of 0.985, which is due two three points which are not in line with the line of best fit or the other data points. This is most likely an issue of human error during the calibration process and this doesn't effect the calibration due to having a sufficient number of data points which match the line of best fit.

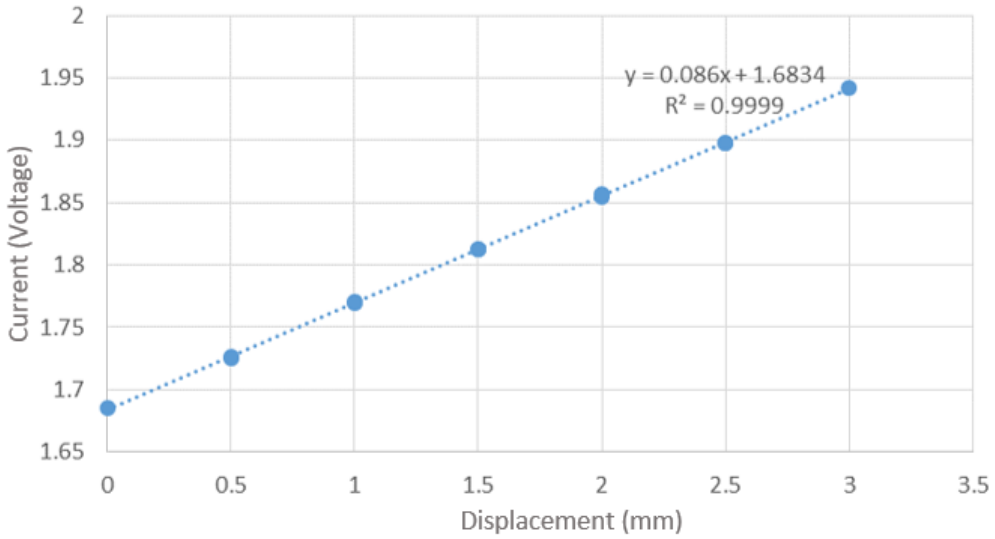

Figure 5.5: The calibration for the LVDT at the centre of the foundation

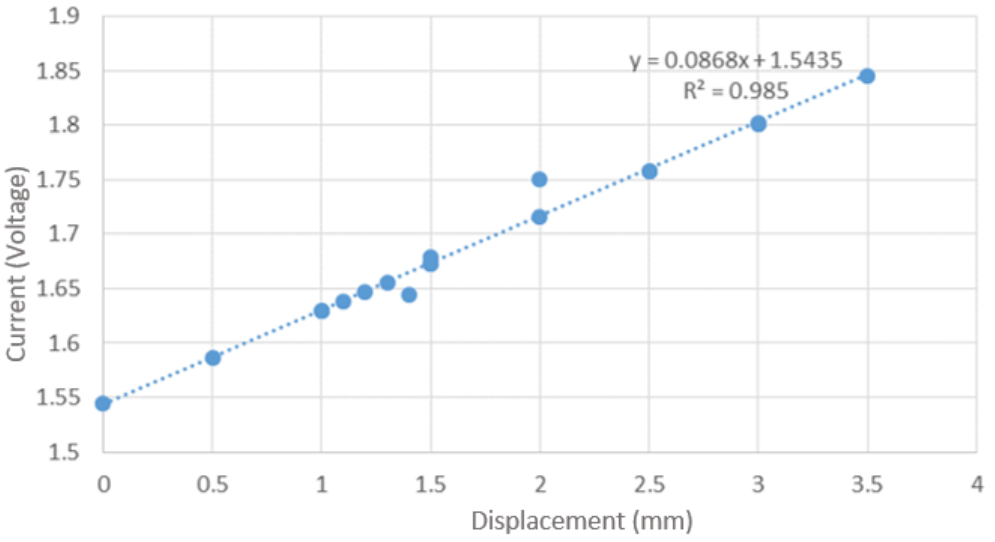

Figure 5.6: The calibration for the LVDT at the edge of the foundation

5.3.4 Accelerometer

The accelerometer used is the same as the one used for the 1g test because it is attached to the structure with super glue, ensuring the direction is correct and always the same for every test for consistency. Further details on the accelerometer and calibration can be found in section 4.2.4.4.

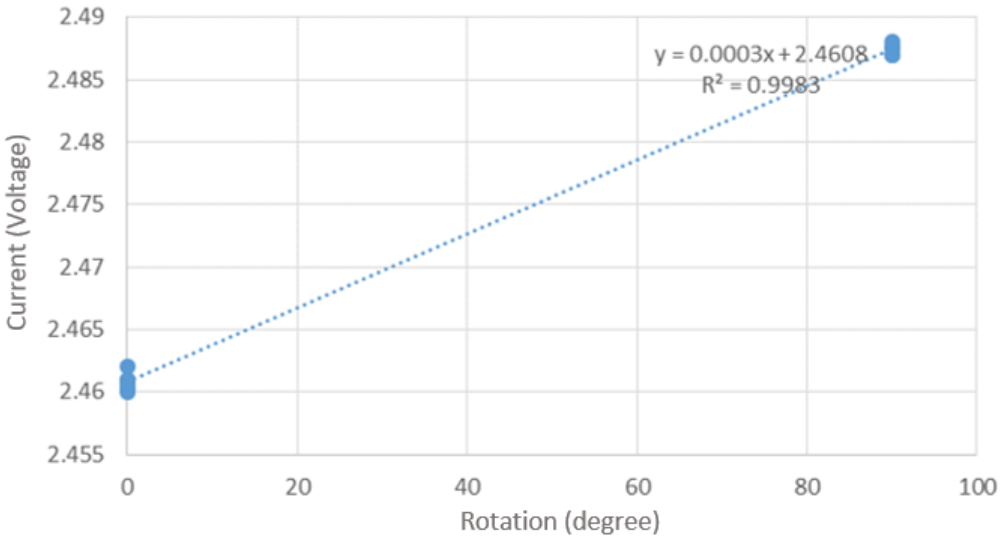

Figure 5.7: The calibration for the accelerometer

Figure 5.7 shows the accelerometer calibration. There are only two points which were measured; 0 and 90 degrees and the R2 is 0.9983, which is acceptable. The calibration factor is 0.0003. No data from the accelerometers could be read though the noise created within the DAQ system and filtering the noise only erased the data.

5.3.5 Pore pressure transducers

Information on the pore pressure transducers can be found in section 4.2.4.3. Similarly to the accelerometer the pore pressure transducers were prepared for both tests and calibrated. No data was obtained from the pore pressure transducers due to the noise created within the DAQ system.

5.3.6 Force sensors

The same instruments were used the 1g testing (section 4.2.4.2), although 100N sensors were used in the centrifuge due to the increased gravity level. However unfortunately the boards in which the sensors are connected to were not able to withstand the increased gravity in the centrifuge and malfunctioned before the centrifuge reached 50g. No data was recorded from the sensors while in-flight.

5.4 Practical Design of the Test Set-up

The placement of instruments in a centrifuge must ensure they are secure and will not move during the flight. There is a limited flexibility in the placement of the structure in the centrifuge box due to the physical size of the actuator, and ensuring there is enough space for the horizontal movement of the robotic actuator. Figure 5.8 shows the layout of the centrifuge test with the LVDTs in position and also how the Actidyn C67 robot is applying the actuation.

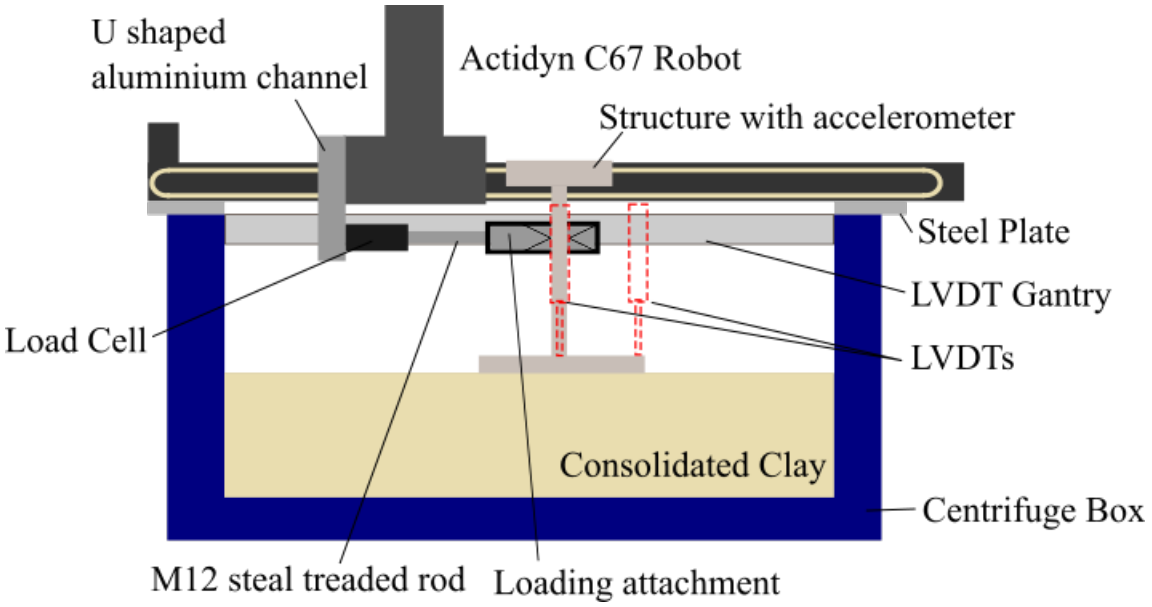

Figure 5.8: The layout of the model for the cyclic centrifuge test

5.4.0.1 Applying the displacement

To apply the displacement to the structure with the robot an attachment is required for the robot to apply the push-pull motion. Under the advice from the Technical Staff at the University of Dundee a U shaped aluminium channel (noted in Figure 5.8) section 200mm in length and 50mm wide with 4 drilled holes at the top to attach to the robot with 4 bolts and nuts. At the base of the channel section there is a single drilled hole which the load cell can be screwed into and double nutted with a M12 threaded rod, and a second section of threaded rod to connect the load cell to the loading attachment (which is also used in the 1g testing Figure 4.14). The load cell can record the force placed upon the structure during the cyclic loading.

5.4.0.2 Gantry

The placement of LVDTs required a gantry to be affixed to the box. It can be seen in Figure 5.9 and also Figure 5.8 as a sketch in the relative placement within the model, the gantry has the LVDT holders attached so they can be positioned in the centre of the foundation and at the edge of the foundation.

5.4.1 Soil

See section 4.2.2 for information on the soil preparation for the experimental modelling. The design of the soil can be found in section 4.2.2.

5.4.2 Structure

Details of the structure and it's design can be found in section 3.3, it is the same model as used in the 1g modelling

5.4.3 Data Acquisition

The centrifuge has two pre-installed data acquisition (DAQ) units, where instruments can be connected to be powered and the feedback data recorded.

The Centrifuge has a computer in the centrifuge cabin with Microsoft Windows operating system with both DAQ systems linked up. A National Instruments LabVIEW software (version 2013) is also installed on the computer which can record the data from both DAQ units. The pressure sensors can be directly connected to the computer via USB connection.

The Fylde micro analogue 2 modular instrument system (FE-MM8) was used in the cyclic test for data acquisition for the load cell, two LVDTs and accelerometer.

The DAQ is positioned in the centrifuge cabin with the on-board computer and connected by USB cable. Duel channel instrument cards (FE-366-TA) allow voltages between 2.5 - 10V for up to 8 instruments to be attached, although at the time only 4 plugs available for the instruments.

5.5 Tests

There was the opportunity for two tests in the centrifuge. The first test was a trial for the robot with the aim of understanding how well it cyclically loads and also to conduct a push-over test. The second test was a cyclic test with normal and storm displacement.

5.5.1 Push-over

Initially, this test was to gain awareness of the robot and how to use it in-flight, as there are two methods of control; it can be pre-programmed or dictated during flight. At the end of the robot familiarisation a push-over test was conducted. The aim of the push-over test is to get a force-displacement curve which will determine the force required to totally displace the structure. This can be checked against the overturning moment that has been calculated in the design of the structure.

The push-over test included displacing the structure the use of accelerometers and PPTs but unfortunately due to the centrifuge on-board DAQ the readings were indistinguishable from noise.

5.5.2 Cyclic test

The cyclic test is an exact copy of the short storm cyclic test (section 4.5.2) that was conducted in the 1g experimental modelling, Figure 4.16 is the same pattern.

For the cyclic test a pre-prepared .txt file was created with all of the cyclic displacement movements, and the directions for the robot to allow for the test preparation. This allows for the test movements to be prepared and removing any possibly of human error during the test. The reasoning for conducting identical cyclic displacements is so that the two methods of modelling can be compared against each other, and also the centrifuge test can be used to verify the 1g modelling method and results, due to the centrifuge modelling having more

accurate output of the soil-structure interaction due to the increased weight of the structure and soil stresses and strains.

The test was continuous but 3 minutes of data was lost when the DAQ software terminated and had to be restarted mid test, this can be seen in the data from the load cell, LVDTs and accelerometer.

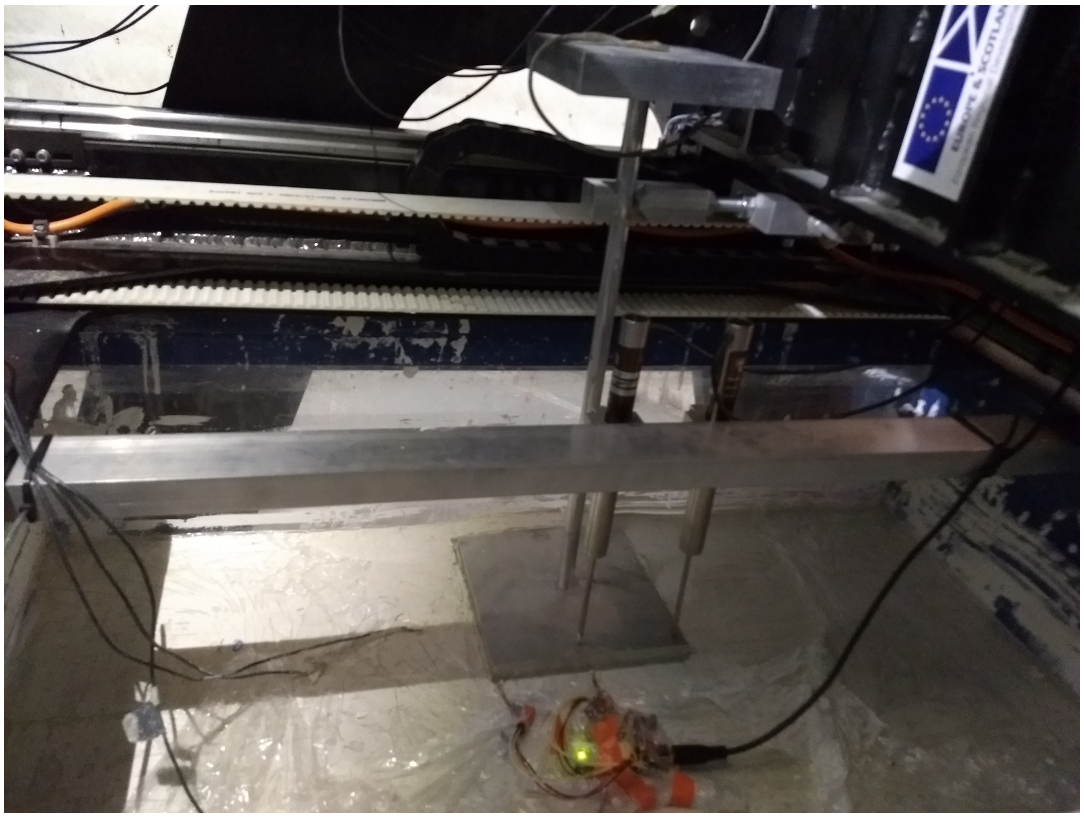

Figure 5.9: The prepared cyclic centrifuge test

5.6 Results

All the results from the centrifuge tests are presented in prototype scale. This allows for the centrifuge results to be compared to the 1g and numerical modelling results as all models are in the same scale. The push-over test is first presented, followed by the cyclic loading test Short Break Storms.

5.6.1 Push-over test

5.6.1.1 Load-displacement

Figure 5.10 shows the results from the push-over test, the structure was displaced in one motion from 0m to 5m. The load data recorded by the load cell had considerable noise, and to overcome the noise the load data was averaged to 10 samples per data point. The displacement positions have been calculated rather than recorded as the displacement data recorded by the robot samples every 1.6-2.4 seconds. Which made for poor recording and inefficient for the

testing conducted, which was unknown before as this was the first use of the robot for recording. Therefore from the speed at which the robot has travelled a position can be calculated.

The maximum force is 245kN which occurred at 3.65m.

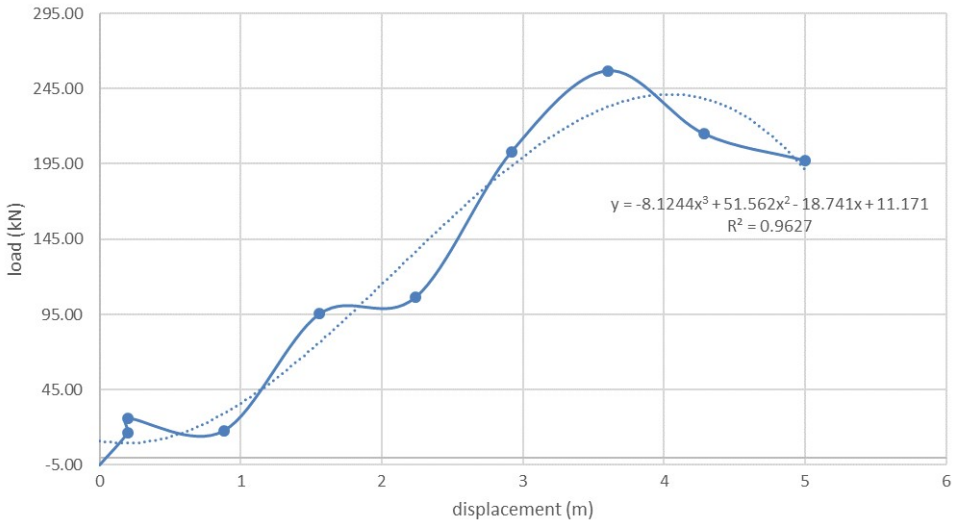

Figure 5.10: The load displacement curve from the pushover test

Figure 5.11 is the structure in position on the soil before the model went into flight, and Figure 5.12 is the foundation at the end of the push-over test once the centrifuge has come to a stop, with considerable uplift and embedment. Also to the left of the foundation a settlement of 100mm (model scale is 2mm) that occurred during the familiarisation stage of the this test.

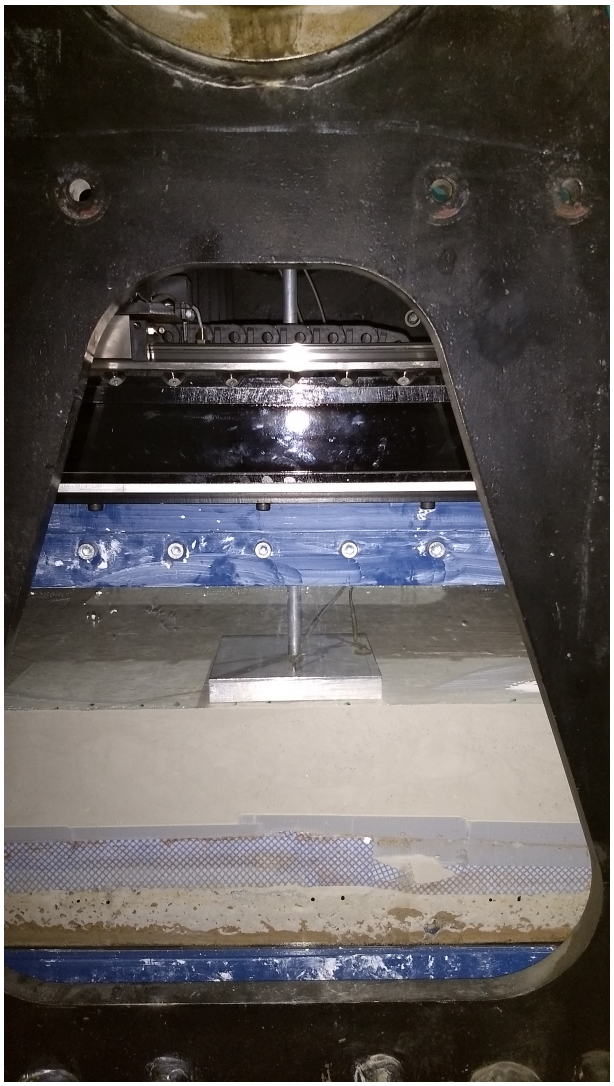

Figure 5.11: The before spinning up for the pushover test

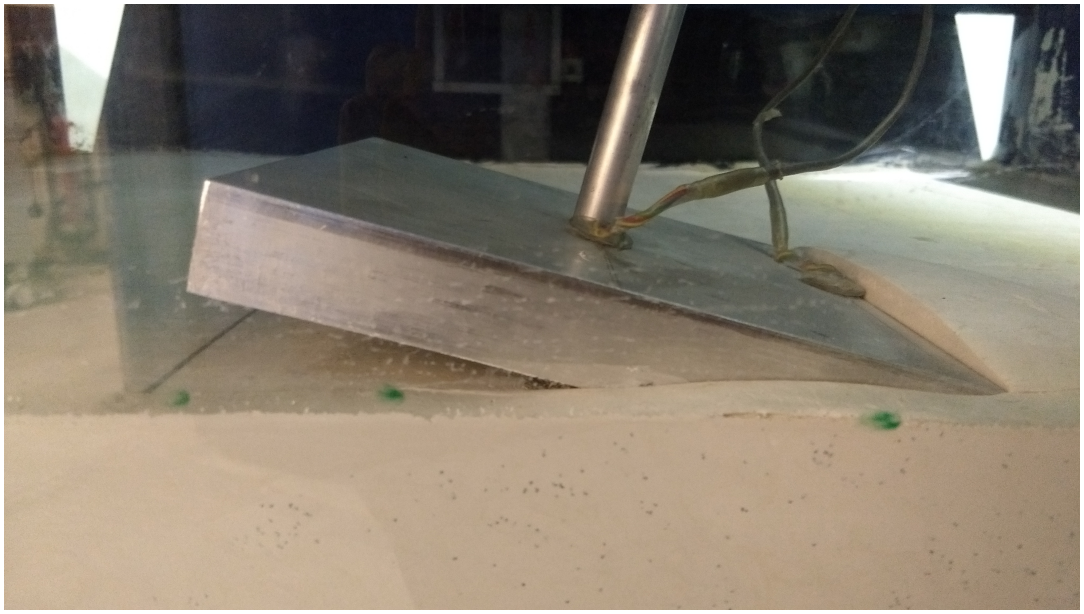

Figure 5.12: The finish position of the pushover test

5.6.1.2 Pore Pressure and accelerometers

No data from the accelerometers or pore pressure transducers could be read though the noise created within the DAQ system. Methods to clean up the data only erased the data that might have been there.

5.6.2 Cyclic test

5.6.2.1 Displacement

The displacement has been recorded by the robot(Figure 5.13), via the Actidyn software at an interval rate of 1.16 second in model scale. This is a larger interval rate than ideal due to occasionally the peaks of the data being missed off where a higher interval rate would record.

The displacement data is presented without any filtering, the maximum displacement of the structure is ±300mm at the point of displacement. The top of structure displacement will be more (a maximum of 338mm), but this was unable to be recorded by a LVDT as in the 1g modelling but has been calculated from the robot data to reflect the data presented in the 1g modelling. (no it hasn't, or its not being shown)

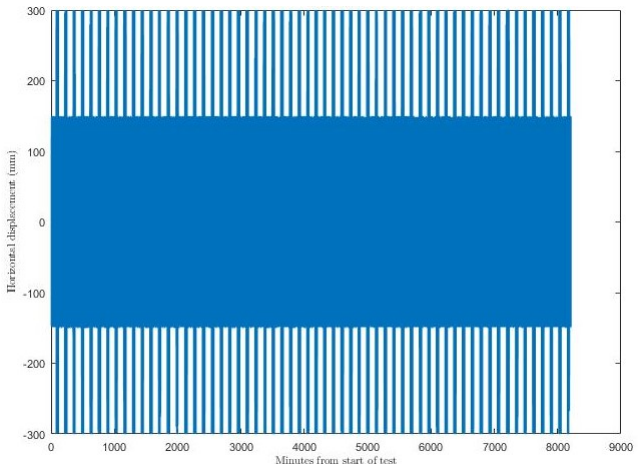

Figure 5.13: Displacement of the structure by the robot actuator

5.6.2.2 Settlement

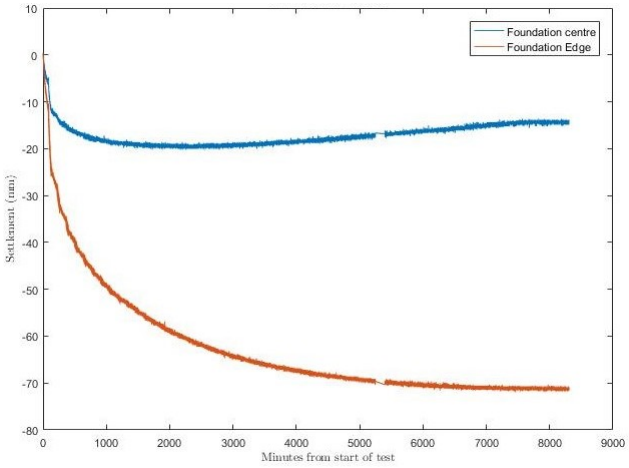

Figure 5.14: Settlement at the centre and edge of the foundation

The settlement can be seen in Figure 5.14, the maximum settlement at the centre of the foundation is 20mm, which occurs 2000 minutes into the test, at 3000 minutes into the test the centre begins to uplift and at the end of the test the finial settlement is 14.5mm.

The First normal phase of cyclic displacement is at 0-50 minutes and has a steady settlement rate but plateaus at 5mm between 50 and 85 minutes. At 85 minutes storm cyclic displacement starts, and the settlement rate increases to a higher rate than seen in the normal phase until the storm phase is over and the next normal phase resumes at 130 minutes, when the total settlement is 12mm. The settlement that occurs after 135 minutes is at a reduced rate and the impact of the normal and storm cycles are less noticeable.

After 3000 minutes of cyclic loading the centre of the foundation starts to rise this could be a result of the foundation rounding as the foundation embeds the soil below the foundation is pushed up, to support this theory significant uplift in the data from the edge of the foundation would be expected, which is not seen. More likely is that at 3000 minutes the LVDT could have started slipping.

In the data from the edge of the foundation the storm and the normal phases of the cyclic displacement are more noticeable, because the storm cyclic displacement has a steeper settlement rate and you can notice the uplift and embedment. From 1900 minutes the storm phases is indistinguishable to the normal phases, which would indicate that the foundation is no longer uplifting. By 6500 minutes the settlement has levelled out to 71mm, which is 59mm more than the centre of the foundation. Which backs up that the LVDT which recorded the movement at the centre of the foundation must have slipped during the test, and given a false reading. The majority of the settlement of the overall foundation occurs at the start of the test, in particularly the first normal and storm phases which were from 0 to 130 minuets where 24.5mm of settlement occurred at the edge of the foundation. This is 34% of the overall settlement that occurs in the test.

5.6.2.3 Force

The force is in kN, and is displayed in Figure 5.15. The data displayed has a moving average of 3 data points (a moving average of 3 because this allowed for some noise to be filtered out without the peaks being altered) to smooth out from the load cell that was attached to the robot applying the displacement to the structure. The start of the test in the first 1000 minutes there is variability in the force required to displace the structure although it is most noticeable in the positive force. The negative force required increases in from 0 to 135 minutes (normal phase -26 to -31kN, and -54 to -61kN in the storm phase), thereafter the force applied in the normal phases is even throughout at -36kN.

The positive force side of the displacement, the normal phases are higher from 0 to 2325 minutes when the force varies from 48kN to 32kN. At 2325 minutes the force has plateaued and is between 25-30kN. This same pattern is seen in the storm phases, but with the plateau force being between 55-61kN.

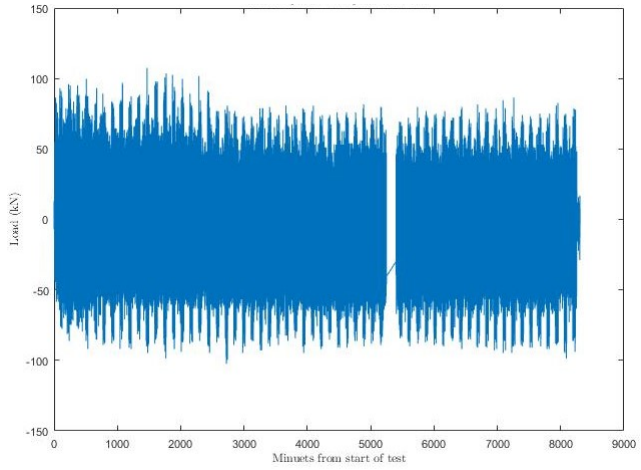

Figure 5.15: The load to displace the structure

The force pattern for the cyclic centrifuge test (Figure 5.16) displays the 1st, 9th, 18th, 38th and 59th storm phases. These are displayed with 10 cycles before the storm and 25 cycles after the storm, in order to see if there are any changes to the force required when the normal storms restart. The data was processed in order to reduce noise increase clarity to the data, this was done by averaging 6 data points at the peak of the loading. There is still some noise but the overall trend is still visible, which means some detail may have been lost in the noise of the centrifuge.

The force pattern in Figure 5.16 shows the force required for maximum displacement, the 1st and the 9th phases require the highest levels of force in the normal and the storm phase. For both the normal displacement requires around 60kN and the storm displacement is double that at 120kN. It does not appear to show any amplification or recovery behaviours which were noted in section 4.6.

The 18th, 38th and 59th phases show to require less force during the normal phases as the cyclic loading continues. The force reduces from around 57kN in phase 18, down to around

53kN in phases 38 and 59. In the recovery section of the normal displacement it does appear phase 59 requires a kN or two less than phase 38. Again in these phases there does not appearer to be any amplification or recovery behaviour.

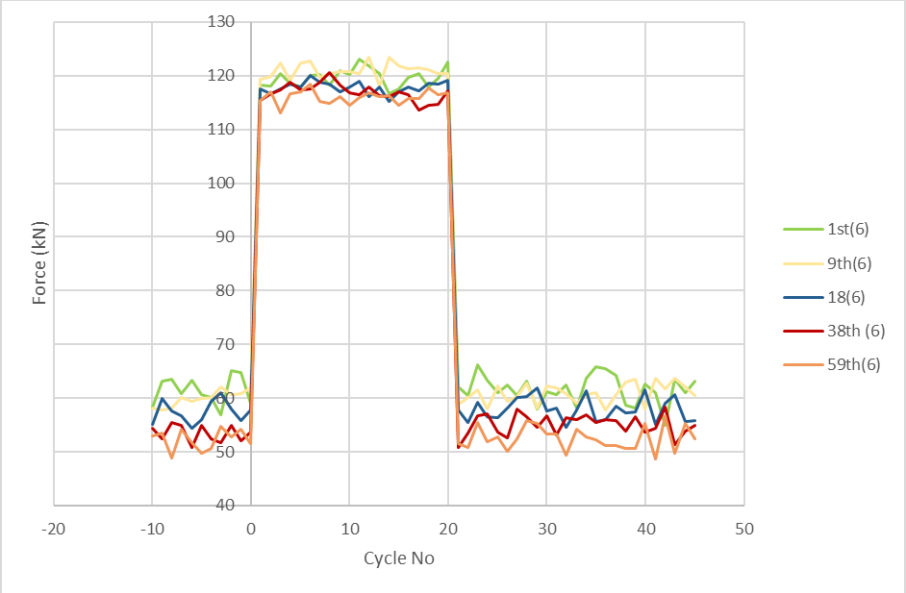

Figure 5.16: The force required for each cycle to displace the structure

5.6.2.4 Rotation

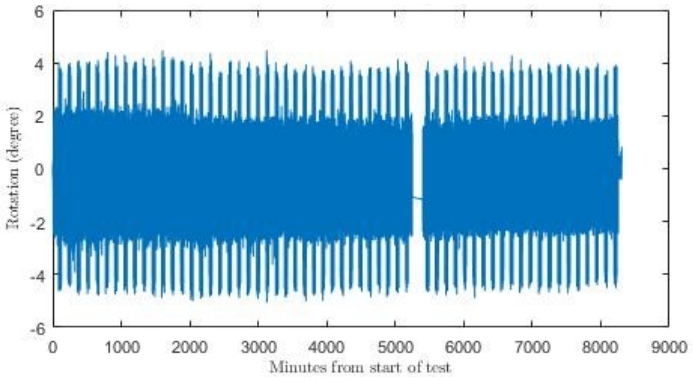

Figure 5.17: The rotation of the structure during the cyclic centrifuge test

The rotation data was recorded via the accelerometer at the top of the structure (Figure 5.17), contained quite a lot of noise, so a moving average filter was used to reduce the noise, a 5 point mean still had the same noise issues whereas a 10 point mean started to erase some of the higher data points, so a 7 point moving mean was chosen. The data does show that there is quite a distinction in the rotation between the normal and storm phases, the normal phase causes a 4-4.5 degree of rotation whereas the storm phase causes a 8-9 degree of rotation to the structure. At the start of the test the rotation for both loading styles is larger than the rotation at the end of the test.

5.6.2.5 Settlement - Rotation

The settlement rotation can be seen in figures 5.18 and 5.19, the rotation data used is from the accelerometer and the settlement data from the edge and centre LVDTs (the settlement data from the edge of the foundation is used due to the issues with the centre settlement data as explained section 5.6.2.2). In Figure 5.18 the maximum rotation is $4.5\mathrm{deg}$ during the storm phases and $3\mathrm{deg}$ in the normal phases, at the maximum rotation in either phases no uplift is present. The settlement data from the edge of the foundation; does not show uplift, although in the storm phases at the maximum rotation is the edge of the foundation has 1mm difference between the maximum positive and negative rotation.

The first phase is of normal displacement which has 12mm of settlement, this is also true of the first storm phase too. The storm phases of 20 cycles the settlement being similar to the initial normal phase indicates that the storm displacement does cause an increased rate of settlement when compared to the normal cyclic displacement. This pattern between the normal phases and storm phases can be seen throughout Figure 5.18, that the storm displacement settle a similar amount to the previous normal phase. It is only once settlement has reached 60mm that distinguishing between phases becomes more difficult this is due to the settlement starting to plateau.

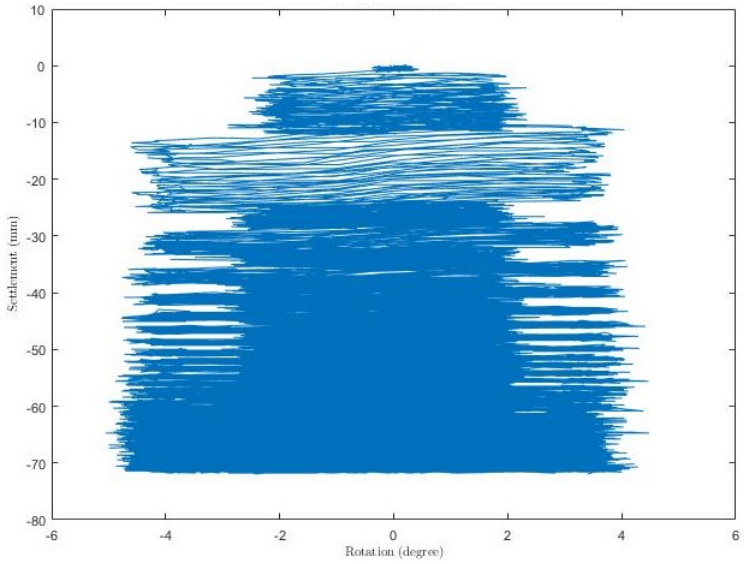

Figure 5.18: The Settlement - rotation during the cyclic test, using settlement data from the edge LVDT

Figure 5.19 is the settlement - rotation using the settlement data from the centre LVDT which has a third less settlement (which in model scale is around 1mm) to the edge LVDT, 20mm in the centre compared to 70mm at the edge. Within the individual cycles there is no uplift being recorded at the centre of the foundation when the structure is rotated/displaced to the maximum. WHen comparing this to the

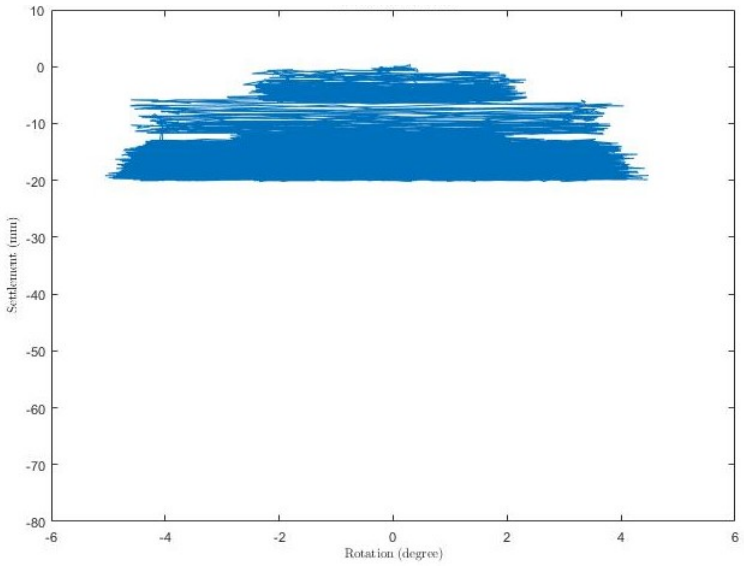

Figure 5.19: The Settlement - rotation during the cyclic test, using data from the centre LVDT

5.6.2.6 Force - Rotation

The data used for the force-rotation Figure 5.20 is a 5 point moving mean for both the force and rotation. The top 3 plots are of the normal displacement and the bottom 3 plots are the storm displacement, the phases plotted are 1st, 30th and 60th. The response from the cyclic displacement changes through out the test, although the force required does not alter. The first normal phase has the widest loop of the three from the normal phase displacements. The loading and unloading slope of the first normal phase is around $40\mathrm{deg}$ where as by the 30th normal phase the angle of the loading and unloading slope in increased to $43\mathrm{deg}$. The shape of the loops also change thought the test, the 30th phase is more compact compared to the first the loop, and the 60th phase is even more.

The force required to rotate the structure is consistent throughout the test, the force-rotation loop narrows from the first phase to the 60th phase, that would be due to the structure becoming more responsive to the displacement. Similar narrowing of the force-rotation loop can be seen for the storm phases as the number of cyclic displacements increase. Due to there being less cycles of displacement for the storm phase compared to the number of cycles in the normal phases (50 normal to 20 storm) it may look as though it is not compacting as much.

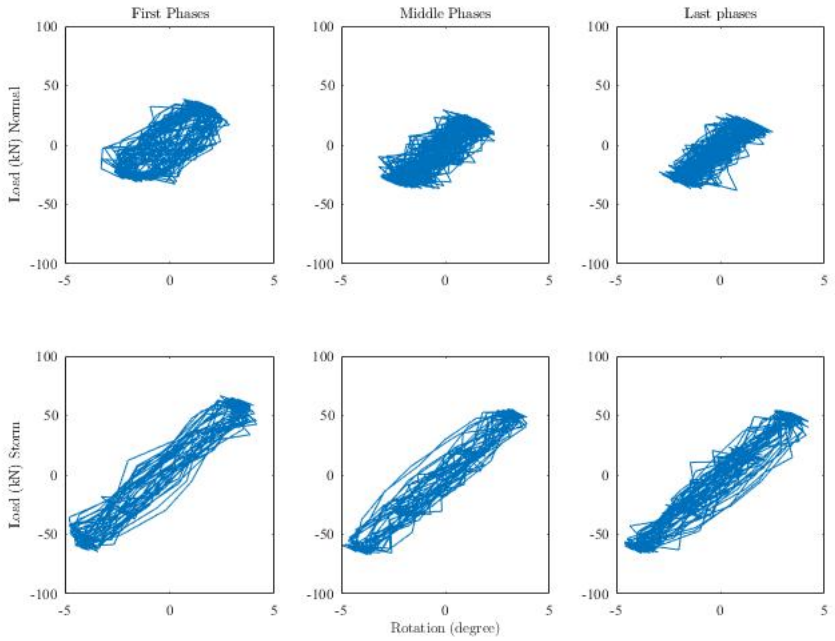

Figure 5.20: The rotation of the structure during the cyclic centrifuge test, displaying the first, middle and last phases of normal and storm loading.

5.7 Discussion

Centrifuge modelling provides a good replication of prototype models due to the increased gravity allowing for better replication of structure weights when compared to 1g modelling. Although in this series of testing adjustments had to be made in order for the model to be appropriate for the centrifuge that was being used. Whereas due to the time being increased within the centrifuge what may take days at 1g is minutes in the centrifuge.

During testing the model is isolated and therefore unable for adjustments during fight is impossible which does not allow for checking or fine adjustments. Such as potentially checking on the centre LVTD which may have slipped 1.5mm during flight. Whereas in 1g testing in the initial tests that did not work, hands on adjustments during testing with feedback via the

Preparation for a centrifuge test is a lengthy process but for each preparation period there was only one chance to flight due to the soil chosen, using clay meant only one sample could be prepared and that equated to one centrifuge test in which after the sample was deformed from settlement and uplift. If sand had been chosen the soil preparation could be done more frequently and therefore allow for more frequent testing in the centrifuge.

Pore pressure transducers were added to the models in the hope they could pick up the fine details of the changes in pressure to the soil below the foundation, when in testing the only readings they gathered was the increase in pore pressure from the centrifuge increasing in gravity. The sensors available were functioning and highly sensitive but due to being in clay rather than sand they were not sensitive enough.

All forms of modelling improve with repetition and an increasing in familerisation on the instruments, the set-up and software. With each aspect having it's own nuanced features that can affect the other parts.

What can't be replicated without assistance of a centrifuge is the consolidation of clay with an increasing strength with depth. Consolidating the clay in the centrifuge allowed for a more realistic soil profile when compared to consolidating clay in a press. The centrifuge consolidation was two-way, and under self weight, the final part of the preparation process was to remove the water on top of the sample and the softer soil. This process is not unlike what might naturally occur in the settlement of a lightly over consolidated clay deposit.

The Actidyn C67 robot has a range of capabilities and adapting them for this set of experiments was in itself an experiment. There were a number of things that were not able to be controlled via the programming one is the speed of the x direction in which it was being used for this project. Also the requirement of being displacement controlled movement at the time was unable to configure how to feed back in information from the load cell in order to produce a load controlled displacement.

Chapter 6

Numerical modelling

6.1 Introduction

In this chapter, numerical modelling has been undertaken to predict the behaviour of a onshore wind turbine with a shallow foundation, furthering the investigation of the effects of long term cyclic loading upon a shallow foundation. The modelling was conducted using the finite element code Plaxis 2D (Brinkgreve et al. 2016). The numerical simulations will be used to gain information about the soil that was not possible to record in the physical modelling, such as pore pressures, stress and strains below the foundation, with a focus on the reaction of the soil due to the uplifting of the rocking foundation. For comparison, the results predicted by the Modified Cam-Clay (MCC) model, for which the material parameters have been calibrated specifically to match the measured undrained behaviour of a kaolin, are presented.

6.2 Critical State Soil Mechanics

The literature covered in this section gives a summary of the MCC soil model used for the numerical simulations to represent the stress-strain relationship of lightly overconsolidated kaolin clay.

The research on normally consolidated clays and over consolidated soils by Rendulic (1937) and Hvorslev (1937) were the building blocks that Roscoe et al. (1958) used to formulate the critical state framework. They used triaxial compression tests on saturated clays to observe behavioural patterns that suggested a relationship between the shear strength and deformation. The critical state of soil was outlined as the stress state for all clays to ultimately reach when under constant loading, being defined when plastic shearing continues without any changes in volume or effective stress. This can be described as a perfectly plastic state, expressed by:

$$\frac{\mathrm{dp}'}{\mathrm{d}\varepsilon_{\mathrm{q}}} = \frac{\mathrm{dq}}{\mathrm{d}\varepsilon_{\mathrm{q}}} = \frac{\mathrm{d}\nu}{\mathrm{d}\varepsilon_{\mathrm{q}}} = 0 \tag{6.1}$$

Where p' is the mean effective stress, q is the deviatoric stress, ν is the specific volume, ε_{p}. It was hypothesized by Roscoe et al. (1958) that there must be a characteristic surface in which

all the possible stress states of soil could be contained with regards to p', q and ν; as shown in Figure 6.1.

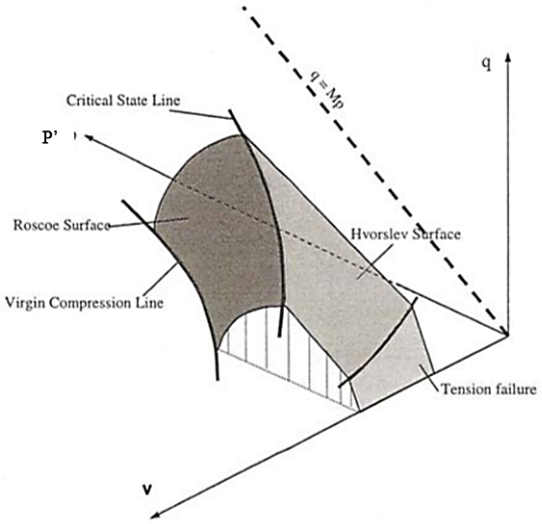

Figure 6.1: The critical state framework boundary as described by Roscoe et al. (1958)

The critical state line (CSL) is defined by:

$$\frac{\mathrm{q}}{\mathrm{p}'} = \mathrm{M} \tag{6.2}$$

which shows as a specific line in the $\mathrm{p}' - \mathrm{q}$'-ν graph in Figure 6.1, where the critical state has been reached for a given soil. During loading, it was noted that the stress path would converge to this critical state. Before reaching the critical state boundary, the deformation is plastic whereas upon reaching the bounding surface the behaviour becomes elasto-plastic.

There are four fundamental properties for the elasto-plastic constitutive model: a yield surface, hardening model, plastic flow rule and a description of elastic material behaviour. The yield surface which contains the elastic domain is given by:

$$\mathrm{F}(\sigma', \kappa) = 0 \tag{6.3}$$

where σ' is the effective stress state, κ is the hardening parameters. If F $= 0$, the behaviour is elasto-plastic whereas when F$<$0 the behaviour is elastic.

The hardening rule determines the size of the yield surface during the development of plastic deformation,and is represented by κ in Equation 6.3. A volumetric hardening rule is adopted in Cam-Clay models, where the change in size of the yield surface is controlled only by plastic volumetric rate, $\mathrm{d}\varepsilon^{\mathrm{p}}$, given by:

$$\mathrm{d}\varepsilon^{\mathrm{p}} = \Lambda \frac{\mathrm{dP}(\sigma', \mathrm{m})}{\mathrm{d}\sigma'} \tag{6.4}$$

where λ is the plastic multiplier. Further information on formulation of the critical state soil framework can be found in Muir Wood (1990).

6.2.1 Cam-Clay model

The development of Cam-Clay started with Roscoe et al. (1963) aiming to use observations from triaxial compression data of saturated clays. Figure 6.2 shows the yield surface in $\mathrm{p}' - \mathrm{q}$ stress space. The yield surface is defined as a logarithmic curve given by:

$$\mathrm{F} = \frac{\mathrm{q}}{\mathrm{p}'\mathrm{M}} + ln(\frac{\mathrm{p}'}{\mathrm{p}'_0}) = 0 \tag{6.5}$$

The yield surface is isotropic on the p' axis and indicates the boundary between the elastic and elasto-plastic behaviour. If the stress state stays within the yield surface then the specimen behaviour is purely elastic and deformation is not permanent. When the stress state contacts the yield surface the soil behaviour becomes elasto-plastic, where a proportion of the strains are plastic and therefore some of the deformation is permanent. On the critical state being crossed by the stress path, a stress state for the clay creates a unique line called the critical state line (CSL). The CSL is formed in $\mathrm{p}' - \mathrm{q}$-ν space, as a straight line which passes through the origin in the $\mathrm{p}' - \mathrm{q}$ plane(as presented in Figure 6.2), with gradient M.

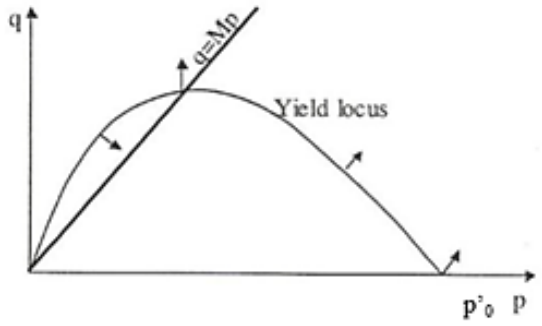

Figure 6.2: The Cam-Clay yield surface in the $\mathrm{p}' - \mathrm{q}$ stress space (Roscoe et al. 1963)

The single biggest issue with the Cam-Clay model is at q=0 where there is a singularity of the yield surface. At this point there are an infinite number of possibilities for a normal to the yield surface, and then an infinite number of flow directions.

6.2.2 Modified Cam-Clay

The original Cam-Clay model was improved by Roscoe and Burland (1968) by changing the yield surface to an ellipsoid in order to avoid infinite flow directions when $\mathrm{q} = 0$. If the soil obeys the normality condition, which imposes that the equation for the yield surface is equal to that for the plastic potential surface, g (Muir Wood 1990):

$$\mathrm{F} = \mathrm{g} = \mathrm{q}^2 - \mathrm{M}^2[\mathrm{p}'(\mathrm{p}'_0 - \mathrm{p}')] = 0 \tag{6.6}$$

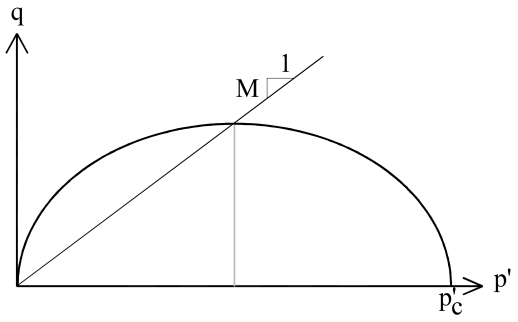

Figure 6.3: The Modified Cam-Clay yield surface in the $\mathrm{p}' - \mathrm{q}$ stress space (Valls-Marquez 2009)

In the MCC model the yield surface in the p'–q-ν space (Figure 6.4) can expand isotropically without changing its position in the stress space. This isotropic hardening can be described by Equation 6.7.

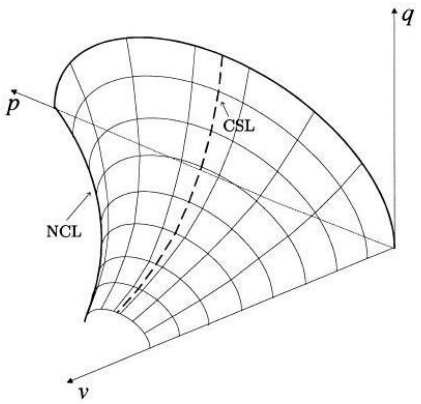

Figure 6.4: The Modified Cam-Clay yield surface in the $\mathrm{p}' - \mathrm{q}$-ν stress space (Elia 2015)

$$\mathrm{dp}'_{\mathrm{c}} = \frac{\mathrm{p}'_{\mathrm{c}}}{(\lambda - \kappa)} \mathrm{d}\nu^{\mathrm{p}} = \mathrm{p}'_{\mathrm{c}} \frac{\nu}{(\lambda - \kappa)} \mathrm{d}\epsilon_{\mathrm{v}}{}^{\mathrm{p}} \tag{6.7}$$

where λ is the compression index, and κ is the swelling index. When the stress path is within the yield surface, the behaviour of the soil is elastic. Elastic behaviour is defined in terms of the bulk and shear moduli, K and G respectively, which are assumed to depend linearly on the mean effective pressure p' as follows:

$$\mathrm{K} = \frac{\nu \mathrm{p}'}{\kappa} \tag{6.8}$$

$$G = \frac{3(1 - 2\mu)}{2(1 + \mu)} \mathrm{K} \tag{6.9}$$

where μ is Poisson's ratio. The elastic parts of the deformation can be expressed as:

$$\begin{bmatrix} \mathrm{d}\epsilon_{\mathrm{v}}{}^{\mathrm{e}} \\ \mathrm{d}\epsilon_{\mathrm{q}}{}^{\mathrm{e}} \end{bmatrix} = \begin{bmatrix} 1/\mathrm{K} & 0 \\ 0 & 1/3\mathrm{G} \end{bmatrix} \begin{bmatrix} \mathrm{dp}' \\ \mathrm{dq} \end{bmatrix} \tag{6.10}$$

where $\mathrm{d}\epsilon_{\mathrm{v}}{}^{\mathrm{e}}$ is the elastic volumetric strain and $\mathrm{d}\epsilon_{\mathrm{q}}{}^{\mathrm{e}}$ is the elastic distortional strain.

The flow rule determines the direction of the plastic increments and is linked to the yield surface because the plastic strain occurs perpendicular to the yield surface:

$$\frac{\mathrm{d}\epsilon_{\mathrm{v}}{}^{\mathrm{p}}}{\mathrm{d}\epsilon_{\mathrm{q}}{}^{\mathrm{p}}} = \frac{\mathrm{M}^2 - \eta^2}{2\eta} \tag{6.11}$$

The plastic stress-strain response is:

$$\begin{bmatrix} \mathrm{d}\epsilon_{\mathrm{v}}{}^{\mathrm{p}} \\ \mathrm{d}\epsilon_{\mathrm{q}}{}^{\mathrm{p}} \end{bmatrix} = \frac{1}{\mathrm{H}} \begin{bmatrix} (\mathrm{M}^2 - \eta^2) & 2\eta \\ 2\eta & 4\eta^2/(\mathrm{M}^2 - \eta^2) \end{bmatrix} \begin{bmatrix} \mathrm{dp}' \\ \mathrm{dq} \end{bmatrix} \tag{6.12}$$

The plastic modulus H (Equation 6.13) is calculated using the specific volume (ν), plastic volume strain ($\epsilon_{\mathrm{v}}{}^{\mathrm{p}}$), plastic distortional strain ($\epsilon_{\mathrm{q}}{}^{\mathrm{p}}$) and stress ratio ($\eta = \frac{\mathrm{q}}{\mathrm{p}'}$).

$$\mathrm{H} = \frac{(1+\mathrm{e})\mathrm{p}'(\mathrm{M}^2 + \eta^2)}{\lambda - \kappa} \tag{6.13}$$

The changes to the Modified Cam-Clay model resolved the issue that occurs in the original Cam-Clay model by removing the singularity point, and was able to reasonably simulate the behaviour of normally and slightly overconsolidated clays. It is capable of capturing features such as pressure sensitivity, hardening response with volumetric compaction, softening response with plastic dilation and coupled volumetric-deviatoric plastic deformations (Borja and Regueiro 2001). There are still issues with the Modified Cam-Clay model though, such as unrealistically large ratios of shear stress over mean stress when the stress state exceeds the CSL and the transition from elastic to elasto-plastic behaviour is sudden and abrupt, which causes a sharp drop in the soil stiffness. In addition, the elastic range is overestimated, meaning that the model cannot predict the accumulation of plastic strains or excess pore water pressures under cyclic loading when the stress path moves inside the yield surface.

6.3 Validation of the Modified Cam-Clay soil model

A soil model can be validated by comparing laboratory test results to the numerical prediction. The Plaxis SoilTest is a constitutive model driver, able to simulate basic laboratory tests such as triaxial, oedometer and direct simple shear, and was used here to validate the material parameters.

The soil model was validated using triaxial experimental data from Robinson (2019). The soil parameters derived by Robinson (2019) were used and are given in Table 6.1.

A comparison of the triaxial data and prediction of the MCC model is presented in Figure 6.5 and shows that the model gives a generally good prediction of the experimental stress path.

Table 6.1: Modified Cam-Clay soil model inputs

Parameter	Value
κ	0.021
λ	0.168
M	0.851
e_{init}	0.5
ν_{ur}	0.15
OCR	1.4
c'	$10 kN/m^2$

At higher confining stresses, the curvature of the stress path is slightly over estimated by the MCC but an excellent fit is produced at the lowest confining stress of 280 kN/m^2, which is most relevant to the modelling in this chapter.

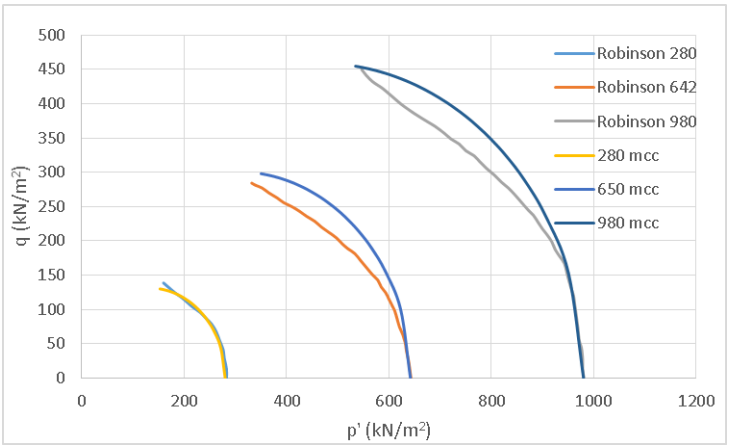

Figure 6.5: The calibration data from Robinson (2019), and the data produced by the Modified Cam-Clay soil model

6.4 Finite element model

A plane strain finite element model was used as the prototype was designed to be simulated in 2D. The choice of seconds for time unit is important for the cyclic loading in order to be accurate in replicating the physical modelling.

The soil is a modelled as a homogenous kaolin speswhite clay, described by the MCC model with parameters given previously. The soil is assumed to be undrained and the effective unit weight is set to $7 kN/m^3$ and the water level set at the base of the model. In the physical modelling a section of soil was excavated so that the undrained shear strength (s_u) at the surface was around 10kPa. To simulate the surface strength in the numerical model, 7m of soil was excavated.

The layout of the numerical model can be seen in Figure 6.6. The soil body is 70m by 27m with an internal section of 18m by 9m for mesh refinement.

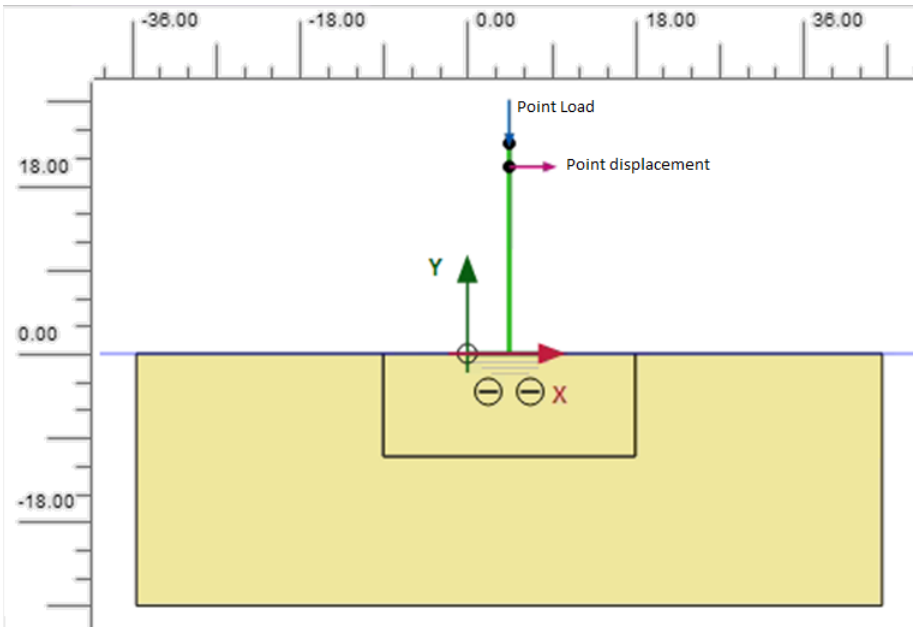

Figure 6.6: The prototype structure and soil in the finite element model

To recreate the physical modelling two plates are used to model the foundation and the superstructure. For the foundation a 9m horizontal plate was placed on the excavated surface; the material properties are given in Table 6.2. Soil-structure interaction is modelled by interface elements, allowing the plate to move independently of the soil. The strength and stiffness of the interface is relative to that of the soil and is controlled by the value of R_{inter} (see section 6.5).

The superstructure is modelled by using a vertical plate, which starts at the centre of the foundation plate and is 22.5m tall. The material properties for the superstructure plate can be seen in Table 6.2. To model the nacelle and the blades a point load is placed at the top of the plate. The point load has a force of -228kN/m which is loaded in the negative y direction (see Figure 6.6).

Table 6.2: Structural properties and loading information

		1g prototype
Foundation weight	kN/m/m	38
Foundation EI	kN/m	14.58 x 10^9
Foundation EA	kN/m	720 x 10^6
Foundation ν		0.32
Superstructure weight	kN/m/m	4.115 x 10^{-6}
Superstructure EI	kN/m	100x 10^3
Superstructure EA	kN/m	1x 10^6
Superstructure ν		0.32
Point load	kN/m	-228

There is a point displacement applied to the superstructure 20m from its base. This point is used to apply the wind displacements, which were described in section 3.3.3. The inputs required to reproduce the normal, storm and gust displacements are shown in Table 6.3.

Table 6.3: Multipliers for cyclic displacement

	Signal	Amplitude (m)	Frequency (Hz)
Normal	Harmonic	0.150	0.03333
Storm	Harmonic	0.300	0.01665
Gust	Harmonic	0.400	0.01111
Exaggerated	Harmonic	0.600	0.0083

Deformation x-axis boundaries are both normally fixed, while the minimum y-axis boundary is fully fixed and the maximum y-axis boundary is free. The x-axis boundaries are both viscous. The viscous boundaries allow for energy that reaches them to be absorbed and therefore not reflected back into the soil body (Brinkgreve et al. 2011).

The calculation process has 3 sections: the initial phase, the turbine construction section which has 4 phases, and the cyclic section which applies the cyclic displacements. The initial stage is a K0 procedure, where the soil body is created in an undisturbed state.

After the initial stresses are generated, 7m of soil is removed from the top the soil body. This is to remove softer soil until the undrained shear strength of the soil at the surface is similar to the 10kPa obtained in the laboratory. The model is constructed in a series of plastic calculation phases. First, the foundation is installed with an active interface against the soil body.

The superstructure is then added in two parts: first the plate element that represents the tower is activated before the nacelle and blades are added as a point load. Finally, the cyclic displacements representing the wind loading are applied as prescribed dynamic displacements across a series of phases to model the configuration of each wind scenario (see Table 6.3).

6.5 Parametric study of the interface values

The interface controls how the structure is connected to the soil. A rough interface ($R_{inter} = 1$) would represent a fully connected/bonded soil interface connection, anything below $R_{inter} = 1$ is a reduction in strength and stiffness of the interface compared to that of the soil body. The aim is to predict the uplift that is seen in the 1g tests, where in normal cyclic displacement the edge of the foundation was recorded moving $\pm$11mm within a single cycle of normal displacement.

Table 6.4: Inputs for the Modified Cam-Clay interface

	Analysis a	Analysis b	Analysis c
c' (kN/m^2)	6	1	10
$\phi(^\circ)$	22	1	30
$\psi(^\circ)$	0	0	0

Initially a study into the interface focused on using a Modified Cam-Clay soil model, which requires values of c', ψ and ϕ. The inputs used can be seen in Table 6.4.

In Figure 6.7 it is possible to see that there is little change between the different values and the reaction from the interface. The resulting movement has an amplitude of 2mm at the foundation edge, which is significantly less than than recorded in the 1g test.

The Mohr-coulomb soil model is soil model which could provide adequate interface behaviour. The input required is a single value for R_{inter}. Instead, a linear elastic Mohr-coulomb material was defined to control the interface. This was assigned the following properties: E, ν, c', ϕ and a value of R_{inter} from 0.035 to 0.08.

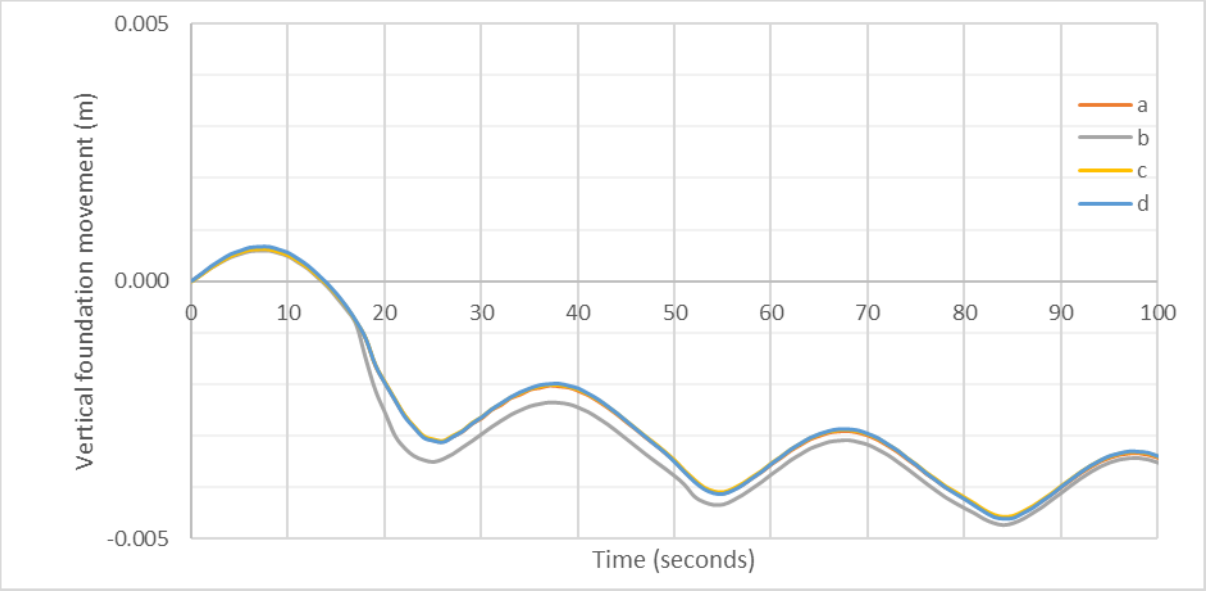

Figure 6.7: Results of the parametric study using an MCC interface using the parameter in Table 6.4

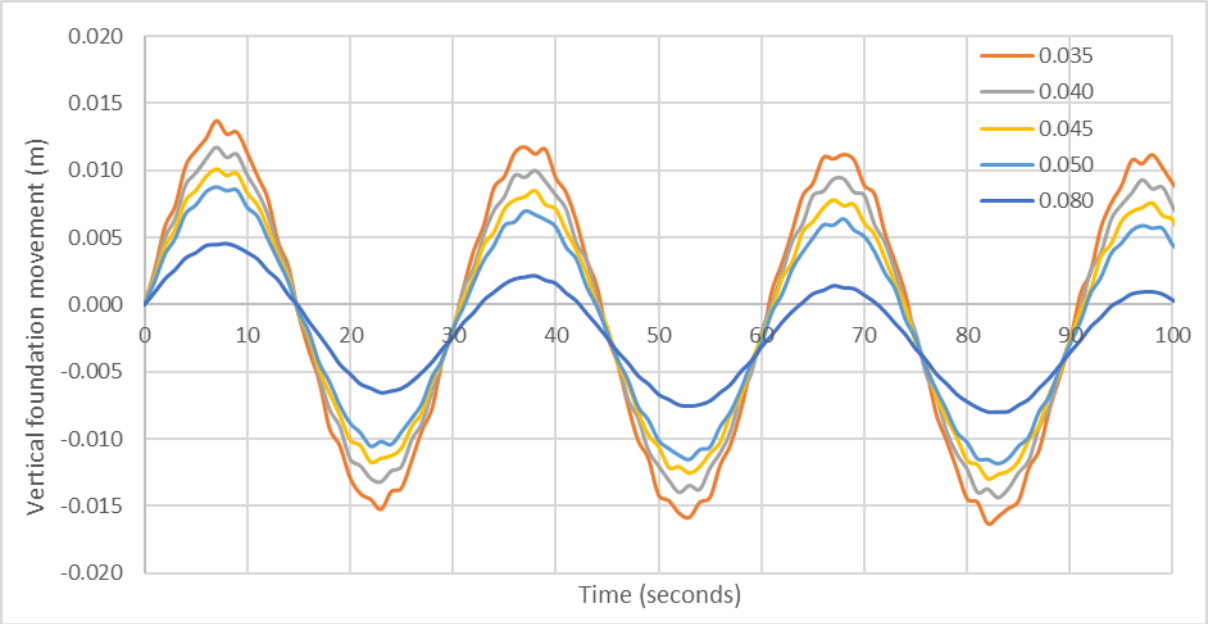

Figure 6.8: Results of the parametric study using a Mohr-coulomb interface

As seen in Figure 6.8 there is a consistent increase of uplift and embedment at the edge of the foundation with a decreasing value of R_{inter}. With the aim of matching the edge of the foundation moving around 22mm within a cycle, a value of R_{inter} of 0.04 was chosen, which produced 23.5mm of movement at the edge of the foundation within a cycle.

6.6 Simulations

The 1g tests that are being simulated are the Baseline, Short break storm and Gust storm. This will include using the same cyclic displacements that are described in section 4.4. The results from the numerical modelling are shown alongside the results from the 1g tests.

6.7 Baseline simulation

The first test to be simulated is the baseline test This 1g test consists of 360 cycles of 150mm displacement. The simulation was extended to 700 cycles.

Figure 6.9 displays the vertical movement at the centre of the foundation. The simulation and 1g test are plotted together for comparison. There is less settlement at the centre of the foundation during the simulation than the test. The simulation also produced less displacement in each cycle, which could be due to either the interface between the soil and structure not allowing for uplift, or the rigidity of the superstructure and the foundation.

The vertical movement at the edge of the foundation (Figure 6.10) does initially involve settlement, but after 6 cycles the settlement has stabilised and the edge of the foundation is just vertically moving within each cycle. The settlement-rotation curves in Figure 6.11 shows that the rotation is similar between the simulation and the 1g test, while the settlement is only similar in-cycles 1-6. The rotation data is taken from a node at the centre of the foundation.

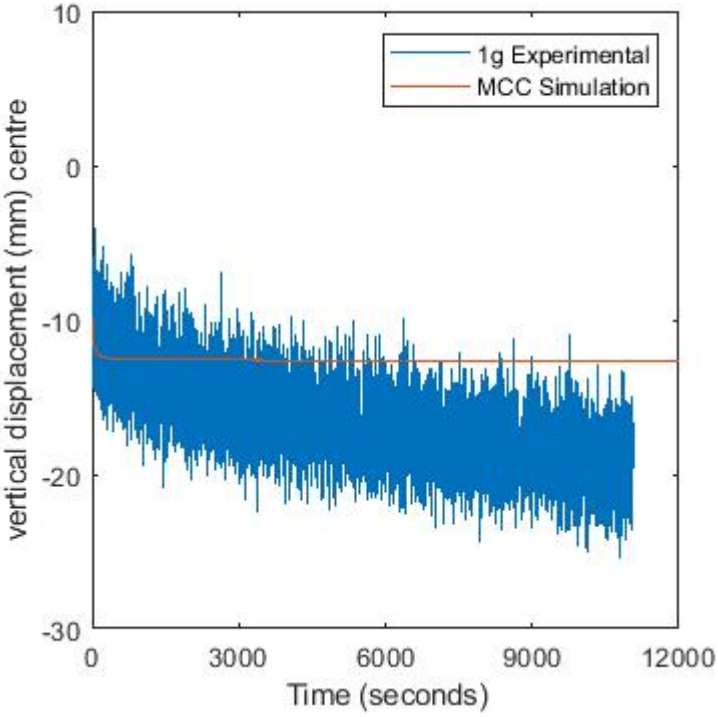

Figure 6.9: Vertical movement at the centre of the foundation - baseline 1g test and MCC simulation

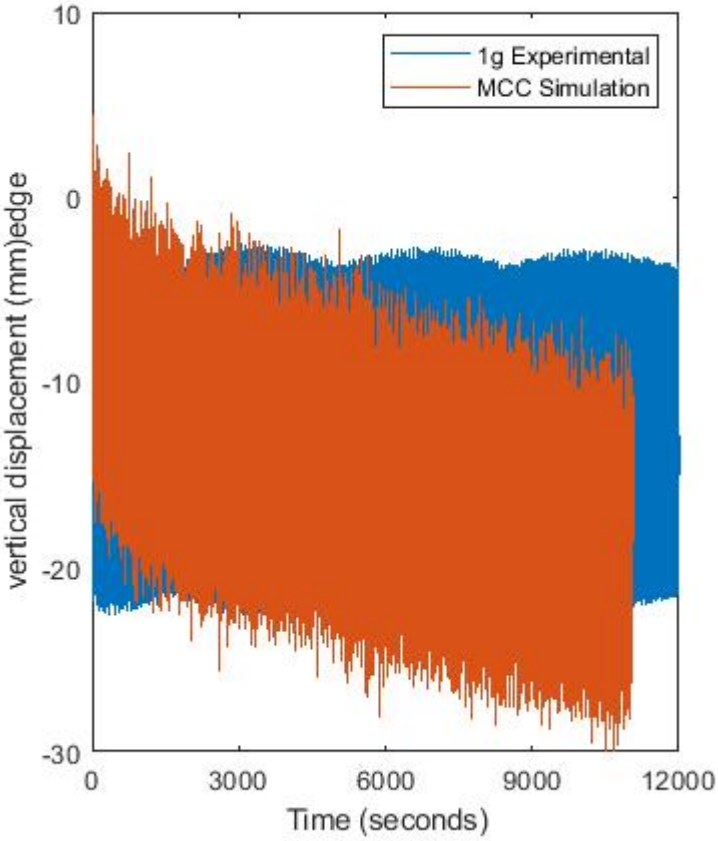

Figure 6.10: Vertical movement at the edge of the foundation - Baseline 1g test and MCC simulation

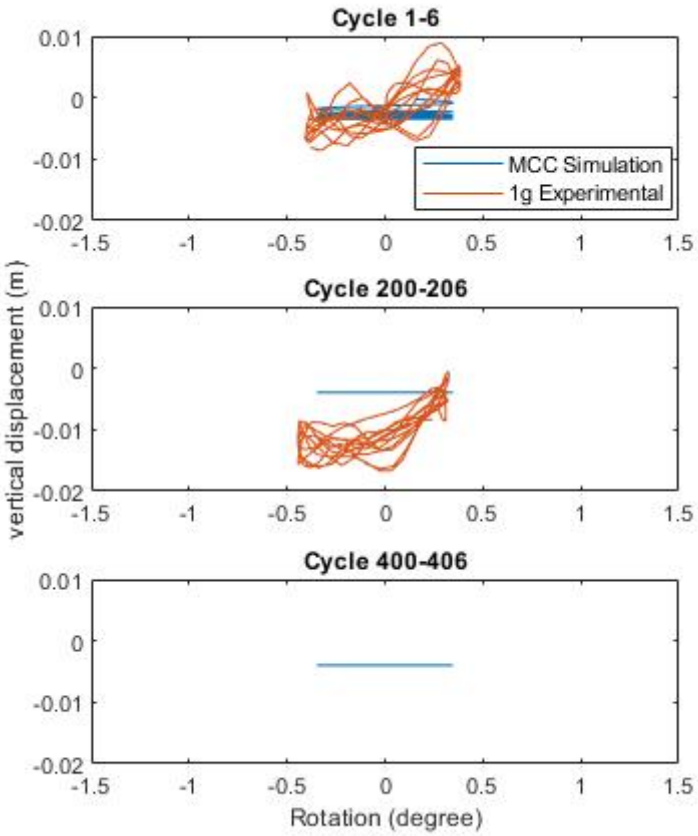

Figure 6.11: Settlement - rotation - baseline 1g test and MCC simulation

The accumulated deviatoric strain - cycle number (Figure 6.12) is displaying the strain below the right hand edge of the foundation, the data used for the figure was taken at 30 second intervals, as the simulated structure has reached the maximum rotation. The strain increases the most from cycle 1-17, where it increased from 1.22 to 1.6 x10^{-4}, and from cycle 25 there is a steady increase in strain but at a much lower rate than in the initial cycles.

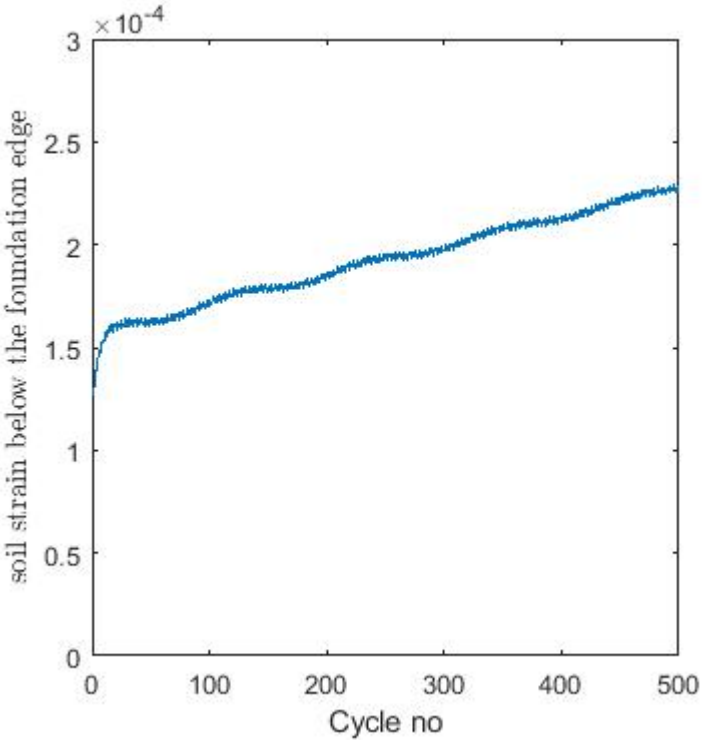

Figure 6.12: Accumulated deviatoric strain - cycle number for the baseline simulation

Figure 6.13 shows the vertical displacement of the soil body during the simulation. The displacement is centred around the foundation, with the highest levels of settlement under the centre of the foundation. The displacement below the foundation is in a 'u' shape, it can be seen that the displacement spreads at depth which could be due to the increasing soil strength with depth.

The deviatoric strain within the soil body is displayed in Figure 6.14. The strain below the foundation is concentrated at the edges, which is due to the cyclic embedment of the foundation. Less strains are produced at the centre, although the centre of the foundation did not lift from the soil during cyclic displacements; this was also noted in Figure 6.9. At depth below the centre of the foundation the shear planes intersects creating a zone of higher strain. The strain dissipates out laterally at depth.

Figure 6.15 shows the incremental deviatoric strain for the simulated phase. From cycle 6 the strain is higher at the edges of the foundation, while there is little at the centre of the foundation. Cycle 206 shows a similar pattern to cycle 6, with decreasing levels of strain. The same occurs for cycle 406 where the incremental deviatoric strain is again reduced. When comparing these outputs to Figure 6.12 it can be seen that the start of the simulation a high strain rate is occurs, while for cycles 206 and 406 the overall strain rate is similar .

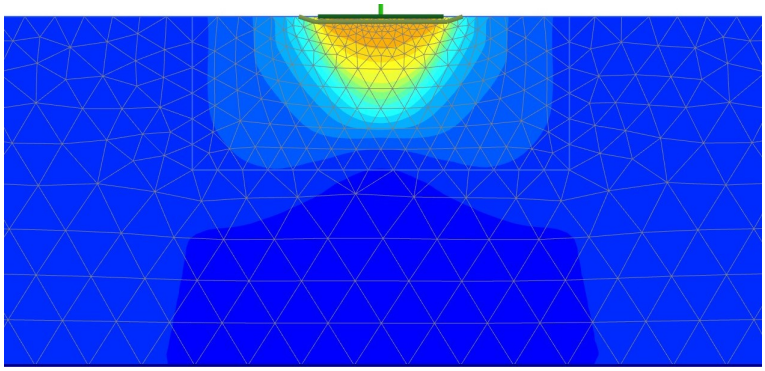

(a) Cycle 6

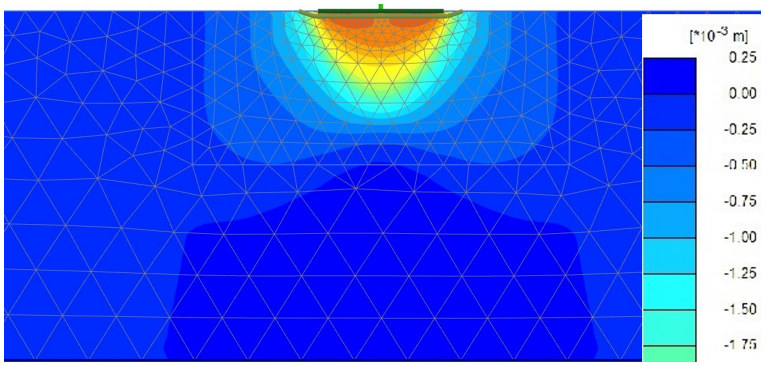

(b) Cycle 206

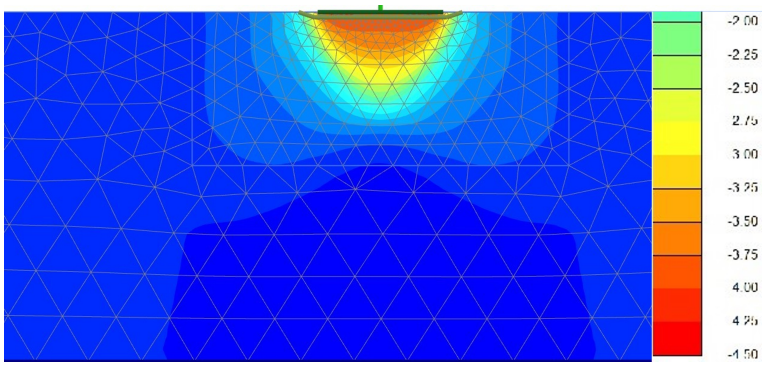

(c) Cycle 406

Figure 6.13: Visual output from Plaxis displaying the vertical displacement within the soil body

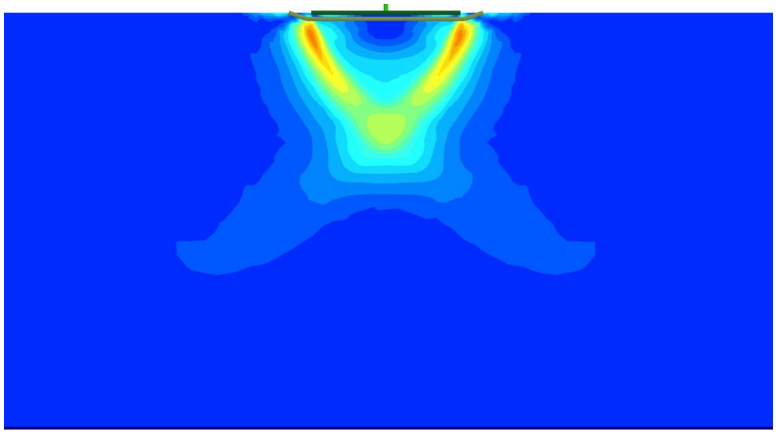

(a) Cycle 6

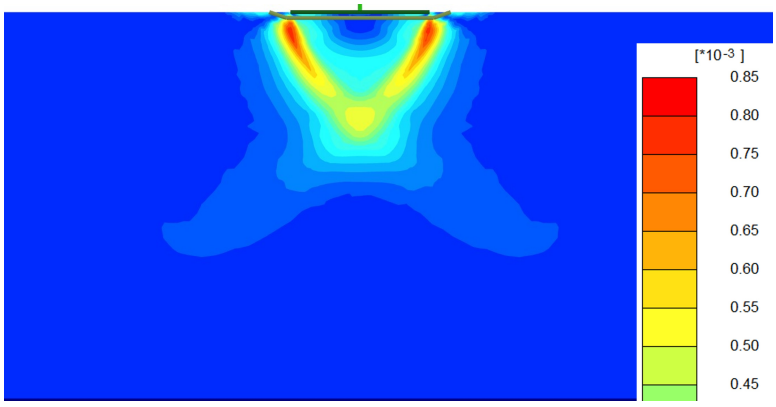

(b) Cycle 206

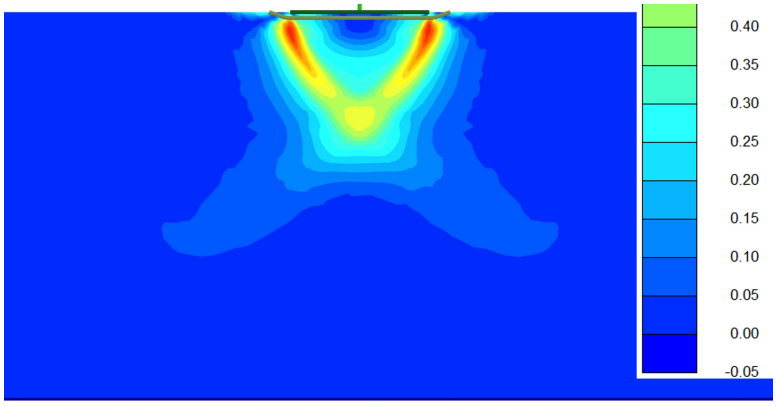

(c) Cycle 406

Figure 6.14: Visual output from Plaxis displaying the accumulated deviatoric strain in the soil body

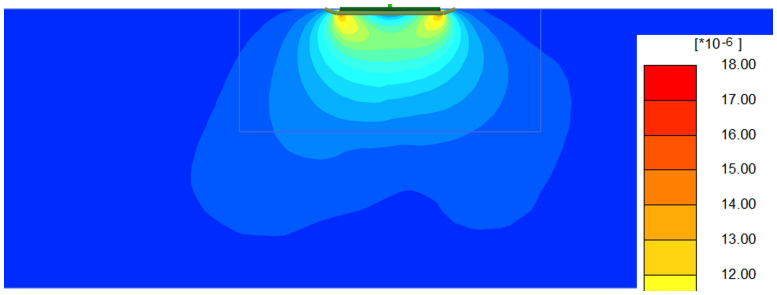

(a) Cycles 6

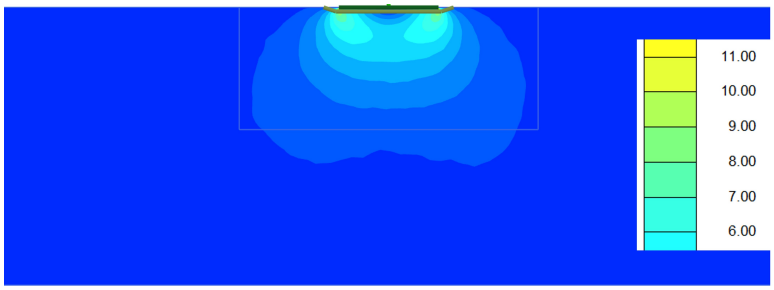

(b) Cycle 206

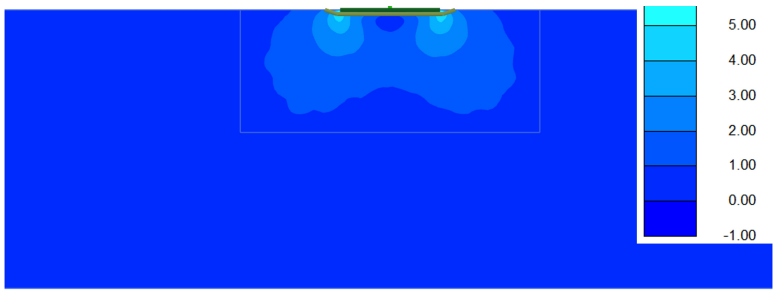

(c) Cycle 406

Figure 6.15: Visual output from Plaxis displaying the incremental deviatoric strain the soil body

The plastic points are displayed to show if any of the soil body showed plastic behaviour. The blue marks in Figure 6.16 (a) represent cap points and occur beneath the foundation, indicating yielding on the subcritical side of the yield surface as the current stress is equivalent to the preconsolidation stress. In subsequent cycles (206 and 406), the initial expansion of the yield surface means that the current stress is now contained inside the yield surface and the soil body shows elastic behaviour.

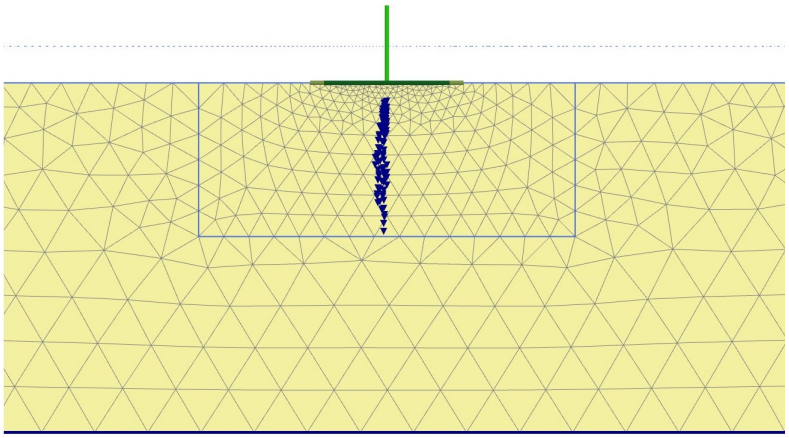

(a) Cycle 6

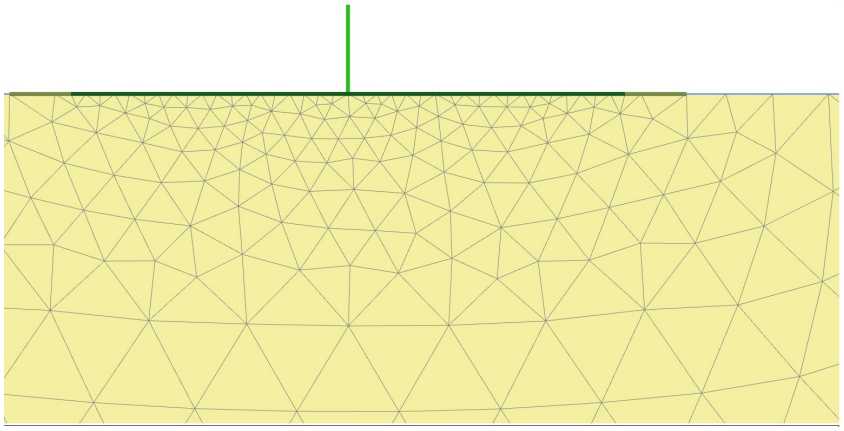

(b) Cycle 206

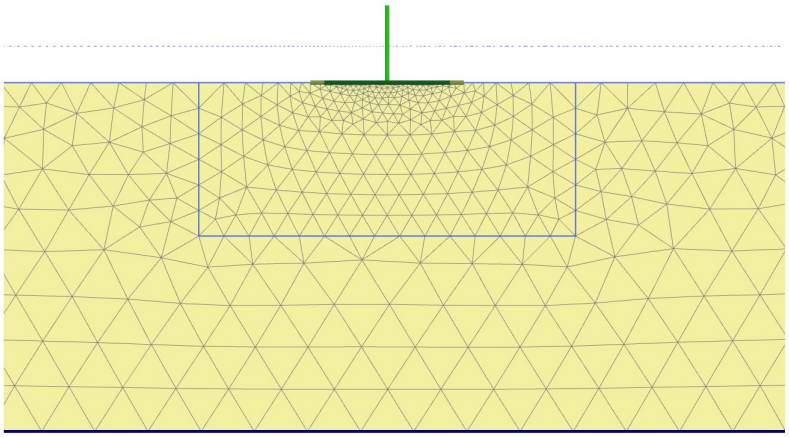

(c) Cycle 406

Figure 6.16: Visual output from Plaxis displaying the plastic points in the soil body. Blue triangles - cap points

Overall the simulated response to the cyclic displacement shows an underestimation of the reaction, when compared to the 1g test. While the interface provided adequate movement at the edge of the foundation, the centre of the foundation does not uplift from the soil. The underestimation of settlement of the centre of the foundation is due to the current stress point moving inside the yield surface after its initial expansion and hence there is no accumulation of plastic strains from cycle to cycle.

6.8 Short break storm simulation

The short break storm simulation is based on the 1g test, which contained 5,400 cycles of 150mm normal and 300mm storm displacements. There are 50 cycles in a normal phase followed by 20 cycles in a storm phase. The numerical simulation only consists of 40 phases: 20 normal and 20 storm phases.

In Figure 6.17 the settlement at the centre of the foundation is displayed until the 20th storm phase. From the 1st normal phase to the 4th storm phase there is a predicted settlement of 135mm. From the 4th storm phase to the 8th storm phase the settlement plateaus and subsequently there is a significant increase.

When comparing the short break storm simulation to the baseline simulation the behaviour is different. In the short break storm simulation the model settles more than its 1g test comparison while the baseline test does not settle as much as its 1g test comparison. The models are exactly the same the only difference is that in the short break storm simulation is longer and contains storm phases.

The same pattern of settlement is seen in Figure 6.18 as in Figure 6.17, although at the edge of the foundation there is in-cycle vertical movement at the edge which was also seen in the baseline simulation.

In Figures 6.19 phases 1, 5 and 10 are shown with their comparative 1g test phase. The normal phases show the simulation and the 1g test initially behave in a similar way, although the 1g rotation did not start at 0. By the 5th normal phase the simulation has settled while the 1g test did not. In addition, there is no uplifting movement predicted in the simulation while it is reaching the maximum rotation. By phase 10 in the 1g test the uplift at the centre of the foundation is evident in the open 'U' shape, which is again is not observed in the simulated results

The open 'U' shape is still not present when the displacement is doubled to $\pm$300mm for the storm phases of settlement - rotation. The interface between the soil and the foundation allows for the edge of the foundation to uplift but the centre shows only settlement.

The accumulated deviatoric strain is shown in Figures 6.20 (a) for the normal phases and (b) for the storm phases. There is little strain accumulation in the first 60 cycles, while from cycle 60 to 280 the strain increases from 0 to 0.11. The accumulation plateaus from cycle 280 to 540, but then there is a rapid increase in the strain until the end of the simulation. When comparing this to the baseline simulation there is significantly more strain accumulation in the short break storm simulations, which occurs after the first storm phase of displacement.

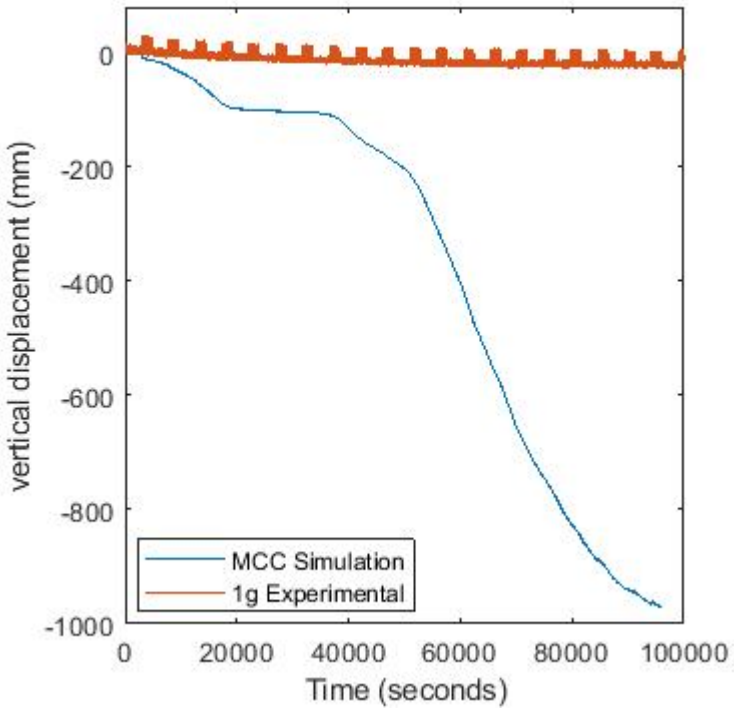

Figure 6.17: Vertical movement at the centre of the foundation - short break storm 1g test and MCC simulation

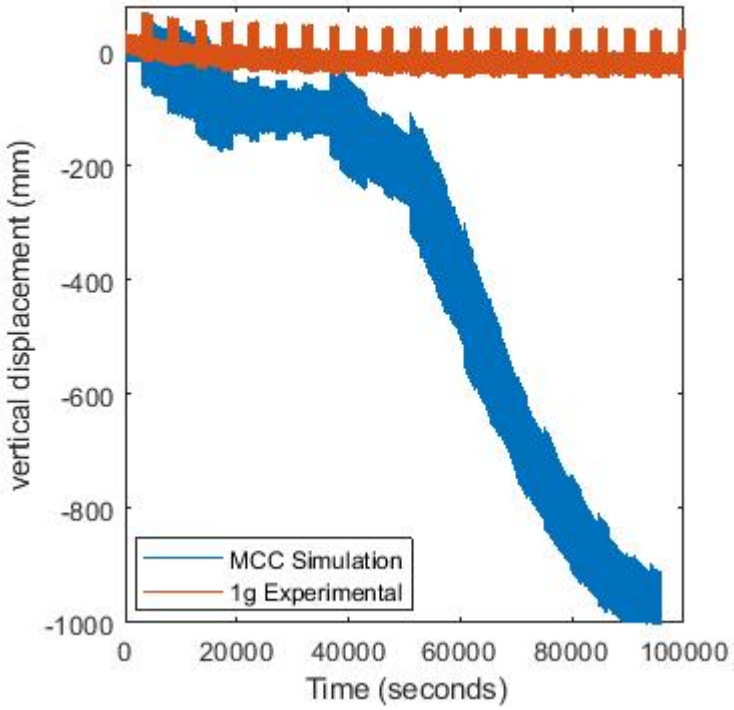

Figure 6.18: Vertical movement at the edge of the foundation - short break storm 1g test and MCC simulation

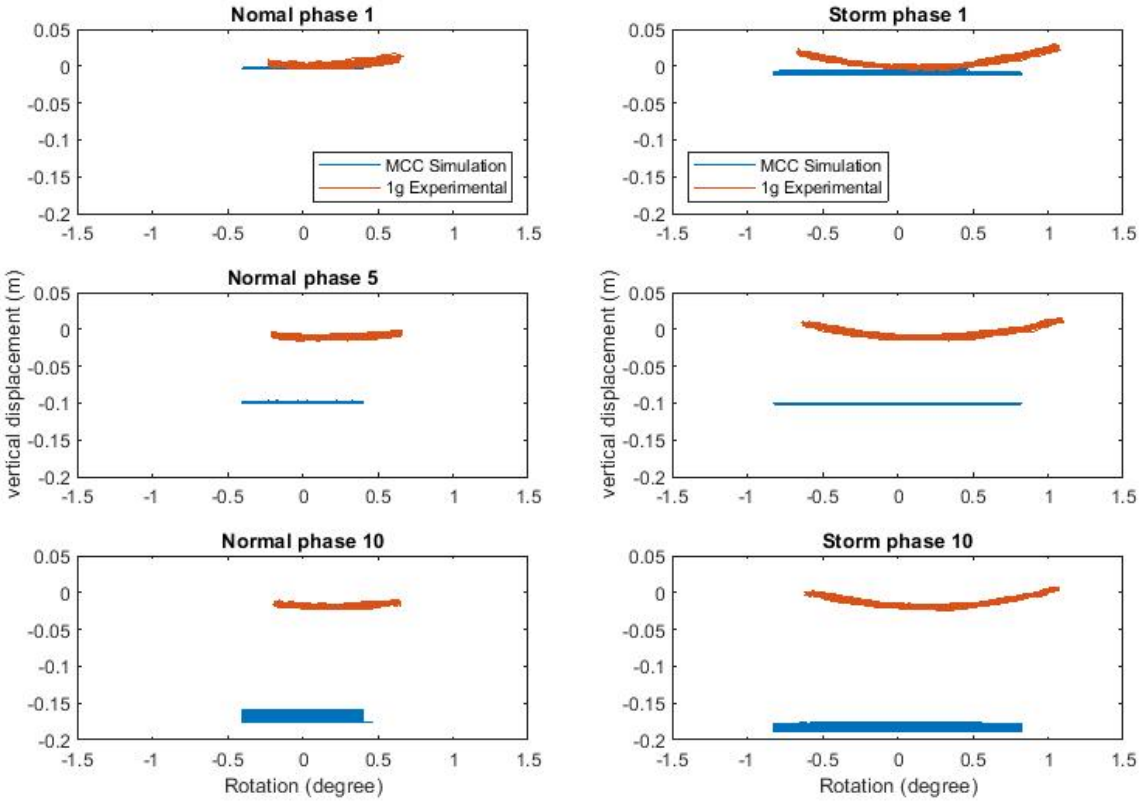

(a) Normal phases **(b)** Storm phases

Figure 6.19: Settlement - rotation, phases 1, 5 and 10 of the Short break storm 1g test and MCC simulation; normal phase (a), storm phase (b)

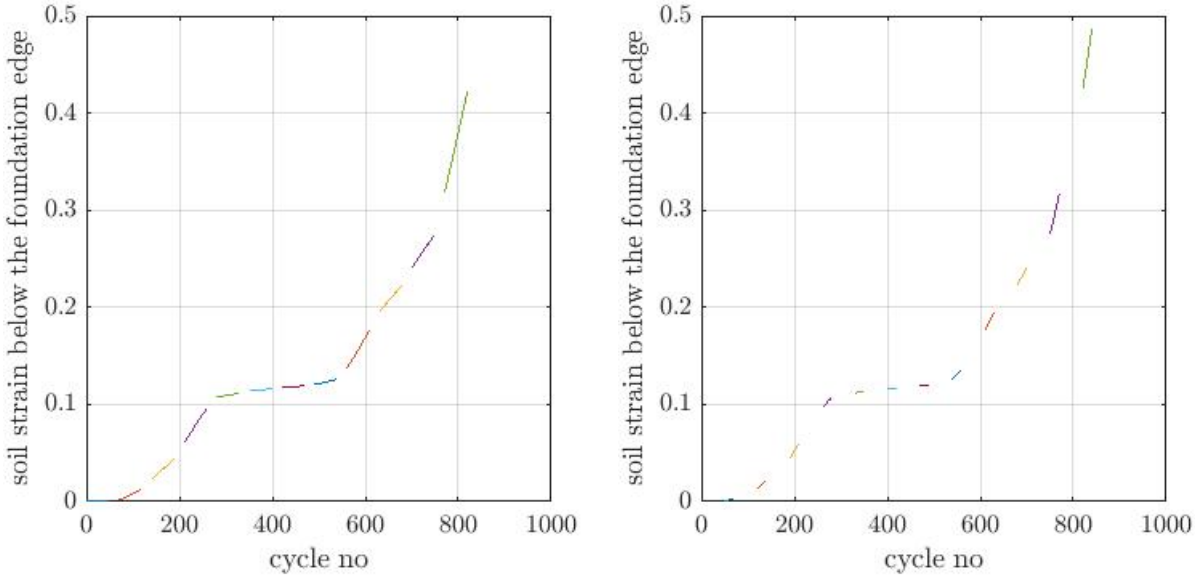

(a) Normal phases **(b)** Storm phases

Figure 6.20: Accumulated deviatoric strain vs cycle number for the short break storm simulation; normal phase (a), storm phase (b)

The displacement in Figures 6.21 shows that the displacement in the soil body in the short break storm simulation is focused at the edge of the foundation. In the first phase (normal and storm) there is no visual change to the soil body, by the 5th normal phase the displacement is focused around the edges of the foundation. The shape of the vertical displacement indicates the soil profile below the foundation is rounding as the edges of the foundation embed into the soil. The displacement in this shape increases in phase 5 storm, and phases 10 and 15 where the displacement intensifies at the edge of the foundation where embedment occurs. By the 15th phases there is settlement at the centre of the foundation, which is the overall structure settlement.

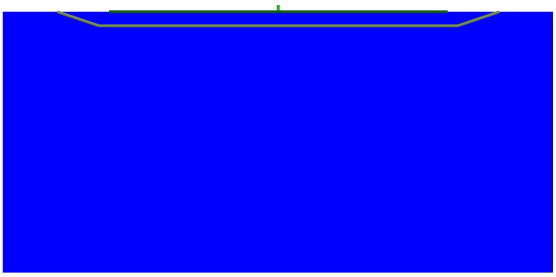

(a) Phase 1: normal

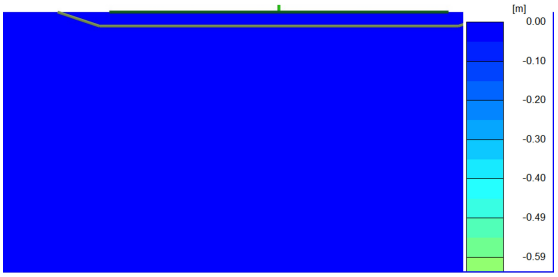

(b) Phase 1: storm

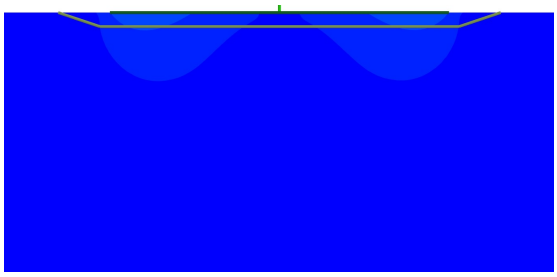

(c) Phase 5: normal

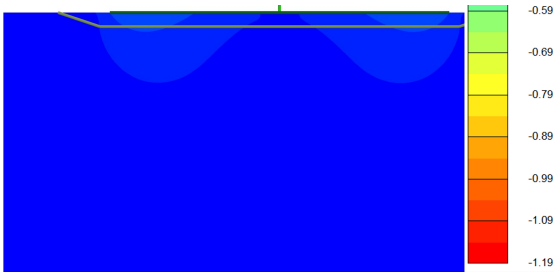

(d) Phase 5: storm

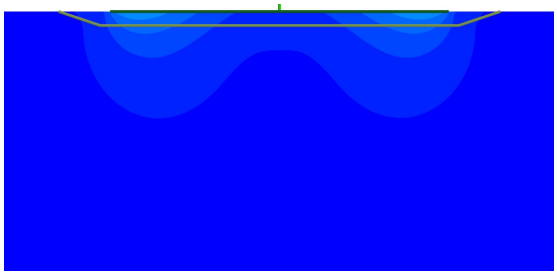

(e) Phase 10: normal

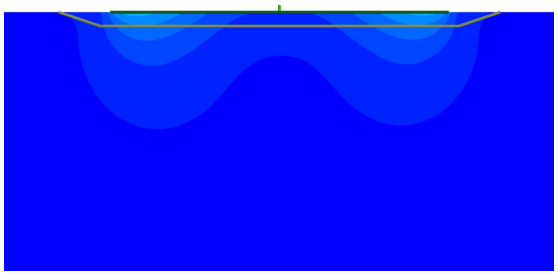

(f) Phase 10: storm

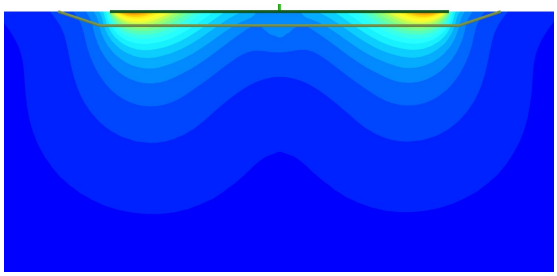

(g) Phase 15: normal

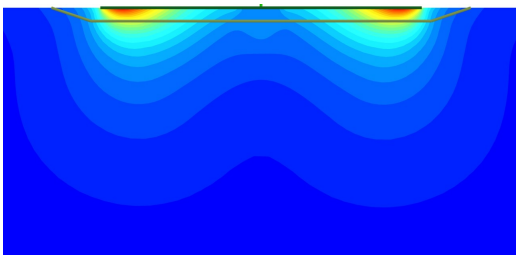

(h) Phase 15: storm

Figure 6.21: Visual output from Plaxis displaying the vertical displacement within the soil body

The incremental deviatoric strain is shown in (Figure 6.22). In the 1st and 5th phases there is no change in the soil body. The 10th normal phase continues the pattern seen during the 5th normal phase, although with a higher intensity of strain at the foundation edge. The 15th normal phase has the highest intensity of strain below the edges of the foundation. It is not matched by phase 15 storm, so the number of cycles has a greater impact on the strain than the additional displacement in the storm phases.

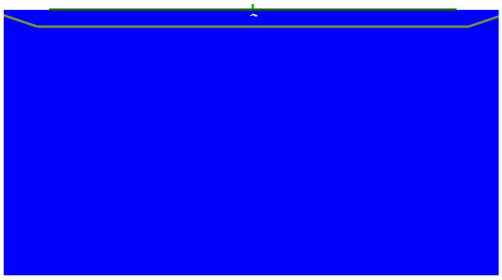

(a) Phase 1: normal

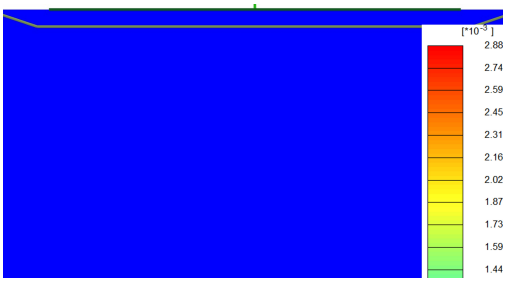

(b) Phase 1: storm

(c) Phase 5: normal

(d) Phase 5: storm

(e) Phase 10: normal

(f) Phase 10: storm

(g) Phase 15: normal

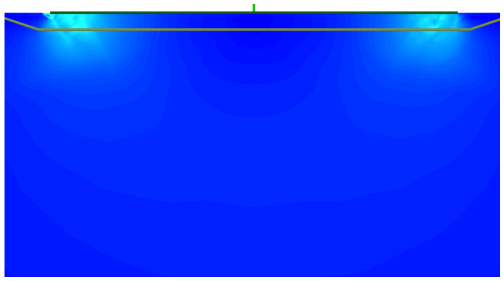

(h) Phase 15: storm

Figure 6.22: Visual output from Plaxis displaying the incremental deviatoric strain in the soil body

Figure 6.23 shows that in the short break storm simulation plastic points develop. Red dots in (b), (c), and (d) indicate a failure point and the stresses lie on the yield surface. The failure points occur near surface under the foundation. Cap points can be seen in all outputs, mainly

focused at the foundation. The 10th storm phase has cap points extending to depth which suggests that expansion of the yield surface in compression occurs throughout the simulation, resulting in the observed settlement accumulation.

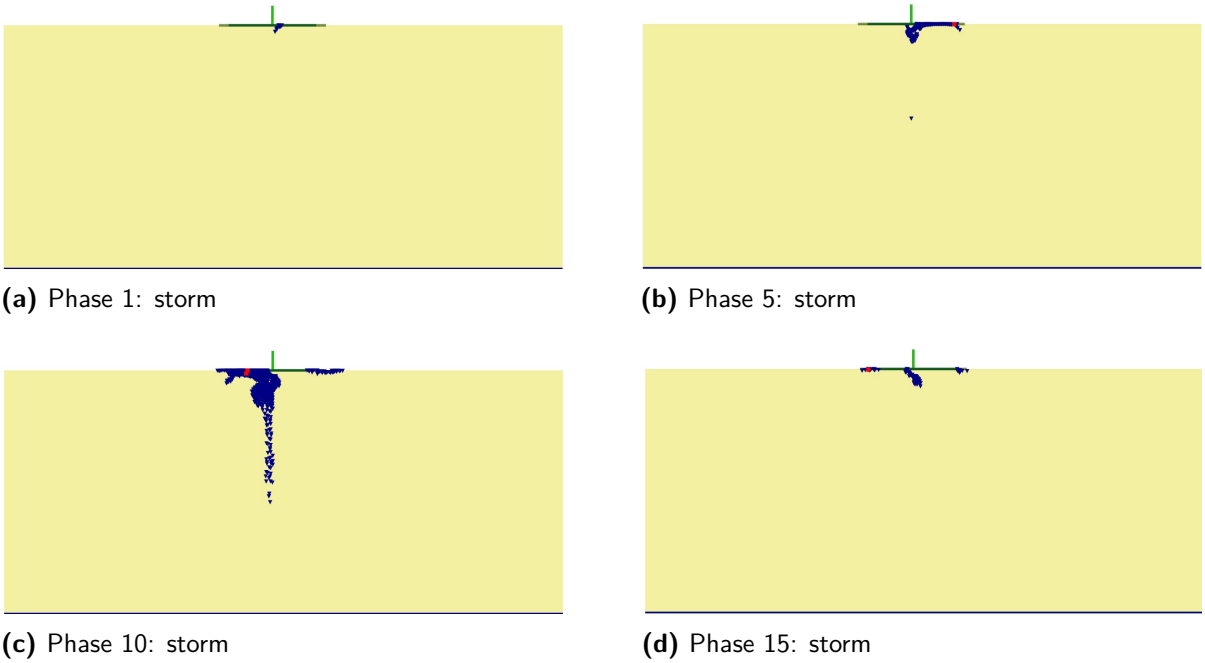

(a) Phase 1: storm

(b) Phase 5: storm

(c) Phase 10: storm

(d) Phase 15: storm

Figure 6.23: Visual output from Plaxis displaying the plastic points in the soil body, red dots = failure points, blue triangles = cap points

6.9 Gust storm simulation

The gust storm simulation is based upon the same 1g test, which contains 3 types of displacement: normal (150mm), storm (300mm), and gust (400mm) displacement, with the respective phases containing 40, 20 or 5 cycles. The simulation contains 5 phases of each displacement.

As evident in Figure 6.24 the vertical movement at the centre of the foundation shows little in-cycle movement. The overall settlement from the simulation is similar to the 1g test until 7000 seconds, which is the 3rd normal phase when the settlement increases.

The vertical displacement at the edge of the foundation is shown in Figure 6.25. The amplitude of the in-cycle movement at the edge of the foundation is over estimated in the first normal phase (0-1200s), whereas for the first storm (1200-2400s) and gust (2400-3000s) phases the simulated and 1g movement are very similar. The simulation does overestimate the embedment at the edge of the foundation. The simulated edge embedding and uplifting occurs in equal amounts, whereas in to the 1g test the uplift at the edge of the foundation is 3 times greater than the embedment.

The in-cycle movement of the foundation edge increases with each phase. In normal phase 4 (9000-10200s) the movement at the edge is 110mm from a displacement of $\pm$ 150mm. The maximum movement at the edge of the foundation from normal cyclic displacement is 60mm.

Figure 6.26 displays the simulated settlement - rotation against the same data from the 1g test for the normal phase (a), storm phase (b) and the gust phase (c).

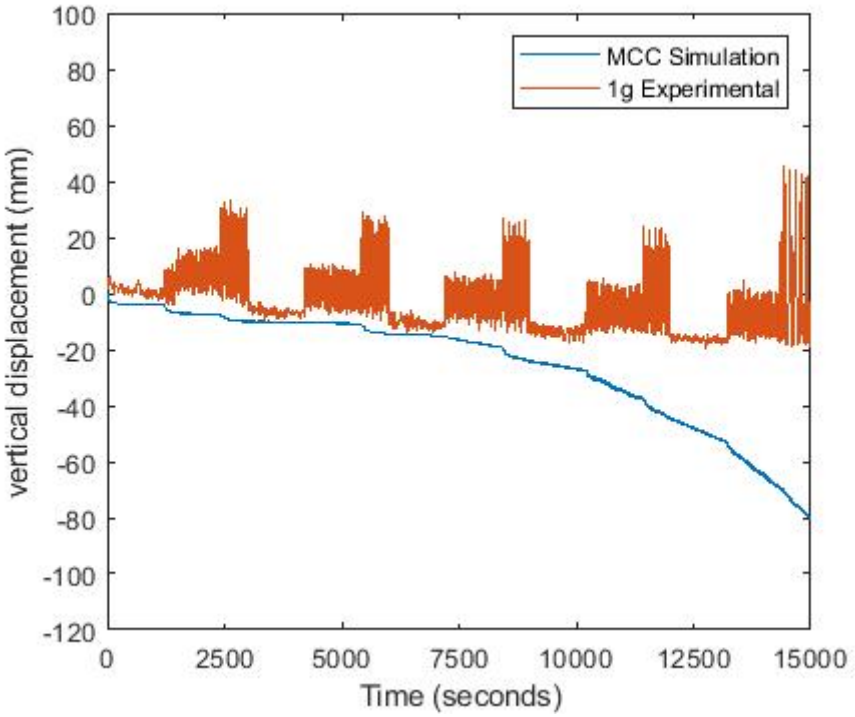

Figure 6.24: Vertical movement at the centre of the foundation - gust storm 1g test and MCC simulation

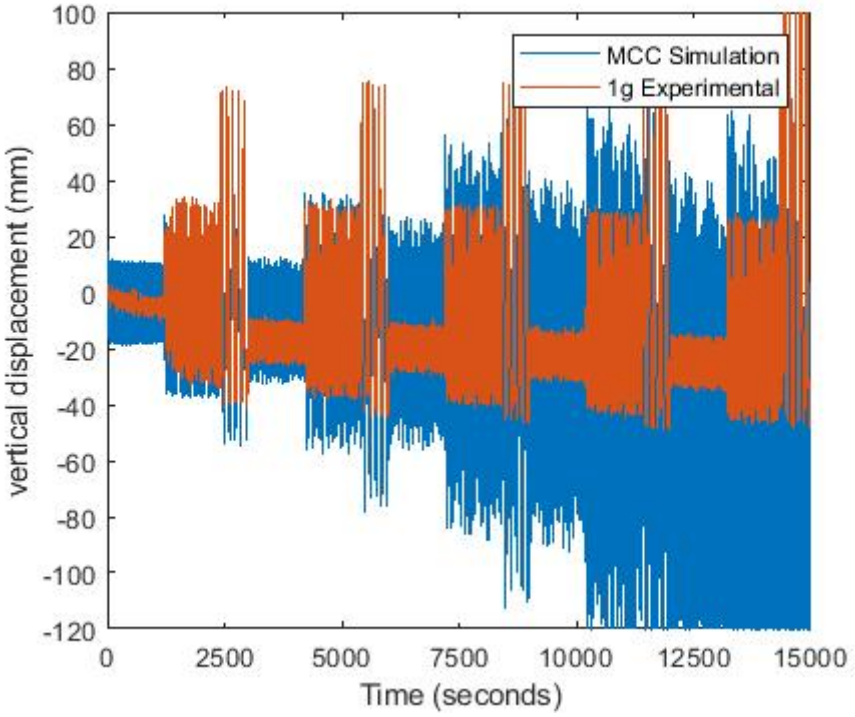

Figure 6.25: Vertical movement at the centre of the foundation - gust storm 1g test and MCC simulation

The normal phases 1-4 match the 1g test outputs well, but by the 5th normal phase the overall settlement in the simulation is more than the 1g. The same pattern of overall settlement continues for the storm and gust phases. In the storm and gust phases the 1g test shows the centre of the foundation uplifting when the rotation is over $\pm$ 0.3°, but this behaviour is not observed in the numerical results.

The rotational movement of the structure in the simulation is focused at the centre of the foundation, whereas for the 1g test the rotation is focused at the embedded edge which allows for uplift at the centre of the foundation.

The deviatoric strain accumulation is shown in Figure 6.27. The strain for the gust storm simulation has a slow increase from 0-170 cycles and within this period there are sharp increases in strain during the gust phase. From cycle 240 until the end of the simulation the strain increases exponentially.

The displacement of the soil body is shown in Figures 6.28. Figures (a) to (e) show the displacement below the foundation is even along the length of the foundation. From the 2nd gust phase, bulbs of displacement start developing from the edge to $1/3$ in from the edge of the foundation.

The displacement continues to increase throughout the phases. At the end of the 3rd, 4th and 5th storm phase the displacement below the foundation is uneven with there being more displacement on the right hand side. This could be due to the phase finishing with the structure leaning to the right. The uneven displacement it not seen in the 3rd, 4th and 5th gust phases suggesting the uneven deformation is not permanent.

The deviatoric strain within the soil body can be seen in Figure 6.29. The strain in the first normal phase (a) starts just below the foundation edge and with depth moves towards the centre of the foundation. As the cycles continue, the strain increases in concentration and expands outwards into the soil body.

The 3rd storm phase (h) is when the strain starts developing adjacent to the foundation edge. The adjacent strain did not develop in other simulations so must be a result of the gust cyclic displacement.

Figure 6.30 displays the soil body and any plastic points that have developed, for the 1st, 2nd, 3rd, 4th and 5th gust phases. In all 5 phases there are cap points which start below the centre of the foundation and continue vertically down where the stress state has equalled the pre-consolidation stress. In phase 4 and 5 (d & e respectively) there is a build up of cap points on under the left half of the foundation.

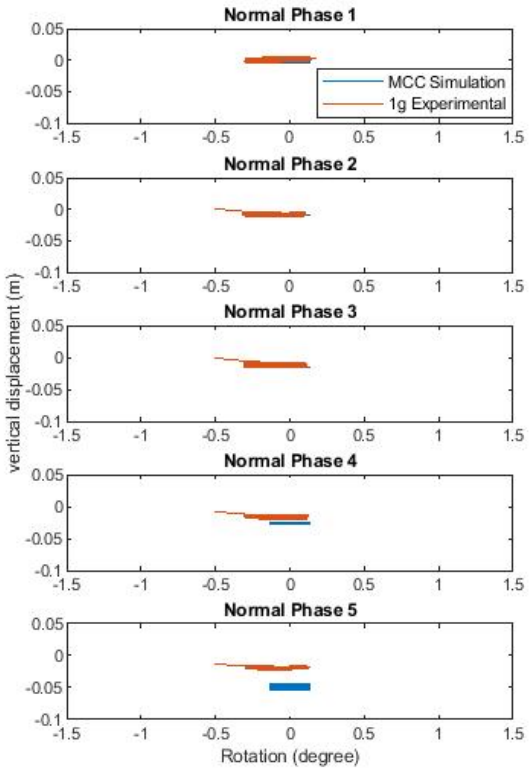

(a) Normal phases

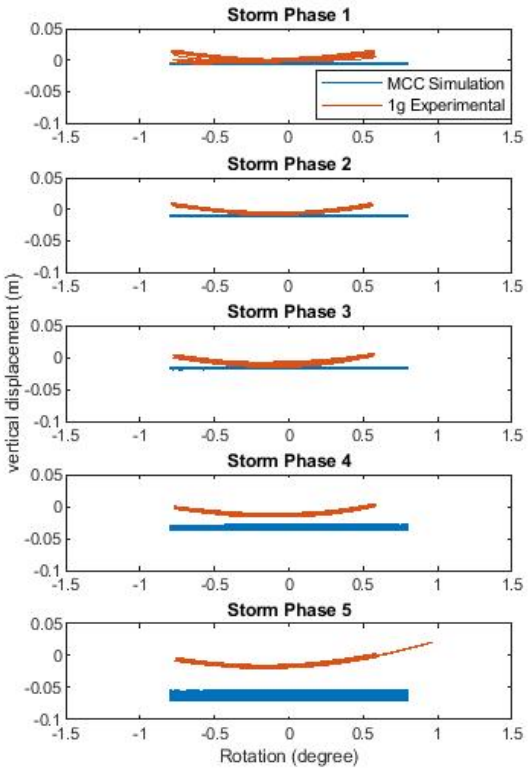

(b) Storm phases

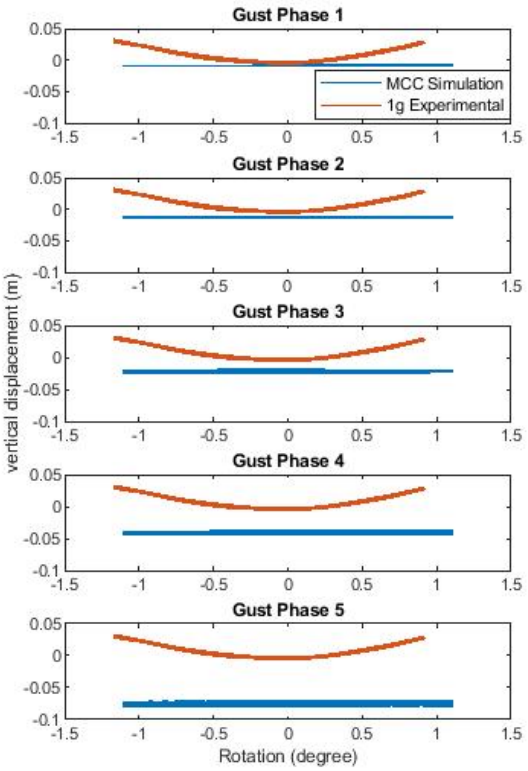

(c) Gust phases

Figure 6.26: Settlement-rotation, phases 1-5 of the Gust storm 1g test and MCC simulation; normal phase (a), storm phase (b), gust phase (c)

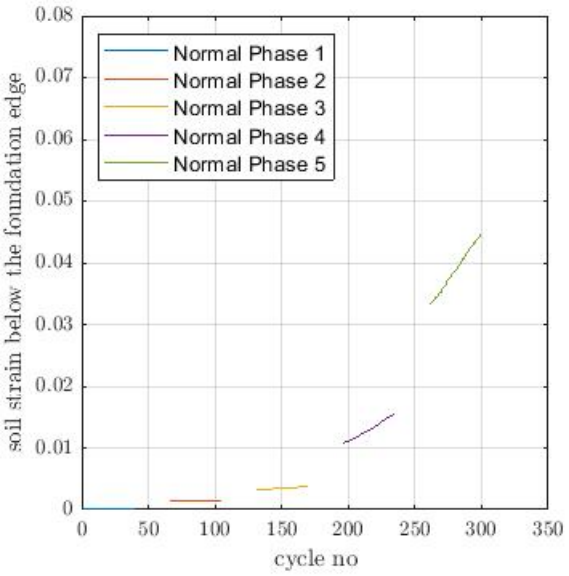

(a) Normal phases

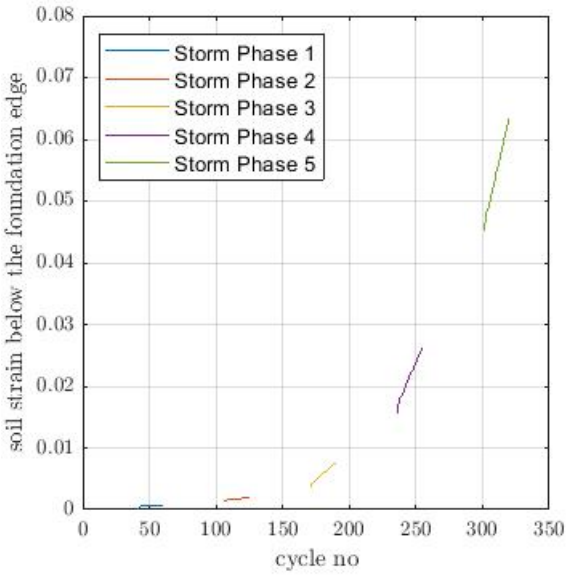

(b) Storm phases

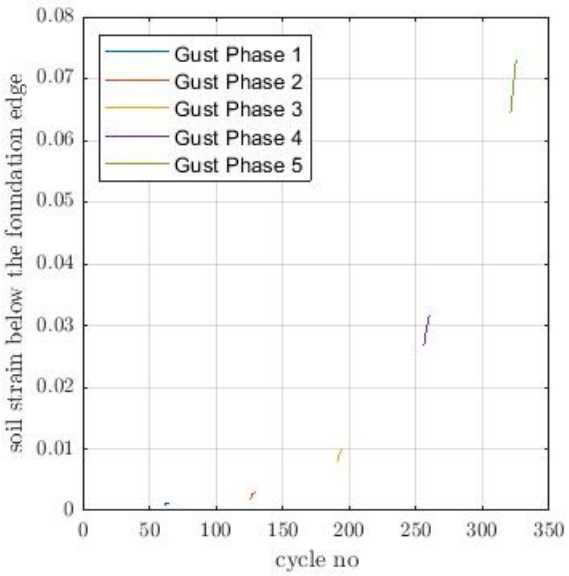

(c) Gust phases

Figure 6.27: Accumulated deviatoric strain vs cycle number for the gust storm simulation; normal phases (a), storm phases (b), and gust phases (c)

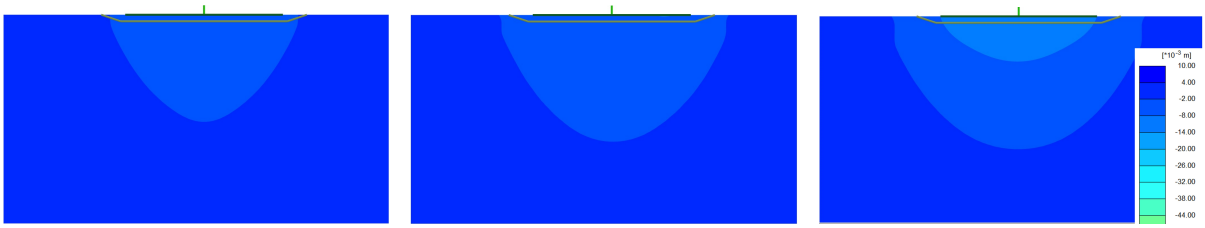

(a) Phase 1: Normal **(b)** Phase 1: Storm **(c)** Phase 1: Gust

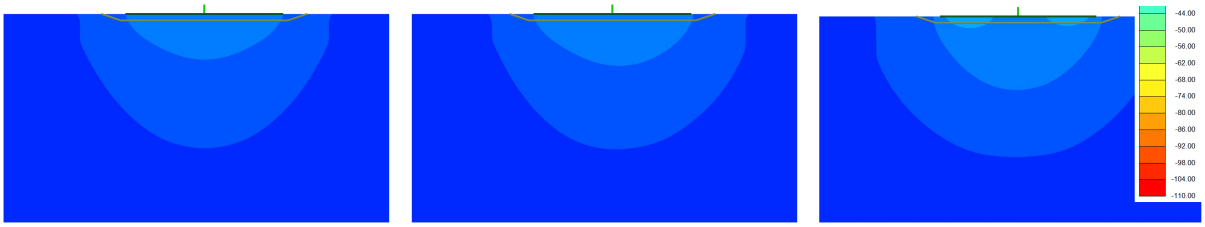

(d) Phase 2: Normal **(e)** Phase 2: Storm **(f)** Phase 2: Gust

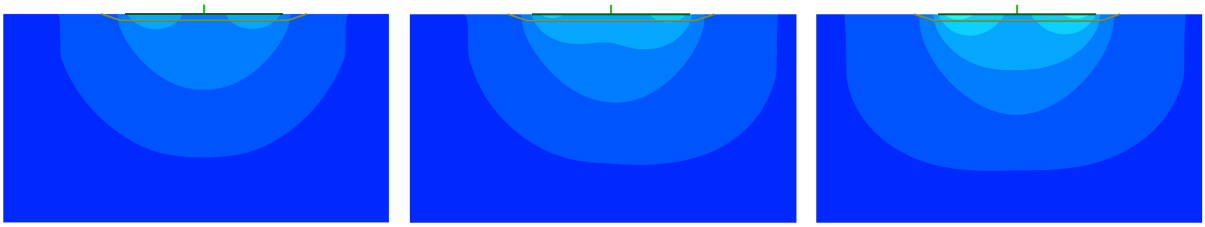

(g) Phase 3: Normal **(h)** Phase 3: Storm **(i)** Phase 3: Gust

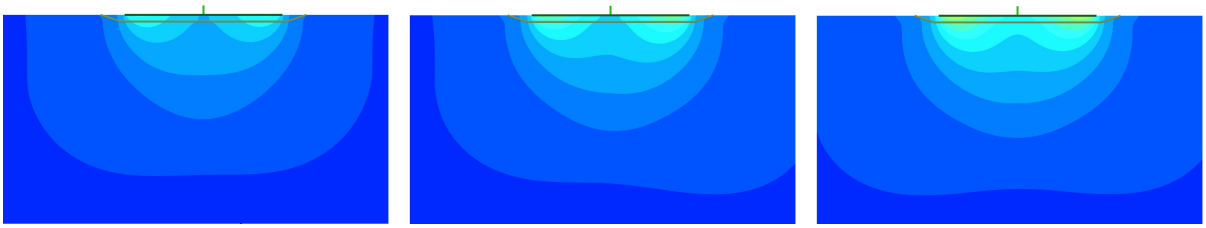

(j) Phase 4: Normal **(k)** Phase 4: Storm **(l)** Phase 4: Gust

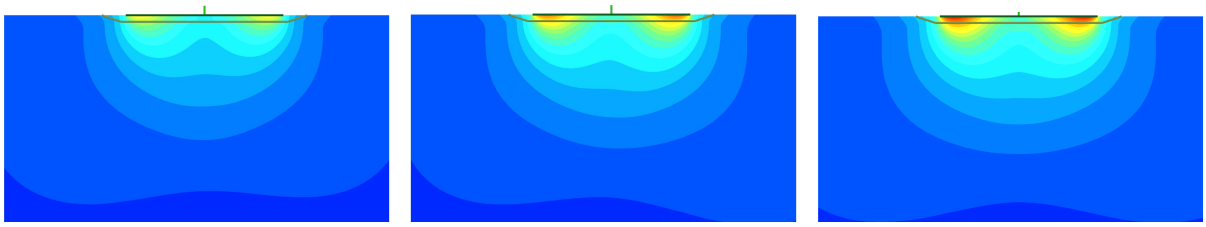

(m) Phase 5: Normal **(n)** Phase 5: Storm **(o)** Phase 5: Gust

Figure 6.28: Visual output from Plaxis displaying the vertical displacement within the soil body

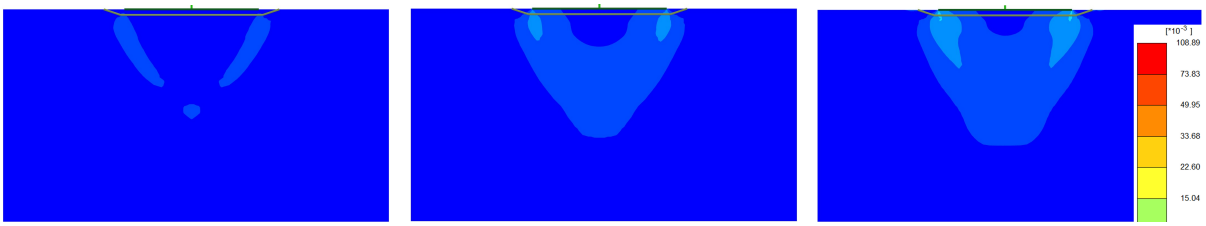

(a) Phase 1:Normal **(b)** Phase 1:Storm **(c)** Phase 1:Gust

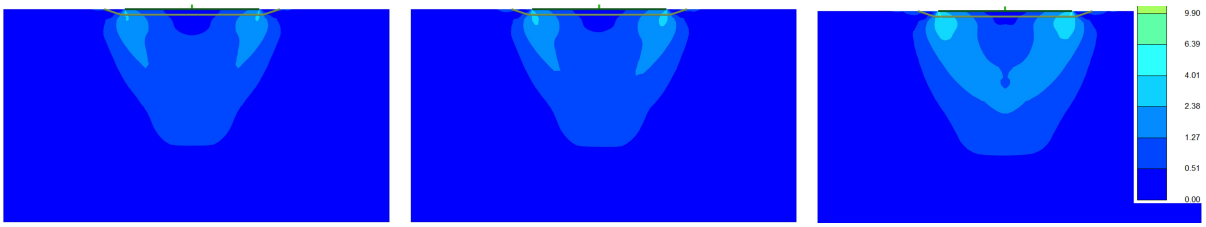

(d) Phase 2:Normal **(e)** Phase 2:Storm **(f)** Phase 2:Gust

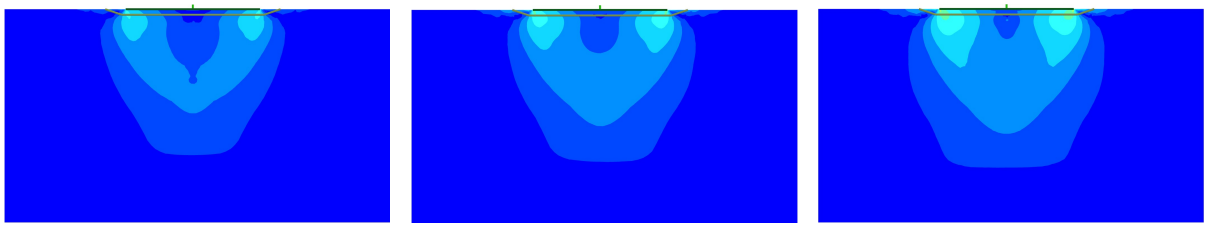

(g) Phase 3:Normal **(h)** Phase 3:Storm **(i)** Phase 3:Gust

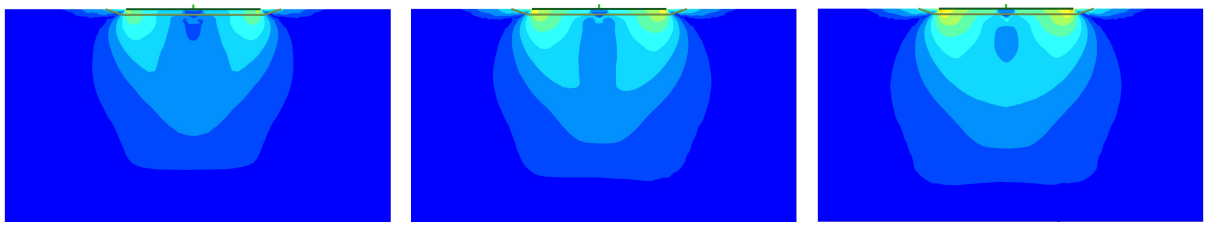

(j) Phase 4:Normal **(k)** Phase 4:Storm **(l)** Phase 4:Gust

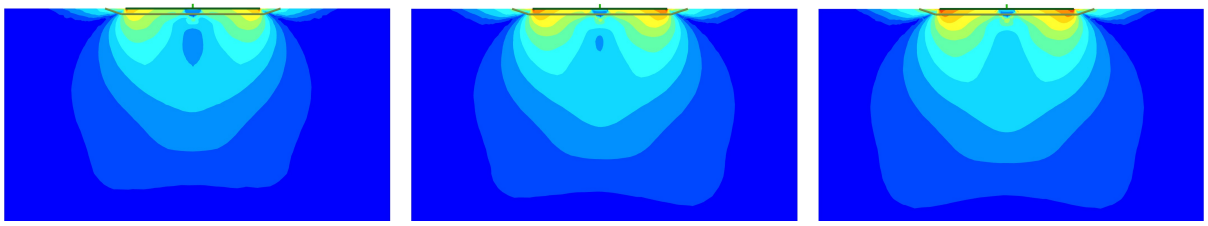

(m) Phase 5:Normal **(n)** Phase 5:Storm **(o)** Phase 5:Gust

Figure 6.29: Visual output from Plaxis displaying the deviatoric strain within the soil body

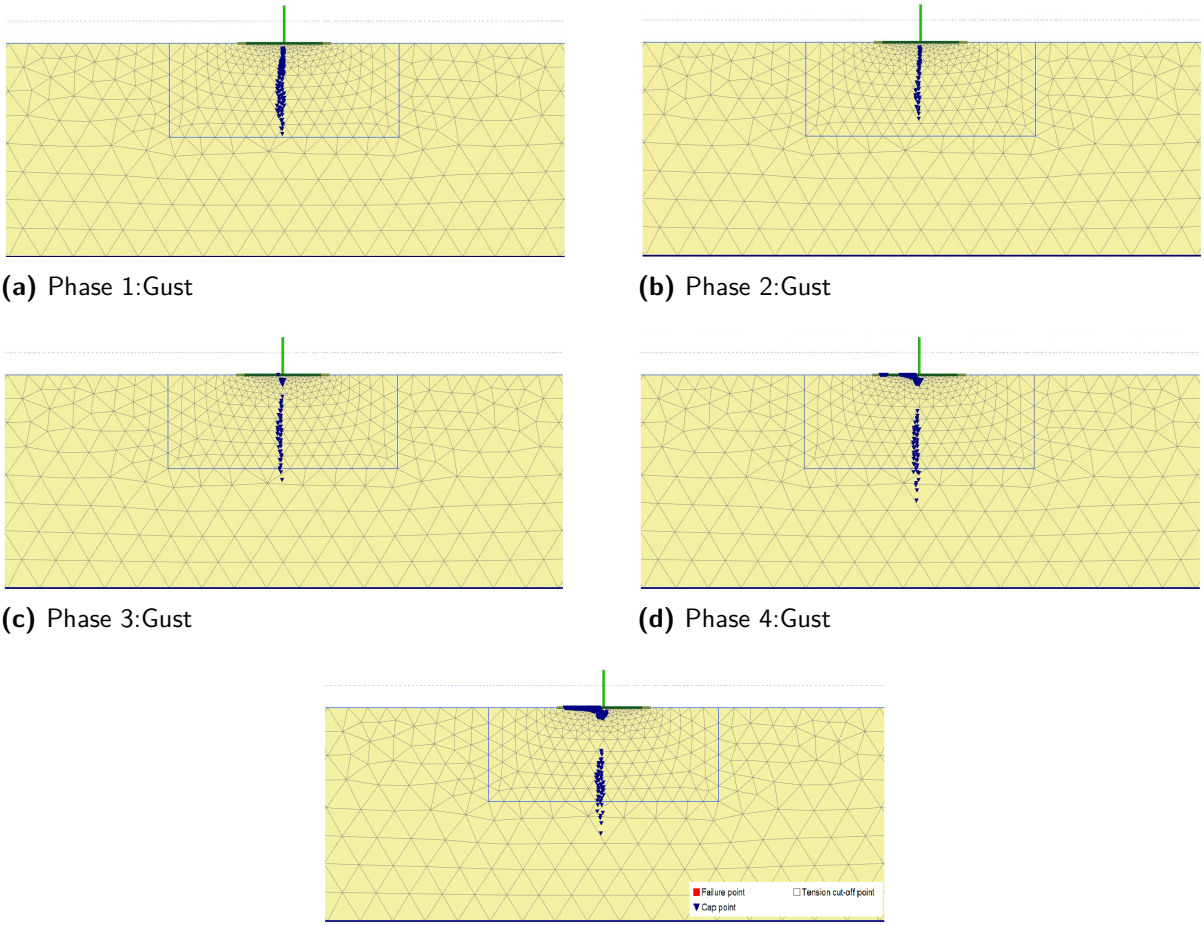

(a) Phase 1:Gust

(b) Phase 2:Gust

(c) Phase 3:Gust

(d) Phase 4:Gust

(e) Phase 5:Gust

Figure 6.30: Visual output from Plaxis displaying the plastic points within the soil body

6.10 Conclusion

The settlement predicted by the numerical model either underestimates the 1g test, as for the baseline simulation, or significantly overestimates the experimental results, as occurs in the more intense wind scenarios (short break storm and gust). In the baseline simulation the response of the soil is predominately elastic and there is minimal permanent deformation, whereas the behaviour in the soil body during the short break storm and gust storm simulations appears to be plastic. This shows the importance of adopting a more realistic constitutive model able to predict plastic strains due to cyclic stress reversals.

There is a relationship between the pattern of strain accumulation and settlement. This is most noticeable in the short break storm test where the both settlement and accumulated strain plateau from 20,000-40,000 seconds. The point of rotation for the structure is the centre of the foundation. The chosen R_{inter} of 0.04 allowed for the edge of the foundation to move freely during embedding and uplifting. The movement at the edge of the foundation was for all simulations similar to the 1g tests in the first 150 cycles.

Gajan et al. (2008) used an interface which allowed for the inclusion of elastic rotation range, without which the model would have predicted more settlement with smaller structural

rotations. Without an interface that includes an elastic rotation range the simulated rocking foundation produced larger settlements for the same rotations as the 1g tests. The interface therefore plays an important part in modelling rocking foundations.

Numerical results will always tend to be more even and consistent than any experimental results due to there being no errors or deformities within the model if not specifically introduced. One example is that of the soil body, which is perfectly uniform and flat at the surface in the numerical model, but in the experiments there may be surface roughness and minor sloping below the foundation. The soil strength increases with depth in the model without the issues of possible layering or air bubbles which may have occurred in the experimental tests, despite all efforts taken to avoid them.

Chapter 7

Conclusions

Multiple forms of modelling (1g, centrifuge and numerical) has been designed and conducted in order to replicate rocking in a wind turbine foundation on a clay soil, from cyclic displacement representing 3 types of wind speeds, functional, shut down and gusts. In order to investigate the soil structure interaction when long term cyclic loading has been applied to a shallow wind turbine foundation based on a slightly overconsolidated kaolin soil.

Multiple forms of modelling (1g, centrifuge and numerical) have been designed and conducted in order to capture rocking of a wind turbine foundation on a clay soil, from cyclic loading representing 3 types of wind speeds: operational, shut down and gusts. A prototype 22.5m wind turbine with a shallow 9m wide foundation was designed for the experimental and numerical modelling. A kaolin soil was selected and tested to produce favourable soil conditions to allow for a shallow foundation to embed without excessive settlements. Five 1g tests were conducted and presented, where foundation rocking occurred causing the soil profile to deform. The main conclusions are as follows:

- Three typical behaviours were observed through out the 1g test consisting of:
  - Amplification behaviour; when the applied displacement is increased between phases, the required force initially increases. With subsequent cycles a decrease in the required force is observed until the response becomes constant or there is a change in the displacement phase. This amplification behaviour results in an increase in embedment and the soil profile below the foundation rounds causing less of the foundation to be in contact with the soil.
  - Constant behaviour; the applied displacement and the force required are consistent until there is a change in the applied displacement. The constant behaviour sees little change in the soil profile the amount of uplift of the foundation, or foundation-soil contact. Settlement still occurs during this behaviour.
  - Recovery behaviour; the applied displacement decreases between phases and the force required significantly decreases. However, with each subsequent cycle the force required increases a small amount for 6-10 cycles and the behaviour becomes

constant. The recovery behaviour flattens the soil profile, uplift is reduced and the foundation-soil contact increases.

- Soil structure interaction was shown to change by measuring the natural frequency of the turbine before and after each test. Where the natural frequency was observed to decrease.

A cyclic centrifuge test was conducted, simulating the short break storm 1g test. Similar behaviours were seen in the 1g and centrifuge tests, such as the force required for displacement decreases when comparing like matching phases.

Numerical modelling was also conducted using 2D finite element analysis. The soil behaviour was described using the Modified Cam-Clay soil model, which was calibrated against the results of laboratory tests on the kaolin clay. Three of the 1g tests were simulated: the baseline, short break storm and gust storm.

- The simulations replicated the general trend of the cyclic displacement, where the larger the displacement applied to the structure, the more deformation occurred in the soil body.

- The simulations predicted an increase of deviatoric strain within the soil body after cyclic loading and larger displacements caused a higher rate of strain accumulation.

The UK's aim at becoming net zero carbon emitter by 2050, renewable energy is essential in reducing carbon emissions and onshore wind turbines can contribute in the transition towards greener energy generation. This research increases knowledge about the foundations of shallow on-shore wind turbines and the capability for these foundation to rock and uplift without significant changes to the stability of the structure.

Allowing for on-shore wind turbine foundations to be slightly under designed using less resources, and possibly even reusing existing pads of decommissioned wind turbines for new larger wind turbines. Where current practices see foundation uplift as a failure of the design it should be seen as a method for structural protection when there are cyclic loads that can cause structural degradation.

After a large cyclic event with large foundation rotations, the ability for the structure to recover and regain strength during the subsequent normal period of cyclic loading, demonstrates the benefits that can be gained from allowing structures to rock.

7.1 Further Work

The recommendations for further works is to increase the volume and complexity of the experimental and numerical modelling, to gain more information about the soil body and represent more realistic wind turbine.

- Duplicates of all the 1g tests to be repeated in the centrifuge, generating more data to confirm the responses shown in the 1g tests.

- Multiple directions of wind loading; wind is not in a single direction in reality, a change in direction would shift where the foundation is in contact with the soil.
- Extending the number of cyclic loads to 10,000 or more to model an entire design life.
- A varied range of wind speeds. Different displacements patterns could be included within the normal phases, representing slower wind speeds during operation.
- Replicating the P1 and P3 loading, creating a complex prototype that has multiple forms of cyclic loading. This would result in a structural relationship with multiple frequencies and complex soil structure interaction.
- Changing the foundation shape from square to either round or hexagonal shapes which are more representative of those used in industry.
- Changing the type of soil to include the use of sand or layered soil. This would indicate if the same behaviours are observed in sands.
- To design the physical modelling to have a visual representation of the stress and strain changes within the soil body. Also to include pressure sensor and pore water pressure sensors below the foundations of the physical modelling, a record of where the pressure is applied blow the foundation as well as the changes in the pore water pressure. Allowing for comparison against numerical simulations.
- The use of a more advanced constitutive model in numerical simulations of the physical experiments. The soil model should be able to capture complex non-linear features of real undrained clay behaviour under cyclic loads, including high stiffness at small strains, the accumulation of plastic strain and associated degradation of stiffness, and generation of excess pore water pressures. These features could be simulated with a critical state model formulated in the framework of kinematic hardening with bounding surface plasticity, such as introduced by Rouainia and Muir Wood (2000).

Bibliography

Adhikari, S. and Bhattacharya, S. (2012), 'Dynamic analysis of wind turbine towers on flexible foundations', *Shock and vibration* **19**(1), 37–56.

Anastasopoulos, I., Gazetas, G., Loli, M., Apostolou, M. and Gerolymos, N. (2010), 'Soil failure can be used for seismic protection of structures', *Bulletin of Earthquake Engineering* **8**(2), 309–326.

Anastasopoulos, I., Gelagoti, F., Kourkoulis, R. and Gazetas, G. (2011), 'Simplified constitutive model for simulation of cyclic response of shallow foundations: validation against laboratory tests', *Journal of Geotechnical and Geoenvironmental Engineering* **137**(12), 1154–1168.

Anastasopoulos, I., Georgarakos, T., Georgiannou, V., Drosos, V. and Kourkoulis, R. (2010), 'Seismic performance of bar-mat reinforced-soil retaining wall: Shaking table testing versus numerical analysis with modified kinematic hardening constitutive model', *Soil Dynamics and Earthquake Engineering* **30**(10), 1089–1105.

Anastasopoulos, I., Kourkoulis, R., Gelagoti, F. and Papadopoulos, E. (2012), 'Rocking response of sdof systems on shallow improved sand: An experimental study', *Soil Dynamics and Earthquake Engineering* **40**, 15–33.

Arany, L., Bhattacharya, S., Adhikari, S., Hogan, S. and Macdonald, J. (2015), 'An analytical model to predict the natural frequency of offshore wind turbines on three-spring flexible foundations using two different beam models', *Soil Dynamics and Earthquake Engineering* **74**, 40–45.

Bhattacharya, S., Lombardi, D. and MuirWood, D. (2011), 'Similitude relationships for physical modelling of monopile-supported offshore wind turbines', *International Journal of Physical Modelling in Geotechnics* **11**, 58–68.

Bhattacharya, S., Nikitas, G., Arany, L. and Nikitas, N. (2017), 'Soil-structure interactions (ssi) for offshore wind turbines', *IET Engineering and Technology Reference* **24**(16).

Bhattacharya, S., Nikitas, G. and Jalbi, S. (2018), On the use of scaled model tests for analysis and design of offshore wind turbines, *in* 'Geotechnics for Natural and Engineered Sustainable Technologies', Springer, pp. 107–129.

Bhattacharya, S., Nikitas, G. and Vimalan, N. (2019), Dynamic ssi of monopile-supported offshore wind turbines, *in* 'Geotechnical Design and Practice', Springer, pp. 113–123.

Bhattacharya, S., Nikitas, N., Garnsey, J., Alexander, N., Cox, J., Lombardi, D., Wood, D. M. and Nash, D. (2013), 'Observed dynamic soil–structure interaction in scale testing of offshore wind turbine foundations', *Soil Dynamics and Earthquake Engineering* **54**, 47–60.

Borja, R. I. and Regueiro, R. A. (2001), 'Strain localization in frictional materials exhibiting displacement jumps', *Computer Methods in Applied Mechanics and Engineering* **190**(20-21), 2555–2580.

Brennan, A., Brown, M., Knappett, J. and McMillan, C. (2016), Breakout loads of subsea structures and pipelines, Technical Note 23rd August 2016, Division of Civil Engineering, University of Dundee, Dundee, UK.

Brinkgreve, R., Kumarswamy, S., Swolfs, W., Waterman, D., Chesaru, A., Bonnier, P. et al. (2016), 'Plaxis 2016', *PLAXIS bv, the Netherlands* .

Brinkgreve, R., Swolfs, W., Engin, E., Waterman, D., Chesaru, A., Bonnier, P. and Galavi, V. (2011), 'Plaxis 2d reference manual', *Delft University of Technology and PLAXIS bv The Netherlands* .

'British-Geological-Socity' (2019), 'Geology of britain viewer, superficial deposits'. Last Accessed: April 2019.
URL: *http://mapapps.bgs.ac.uk/geologyofbritain/home.html*

'British-Standard-Intitution' (1990), 'Methods of test for soils for civil engineering purposes, part 4, compaction realted tests, bs1377-4'. Date accessed: November 2016.
URL: *https://bsol-bsigroup-com.libproxy.ncl.ac.uk/Search/Search?searchKey=1377-4OriginPage=Header+Search+BoxautoSuggestion=false*

BRITISH-STANDARDS-INSTITUTION (1995), 'Eurocode 7. part 1, general rules (together with united kingdom national application document)', **1**.

'British-Standards-Intitution' (1990), 'Methods of test for soils for civil engineering purposes, part 9, in-situ tests, bs 1377-9'. date accessed: Novemeber 2016.
URL: *https://bsol-bsigroup-com.libproxy.ncl.ac.uk/Search/Search?searchKey=1377-9OriginPage=Header+Search+BoxautoSuggestion=false*

Byrne, B. (2000), Performance of shallow foundations on sand, *in* 'Sixth Young Geotechnical Engineers Symposium', Thomas Telford Publishing, pp. 3–4.

Byrne, B. W., Burd, H. J., Gavin, K. G., Houlsby, G. T., Jardine, R. J., McAdam, R. A., Martin, C. M., Potts, D. M., Taborda, D. M. and Zdravkovic, L. (2018), Pisa: Recent developments in offshore wind turbine monopile design, *in* 'Vietnam Symposium on Advances in Offshore Engineering', Springer, pp. 350–355.

Cabangon, L., Elia, G. and Rouainia, M. (2017), 'Advanced numerical modelling of the transverse behaviour of tunnels under seismic loading', *EURO:TUN 2017* .

Chopra, A. K. (1995), *Dynamics of structures: theory and applications to earthquake engineering*, Prentice Hall.

Corbetta, G., Mbistrova, A., Ho, A., Pineda, I. and Ruby, K. (2016), 'Wind in power: 2015 european statistics', *Brussels. European Wind Energy Association* p. 14.

Currie, M., Saafi, M., Tachtatzis, C. and Quail, F. (2015), 'Structural integrity monitoring of onshore wind turbine concrete foundations', *Renewable energy* **83**, 1131–1138.

Deng, L., Kutter, B. L. and Kunnath, S. K. (2011), 'Centrifuge modeling of bridge systems designed for rocking foundations', *Journal of Geotechnical and Geoenvironmental Engineering* **138**(3), 335–344.

Deng, Z.-W., Gao, Q.-F., Dong, H. and Li, L.-X. (2018), 'Dynamic responses of the shallow foundation of an onshore wind turbine', *International Journal of Physical Modelling in Geotechnics* pp. 1–14.

Det Norske Veritas (2010), 'Design and manufacture of wind turbine blades, offshore and onshore wind turbines', *Det Norske Veritas* .

Drosos, V., Georgarakos, T., Loli, M., Anastasopoulos, I., Zarzouras, O. and Gazetas, G. (2012), 'Soil-foundation-structure interaction with mobilization of bearing capacity: Experimental study on sand', *Journal of Geotechnical and Geoenvironmental Engineering* **138**(11), 1369–1386.

Elia, G. (2015), 'Site response for seismic hazard assessment', *Encyclopedia of Earthquake Engineering* p. 3266â3287.

Gajan, S., Hutchinson, T. C., Kutter, B. L., Raychowdhury, P., Ugalde, J. A. and Stewart, J. P. (2008), *Numerical models for analysis and performance-based design of shallow foundations subjected to seismic loading*, Pacific Earthquake Engineering Research Center.

Gajan, S. and Kutter, B. L. (2008), 'Capacity, settlement, and energy dissipation of shallow footings subjected to rocking', *Journal of Geotechnical and Geoenvironmental Engineering* **134**(8), 1129–1141.

Gajan, S. and Kutter, B. L. (2009), 'Effects of moment-to-shear ratio on combined cyclic load-displacement behavior of shallow foundations from centrifuge experiments', *Journal of geotechnical and geoenvironmental engineering* **135**(8), 1044–1055.

Gajan, S., Kutter, B. L., Phalen, J. D., Hutchinson, T. C. and Martin, G. R. (2005), 'Centrifuge modeling of load-deformation behavior of rocking shallow foundations', *Soil Dynamics and Earthquake Engineering* **25**(7-10), 773–783.

Gajan, S. and Saravanathiiban, D. S. (2011), 'Modeling of energy dissipation in structural devices and foundation soil during seismic loading', *Soil Dynamics and Earthquake Engineering* **31**(8), 1106–1122.

Gazetas, G., Anastasopoulos, I. and Garini, E. (2014), 'Geotechnical design with apparent seismic safety factors well-bellow 1', *Soil Dynamics and Earthquake Engineering* **57**, 37–45.

GDS-Instruments (2009), 'Gdsfa - data sheet'. Last accessed: May 2018.
URL: *http://www.gdsinstruments.com/__assets__/Products/00032/GDSFA_Force_Actuator_Datasheet.pdf*

Hakhamaneshi, M., Kutter, B., Deng, L., Hutchinson, T. and Liu, W. (2012), 'New findings from centrifuge modeling of rocking shallow foundations in clayey ground', *ASCE GeoCongress* .

Harte, M., Basu, B. and Nielsen, S. R. (2012), 'Dynamic analysis of wind turbines including soil-structure interaction', *Engineering Structures* **45**, 509–518.

He, M., Bai, X., Ma, R. and Huang, D. (2019), 'Structural monitoring of an onshore wind turbine foundation using strain sensors', *Structure and Infrastructure engineering* **15**(3), 314–333.

Houlsby, G. (1999), 'Model tests on suction caissons in dense sand', *Final Report on EPSRC Grant GR/L/67547, Department of Engineering Science, University of Oxford* .

Houlsby, G., Kelly, R., Huxtable, J. and Byrne, B. (2005), 'Field trials of suction caissons in clay for offshore wind turbine foundations', *Géotechnique* **55**(4).

Houlsby, G., Kelly, R., Huxtable, J. and Byrne, B. (2006), 'Field trials of suction caissons in sand for offshore wind turbine foundations', *Géotechnique* **56**(1).

Houlsby, G. T. and Byrne, B. W. (2000), 'Suction caisson foundations for offshore wind turbines and anemometer masts', *Wind engineering* **24**(4), 249–255.

House, A., Oliveira, J. and Randolph, M. (2001), 'Evaluating the coefficient of consolidation using penetration tests', *International Journal of Physical Modelling in Geotechnics* **1**(3), 17–26.

Hvorslev, M. (1937), Über die Festigkeitseigenschaften gestörter bindiger Böden. Ingeniorvidenskabelige Skrifter A Nr. 45, Danmarks Naturvidenskabelige Samfund, PhD thesis, Dissertation, Kopenhagen.

Kutter, B. L., Hutchinson, T. C., Moore, M. A., Kunnath, S. and Deng, L. (2012), Influence of physical modeling on adoption of rocking foundations in practice, *in* 'GeoCongress 2012: State of the Art and Practice in Geotechnical Engineering', GeoCongress, pp. 2017–2026.

Lazcano, D. R. P., Aires, R. G. and Nieto, H. P. (2020), 'Bearing capacity of shallow foundation under cyclic load on cohesive soil', *Computers and Geotechnics* **123**, 103556.

LeBlanc, C., Houlsby, G. and Byrne, B. (2010), 'Response of stiff piles in sand to long-term cyclic lateral loading', *Géotechnique* **60**(2), 79–90.

Li, Z., Haigh, S. and Bolton, M. (2010), 'Centrifuge modelling of mono-pile under cyclic lateral loads', *Physical Modelling in Geotechnics* pp. 965–970.

Lombardi, D., Bhattacharya, S. and Wood, D. M. (2013), 'Dynamic soil–structure interaction of monopile supported wind turbines in cohesive soil', *Soil Dynamics and Earthquake Engineering* **49**, 165–180.

Madabhushi, G. (2014), *Centrifuge modelling for civil engineers*, 1st edn, CRC Press, Florida, USA.

Muir Wood, D. (1990), *Soil behaviour and critical state soil mechanics*, Cambridge university press.

Muir Wood, D. (2004), *Geotechnical modelling*, 1 edn, CRC press, Oxfordshire, UK.

Ntambakwa, E., Yu, H., Guzman, C. and Rogers, M. (2016), Geotechnical design considerations for onshore wind turbine shallow foundations, *in* 'Geotechnical and Structural Engineering Congress 2016', pp. 1153–1165.

Okawa, M., Fujiyama, C., Koda, Y. and Kado, M. (2018), Damage investigation of existing onshore wind turbine foundation, *in* 'Grand Renewable Energy proceedings Japan council for Renewable Energy', Japan Council for Renewable Energy, p. 133.

Okur, D. and Ansal, A. (2007), 'Stiffness degradation of natural fine grained soils during cyclic loading', *Soil Dynamics and Earthquake Engineering* **27**(9), 843–854.

Oliveira, G., Magalhães, F., Cunha, Á. and Caetano, E. (2018), 'Vibration-based damage detection in a wind turbine using 1 year of data', *Structural Control and Health Monitoring* **25**(11), e2238.

Oliveto, G., Calio, I. and Greco, A. (2003), 'Large displacement behaviour of a structural model with foundation uplift under impulsive and earthquake excitations', *Earthquake engineering & structural dynamics* **32**(3), 369–393.

Paolucci, R., Shirato, M. and Yilmaz, M. T. (2008), 'Seismic behaviour of shallow foundations: Shaking table experiments vs numerical modelling', *Earthquake Engineering & Structural Dynamics* **37**(4), 577–595.

Rendulic, L. (1937), 'Das grundgesetz der tonmechanik und sein experimenteller beweis', *Bauingenieur* **18**, 0–31.

Robinson, S. (2019), Rate effect behaivour of different clays from high speed triaxial element testing, Doctorial thesis, School of Engineering, University of Dundee.

Roscoe, K. and Burland, J. (1968), 'On the generalized stress-strain behaviour of wet clay', *Geotechnique* .

Roscoe, K. H., Schofield, A. and Wroth, a. P. (1958), 'On the yielding of soils', *Geotechnique* **8**(1), 22–53.

Roscoe, K., Schofield, A. and Thurairajah, A. (1963), 'Yielding of clays in states wetter than critical', *Geotechnique* **13**(3), 211–240.

Rouainia, M. and Muir Wood, D. (2000), 'A kinematic hardening constitutive model for natural clays with loss of structure', *Géotechnique* **50**(2), 153–164.

Salawu, O. (1997), 'Detection of structural damage through changes in frequency: a review', *Engineering structures* **19**(9), 718–723.

Seymour, S. (2018), Numerical modelling of onshore wind turbine gravity foundations susceptible to cyclic soil degradation, Msc thesis, School of Engineering, University of Cape Town.

Siemens (2009), Foundation loads swt-2.3-93, Confidental Corrorspendance with Arup SWT-23-93, 78.3m hh, Siemens Wind Power A/S.

Stewart, D. and Randolph, M. (1991), 'A new site investigation tool for the centrifuge.', *Proc., Int. Conf. Centrifuge 1991* pp. 531–538.

Taddei, F., Butenweg, C. and Klinkel, S. (2015), 'Parametric investigation of the soil–structure interaction effects on the dynamic behaviour of a shallow foundation supported wind turbine considering a layered soil', *Wind Energy* **18**(3), 399–417.

The-Wind-Power (2019), 'Swt-2.3-93'. last accessed 2019-08-06.
URL: *https://www.thewindpower.net/scripts/fpdf181/turbine.php?id=22*

Valls-Marquez, M. (2009), Evaluating the capabilities of some constitutive models in reproducing the experimental behaviour of stiff clay subjected to tunnelling stress paths, PhD thesis, University of Birmingham.

Yu, H., Guzman, C. and Ntambakwa, E. (2016), Consideration of the cyclic degradation of cohesive soils in pile foundation design for onshore wind turbines, *in* 'Geo-Chicago 2016', Chicago Illinois, pp. 195–206.

Yu, L.-q., Wang, L.-Z., Guo, Z., Bhattacharya, S., Nikitas, G., Li, L.-L. and Xing, Y.-L. (2015), 'Long-term dynamic behavior of monopile supported offshore wind turbines in sand', *Theoretical and Applied Mechanics Letters* **5**(2), 80–84.

Zania, V. (2014), 'Natural vibration frequency and damping of slender structures founded on monopiles', *Soil dynamics and Earthquake engineering* **59**, 8–20.

Zhu, B., Byrne, B. and Houlsby, G. (2012), 'Long-term lateral cyclic response of suction caisson foundations in sand', *Journal of Geotechnical and Geoenvironmental Engineering* **139**(1), 73–83.

Ziegler, L., Gonzalez, E., Rubert, T., Smolka, U. and Melero, J. J. (2018), 'Lifetime extension of onshore wind turbines: A review covering germany, spain, denmark, and the uk', *Renewable and Sustainable Energy Reviews* **82**, 1261–1271.